UNIVERSITY OF CALIFORNIA SAN DIEGO

Mechanisms of Intermicrobial Interactions in the Cheese Rind Microbiome

A dissertation submitted in partial satisfaction of the requirements for
the degree Doctor of Philosophy

in

Biology

by

Emily C. Pierce

Committee in Charge:

Professor Rachel J. Dutton, Chair
Professor Susan S. Golden
Professor Sergey Kryazhimskiy
Professor Joseph Pogliano
Professor Manuela Raffatellu

2021

The dissertation of Emily C. Pierce is approved, and it is acceptable in quality and form for publication on microfilm and electronically.

University of California San Diego

2021

DEDICATION

This dissertation is dedicated to Peaches, a loyal friend.

TABLE OF CONTENTS

LIST OF FIGURES

LIST OF TABLES

ACKNOWLEDGMENTS

I would like to first thank my committee members for their service and for their thoughtful consideration of my project over the years. This dissertation has been vastly improved by their input. Thank you especially to Professor Rachel Dutton. Whenever people ask how I decided on a thesis lab, my answer is always immediately that I chose it to work with you. It has been an honor to be your 'first pancake'. Thank you for letting me work on a project that perfectly suited my interests, for helping me to develop as a scientist, and for accepting me despite my inability to cut proper circles. From the beginning, I felt that you were not only an admirable and revolutionary scientist, but mostly that you were someone I felt at home with. Your leadership over the past five years has certainly turned our lab into a home-away-from-home, in large part because of the people you have chosen to work for you. To my labmates, I have been incredibly lucky to know you scientifically and personally. You make every day more fun. Thank you especially to Manon, for your delicious bakes, for laughing with me at inappropriate times (even though you hide it in your scarf), and for being a scientific role model. I have often thought that we are eerily similar, so it is no surprise we ended up on team RB-TnSeq together. You have taught me so much, and this work would absolutely not have been possible without you. I am so glad I chose to sit in your office.

Completion of this dissertation was also made possible by the support of the amazing female scientists in my cohort, aka 'Da Ladies.' Their friendships have filled this chapter of my life with love and laughter, and I have great professional and personal admiration for each of them. Thank you especially to Brooke, for lending me Harry Potter books in my darkest hours, for romcom champagne sessions, and for being a shoulder to cry on. Angela, from our 'first day of school' on, you have been a kind and thoughtful friend, with an extraordinary ability to put

my heart at ease. I am forever grateful that we shared a New York hotel room. Laura, thank you for sharing your beachside estate and for being the best aunt a bunny could ask for. Your unforgettable crab dance has been an inspiration in times of struggle. To Ben, thank you for your support and advice over the years. I'm not sure I ever really meditated, but I always enjoyed the company.

To my best friend Hopsy, you are the greatest and most loved. You may be small, but you have been a huge presence in my life. Thank you for being a constant source of joy. Elliot, thank you for taking me literally and figuratively to new heights, for cooking dinner so that I could work on this dissertation, for exploring the world with me, and for bringing constant hilarity to our home. Your support has been invaluable.

Lastly, to my family, thank you for a lifetime of encouragement. I would never have made it here without you. It has been hard being far away over the last few years, but I want you to know that I appreciate the sacrifices you have made in helping me to succeed. Thank you to my parents for traveling across the country with rabbits in tow to get me settled, for talking to me every day as I risked my life crossing La Jolla Shores, and for always having my back.

I would also like to acknowledge scientific contributions to this dissertation. Chapter 1 consists of material from a manuscript in preparation for publication. The manuscript in preparation is: Emily C. Pierce and Rachel J. Dutton. Identifying molecular mechanisms of species interactions within communities. (In preparation for *Current Opinion in Microbiology*). The dissertation author is the primary author of this manuscript in preparation.

Chapter 2, in part, is made up of a reprint of the following published manuscript: Morin, Manon, Emily C. Pierce, and Rachel J. Dutton. Changes in the genetic requirements for microbial interactions with increasing community complexity. *Elife* 7 (2018): e37072. The dissertation author was the secondary author of this paper.

Chapter 3, in part, is made up of a reprint of the following published manuscript: Pierce, E.C., Morin, M., Little, J.C., Liu, R.B., Tannous, J., Keller, N.P., Pogliano, K., Wolfe, B.E., Sanchez, L.M., and Dutton, R.J. Bacterial–fungal interactions revealed by genome-wide analysis of bacterial mutant fitness. *Nat Microbiol* (2020). https://doi.org/10.1038/s41564-020-00800- z. The dissertation author was the primary author of this paper.

Chapter 4 consists of unpublished material. The dissertation author is the primary author of this material. The following individuals are also authors on this work: Section 4.2- Rachel Dutton (UCSD); Section 4.3- Kit Pogliano (UCSD), Roland Liu (UCSD), Rachel Dutton (UCSD); Section 4.4- Manon Morin (UCSD), Rachel Dutton (UCSD).

VITA

Education

University of California San Diego — San Diego, CA
Ph.D. in Biological Sciences — 2015-2021
Micro-MBA, Rady School of Management

University of Georgia — Athens, GA
B.S. in Applied Biotechnology — 2007-2012
M.S. in Plant Breeding, Genetics, and Genomics
summa cum laude
Combined MS/BS Program
Honors Program

ETH Zürich — Zurich, Switzerland
International Exchange Program Masters Student — February-June 2012

Industry Experience

Illumina — San Diego, CA
iAspire intern with Jonathan Hetzel in Genomic Applications — June-August 2019
Solutions for detection of antimicrobial resistance in sequencing data

DuPont Pioneer — Wilmington, DE
Research assistant with Dr. Howard Damude and Dr. Brian McGonigle — 2013-2015
Genetic Engineering of Soybean for Oleic Oil Production and Insect Resistance

Research Experience

University of California San Diego — San Diego, CA
Graduate research in the laboratory of Dr. Rachel Dutton — 2015-2021
Mechanisms of Intermicrobial Interaction
in the Cheese Rind Model Microbiome
Collaboration with Ballast Point Brewing Company
Development of a Microbial Community in a Virgin Oak Foeder

University of California, Santa Barbara — Santa Barbara, CA
Kavli Institute for Theoretical Physics' Advanced School of Quantitative Biology — June-August 2017
Eco-Evolutionary Dynamics in Microbial Communities

University of Georgia — Athens, GA
Undergraduate and graduate research in the laboratory of Dr. Wayne Parrott — 2008-2012
Metabolic Engineering of Ketocarotenoid Production in Soybean

Publications

Pierce EC, Morin M, Little JC, Liu RB, Tannous J, Keller NP, Pogliano K, Wolfe BE, Sanchez LM, Dutton RJ (2020). Bacterial-fungal interactions revealed by genome-wide analysis of bacterial mutant fitness. *Nature Microbiology*.

Cleary JL, Luu GT**, Pierce EC**, Dutton RJ, Sanchez LM (2019). BLANKA: An Algorithm for Blank Subtraction in Mass Spectrometry of Complex Biological Samples. *Journal of The American Society for Mass Spectrometry, 30*(8), 1426-1434.

Morin M, **Pierce EC**, Dutton RJ (2018). Changes in the genetic requirements for microbial interactions with increasing community complexity. *eLife, 7*, e37072.

Rubin BE, Huynh TN, Welkie DG, Diamond S, Simkovsky R, **Pierce EC,** Taton A, Lowe LC, Lee JJ, Rifkin SA, Woodward JJ, Golden, SS (2018). High-throughput interaction screens illuminate the role of c-di-AMP in cyanobacterial nighttime survival. *PLoS Genetics, 14*(4), e1007301.

Pierce EC, LaFayette PR, Ortega MA, Joyce BL, Kopsell DA, Parrott WA (2015) Ketocarotenoid Production in Soybean Seeds through Metabolic Engineering. *PLoS ONE, 10*(9), e0138196.

Awards, Honors, and Grants

McElroy Award, UCSD	2020
Illumina NovaSeq Sequencing Mini-Grant	2020
3rd Place Grad SLAM UCSD Speaking Competition	2019
NSF Graduate Research Fellowship Honorable Mention	2016, 2017
Center for Microbiome Innovation Seed Grant	2016
Ruth Stern Award, UCSD	2016
Cell and Molecular Genetics Training Program Grant	2016
CURO Undergraduate Research Scholar	2012
Foundation for Global Scholars Travel Scholarship	2012
UGA Graduate School Research Assistantship	2010
UGA CURO Summer Research Fellowship	2009

Presentations

Center for Microbiome Innovation Research Summit — San Diego, CA, 2020
Pierce EC, Morin M, and Dutton RJ. *Insights from Multi-Omic Investigations of the Cheese Microbiome*

Lake Arrowhead Microbial Genomics Conference — Lake Arrowhead, CA, 2018
Pierce EC, Morin M, and Dutton RJ. *Bacterial-fungal Interactions in the Cheese Rind Model Microbiome.* Student Poster Award.

American Society of Brewing Chemists Brewing Summit — San Diego, CA, 2018
Pierce EC, Moritz C, Nagle ED, Heussler GE, Dell Z, Dutton RJ. *Development of a Microbial Community in a Virgin Oak Foeder and its Impact on Sugar Utilization and Acid Production.* Poster.

Cell and Molecular Genetics Training Program Colloquium — San Diego, CA

Pierce EC, Morin M, and Dutton RJ. *Mechanisms of microbial interactions in a model community.* Oral presentation. 2018

ASM Interbacterial Cooperation and Competition Conference Washington, D.C.
Pierce EC, Morin M, and Dutton RJ. *High-throughput Genetic Screen for Species Interactions in a Model Microbial Community.* Poster. 2017

Molecular and Cellular Biology of the Soybean Conference Des Moines, IA
Pierce EC, LaFayette P, Tucker D, Kopsell D, and Parrott WA. *Metabolic Engineering of Soybean for Carotenoid Production.* Oral Presentation, selected from abstracts. 2012

Teaching Experience

University of California San Diego San Diego, CA
Instructional Assistant 2017-2019
Recombinant DNA Techniques, Genomics Research Initiative Lab II, and Microbiology

University of Georgia Athens, GA
Research Mentor for Young Scholars Internship Program 2011

Activities

Mentor for UCSD Biology Undergraduate and Master's Mentorship Program. 2020
Organizer of Microbiology Graduate Student Seminar Series 2018
Organizer of CMG Training Program Symposium 2017
Member of PhD Student Recruitment Committee 2016, 2017
Volunteer for Fleet Science Center, San Diego 2016
Mentor for Women Organization for Research Mentoring in STEM 2016
Guest lecturer at Science Saturday for Girls 2016
Volunteer for Better Education for Women in Science and Engineering 2016
Guest lecturer for middle school science class, Mar Vista Academy, San Diego 2016

ABSTRACT OF THE DISSERTATION

Mechanisms of Intermicrobial Interactions in the Cheese Rind Microbiome

by

Emily C. Pierce

Doctor of Philosophy in Biology

University of California San Diego, 2021

Professor Rachel J. Dutton, Chair

Despite having traditionally been studied in isolation, the natural context of microbial growth is in the presence of other species. Research on microbes in interactive contexts has previously been challenging due to the complexity of natural microbiomes and an inability to culture non-model organisms. To address these challenges, a model microbiome based on the cheese rind has been developed. This system is of intermediate diversity and contains genetically tractable and culturable organisms, enabling mechanistic study of microbial interactions. Using species from this model microbiome, we apply cutting-edge genetic, metabolomic, and imaging techniques to investigate mechanisms of intermicrobial interactions. Chapter 1 reviews recent

findings regarding intermicrobial interactions. Chapter 2 reports on the development of an RB-TnSeq library in cheese-associated bacterium *Pseudomonas psychrophila* and the use of this library in a three-member cheese rind model community to identify intermicrobial interactions. Chapter 3 presents the application of RB-TnSeq to the study of mechanisms related to bacterial-fungal interactions. This chapter also introduces a custom analysis pipeline developed for cross-condition RB-TnSeq comparisons. Chapter 4 describes three projects stemming from Chapter 3, which relate to an *E. coli* gene of unknown function, a fungal protein with potential antibiotic activity, and the application of RB-TnSeq to the study of bacterial-bacterial interactions, including the creation and characterization of an RB-TnSeq library in another cheese-associated bacterium *Hafnia* sp. str. JB232. Finally, Chapter 5 discusses potential future directions for this work and provides concluding remarks.

CHAPTER 1: Introduction

1.1 Recent Insights into Intermicrobial Interactions

Next generation sequencing has revealed the enormous diversity of microbial species present in almost every imaginable habitat on the planet, and the important roles these microbes have is becoming increasingly clear. However, due in part to the complexity of microbial communities, or microbiomes, understanding how microbes within a system interact and how these interactions affect community-level phenotypes is extremely challenging. The ability to uncover and characterize these interactions has the potential to reveal large amounts of new biological information about microbes, and can provide insights into how to manipulate microbiomes for improved medicinal, agricultural, and environmental outcomes.

Despite the challenges associated with the study of species interactions, researchers have continued to work towards uncovering the mechanisms that drive interactions in diverse systems. Here, we review highlights from recent literature on the molecular mechanisms of intermicrobial interactions. Across diverse systems, we find common themes in how microbes interact with their neighbors (Figure 1.1-1). We have thus grouped these studies based on the mechanistic themes that were identified, including interactions mediated by access to metals, toxic molecules, signaling mechanisms, nutrients, pH changes, and physical relationships. The combination of genetic, metabolomic, and imaging techniques seen in a number of recent studies has proven to be a powerful approach to elucidating these mechanisms. We also highlight some of the emerging approaches to studying mechanisms of intermicrobial interactions that have made these discoveries possible.

Iron as a key driver of species interactions

Iron has long been recognized as a key and often limiting nutrient for microbial growth. Microbes have evolved a number of strategies to deal with this limitation, including the secretion of iron-binding specialized metabolites called siderophores. Siderophores have been indicated in a number of intermicrobial interactions, including competition, cooperation, and cheating (Kramer, Özkaya, and Kümmerli 2020). It is therefore not surprising that interactions revolving around iron access continue to be uncovered in diverse systems.

In a recent study with nasal bacteria, *Corynebacterium* species that strongly inhibited coagulase-negative *Staphylococcus* via iron starvation were found to possess a gene cluster for the siderophore dehydroxynocardamine. This cluster is expressed in nasal metatranscriptomes, suggesting that *Corynebacterium*-mediated iron starvation of other bacteria may be relevant to the human nasal microbiome (Stubbendieck et al. 2019). Siderophore interactions are also relevant to non-host associated microbiomes. Building on an existing body of literature on interactions related to the *Pseudomonas* siderophore pyoverdine, Butaité *et al*. examined how these interactions play out among natural isolates in communities, where producers and non-producers frequently co-exist. They find that pyoverdine interactions not only involve cheating, whereby non-producers benefit directly from producers, but also growth inhibition, where non-producer pseudomonads cannot benefit from pyoverdine due to incompatible receptors (Butaitė et al. 2017).

Although siderophore-based interactions have received a lot of attention in bacterial-bacterial dynamics, recent work in a model microbiome based on the cheese rind have shown that fungal siderophores may also play important roles in microbiome dynamics, as they can positively impact the fitness of their bacterial neighbors and influence the distribution of closely-

related species (Kastman et al. 2016; Pierce et al. 2020). Despite a common focus on iron, access to other trace metals like zinc and copper can also drive intermicrobial interactions (Cleary et al. 2018; Han et al. 2019).

Antibiosis

Production of specialized metabolites and proteins that are toxic to other microbes is an important competitive strategy for microbes in community contexts (García-Bayona and Comstock 2018). In the human skin microbiome, a gene cluster for an antibiotic thiopeptide produced by many isolates of the common skin bacterium *Cutibacterium* was found to be upregulated when co-cultured with *Staphylococcus* species. This antibiotic does not affect commensal Actinobacteria, but does lead to higher ratios of *C. acnes* to *S. epidermidis*, suggesting that this antibiotic may impact the composition of hair follicle microbiomes (Claesen et al. 2020). Bacterially-derived peptides have also been shown to have a role in bacterial-fungal interactions in plant-associated species; *Ralstonia solanacearum* peptides trigger fungal antibiotic production (Spraker et al. 2018). Among rhizosphere species, *Pseudomonas* spp. can produce a family of alkaloids that inhibit Bacteroidetes. Production of related metabolites has convergently evolved in plants, suggesting that these bacterial metabolites may have similar roles in plant development or protection (Lozano, Park, et al. 2019). A root nodule model microbiome composed of *Brevibacillus brevis*, *Paenibacillus* sp., *Pantoea agglomerans*, and *Pseudomonas* sp. was recently used to identify cooperative and competitive interactions. This study included the use of metabolomics to identify a novel family of *B. brevis* antibiotic metabolites (B. L. Hansen et al. 2020).

Bacteria must also defend themselves against contact-dependent antagonism such as type VI secretion. Bacteria use type VI secretion systems to directly deliver toxic proteins into competitor bacterial cells. These systems play important roles in intermicrobial dynamics in diverse systems including the human gut (Ross et al. 2019), squid light organs (Speare et al. 2018), and legume root nodules (Salinero-Lanzarote et al. 2019). Interkingdom antibiosis was observed in a study using a combination of genetic and cell imaging techniques to investigate mechanisms of bacterial-fungal interactions in cheese rind microbiomes (Pierce et al. 2020).

Signaling-based Interactions

Signaling molecules are key to microbial communication and quorum sensing, which allows bacteria to adjust gene expression based on the surrounding population. Two recent studies highlighted the role of quorum sensing inhibition in interactions with *Staphylococcus*. A *Staphylococcus caprae* skin commensal can reduce skin infection burden of *S. aureus*, and probiotic *B. subtilis* reduced colonization of *S. aureus* in the intestine. Both of these interactions were linked to the production of peptides that inhibited *S. aureus* quorum sensing (Paharik et al. 2017; Piewngam et al. 2018). In *Chromobacterium violaceum*, quorum sensing regulates the expression of a drug efflux pump that increases resistance to bactobolin produced by *Burkholderia thailandensis*. Loss of quorum-sensing decreased competitive fitness of *C. violaceum* growing with *B. thailandensis*, and the presence of bactobolin restrained the evolution of *C. violaceum* quorum sensing cheaters, suggesting that interspecies interactions can constrain cheaters that exploit public goods (Evans et al. 2018). Predators can also eavesdrop on quorum sensing to detect their prey, as seen by the increased predatory behavior of a bacteria-consuming myxobacterium in response to quorum sensing molecules (Lloyd and Whitworth 2017).

Interactions related to pH

Environmental modifications related to physiochemical changes can also drive intermicrobial interactions. One common mechanism is the alteration of pH, as changes in pH can influence community structure across diverse ecosystems through promoting or inhibiting the growth of acid-sensitive or acid-tolerant species (Thompson et al. 2017). Recent work showed that the outcome of bacterial pairwise co-cultures could be predicted from a simple model based on how individual organisms manipulate and respond to environmental pH (Ratzke and Gore 2018). Co-culturing of two species from the fruit fly gut microbiome, *Lactobacillus plantarum* and *Acetobacter* sp., led to increased antibiotic tolerance of *L. plantarum* through a pH-based mechanism. When co-cultured, *Acetobacter* consumed lactate produced by *L. plantarum*, resulting in deacidification that favorably altered the *L. plantarum* growth (Aranda-Díaz et al. 2020).

Trophic Interactions

Trophic interactions such as nutrient cross-feeding or competition are important in many systems. Genetic and proteomic studies of bacteria growing alone or in consortia with other species have demonstrated that amino acid cross-feeding and/or competition among bacteria is seen in a model system from soil (L. B. S. Hansen et al. 2017; Herschend et al. 2017), between enteric pathogen species (Abdel-Haleem et al. 2020), among microbes in a cheese rind model microbiome (Morin, Pierce, and Dutton 2018), and with species associated with polymicrobial urinary tract infections (Armbruster et al. 2017). Competition and cross-feeding of vitamins have also been found to be important in interactions between bacteria and both other bacteria and microeukaryotes associated with fermented foods, marine systems, and the human gut (Cooper et

al. 2019; Pierce et al. 2020; Soto-Martin et al. 2020). In human gut metagenomes, positive associations are observed between bacterial *Christensenella* spp. and the hydrogen-consuming archaeon *Methanobrevibacter smithii*, two organisms whose abundance is correlated with host leanness. Ruaud *et al*. show that *Christensenella minuta* supports the growth of *M. smithii* through interspecies H_2 transfer, a process that is facilitated by physical associations (Ruaud et al. 2020). Other recent findings related to trophic interactions include cross-feeding of purines between bacteria (Abdel-Haleem et al. 2020; LaSarre et al. 2020) and interbacterial competition for carbon sources (Hall, Harrison, and Brockhurst 2018).

Trophic interactions have been shown to impact community-level phenotypes. They can mediate microbial community succession, as demonstrated in communities that self-assemble on organic marine particulates. Succession in these communities is determined by degradation of the particle by a primary group which provides carbon sources that facilitate a second group of "consumers." These consumers then inhibit the growth of the primary degraders by taking up space and interfering with degrader colonization (Datta et al. 2016; Enke et al. 2018). New work with eight soil bacteria showed that spent media from species grown in high nutrient concentrations led to more negative interactions with the other species relative to media from bacteria grown in low nutrient concentration. This is perhaps because interactions became driven by toxic metabolites rather than nutrient competition. The authors suggest that under higher nutrient conditions, interactions are stronger and more negative, which could lead to less biodiversity in these conditions (Ratzke, Barrere, and Gore 2020). Nutrient cross-feeding interactions can also constrain evolution of traits like antibiotic resistance, as the success of one member will be limited by the success of its cross-feeding partner; this could inform more

effective antibiotic treatment strategies (Adamowicz and Harcombe 2020; Adamowicz et al. 2020; Flynn et al. 2020).

Physical Interactions

Intermicrobial interactions can both influence and be influenced by physical structures and spatial organization in mixed biofilms. Spatially structured systems may limit the interactions of microbes to other microbes in close range (Dal Co et al. 2020). Combining transcriptomics and visual imaging, Liu *et al*. found that increased biomass production in a biofilm of four soil species relative to three-species communities was due to a fine-tuned spatial organization dependent on interspecies interactions (Liu et al. 2019). Interactions between bacteria isolated from marine biofilms led to the production of a newly secreted exopolysaccharide that may have increased biofilm formation in two-species communities (Guillonneau et al. 2018). Two soil bacteria, *Bacillus subtilis* and *Pantoea agglomerans*, were also shown to produce a biofilm structure not present in either monoculture that was dependent on contributions from both species. This structure protected *P. agglomerans* from antibiotic killing (Yannarell et al. 2019). Two other soil bacteria, *Pseudomonas fluorescens* and *Pedobacter* sp., have an emergent motility phenotype when grown together (McCully et al. 2019). A model microbiome from the soybean rhizosphere consisting of three bacterial species also displayed emergent motility and biofilm properties when species were grown in interactive contexts (Lozano, Bravo, et al. 2019). Emergent biofilm properties and physical interactions also occur in bacterial-fungal interactions. The presence of *Candida* metabolites stimulates biofilm growth of *Streptococcus* in dental cavities (Kim et al. 2017). Applying 'transparent soil' models to investigate soil microbial communities, Sharma *et al*. find that bacteria physically attached to

dead fungal hyphal structures are more metabolically active following a desiccation event (Sharma et al. 2020). In cheese rind microbiomes, motile Proteobacteria are able to use mycelial networks to disperse, giving them a fitness advantage in multispecies communities (Zhang et al. 2018).

Emerging Techniques for Investigating Interactions

Technological advances have enabled new approaches to studying microbial interactions (Figure 1.1-1). Multiple groups have recently developed microfluidic droplet based platforms to study synthetic microbial communities made up of combinatorial interactions (Hsu et al. 2019; Kehe et al. 2019). Kehe *et al.* used their platform to screen 100,000 multispecies communities made up of 19 soil isolates, and were able to find sets of isolates that consistently promoted growth of a plant symbiont (Kehe et al. 2019). Variations of transposon insertion sequencing, which combines transposon mutant screening and next generation sequencing, have been used to determine genes important for bacterial growth in community contexts using species from cheese rinds, oral microbiomes, and a synthetic bacterial mutualism (LaSarre et al. 2020; Lewin et al. 2019; Morin, Pierce, and Dutton 2018; Pierce et al. 2020). Rather than relying on inferring interactions from net outcomes such as changes in growth during co-culture, mutant screening techniques enable a more mechanistic understanding of intermicrobial interactions. Recently, droplet microfluidics has been combined with transposon mutant sequencing, enabling detection of fitness impacts related to public goods by separating individual mutants into their own compartments. Using this technology, the authors were able to observe interactions between *Streptococcus pneumoniae* strains (Thibault et al. 2019).

Conclusion

There are many open questions related to the types of interactions that occur within microbiomes. As seen in a number of the studies discussed above, these questions have led to increasing interest in the development of model microbial communities for the study of interaction mechanisms (Enke et al. 2018; B. L. Hansen et al. 2020; Lozano, Bravo, et al. 2019; May et al. 2019; Morin, Pierce, and Dutton 2018; Zengler et al. 2019). Although bacteria have received a lot of attention in intermicrobial dynamics, fungi play important roles in many systems and should be incorporated into model communities when relevant. The further development of model microbiomes that enable controlled experiments in more realistic contexts is a promising avenue for advancing this field.

Here, we have reviewed some of the most recent literature on microbial interaction mechanisms. Notably, many of these mechanisms are found across multiple systems, suggesting that findings in one microbiome can provide insights into other systems. Further study on translatability of mechanistic findings to other microbiomes and more intentional cross-system comparisons will undoubtedly be key to our ability to define fundamental principles of microbiome assembly and function.

Figure

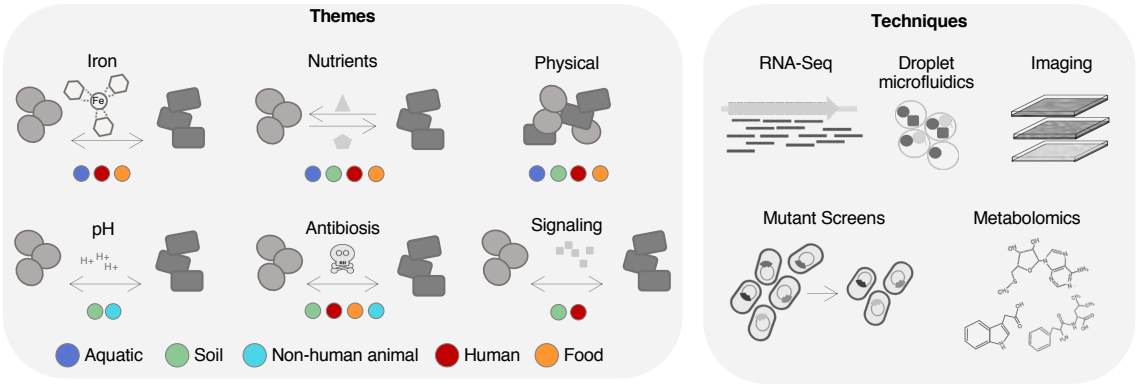

Figure 1.1-1. Recent Work on Intermicrobial Interaction Mechanisms. Left, Mechanistic themes found in intermicrobial interactions and microbiomes in which these mechanisms have recently been described. **Right,** Emerging techniques for studying intermicrobial interaction mechanisms.

1.2 Acknowledgments

Chapter 1 consists of material from a manuscript in preparation for publication. The manuscript in preparation is: Pierce, EC and Dutton, RJ. Identifying molecular mechanisms of species interactions within communities. (In preparation for *Current Opinion in Microbiology*). The dissertation author is the primary author of this manuscript in preparation.

CHAPTER 2: Characterization of Interactions in a 3-Member Microbiome

2.1 Chapter Summary

Initial studies on the development of cheese rind microbiomes showed that microbial interactions were widespread (Wolfe et al. 2014). However, the only readout of these interactions was a net growth impact observed during co-culture. In order to understand the underlying genetic basis of these interactions, we wanted to use a newly available technology, RB-TnSeq, to capture information on what genes impact bacterial fitness in cheese rind communities. This was the topic of a paper published in *eLife* on which I was second author, which is provided in this chapter in Section 2.2**.**

In this paper, we chose to work with a simple three-member community made up of *Hafnia alvei* str. JB232 (cheese bacterium), *Geotrichum candidum* str. GEO13 (cheese yeast), and *Penicillium camemberti* SAM3 (cheese mold). These species are the main members of Brie cheese rind communities. For RB-TnSeq assays, we grew a pooled library of barcoded *E. coli* or *P. psychrophila* str. JB418 (cheese bacterium) transposon mutants alone, in pairwise combinations with the Brie community species, or with all three Brie community members. For this work, I created and characterized the *P. psychrophila* str. JB418 transposon mutant library that was used in this work, performed the *P. psychrophila* RB-TnSeq experiments in the Brie community, and contributed to data analysis and writing of the manuscript. The *P. psychrophila* library contains 143,491 mutants with barcoded transposons centrally inserted in protein-coding genes.

Using RB-TnSeq assays, we were able to determine the impact of each community member on the fitness of individual mutants in the bacterial libraries and were able to determine

how these impacts changed when the full community was present. Analysis of community member impacts on bacteria allowed us to identify a few key functions related to microbial interactions, which included cross-feeding of amino acids between species and competition for iron and nitrogen. While half of the interactions were maintained from pairwise interactions in the full community, half were not, suggesting that a different network of interactions may emerge with increasing community complexity.

2.2 Interactions in the Brie Rind Model Community

eLIFE elifesciences.org

RESEARCH ARTICLE

Changes in the genetic requirements for microbial interactions with increasing community complexity

Manon Morin[1], Emily C Pierce[1], Rachel J Dutton[1,2]*

[1]Division of Biological Sciences, University of California, San Diego, La Jolla, United States; [2]Center for Microbiome Innovation, Jacobs School of Engineering, University of California San Diego, La Jolla, United States

Abstract Microbial community structure and function rely on complex interactions whose underlying molecular mechanisms are poorly understood. To investigate these interactions in a simple microbiome, we introduced *E. coli* into an experimental community based on a cheese rind and identified the differences in *E. coli*'s genetic requirements for growth in interactive and non-interactive contexts using Random Barcode Transposon Sequencing (RB-TnSeq) and RNASeq. Genetic requirements varied among pairwise growth conditions and between pairwise and community conditions. Our analysis points to mechanisms by which growth conditions change as a result of increasing community complexity and suggests that growth within a community relies on a combination of pairwise and higher-order interactions. Our work provides a framework for using the model organism *E. coli* as a readout to investigate microbial interactions regardless of the genetic tractability of members of the studied ecosystem.
DOI: https://doi.org/10.7554/eLife.37072.001

***For correspondence:** rjdutton@ucsd.edu

Competing interests: The authors declare that no competing interests exist.

Funding: See page 23

Received: 28 March 2018
Accepted: 09 September 2018
Published: 13 September 2018

Introduction

Microorganisms rarely grow as single isolated species but rather as part of diverse microbial communities. In these communities, bacteria, archaea, protists, viruses and fungi can coexist and perform complex functions impacting biogeochemical cycles and human health (***Falkowski et al., 2008***; ***Flint et al., 2012***). Deciphering microbial growth principles within a community is challenging due to the intricate interactions between microorganisms, and between microorganisms and their environment. While interest in microbial communities has dramatically increased, our understanding of microbial interactions within communities is lagging significantly behind our ability to describe the composition of a given community.

Approaches relying on 16S rDNA sequencing analyses of microbial communities can be used to reconstruct ecosystem networks and detect patterns of co-occurrence to infer general interactions such as competition, mutualism and commensalism (***Faust and Raes, 2012***). However, the molecular mechanisms underlying these interactions remain largely uncharacterized. Further, the way in which these interactions are organized within a community, such as whether they consist of predominantly pairwise or higher-order interactions, is even less clear. A more precise understanding of microbial interactions, their underlying mechanisms, and how these interactions are structured within a community, are all necessary to elucidate the principles by which a community is shaped. In this study, we combine genome-scale genetic and transcriptomic approaches within an experimentally tractable model microbial community to begin to address these questions.

Genome-scale approaches, such as transposon mutagenesis coupled to next-generation sequencing (TnSeq approaches) have been successfully used to quantify the contribution and thus the importance of individual genes to a given phenotype (***van Opijnen and Camilli, 2013***). These techniques

eLife digest Microorganisms live almost everywhere on Earth. Whether it is rainforest soil or human skin, each environment hosts a unique community of microbes, referred to as its microbiome. There can be upwards of hundreds of species in a single microbiome, and these species can interact in a variety of ways; some cooperate, others compete, and some can kill other species. Deciphering the nature of these interactions is crucial to knowing how microbiomes work, and how they might be manipulated, for example, to improve human health. Yet studies into these interactions have proven difficult, not least because most of the species involved are difficult to grow in controlled experiments.

One environment that is home to a rich community of microbes is the outer surface of cheese, known as the cheese rind. The cheese rind microbiome is a useful system for laboratory experiments, because it is relatively easy to replicate and its microbes can be grown on their own or in combinations with others.

To explore the nature of interactions in microbiomes, Morin et al. have now grown a large collection of *E. coli* mutants as members of simplified microbiomes based on the cheese rind. The mutant bacteria were grown on cheese either alone, paired with one other species, or alongside a community of three species. The aim was to see which mutants grew poorly when other species were present, thus allowing Morin et al. to identify specific genes that are important for interactions within the experimental microbiomes.

Even in these simplified microbiomes, the microbes interacted in a variety of ways. Some microbes competed with *E. coli* for elements like iron and nitrogen; others cooperated by sharing the building blocks needed to make larger molecules. Many of the interactions that happened when *E. coli* was paired with one species were not seen when more species were added to the community. Similarly, some interactions were only seen when *E. coli* was grown alongside a community of microbes, and not when it was paired with any of the three species on their own.

These findings show that complex interactions are present even in a simplified microbiome. This experimental approach can now be applied to other microbiomes that can be grown in the laboratory to examine whether the patterns of interactions seen are generalizable or specific to the cheese rind system.

DOI: https://doi.org/10.7554/eLife.37072.002

use a pooled library of transposon insertion mutants whose frequency is measured to identify genes important for growth in a given condition. Recently, the generation and introduction of unique random barcodes into transposon mutant libraries made this approach more high-throughput, enabling screens of important genes across hundreds of conditions and for numerous genetically tractable microorganisms (***Wetmore et al., 2015***; ***Price et al., 2018***).

To investigate the genetic basis of microbial interactions, we have adapted this approach to identify and compare genetic requirements in single-species (non-interactive) and multi-species (interactive) conditions. We used a large and diverse transposon library previously generated in the genetically-tractable model bacterium *E. coli* K12 (***Wetmore et al., 2015***) to characterize the genetic requirements of interactions within a model community based on the rind of cheese (***Wolfe et al., 2014***). The fact that the *E. coli* genome has undergone extensive characterization can help more effectively interpret the genetic requirements introduced by growth within communities. Although *E. coli* K12 is not a typical endogenous species of this particular microbiome, non-pathogenic *E. coli* strains can be found in raw milk and raw-milk cheese (***Trmčić et al., 2016***). Shiga-toxin-producing *E. coli* 0157:H7 and non-0157 pathogenic *E. coli* species are common invaders of the cheese environment and can survive during cheese making causing mild to life-threatening symptoms after ingestion (***Coia et al., 2001***; ***Montet et al., 2009***; ***Frank et al., 1977***).

Using the *E. coli* transposon library, we (i) identified the set of genes important for growth alone in the cheese environment, (ii) identified the set of genes important for growth in pairwise conditions with each individual community member and (iii) identified the set of genes important for growth in the presence of the complete community. Characterization of the functions or pathways associated with growth in interactive versus non-interactive conditions were then used to infer the biological

processes involved in interactions within the model microbiome. Additionally, we compared the set of genes important for growth in pairwise conditions with the ones important for growth in a community to investigate how microbial interactions change depending on the complexity of the interactive context. We also performed a similar RB-TnSeq analysis during non-interactive and interactive conditions using a transposon library we generated in the cheese-endogenous species *Pseudomonas psychrophila* JB418. Finally, we measured changes in the transcriptional profile of *E. coli* during growth alone, growth in pairwise conditions, and within the community using RNAseq as a complementary approach to RB-TnSeq in defining microbial interactions. This analysis revealed a deep reorganization of gene expression whenever *E. coli* is in the presence of other species.

This work revealed numerous interactions between species, such as metabolic competition for iron and nitrogen, as well as cross-feeding from fungal partners for certain amino acids. Our analysis showed that most of the metabolic interactions (competition and cross-feeding) observed in pairwise conditions are maintained and amplified by the addition of all partners in the community context. However, around half of the genetic requirements observed in pairwise conditions were no longer apparent in the community, suggesting that higher-order interactions emerge in a community.

Results

Identification of the basic genetic requirements for growth of *E. coli* in isolation

We used the *E. coli* Keio_ML9 RB-TnSeq library from ***Wetmore et al., 2015***, containing a pool of 152,018 different insertion mutants (with a median of 16 insertion mutants per gene; covering 3728 of 4146 protein-coding genes), each associated with a unique 20 nucleotide barcode. This library was originally generated in and maintained on lysogeny broth medium (LB) and was used previously to identify genes required for growth across a variety of conditions (***Wetmore et al., 2015***; ***Price et al., 2018***). To determine genes important for growth on our cheese-based medium, we grew the pooled library by itself on sterile cheese curd agar plates (CCA: 10% freeze-dried fresh cheese, 3% NaCl, 0.5% xanthan gum, 1.7% agar), the same medium used in all further experiments and used previously to demonstrate that cheese communities could be successfully reconstructed *in vitro* (***Wolfe et al., 2014***). As the library is composed of multiple insertion mutants for a gene, we expect the individual insertion mutants to be evenly distributed in the experimental environment, minimizing the effect on any individual insertion mutant due to stochastic processes such as genetic drift or localized effects related to spatial structure (***Hallatschek et al., 2007***). During growth, we expect the library to modify the environment by taking up nutrients and excreting molecules (waste products, enzymes, etc). Consequently, we expect that some genetic requirements will change during growth. Thus, to provide a comprehensive overview of the genetic requirements for growth, we grew the pooled library on CCA and collected samples after 1, 2 and 3 days. For each time point, we harvested the library from the surface of the cheese plate, extracted genomic DNA, used PCR to amplify the barcoded regions of the transposons, and then sequenced these products to measure the abundance (*i.e.* the number of sequencing reads associated with each barcode) of each transposon mutant over time (see Materials and Methods).

The fitness of each insertion mutant was calculated as the $\log_2$ of the ratio of its abundance at a given timepoint compared to its abundance at T0 (the inoculum). We calculated the raw fitness of a gene as the weighted average of the fitness of all insertion mutants of that gene. Gene fitness values were then normalized. First, fitness values are corrected to account for changes in copy number along the chromosome as insertions near the replication fork are expected to have higher copies in dividing cells. Then, fitness values were normalized based on the assumption that disruption of most of the genes leads to little or no fitness effect (see Materials and Methods and (***Wetmore et al., 2015***) for details). Consequently, most of the fitness values are expected to be close to 0, indicating that disruption of these genes leads to no particular growth modification compared to the rest of the library. Negative gene fitness values, however, identify mutants that are growing slower than the rest of the library and therefore, genes that are of particular importance for growth in the studied condition. A t-score, calculated as a moderated t-statistic, is determined for each gene fitness value to assess if the fitness value is reliably different from 0 (see Materials and Methods and

(**Wetmore et al., 2015**) for details). The RB-TnSeq pipeline from experimental set-up to gene fitness calculation is summarized in **Figure 1—figure supplement 1**.

At each timepoint, we were able to calculate the fitness and a corresponding t-score for 3298 protein-coding genes (**Figure 1A**, **Figure 1—source data 1**). Because we were interested in genes with a strong fitness defect (significant negative fitness values), we first removed genes with an absolute t-score <= 3. This t-score threshold was set to identify strong negative fitness values while minimizing potential false positives (false discovery rate of 0.2%). The t-score assesses how reliably a fitness value is different from 0. In each condition, most genes have no detectable fitness effect, and thus have a fitness value close to 0. Thus, in our dataset, most of the genes below this t-score also have a fitness value close to 0. On average, 97% of the fitness values were associated with a t-score that falls below our threshold. Within the fitness values that pass the t-score threshold, we then removed genes associated with positive fitness values. Thus, we only retained the genes whose deletion leads to a consistent growth defect for *E. coli* on CCA compared to the rest of the library. This filtering process revealed 160 genes that were important for *E. coli* growth alone on CCA (**Figure 1A**).

To identify the functions associated with these 160 genes, we mapped them to the KEGG BRITE database (**Figure 1B**). 84 genes were assigned to KEGG modules and 64 of them were associated with *E. coli* metabolism. Within these metabolic genes, we found 28 genes associated with amino acid metabolism, specifically the biosynthesis of all amino acids except for proline, lysine and histidine. Quantification of free amino acids in our medium highlighted very low concentrations of all amino acids (**Figure 1—figure supplement 2**) suggesting that a limited supply of free amino acids leads to a genetic requirement for amino acid biosynthesis. This is supported by the observation that both *spoT* and *relA*, regulators of the stringent response which can be triggered by amino acid starvation (**Cashel et al., 1996**), are also associated with a negative fitness value. Additionally, we observed the importance of the regulator *gcvR*, that inhibits catabolism of glycine into C1 metabolism. In fact, GcvR inhibits the glycine cleavage complex, a multienzyme complex that oxidizes glycine (**Ghrist and Stauffer, 1995**; **Ghrist et al., 2001**). Furthermore, mutants of the glycine cleavage complex displayed a significant positive fitness, suggesting that absence of glycine utilization through C1 metabolism is beneficial in our amino acid-deficient environment. Altogether, this observation also underlines that amino acids are limiting in the environment and that their biosynthesis and utilization control is important for growth. 19 of the 160 genes were associated with energy metabolism and, more specifically, with sulfur assimilation (n = 7 genes) and respiration (n = 8 genes). Here, we deduce that importance of sulfur assimilation is directly caused by the lack of the amino acids cysteine and methionine, which are the major pools of sulfur-containing compounds in the cell. As a non-endogenous species, *E. coli* might not possess the adequate peptidases or proteases to degrade and use the highly available protein casein. Identification of two of the three genes of the Leloir pathway (*galE* and *galT*), involved in the uptake and conversion of galactose into glucose, suggests that galactose might be a crucial nutrient for *E. coli* growth on CCA.

Eight genes mapped to membrane transport and were associated with two specific pathways: ferric-enterobactin transport and glycine-betaine transport. Ferric-enterobactin transport allows the cells to scavenge iron in a low-iron environment (**Raymond et al., 2003**; **Hider and Kong, 2010**). Iron is an essential micronutrient and cheese is known to be iron-limited (**Albar et al., 2014**). Glycine betaine is used by cells as an osmoprotectant in high osmolarity environments. During cheese curd processing, high concentrations of NaCl are added (**Guinee, 2004**), and our CCA medium contains 3% NaCl to mimic these conditions. The importance for *E. coli* to maintain its cell osmolarity is also suggested by the requirement of genes responsible for the transport of the ions sodium, potassium and zinc.

In our experiment, the fact that all of the mutants are pooled together limits our ability to identify genes whose phenotypes can be complemented by common goods (molecules released in the environment) produced by neighboring cells. For example, given that iron is limiting in cheese, we expect that enterobactin biosynthesis is an important pathway for growth in this environment. However, no genes from the enterobactin biosynthesis pathway (*entCEBAH*, *entD* and *entF*) had a significant negative fitness value (average fitness of the enterobactin biosynthesis pathway: 0.1), while individual growth of these enterobactin biosynthesis mutants from the KEIO collection was limited on CCA compared to a rich, non-iron-limited medium (**Figure 1—figure supplement 3**).

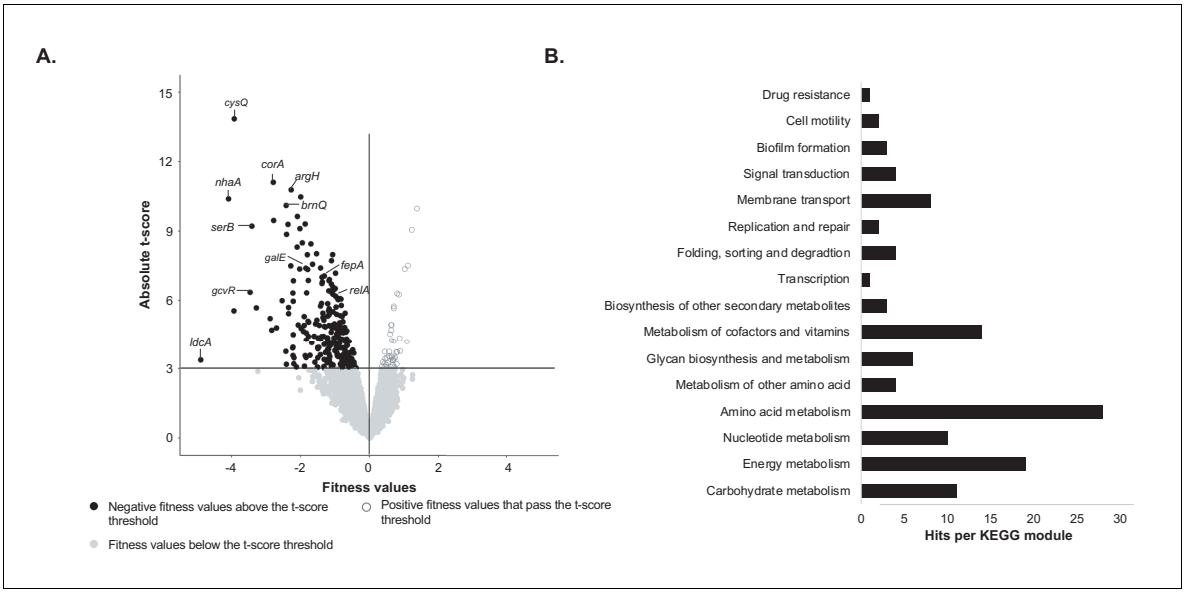

Figure 1. Identification of genes important for growth of *E. coli* alone on cheese curd agar (***Figure 1—source data 1***). (**A**) The pooled *E. coli* RB-TnSeq library Keio_ML9 (***Wetmore et al., 2015***) was grown alone on cheese curd agar (CCA). Gene fitness values were calculated for 3298 genes at days 1, 2, and 3 along with a t-score, which assesses how reliably the fitness value differs from 0. The fitness values obtained at the three timepoints are displayed on a single volcano plot (3 points per gene). A t-score threshold of absolute(t-score)≥3 was used to identify genes with strong fitness effects. 97% of the genes fell below this threshold and have no strong and significant fitness effect. Black dots represent genes with strong negative fitness effects. Altogether, they represent 160 different genes that are associated with a significant fitness value for at least one timepoint. (**B**) These 160 genes were mapped to the KEGG BRITE Database for functional analysis and identification of required functions for *E. coli* growth on CCA. 84 of the 160 genes had hits when mapped to the KEGG BRITE database.

DOI: https://doi.org/10.7554/eLife.37072.003

The following source data and figure supplements are available for figure 1:

Source data 1. RB-TnSeq analysis of *E. coli's* growth alone on 10% cheese curd agar, pH7.

DOI: https://doi.org/10.7554/eLife.37072.012

Figure supplement 1. Pipeline of RB-TnSeq experiment using the *E. coli* Keio M9 library: from experimental set-up to normalized gene fitness and t-score calculation.

DOI: https://doi.org/10.7554/eLife.37072.004

Figure supplement 2. Quantification of free amino acids in CCA.

DOI: https://doi.org/10.7554/eLife.37072.005

Figure supplement 3. Comparison of individual growth of enterobactin biosynthesis mutants on LB and CCA.

DOI: https://doi.org/10.7554/eLife.37072.006

Figure supplement 4. RB-TnSeq experiments using the P. psychrophila JB418 library.

DOI: https://doi.org/10.7554/eLife.37072.007

Figure supplement 4—source data 1. RB-TnSeq analysis of *P. psychrophila's* growth alone, in pairwise conditions and with the community on 10% cheese curd agar, pH7.

DOI: https://doi.org/10.7554/eLife.37072.008

Figure supplement 5. Competitive assays of 25 mutants of the Keio collection (***Baba et al., 2006***).

DOI: https://doi.org/10.7554/eLife.37072.009

Figure supplement 6. Map of the JB418_ECP1 transposon library generated in *P. psychrophila* JB418.

DOI: https://doi.org/10.7554/eLife.37072.010

Figure supplement 7. Quality assessment of all RB-TnSeq experiments.

DOI: https://doi.org/10.7554/eLife.37072.011

In summary, functions of major importance for *E. coli* to grow alone in our experimental environment involved (i) response to low iron availability, (ii) response to osmotic stress and (iii) response to limited available nutrients (specifically free amino acids). These required functions are consistent with recently published results on the requirements of the mammary pathogenic *E. coli* (MPEC) during growth in milk (***Olson et al., 2018***) except for resistance to osmotic stress which does not occur in milk. We also generated an RB-TnSeq library in the bloomy rind cheese endogenous species *P. psychrophila* JB418 and found comparable requirements for growth alone on cheese (***Figure 1—figure supplement 4***).

To validate the results obtained with the RB-TnSeq library, we measured the fitness of individual knockout mutants from the *E. coli* Keio collection (***Baba et al., 2006***). We tested 25 knockout mutants corresponding to genes with a strong growth defect observed after one day of growth. We carried out competitive assays between each knockout mutant and the wild-type strain on CCA. We calculated each knockout mutant fitness as the log2 of the fold change of its abundance after one day of growth. A z-score was also calculated to assess the confidence of that fitness. 21 of 25 knockout mutants displayed a fitness value lower than 0 with at least 95% confidence (***Figure 1—figure supplement 5***). The remaining four mutant strains (*brnQ*, *cysK*, *serA* and *trxA*) were associated with high fitness value variability across replicate experiments and had a lower z-score. Altogether, this supports the reliability and validity of RB-TnSeq results.

Identification of *E. coli* genetic requirements for growth in pairwise conditions

The growth of the *E. coli* library alone allowed us to determine the baseline set of genes required for optimal growth in the model cheese environment. We next wanted to identify genes with negative fitness during growth when another species is present. First, we analyzed the growth of *E. coli* and the partner species. We grew *E. coli* for 3 days on CCA in the presence of either *H. alvei*, *G. candidum* or *P. camemberti*. In addition to belonging to distinct domains or phyla, these three partners are the typical members of a bloomy rind cheese community (such as Brie or Camembert). The presence of *E. coli* did not influence the growth of any partner species (***Figure 2—figure supplement 1***). However, *E. coli*'s growth was reduced in the presence of each partner after three days of growth (***Figure 2A***).

We then determined the genes associated with negative fitness during *E. coli* growth in each pairwise condition using RB-TnSeq (*i.e.* genes whose fitness value is negative and associated with an absolute t-score greater than three in the pairwise condition) (***Figure 2B***, ***Figure 2—source data 1***). As performed above, barcode frequencies were compared between T0 and after growth with each partner (at days 1, 2 and 3). As our goal is to compare genetic requirements for growth in interactive and non-interactive conditions rather than to examine changes in requirements over time, we grouped genes with a significant negative fitness for at least one timepoint as a single set of genes for each pairwise condition. We identified 145 genes with negative fitness values in *E. coli* for growth with *H. alvei*, 142 genes for growth with *G. candidum* and 131 genes for growth with *P. camemberti*. Altogether they constitute a set of 153 genes that are required for optimal growth in at least one pairwise culture.

Comparison of genes with negative fitness identified when *E. coli* is grown alone with the genes identified when *E. coli* is grown in pairwise conditions is expected to highlight differences brought about by the presence of another species (***Figure 2C***). Consistent presence of multiple genes of the same pathway within only one of these sets of genes associated with negative fitness is likely to point out a pathway specifically important in one condition. Thus, we can infer possible interactions based on the different relevant pathways between interactive and non-interactive growth conditions. Altogether, the 153 genes with a negative fitness in pairwise conditions and the 160 genes for *E. coli* growth alone represent 235 unique genes (***Figure 2C***). These can be divided into three groups of genes: (i) conserved negative fitness: genes with negative fitness in both growth alone and in all pairwise conditions (n = 78), (ii) pairwise-alleviated negative fitness: any gene found to have a negative fitness during *E. coli* growth alone that was not associated with a negative fitness in at least one of the three pairwise cultures (n = 82), and (iii) pairwise-induced negative fitness: any gene with negative fitness in the presence of at least one of the partners but not associated with a negative fitness during growth alone (n = 75) (***Figure 2C and D*** and ***Figure 2—figure supplement 2***). We further

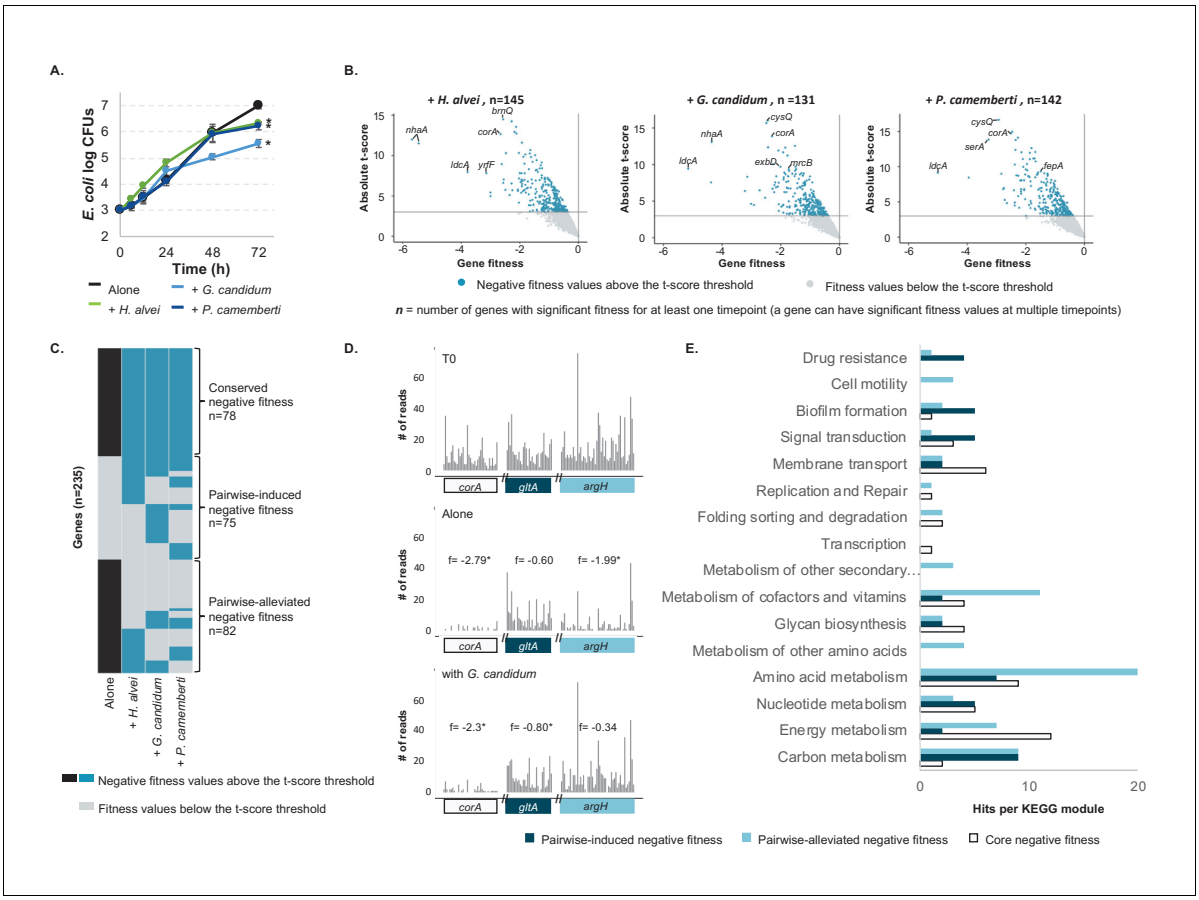

Figure 2. *E. coli* genes with negative fitness during growth in pairwise conditions (***Figure 2—source data 1***). (**A**) We grew *E. coli* in pairwise conditions on CCA with either *H. alvei*, *G. candidum* or *P. camemberti*. Asterisks indicate significant differences in growth of *E. coli* as compared to growth alone at day 3 (Dunnett's test, adjusted p-value≤5%) (**B**) Using the *E. coli* RB-TnSeq library, we identified genes with negative fitness in each pairwise condition at three timepoints (days 1, 2, 3). Each volcano plot shows fitness values of all 3298 genes at all timepoints (three points per gene). We identified 145 genes with a negative fitness in the presence of *H. alvei* in at least one timepoint, 131 genes in pairwise culture with *G. candidum* and 142 genes in pairwise culture with *P. camemberti*. Altogether, they constitute 153 genes with negative fitness in pairwise conditions. (**C**) Comparing these genes (dark blue) to the 160 genes with a negative fitness during *E. coli* growth alone (black), we obtained a total of 235 unique genes and identified 78 genes that have a negative fitness both during growth alone and all pairwise conditions (conserved negative fitness), 75 genes that have a negative fitness in at least one pairwise condition but not alone (pairwise-induced negative fitness) and 82 genes with a negative fitness in growth alone but not in at least one pairwise condition (pairwise-alleviated negative fitness). (**D**) We selected a gene to illustrate conserved negative fitness (*corA*, 37 insertion mutants), pairwise-induced negative fitness (*lpoB*, 31 insertion mutants), and to illustrate pairwise-alleviated negative fitness (*argH*, 50 insertion mutants). For each gene, we display the number of sequencing reads for associated insertion mutants in the T0 sample, in growth alone day 3 and growth with *G. candidum* day 3. These sequencing reads are the raw data accounting for mutant abundance and used for fitness calculation (f represents each gene's fitness value). While reads are not rarefied in the fitness calculation pipeline, we used rarefied reads for the purpose of the figure. Asterisks indicate genes with significant fitness values (consistent decrease in the number of reads per insertion mutant in the condition compared to T0). (**E**) We mapped the genes associated with conserved, pairwise-induced, and pairwise-alleviated negative fitness to the KEGG BRITE database. 41/75, 45/82 and 33/77 genes had hits.

DOI: https://doi.org/10.7554/eLife.37072.013

The following source data and figure supplements are available for figure 2:

Source data 1. RB-TnSeq analysis of *E. coli*'s growth in pairwise conditions on 10% cheese curd agar, pH7.

DOI: https://doi.org/10.7554/eLife.37072.016

Figure supplement 1. *E. coli* and community member growth curves alone, in pairwise conditions or during community growth.

Figure 2 continued on next page

Figure 2 continued

DOI: https://doi.org/10.7554/eLife.37072.014

Figure supplement 2. Comparison of the genes important for *E. coli* growth alone, in each pairwise condition or with the community.

DOI: https://doi.org/10.7554/eLife.37072.015

focused on the pairwise-alleviated and pairwise-induced negative fitness as these groups contain genes potentially related to interactions.

Genes whose negative fitness is alleviated by pairwise growth can highlight processes that are of importance for growth alone but no longer important because of the presence of a partner, thus suggesting interactions between *E. coli* and the partner. Just over half of the genes with negative fitness alone appeared to be relieved by the presence of a partner (n = 82 genes, ***Figure 2C***), suggesting major modifications of growth conditions following the introduction of a partner. We mapped these 82 alleviated genes to the KEGG BRITE database to identify functions and pathways that are no longer critical in the presence of a partner (***Figure 2E***). 16 genes were associated with unknown or predicted proteins and did not map to any field of the database. Of the remaining genes, 45 mapped to modules of the KEGG orthology hierarchy.

Most of the genes with alleviated negative fitness were associated with the KEGG metabolism module and are thus part of metabolic pathways. It is especially evident that pairwise growth leads to major changes in the need for amino acid biosynthesis. For example, 6 out of the 8 genes of valine and isoleucine biosynthetic pathways are no longer associated with a negative fitness during pairwise growth (***Figure 3C***). In addition, 2 genes of arginine biosynthesis, 2 genes of methionine biosynthesis as well as final steps of homoserine, aspartate and glutamate biosynthesis are no longer required. Moreover, *ilvY*, the transcriptional activator of valine and isoleucine biosynthesis was also among the genes no longer required for pairwise growth. Here, the dominant presence of amino acid biosynthesis genes in the alleviated functions suggests cross-feeding of the pathway end-products or intermediates which are either provided directly by the partner species or made more available in the environment as a consequence of the partner's metabolic activity. Thus, our data suggest that pairwise growth may allow cross-feeding of the amino acids valine, isoleucine, arginine, methionine, homoserine, aspartate and glutamate. Isoleucine and methionine are also intermediates of cofactor biosynthesis, and genes associated with their biosynthesis were also mapped to metabolism of cofactors and vitamins.

To understand if the genes with pairwise-alleviated negative fitness were related to a specific partner, we investigated how each partner contributed to this gene set (***Figure 2—figure supplement 2***). Of the 82 total genes, 36 were alleviated in all pairwise conditions, suggesting that any partner leads to the compensation of these requirements. They included genes associated with amino acid metabolism specific to homoserine and methionine biosynthesis. Of the remaining genes, eight were specifically not required in the presence of *H. alvei*, nine were specifically not required in the presence of *G. candidum* and nine were specifically not required in the presence of *P. camemberti*. Alleviation of leucine and valine biosynthesis was observed with both fungal partners, while biosynthesis of arginine appeared to be no longer required specifically in the presence of *G. candidum*. Fungal species are known to secrete proteases that digest small peptides and proteins (***Kastman et al., 2016***; ***Boutrou et al., 2006b***; ***Boutrou et al., 2006a***) and may lead to increased availability of amino acids in the environment.

We then analyzed the 74 genes with pairwise-induced negative fitness in order to identify functions or pathways that become important in the presence of a partner (***Figure 2E***). These genes represent almost half (75 out of 153 – ***Figure 2C***) of the genes with negative fitness in pairwise conditions, suggesting that presence of a partner introduces new selection pressures. 33 genes mapped to KEGG orthology terms. Among this gene set are pathways associated with signal transduction, biofilm formation and drug resistance. They were related to three major responses: metabolic switch (*creB*: carbon source responsive response regulator), response to stress and toxic compounds (*cpxA*: sensory histidine kinase, *oxyR*: oxidative stress regulator, *acrAB*: multidrug efflux) and biofilm formation (*rcsC* and *rcsB*: regulator of capsular synthesis, *pgaC*: poly-*N*-acetyl-D-glucosamine synthase subunit). Biofilms are microbial structures known to provide resistance to different stresses, including resistance to antibiotics, and biofilm-inducing genes can be activated in the presence of stress events (***Landini, 2009***). The transcriptional regulator OxyR and the transduction

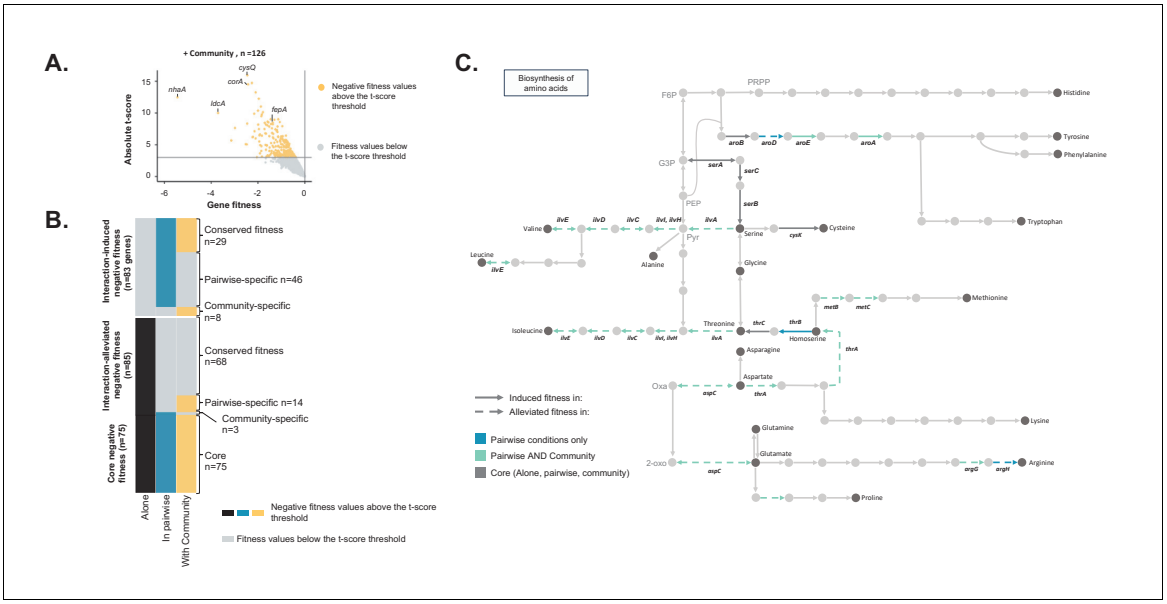

Figure 3. Comparison of *E. coli* genes with negative fitness within the community and in pairwise conditions (***Figure 3—source data 1***). (**A**) Using the *E. coli* RB-TnSeq library, we identified genes required to grow with the community (*H. alvei* + G. candidum + *P. camemberti*). During growth with the community, we identified a total of 126 genes with a negative fitness. (**B**) We compared the pairwise-induced and community-induced genes (Interaction-induced genes) as well as the pairwise-alleviated and community-alleviated genes (Interaction-alleviated genes) to identify conservation of interactions from pairwise to community and emergence of higher-order interactions. (**C**) Within the alleviated negative fitness, genes associated with numerous amino acid biosynthetic pathways were identified. F6P: fructose-6-phosphate, PRPP: 5-phospho-ribose-1-di-phosphate, G3P: Glyceraldehyde-3-phosphate, PEP: phosphoenol-pyruvate, Pyr: Pyruvate, Oxa: Oxaloacetate, 2-oxo: 2-oxoglutarate.

DOI: https://doi.org/10.7554/eLife.37072.017

The following source data is available for figure 3:

Source data 1. RB-TnSeq analysis of *E. coli*'s growth with the community on 10% cheese curd agar, pH7.

DOI: https://doi.org/10.7554/eLife.37072.018

system CpxA and CpxB are known coordinators of stress response and biofilm formation (***Gambino and Cappitelli, 2016***; ***Dorel et al., 2006***). While these genes represent only a small subset of the pairwise-induced gene set, they could suggest that partner species are producing toxic compounds or oxidative stress-inducing compounds.

We again investigated if these responses were partner-specific (***Figure 2—figure supplement 2***). Of the 74 pairwise-induced negative fitness, 11 were found to have a negative fitness in the presence of all partners, 13 were specific to the presence of *H. alvei*, 24 were specific to the presence of *G. candidum* and 11 were specific to the presence of *P. camemberti*. Despite involving different genes, necessity of biofilm formation and response to toxic stress were associated with the presence of all partners.

Finally, functional analysis of the conserved genes with negative fitness highlighted that functions associated with membrane transport, including resistance to high osmolarity and iron transport as well as functions associated with energy metabolism and aromatic amino acid biosynthesis were still important to grow in the presence of a partner (***Figure 2E***).

We performed similar pairwise assays using the RB-TnSeq library of *P. psychrophila* JB418 with *H. alvei*, *G. candidum* or *P. camemberti*. We identified a similar number of genes associated with pairwise-alleviated and pairwise-induced requirements (***Figure 1—figure supplement 4***) as we did when using the *E. coli* library. As with *E. coli*, we can infer production of toxic stress by the partners as

genes associated to DNA repair were identified with a negative fitness in pairwise conditions in the functional analysis. However, cross-feeding by fungal partners was not as striking as for *E. coli*.

Identification of *E. coli* genetic requirements for growth within the community and comparison to pairwise conditions

We next aimed to investigate the differences between genes with a negative fitness during growth in a community (complex interactive condition) and genes with a negative fitness during growth in associated pairwise conditions (simple interactive conditions) (***Figure 2—figure supplement 2***). We grew the *E. coli* library with the complete community composed of *H. alvei*, *G. candidum* and *P. camemberti* and we identified 126 genes with a reliable negative fitness (***Figure 3A***, ***Figure 3—source data 1***). *E. coli's* final biomass was more reduced by the presence of the community than by a single partner. However, the growth of each community member remained unaffected (***Figure 2—figure supplement 1***).

We first identified community-induced and community-alleviated genes by comparing the genes with a negative fitness in the community with the genes with a negative fitness during growth alone. We identified 89 genes that had negative fitness for both community and alone (conserved negative fitness), 37 genes with negative fitness only with the community (community-induced negative fitness) and 71 genes with negative fitness only for growth alone (community-alleviated negative fitness). As with a single partner, the presence of a complex community potentially relieves some fitness effects while introducing new ones.

Comparing community-induced and pairwise-induced genes can reveal if and how community complexity modifies the genes that are important in different interactive contexts compared to growth alone (***Figure 3B*** – Interaction-induced negative fitness). We identified 29 genes with a negative fitness in both pairwise and community growth compared to growth alone (conserved interaction-induced negative fitness). These include genes associated with oxidative stress and biofilm formation. These genes are likely to be associated with pairwise interactions which are maintained in a community context.

Meanwhile, eight genes appeared to be specifically associated with negative fitness in the presence of the community (***Figure 3B***, community-specific induced genes), highlighting higher-order interactions that emerge from a higher level of complexity in the community composition. Interestingly, these genes represent only a small fraction (22%) of the community-induced requirements, suggesting that most of the negative fitness effects observed in the community are derived from pairwise interactions.

Finally, we identified 46 genes that have a negative fitness in pairwise conditions, but not during growth alone or within the community (***Figure 3B***, pairwise-specific induced genes). These genes could be related to interactions that are either alleviated or counteracted in a community, either by the presence of a specific species or by the community as a whole. For example, some of the identified genes were associated with antimicrobial resistance, and, in a diverse community, other species could degrade the putative antimicrobial molecules or prevent the producing species from secreting it. Consequently, *E. coli* would be exposed to a lower level of antimicrobials, suppressing the necessity of a resistance gene. Thus, the complex pattern of requirements for these genes may reflect higher-order interactions.

We next investigated if the interactions related to pairwise-alleviated negative fitness and community-alleviated negative fitness were similar (***Figure 3B*** – Interaction-alleviated negative fitness). 68 genes were no longer associated with a negative fitness in both pairwise conditions and with the community compared to growth alone (conserved interaction-alleviated negative fitness). These genes may represent pairwise interactions maintained in the community context. Amino acid biosynthesis was highly represented within these genes and more specifically biosynthesis of valine, isoleucine, methionine, homoserine, aspartate and glutamate (***Figure 3C***). This suggests that, despite the presence of more species, these amino acids are still cross-fed.

We also identified 14 genes that no longer had a negative fitness in pairwise conditions compared to growth alone yet remained with a negative fitness in growth with the community (pairwise-specific alleviated negative fitness). These 14 genes represent a small fraction of the pairwise-alleviated, thus suggesting that most of interactions related to pairwise-alleviation are maintained in the community. Finally, only three genes were specifically alleviated in the community (community-specific alleviated fitness). This points out that presence of the full community does not lead to

emergence of specific alleviation of fitness effects but that most of the fitness effect alleviations observed in the community are conserved from pairwise interactions. In both cases, these 14 pairwise-specific and three community-specific alleviated genes could highlight existence of more higher-order interactions. However, too few genes are involved to determine the exact nature of these interactions.

Finally, we identified 75 genes with negative fitness in all conditions (core negative fitness). These genes encompass functions including iron uptake and response to high osmolarity. Overall, they are associated with response to environmental parameters that other species do not alleviate.

To summarize, the community-induced genes were mostly maintained from pairwise-induced genes. Similarly, the genes that were community-alleviated were highly similar to the pairwise-alleviated genes. However, we also observed emergence of higher-order interactions in the community condition as numerous interactions observed in pairwise conditions (n = 46 + 14) were not conserved in the community condition and specific interactions (n = 8 + 3) were observed in the community condition. Altogether, 58% of the interactions observed in the community were from pairwise interactions while 42% emerged from higher community complexity.

Again, we carried out similar experiments and analysis using the *P. psychrophila* JB418 RB-TnSeq library generated in our laboratory. The results were highly similar to the ones observed with *E. coli* in terms of number of genetic requirements alleviated in the presence of the community compared to growth alone as well as the number genes specifically important to grow with the community compared to growth alone (***Figure 1—figure supplement 4***). Finally, we consistently observed importance of higher-order interactions, 61% of the observed interactions in the community were conserved from pairwise interactions and 39% were higher-order interactions.

Differential expression analysis of *E. coli* in interactive conditions versus growth alone

So far, we used a genome-scale genetic approach to investigate potential microbial interactions. As a complementary strategy, we generated transcriptomic data for *E. coli* during growth in each previously described condition. Changes in transcriptional profiles can be a powerful indicator of an organism's response to an environment and have been used to identify *E. coli* pathways involved in interactions (***Croucher and Thomson, 2010***; ***McAdam et al., 2014***; ***Galia et al., 2017***).

To measure *E. coli* gene expression, we extracted and sequenced RNA from each timepoint and condition of the same samples used for RB-TnSeq above (after 1, 2 and 3 days of growth when grown alone, in pairwise conditions or with the community). Comparison of transcriptional profiles suggests a strong reorganization of *E. coli* gene expression in response to the presence of a partner (***Figure 4A***, ***Figure 4—source data 1*** and ***Figure 4—figure supplement 1***).

We first focused on the genes differentially expressed between growth in pairwise conditions and growth alone. We calculated the fold change of gene expression between pairwise growth and growth alone and identified differentially expressed genes by screening for adjusted p-values lower than 1% (Benjamini-Hochberg correction for multiple testing) and an absolute log2 of fold change (logFC) greater than 1. To remain consistent with the analysis performed for the genetic requirements, we pooled the data of all timepoints after identifying the upregulated or downregulated genes for each timepoint. We found a total of 966 upregulated and 977 downregulated genes across all partners (482 upregulated genes and 478 downregulated genes in presence of *H. alvei*, 633 upregulated genes and 719 downregulated genes in presence of *G. candidum*, 626 upregulated genes and 694 downregulated genes in presence of *P. camemberti*, ***Figure 4A***). Almost half of *E. coli*'s genome is subjected to expression modification, suggesting a global response to the presence of a partner. We further investigated if differential expression in pairwise conditions is partner-specific (***Figure 4—figure supplement 1***). Around half of *E. coli* gene expression regulation in the presence of a partner appears to be independent of which partner is present. Also, a number of genes were differentially expressed depending on the partner: 66 genes were specifically upregulated and 60 genes downregulated with *H. alvei*, 213 upregulated and 182 downregulated with *G. candidum*, and 183 upregulated and 161 downregulated with *P. camemberti*.

Due to the larger gene set compared to RB-TnSeq, we performed KEGG pathway enrichment analyses on the differentially expressed genes in pairwise conditions to determine upregulated functions and pathways (***Figure 4B***). First, almost all of the aminoacyl-tRNA-synthetases and functions associated with energy production were upregulated. Interestingly upregulation of energy

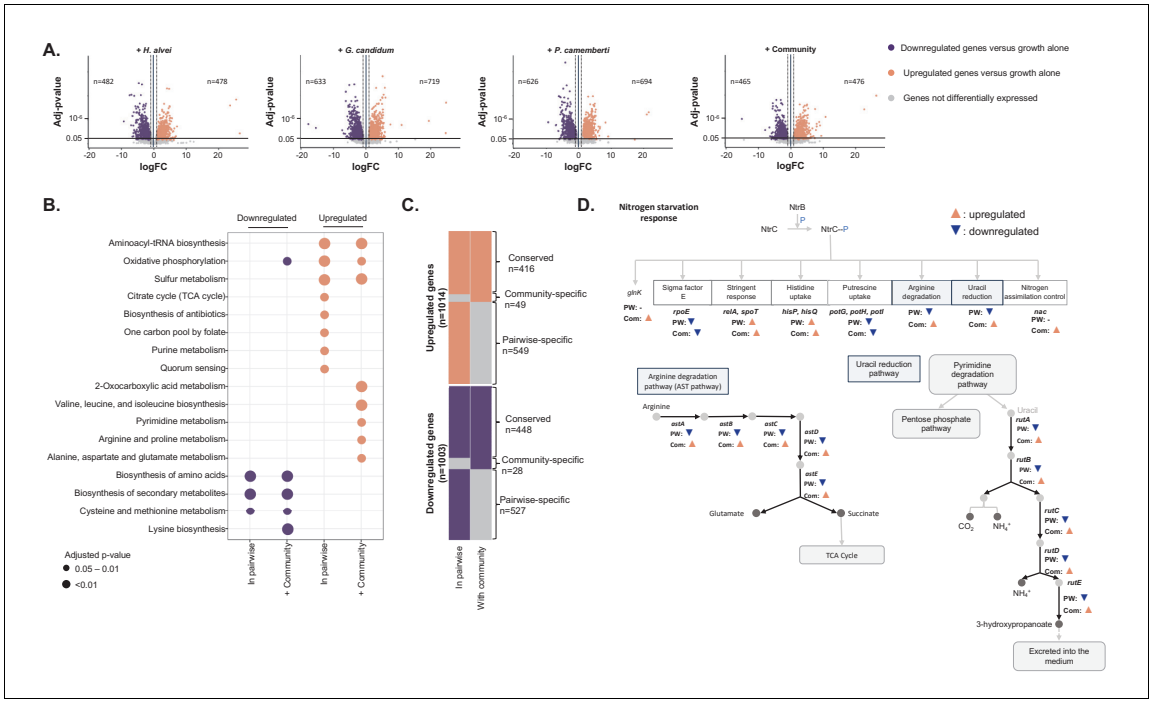

Figure 4. Differential expression analysis of *E. coli* during interactive and non-interactive growth conditions (***Figure 4—source data 1***). We used RNASeq to investigate *E. coli* gene expression at three timepoints (1, 2 and 3 days) during growth on CCA alone, in pairwise conditions (with *H. alvei*, *G. candidum* or *P. camemberti*) and with the community. (**A**) Using DESeq2 (***Love et al., 2015***), we identified up and downregulated genes during growth in each pairwise condition compared to growth alone as well as up and downregulated genes during growth with the community compared to growth alone. Differential expression analysis has been performed at three timepoints, however, we displayed the results of the three timepoints on a single volcano plot. Only genes associated with an adjusted p-value lower than 1% (Benjamini-Hochberg correction for multiple testing) and an absolute logFC higher than one were considered differentially expressed. (**B**) We regroup any genes upregulated in at least one pairwise condition as a single set of pairwise-upregulated genes and did the same for pairwise-downregulated genes. Then, we performed functional enrichment analysis on KEGG pathways for pairwise-downregulated genes, community-downregulated genes, pairwise-upregulated genes and community-upregulated genes. Functional enrichment was performed using the R package clusterProfiler (***Yu et al., 2012***) and only the KEGG pathways enriched with an adjusted p-value lower than 5% (Benjamini-Hochberg correction for multiple testing) were considered. (**C**) We compared pairwise-upregulated genes with community-upregulated genes and pairwise-downregulated genes with community-downregulated genes to identify if expression regulation from pairwise conditions is conserved in the community context and if we observe specific changes in pairwise or community conditions. (**D**) Within the genes specifically upregulated during growth with the community, we observed the upregulation of multiple genes associated with the nitrogen starvation response. Most of these genes were also downregulated in pairwise conditions.

DOI: https://doi.org/10.7554/eLife.37072.019

The following source data and figure supplement are available for figure 4:

Source data 1. Differential expression analysis of *E. coli*'s growth in pairwise and with the community versus growth alone.

DOI: https://doi.org/10.7554/eLife.37072.021

Figure supplement 1. RNASeq analysis of *E. coli* gene expression during growth alone and in pairwise conditions.

DOI: https://doi.org/10.7554/eLife.37072.020

production through aerobic respiration and the TCA cycle happened after 3 days of growth. Oxygen availability (***Gunsalus, 1992***) and growth phase (***Wackwitz et al., 1999***) are the two known regulators of aerobic respiration. At day 3, *E. coli* was observed to be in log phase when alone, whereas in the presence of a partner, and especially with *P. camemberti*, *E.coli* was observed to enter the stationary phase between day 2 and day 3 (***Figure 2*** – figure supplement 1). Therefore, upregulation of aerobic respiration is most likely associated with the growth stage difference between *E. coli* alone

and with a partner. While these functions were upregulated regardless of the partner, more genes were upregulated in the presence of *G. candidum* than the other partners and thus, several pathways associated with nucleotide biosynthesis (C1-pool by folate, purine metabolism, and pyrimidine metabolism) were specifically upregulated with this partner. This suggests that either *E. coli* and *G. candidum* compete for nucleotide compounds from the environment or that presence of *G. candidum* leads to an increased demand of nucleotide compounds for *E. coli's* metabolism and growth.

We performed a similar KEGG pathway enrichment analysis on the downregulated genes in pairwise conditions. Pathways involved in the biosynthesis of amino acids, specifically tyrosine, phenylalanine, tryptophan, methionine, lysine, arginine, homoserine, leucine, glutamate, threonine and glycine, appeared to be the principal downregulated functions in the presence of a partner and more particularly with a fungal partner. Interestingly, some amino acid biosynthetic pathways were upregulated later in the growth but not significantly enriched in the enrichment analysis (phenylalanine, tyrosine and leucine). Downregulation of amino acid biosynthesis suggests that the partner species generates amino acids available for cross-feeding. The observation of this interaction in the transcriptome data is consistent with our interpretation of RB-TnSeq results and reinforces the likelihood of such an interaction. However, late upregulation of some amino acid biosynthesis suggests that as the partner grows along with *E. coli* they eventually end up competing for amino acids, leading to biosynthesis upregulation. This late competition was unlikely to be detected by RB-TnSeq using our current analysis.

To summarize, presence of a partner triggers a significant and dynamic reorganization of *E. coli* gene expression. Most of these modifications restructure *E. coli* metabolic activity: mostly in response to modification of growth phase, but also in response to nutrient availability changes and for example to benefit from cross-feeding and common goods.

Next, we aimed to determine whether *E. coli* gene expression reorganization significantly changes when grown with the full community as compared to growth in pairwise conditions. To do so, we first calculated *E. coli* gene logFC at each timepoint between growth with the community and growth alone. We further analyzed genes with adjusted p-values lower than 1% (Benjamini-Hochberg correction for multiple testing) and absolute logFC greater than 1. After pooling across timepoints, we identified 465 upregulated and 476 downregulated genes in the presence of the community versus growth alone (***Figure 4A***). We then compared these genes to the 966 upregulated genes and 977 downregulated genes in pairwise conditions versus growth alone (***Figure 4B and C***).

First, 416 genes were found to be upregulated in both pairwise and community growth versus growth alone (conserved upregulated genes). Enrichment analysis highlighted functions that were previously described as upregulated in most of the pairwise conditions: aminoacyl-tRNA-synthetase and energy metabolism (***Figure 4B***). This suggests that certain interactions that *E. coli* experienced in pairwise conditions are conserved in the community context. To investigate if the addition of similar interactions from different partners leads to an amplified response, we explored if the magnitude of expression changes in these pathways is higher in the community. We performed differential expression analysis on the genes comparably regulated in pairwise conditions and with the community (***Figure 4—figure supplement 1***). 50 of the 416 conserved upregulated genes were significantly more upregulated in community growth compared to pairwise growth. Among them, sulfate assimilation genes were overrepresented. This suggests that similar pairwise interactions may be additive in the community, leading to a stronger transcriptional response.

Next, we identified 549 genes that were specifically upregulated in pairwise conditions versus growth alone and not upregulated in community versus growth alone (pairwise-specific upregulated genes). KEGG pathway enrichment analysis highlighted that these genes were mostly associated with quorum sensing, fatty acid metabolism and oxidative phosphorylation (***Figure 4B***). This observation suggests that the presence of additional species in the community counteracts or prevents certain pairwise interactions. It supports the presence of higher-order interactions as highlighted with the RB-TnSeq experiments. Indeed, more than half of the upregulated genes observed in pairwise conditions are not conserved with the community.

Finally, 49 genes were specifically upregulated during community growth versus growth alone (community-specific upregulated genes). Emergence of specific expression patterns with the community also suggests the existence of higher-order interactions. However, these community-specific upregulated genes represent only a small fraction (10%) of upregulated genes within the community. Thus, most expression upregulation observed with the community is conserved from expression

upregulation observed in pairwise conditions. Genes specifically upregulated with the community were associated with the biosynthesis of valine, leucine, and isoleucine, pyrimidine metabolism as well as arginine and proline metabolism (***Figure 4B***). Upregulation of certain amino acid biosynthesis pathways suggests that despite potential cross-feeding from individual partners, addition of many partners eventually leads to competition. Upregulation of pyrimidine, arginine and proline metabolism however is part of a larger response; the response to nitrogen starvation (***Figure 4D***). This response facilitates cell survival under nitrogen-limited conditions. Specifically, upregulated genes included all the genes involved in the regulatory loop of the transcriptional regulator NtrC (*glnL*) and nitrogen utilization as well as NtrC transcriptional targets: the transcriptional regulator Nac (*nac*), the operon *rutABCDEFG* involved in ammonium production by uracil catabolism, the *astABCDE* operon constituting the arginine degradation pathway (AST pathway) and the two regulators of the stringent response, *relA* and *spoT*. Thus, the presence of additional species in the community specifically triggers the activation of the response to nitrogen starvation, which suggests a potential higher competition for nitrogen in the community context.

We performed a similar analysis on downregulated genes in pairwise conditions and with the community versus growth alone to investigate if transcriptional downregulation in pairwise and community conditions are similar (***Figure 4C***). We identified 448 genes that were downregulated during both pairwise and community growth conditions versus growth alone (conserved downregulated genes). Enrichment analysis pointed to the downregulation of amino acid biosynthesis as well as cysteine and methionine metabolism. Therefore, consistent with our RB-TnSeq data, this suggests that cross-feeding from a single partner is maintained in a more complex context. 527 genes were specifically downregulated in pairwise conditions and not with the community (pairwise-specific downregulated genes). Despite the large number of genes, no specific functions were enriched. However, the *rutABCDEFG* and *astABCDE* operons associated with the response to nitrogen starvation were downregulated in each pairwise condition (***Figure 4D***). Altogether, pairwise-specific downregulated genes represent 54% of the genes downregulated in pairwise conditions, thus strongly suggesting higher-order interactions. Here, the presence of the community may trigger a highly specific response that would otherwise be downregulated in the presence of only one species. Finally, also highlighting potential higher-order interactions, 28 genes were specifically downregulated when *E. coli* is grown with the community (community-specific downregulated genes). However, this represents only 6% of the observed downregulated genes in the community, highlighting again that most of the gene expression regulations in the presence of the community are conserved from gene expression regulations pairwise interactions.

To conclude, most of the changes in *E. coli* gene expression during growth with the community were similar to a subset of expression changes observed in pairwise conditions. Moreover, some of these changes were amplified in the community compared to pairwise. This suggests that while a large part of transcriptional regulation in the community results from pairwise interactions, similar interactions from different partners may be additive in the community and exert a stronger impact on transcription. Also, the observed changes in nitrogen availability-related transcription suggest that community growth may induce new metabolic limitations.

Discussion

In this work, we used the model organism *E. coli* as a readout for microbial interactions in a model cheese rind microbiome. We used genome-scale approaches to determine the changes in *E. coli's* genetic requirements and gene expression profiles in conditions with increasing levels of community complexity. Our analysis highlighted both important changes in *E. coli's* genetic requirements between interactive and non-interactive conditions as well as deep reorganization of *E. coli*'s gene expression patterns. We identified a variety of interactive mechanisms in the different interactive contexts. Our data revealed that interactions within the community include both competitive and beneficial interactions. By reconstructing a community from the bottom up, we were able to investigate how interactions in a community change as a consequence of being in a more complex, albeit still simple, community. RNASeq and RB-TnSeq consistently showed that around half of the interactions in a community can be attributed to pairwise interactions and the other half can be attributed to higher-order interactions. Although community structure is argued to be predictable from pairwise interactions in specific cases, higher-order interactions are believed to be responsible for the

general lack of predictability (**Billick and Case, 1994**; **Friedman et al., 2017**; **Momeni et al., 2017**). Similarly, such higher-order interactions have been shown to be responsible for the unpredictability of community function from individual species traits (**Sanchez-Gorostiaga et al., 2018**). Our work demonstrates the existence and prevalence of these higher-order interactions even within a simple community.

Together, RB-TnSeq and RNASeq provided insight into mechanisms of mutualism between microbial species in this model system. One major interaction mechanism appears to be cross-feeding of amino acids from fungal partners. Although amino acid biosynthesis pathways were strongly required when *E. coli* grew alone, the presence of fungal species, but not bacterial species, led to fitness effect alleviation and downregulation of amino acid biosynthesis. This suggests that fungi increase the availability of free amino acids in the environment. Cheese-associated fungal species are known to secrete proteases that can degrade casein, the major protein found in cheese (**Kastman et al., 2016**; **Boutrou et al., 2006b**; **Boutrou et al., 2006a**), and therefore may increase the availability of an otherwise limiting resource. Although our model system is based on cheese, interactions based on cross-feeding are widely observed in other environments, such as soil, the ocean or the human gut (**Freilich et al., 2011**; **Pacheco et al., 2018**; **Goldford et al., 2018**). For example, in the gut microbiome, Bifidobacteria can ferment starch and fructooligosaccharides and produce fermentation products including organic acids such as acetate which can in turn be consumed by butyrate-producing bacteria like *Eubacterium hallii* (**Belenguer et al., 2006**; **De Vuyst and Leroy, 2011**; **Flint et al., 2012**). Cross-feeding of other nutrients in the gut has also been uncovered using a related approach (INSeq) which found that vitamin B12 from Firmicutes or Actinobacteria was important for the establishment of *Bacteroides thetaiotaomicron* in mice (**Goodman et al., 2009**).

Our results also revealed mechanisms of competition within the community. RNASeq highlighted that both siderophore production and uptake are upregulated in interactive conditions, suggesting that there is competition for iron between species. Competition for iron is frequently observed across many environments, including cheese, as iron is an essential micronutrient for microbial growth and often a limited resource (**Monnet et al., 2012**; **Albar et al., 2014**; **Stubbendieck and Straight, 2016**; **Traxler et al., 2012**). Interestingly, although we were able to detect fitness defects for siderophore uptake using RB-TnSeq, we did not see fitness defects for siderophore biosynthesis mutants. Because RB-TnSeq relies on a pooled library of mutants, one of the limitations to this approach is that it is difficult to detect fitness effects for genes associated with the production of common goods. For example, in the pooled library, most cells have wild-type siderophore biosynthesis genes, and thus produce and secrete siderophores into the environment under iron limitation. A consequence of this is that any cell that has lost the ability to produce siderophores can readily access the siderophores produced by neighboring cells. In contrast, the genes for uptake of common goods should remain crucial, and accordingly, we do observe fitness defects in the siderophore uptake genes. For this reason, using RNASeq can help overcome some of the limitations, such as pooling effects, associated with RB-TnSeq.

Interactions between species also appeared to lead to stressful growth conditions, as RB-TnSeq showed the need for genes to deal with growth in the presence of toxic compounds. *G. candidum* is known to produce and excrete D-3-phenyllactic acid and D-3-indollactic acid, which inhibit the growth of Gram-negative and Gram-positive bacteria in the cheese environment (**Boutrou and Guéguen, 2005**; **Dieuleveux et al., 1998**). Also, strains of *H. alvei* isolated from meat have been shown to produce compounds inhibiting biofilm formation in *Salmonella enterica* serovar Enteritidis (**Chorianopoulos et al., 2010**). To begin to understand the extent to which the interactions we detected with *E. coli* were specific to this species, or more general, we performed similar RB-TnSeq experiments with the cheese isolate *Pseudomonas psychrophila.* This comparative approach showed that some responses to growth with other species are conserved, such as those needed to survive stress conditions, while others differ between the two species such as amino acid cross-feeding. This further highlights the ability to detect the dynamic nature of interactions, which not only change with community complexity, but also with the composition of the community.

While our analysis highlighted global changes occurring as a consequence of interactions, and some of the key underlying interaction mechanisms, many more aspects of the biology occurring within communities are likely to be uncovered even within this simple model system. For example, much of our current analysis is limited to well-characterized pathways with strong negative fitness

effects, yet many uncharacterized genes were also identified as potentially involved in interactions. Further investigation of these genes could uncover novel interaction pathways. Additionally, analysis of the exact ways in which community members modify the growth environment, such as through the production of extracellular metabolites, will be important to fully understand the molecular mechanisms of interactions.

Altogether, this study revealed the intricacy, redundancy and specificity of the many interactions governing a simple microbial community. The ability of *E. coli* to act as a probe for molecular interactions, the robustness of RB-TnSeq, and its complementarity with RNASeq open new paths for investigating molecular interactions in more complex communities, independently of the genetic tractability of their members, and can contribute to a better understanding of the complexity and diversity of interactions within microbiomes. Finally, our work provides a starting point for better understanding the exact nature of higher-order interactions, and how they impact microbial communities.

Materials and methods

Key resources table

Reagent type (species) or resource	Designation	Source or reference	Identifiers	Additional information
Library, strain background (*Escherichia coli* K12)	Keio collection	PMID: 16738554	CGSC, RRID:SCR_002303	Collection of 3,818 *E. coli* knockout strains
Library, strain background (*Escherichia coli* K12)	Keio_ML9	PMID: 25968644	RB-TnSeq library of *E. coli* K12 BW25113 (152,018 pooled insertion mutants)	
Library, strain background (*Pseudomonas psychrophila*)	JB418_ECP1	this paper		RB-TnSeq library generated in the *P. psychrophila* JB418 strain isolated from cheese (272,329 pooled insertion mutants)
Strain, strain background (*Escherichia coli* K12)	Keio ME9062	PMID: 16738554	CGSC#: 7636	Parent strain of the Keio collection mutants. Also referred as *E. coli* K12 BW25113
Strain, strain background (*Hafnia alvei*)	*Hafnia alvei JB232*	this paper		Strain isolated from cheese
Strain, strain background (*Geotrichum candidum*)	*Geotrichum candidum*	Danisco - CHOOZIT	GEO13 LYO 2D	Industrial starter for cheese production
Strain, strain background (*Penicillium camemberti*)	*Penicllium camemberti*	Danisco - CHOOZIT	PC SAM 3 LYO 10D	Industrial starter for cheese production
Strain, strain background (*P. psychrophila*)	*Pseudomonas psychrophila JB418*	this paper		Strain isolated from cheese
Strain, strain background (*E. coli*)	*E. coli APA766*	PMID: 25968644		donor WM3064 which carries the pKMW7 Tn5 vector library containing 20 bp barcodes
Sequence-based reagent	NEBNext Multiplex Oligos for Illumina (Set 1); NEBNext multiplex Oligos for Illumina (Set 2)	New England Biolabs	NEB #E7335 (lot 0091412);, NEB #E7500 (lot 0071412)	
Sequence-based reagent	Nspacer_barseq_pHIMAR; P7_MOD_TS_index3 primers	PMID: 25968644		Primers for transposon-insertion sites amplication for *P. psychrophila* RB-TnSeq library characterization
Sequence-based reagent	BarSeq_P1; BarSeq_P2_ITXXX	PMID: 25968644		Primers for RB-TnSeq PCR (amplification of the barcode region of the transposon)
Commercial assay or kit	NEBNext Ultra DNA Library Prep Kit for Illumina	New England Biolabs	NEB #E7645	
Commercial assay or kit	MinElute purification kit	Qiagen	ID:28004	
Commercial assay or kit	Turbo DNA-free kit	AMBION, Life Technologies	AM1907	

Continued on next page

Continued

Reagent type (species) or resource	Designation	Source or reference	Identifiers	Additional information
Commercial assay or kit	MEGAclear Kit Purification for Large Scale Transcription Reactions	AMBION, Life Technologies	AM1908	
Commercial assay or kit	Ribo-Zero rRNA removal kit (bacteria); Ribo-Zero rRNA removal kit (yeast)	Illumina	MRZMB126; MRZY1306	
Commercial assay or kit	NEBNextUltraTM RNA Library Prep Kit for Illumina	New England Biolabs	NEB #E7770	
Software, algorithm	Geneious	http://www.geneious.com		
Software, algorithm	Perl	https://www.perl.org/		
Software, algorithm	R	https://www.r-project.org/		
Other	MapTnSeq.pl; DesignRandomPool.pl; BarSeqTest.pl	PMID: 25968644		Perl scripts for RB-TnSeq library characterization and RB-TnSeq analysis - https://bitbucket.org/berkeleylab/feba
Other	DESeq2	PMID: 25516281		R package for RNASeq analysis

Strains and media

Strains

The following strains have been used to reconstruct the bloomy rind cheese community: *H. alvei* JB232 isolated previously from cheese (**Wolfe et al., 2014**) and two industrial cheese strains: *G. candidum* (*Geotrichum candidum* GEO13 LYO 2D, Danisco – CHOOZIT^{TM}, Copenhagen, Denmark) and *P. camemberti* (PC SAM 3 LYO 10D, Danisco - CHOOZIT^{TM}). The strain *P. psychrophila* JB418 was isolated from a sample of Robiola due latti (Italy) (**Wolfe et al., 2014**) and used for all the experiments involving *Pseudomonas*. All the *E. coli* strains used in this study shared the same genetic background of the initial strain *E. coli* K12 BW25113. The use of the different strains is described in **Table 1**.

Medium

All growth assays have been carried out on 10% cheese curd agar, pH7 (CCA) (10% freeze-dried Bayley Hazen Blue cheese curd (Jasper Hill Farm, VT), 3% NaCl, 0.5% xanthan gum and 1.7% agar). The pH of the CCA was buffered from 5.5 to 7 using 10M NaOH.

Growth curve assays on 10% cheese curd agar, pH7

The following growth assays are distinct from the growths carried out for RB-TnSeq and fitness analysis (see below).

Assays have been performed in at least triplicates. Growth assays have been carried out for the *E. coli* JW0024 strain (**Baba et al., 2006**) and *P. psychrophila* JB418 during growth alone, in pairwise conditions with either *H. alvei* JB232, *G. candidum* or *P. camemberti* and with the full community.

E. coli was pre-cultured overnight in liquid LB-kanamycin (50 µg/ml) at 37°C and *P. psychrophila* JB418 was pre-cultured overnight in LB at room temperature (RT) . Then, for growth alone assays, 1000 cells of *E. coli* or *P. psychrophila* JB418 were inoculated on a 96 well plate containing 200 µL of

Table 1. *E. coli* strains used during the study.

Experiment	*E. coli* strain(s)	Reference
RB-TnSeq	*E. coli* Keio_ML9 library	(**Wetmore et al., 2015**)
Growth assays	*E. coli* JW0024 strain (undisrupted mutant)	(**Baba et al., 2006**)
Competition assays	WT: Keio ME9062 Mutants: (**Figure 1—figure supplement 5**)	(**Baba et al., 2006**)

DOI: https://doi.org/10.7554/eLife.37072.022

CCA per well. For pairwise growth assays, either *E. coli* or *P. psychrophila* JB418 was co-inoculated with either *H. alvei* JB232, *G. candidum* or *P. camemberti* at a ratio of 1:1 cell (1000 cells of *E. coli* and 1000 cells of the partner). Finally, for growth assay with the community, *E. coli* or *P. psychrophila* JB418 have been co-inoculated with *H. alvei* JB232, *G. candidum* and *P. camemberti* at a ratio of 10:10:10:1 cells.

Growth assays were then carried out for 3 days at RT. Agar plugs from 96 well plates were harvested at T = 0 hr, 6 hr, 12 hr, 24 hr, 36 hr, 48 hr, 72 hr and 120 hr for *E. coli* growth assays and T = 0 hr, 12 hr, 24 hr, 48 hr and 72 hr for *P. psychrophila* JB418 growth assays. Agar plugs were homogenized in 1 mL of PBS1X-Tween0.05% and three dilutions were plated on different media to measure growth of each species (see **Table 2**). Plates were incubated for 24 hr at 37°C for *E. coli* and 2 days at RT for *P. psychrophila* JB418. After incubation, colony forming units (CFUs) were counted to estimate the number of bacterial cells on the cheese curd agar plates.

Growth alone of *H. alvei* JB232, *G. candidum* and *P. camemberti* have also been carried out similarly to *E. coli* and *P. psychrophila* JB418 growth alone.

P. psychrophila JB418 genome sequencing, assembly and annotation

P. psychrophila JB418 gDNA was sequenced using Pacific Biosciences (PacBio), Oxford Nanopore Minion (Oxford Nanopore, Oxford, UK) and Illumina sequencing. PacBio library preparation and sequencing were performed by the IGM Genomics Center at the University of California San Diego. Nanopore library preparation and sequencing were done at the University of California, Santa Barbara as part of the Eco-Evolutionary Dynamics in Nature and the Lab (ECOEVO17). Illumina library preparation and sequencing were done at the Harvard University Center for Systems Biology. Canu was used to assemble the PacBio and nanopore reads (**Koren et al., 2017**). Illumina data was then used to correct sequencing error using the software Pilon (**Walker et al., 2014**). The assembled genome was annotated using the Integrated Microbial Genomes and Microbiomes (IMG/M) system (**Markowitz et al., 2012**). The *P. psychrophila* JB418 genome is 6,072,477 nucleotides long. It contains a single circular chromosome of 5.85 Mb and 4 plasmids of 172.2 Kb, 37.7 Kb, 5.8 Kb and 2.4 Kb. 6060 genes including 5788 open reading frames were identified. This genome is publicly available on the IMG/M website as IMG Genome ID 2751185442.

Transposon mutant library construction in *P. psychrophila* JB418

P. psychrophila JB418 was mutagenized by conjugation with *E. coli* strain APA766 (donor WM3064 which carries the pKMW7 Tn5 vector library containing 20 bp barcodes) (**Wetmore et al., 2015**). This donor strain is auxotrophic for diaminopimelic acid (DAP). The full collection of the APA766 donor strain (1 mL) was grown up at 37°C overnight at 200 rpm. Four 25 mL cultures (each started with 250 µL of APA766 stock) were grown in LB-kanamycin:DAP (50 µg/mL kanamycin and 60 µg/mL DAP). A 20 mL culture was started from an individual *P. psychrophila* JB418 colony in LB broth and grown at RT overnight at 200 rpm. *E. coli* donor cells were washed twice with LB and resuspended in 25 mL LB. Donor and recipient cells were then mixed at a 1:1 cell ratio based on OD600 measurements, pelleted, and resuspended in 100 µL. This was done separately for each of the four *E. coli* cultures. 40 µL were plated on nitrocellulose filters on LB plates with 60 µg/mL DAP. Two filters were used for each of the four conjugation mixtures (eight total conjugations). The conjugations took place for 6 hr at RT. After 6 hr, the filters were each resuspended in 2 mL of LB broth and then plated on LB:kanamycin (50 µg/mL) for selection of transconjugants. 20 plates were plated of a 1:2

Table 2. Organization of CFU's quantification for growth assays.

***E. coli* + *H. alvei* JB232**	**LB (*E. coli* + *H. alvei* JB232 CFUs) LB-kanamycin (50 µg/ml) (*E. coli* CFUs)**
E. coli + *G. candidum*	LB-kanamycin:cycloheximide (50 µg/ml and 10 µg/ml) (*E. coli* CFUs) LB-chloramphenicol (*G. candidum* CFU's)
E. coli + *P. camemberti*	LB-kanamycin:cyclohexamide (50 µg/ml and 10 µg/ml) (*E. coli* CFUs) LB-chloramphenicol (50 µg/ml)(*P. camemberti* CFU's)
E. coli + Community	LB-cyclohexamide (10 µg /mL) (*E. coli* and *H. alvei* JB232 CFU's), LB-kanamycin:cyclohexamide (50 µg/ml and 10 µg/ml) (*E. coli* CFU's) and LB-chloramphenicol (50 µg/ml) (*G. candidum* and *P. camemberti* CFU's)

DOI: https://doi.org/10.7554/eLife.37072.023

dilution for each conjugation (160 plates total). Transconjugants were pooled and harvested after three days of growth on selection plates. The pooled mixture was diluted back to 0.25 in 100 mL of LB:kanamycin (50 μg/mL). The culture was then grown at RT to an OD600 of 1.3 before glycerol was added to 10% final volume and 1 mL aliquots of the library (named JB418_ECP1) were made and stored at −80°C for future use.

TnSeq sequencing library preparation for *P. psychrophila* JB418 and TnSeq data analysis

Library preparation was performed as in ***Wetmore et al., 2015*** with slight modifications (***Wetmore et al., 2015***).

DNA extraction

DNA was extracted from the *P. psychrophila* JB418_ECP1 RB-TnSeq library by phenol:chloroform extraction. Briefly, the cell pellet was vortexed at maximum speed for 3 min in the presence of 500 μL buffer B (200 mM NaCl,20mM EDTA sterilized by filtration), 210 μL of 20% SDS, a 1:1 mixture of 425–600 μM and 150–212 μm acid-washed beads, and 500 μL of phenol:chloroform, pH 8. The sample was then centrifuged for 3 min at 4°C at 8000 rpm prior to removing the aqueous phase to a new tube. 1/10 of sample aqueous phase volume of 3M sodium acetate was then added along with one aqueous phase volume of ice cold isopropanol. The sample was then placed for ten minutes at −80°C before centrifugation for five minutes at 4°C at 13000 rpm. The supernatant was discarded and 750 μL of ice cold 70% ethanol was added before another centrifugation for five minutes at 4°C at 13000 rpm. The supernatant was discarded and the DNA pellet was allowed to air dry before resuspension in 50 μL of nuclease-free water. DNA was quantified with Qubit double-stranded DNA high-sensitivity assay kit (Invitrogen, Carlsbad, CA).

DNA fragmentation and size selection

2 μg of DNA was sheared with a Covaris E220 focused-ultrasonicator with the following settings: 10% duty cycle, intensity 5, 200 cycles per burst, 150 s. DNA was split into two aliquots (1 μg each) and samples were size-selected for fragments of 300 bp using 0.85X Agencourt AMPure XP beads (Invitrogen) with a 1.4x ratio following the manufacturer's instructions.

Library preparation

The entire 20 μL volume of these two size-selected samples were then each used as input into the NEBNext End Prep step 1.1 of the NEBNext Ultra DNA Library Prep Kit for Illumina (New England Biolabs, Ipswich, MA) protocol. The remainder of the manufacturer's protocol was then followed with the exception that for adapter ligation, we used 0.8 μL of 15 μM double-stranded Y adapters. Adapters were prepared by first combining 5 μL of 100 μM Mod2_TS_Univ (ACGCTCTTCCGATC*T) and 5 μL of 100 μM Mod2_TruSeq (/5'P/GATCGGAAGAGCACACGTCTGAACTCCAGTCA. This mixture was then incubated in a thermocycler for 30 min at 37°C, followed by ramping at 0.5°C per second to 97.5°C before a hold at 97.5°C for 155 s. The temperature was then decreased by 0.1°C per five seconds for 775 cycles, followed by a hold at 4°C. Annealed adapters were diluted to 15 μM in TE and stored at −80°C before use. AMPure XP ratios for a 200 bp insert size were used as recommended in ***Table 1.1*** of the NEBNext Ultra DNA Library Prep Kit for Illumina manual.

To enrich for transposon-insertion sites, PCR amplification was done on the adapter-ligated DNA with NEBNext Q5 Hot Start HiFi Master Mix and Nspacer_barseq_pHIMAR and P7_MOD_TS_index3 primers (***Wetmore et al., 2015***) with the following program: 98°C 30 s, 98°C 10 s, 65°C 75 s, repeat steps 2–3 24X, 65°C 5 min, and then maintained at 4°C. Following PCR and clean-up of step 1.5 of the NEBNext Ultra DNA Library Prep Kit for Illumina manual, the two preps were pooled and the concentration was quantified with Qubit double-stranded DNA high-sensitivity assay kit (Invitrogen). A second size selection clean-up was performed by repeating step 1.5 of the NEBNext Ultra DNA Library Prep Kit for Illumina manual.

Library sequencing

The sample was analyzed on an Agilent TapeStation and the average size was 380 bp and the concentration was 57 pg/µL. This sample was then submitted for sequencing on a HiSeq 2500 Rapid Run (150 bp fragments, paired-end) at the UCSD IGM Genomics Center.

Library characterization

TnSeq reads were analyzed with the Perl script MapTnSeq.pl from (***Wetmore et al., 2015***). This script maps each read to the *P. psychrophila* genome. The script DesignRandomPool.pl (***Wetmore et al., 2015***) was used to generate the file containing the list of barcodes that consistently map to a unique location as well as their location. We obtained a total of 272,329 insertion mutants. The transposon was inserted in the central part of a gene for 143,491 of these insertion mutants covering 83% of *P. psychrophila* JB418 genome (***Figure 1—figure supplement 6***).

RB-TnSeq experiments for *E. coli* and *P. psychrophila* JB418

The *E. coli* barcoded transposon library Keio_ML9 and the *P. psychrophila* strain JB418 library were used for RB-TnSeq fitness assays on CCA during growth alone, growth in pairwise condition with each bloomy rind cheese community member and during growth with the full community. ***Figure 1—figure supplement 1*** provides a description of the fitness assays as well as fitness calculation.

Library pre-culture

Each library has to be initially amplified before use. One aliquot of each library was thawed and inoculated into 25 mL of liquid LB-kanamycin (50 µg/mL). Once the culture reached mid-log phase (OD = 0.6–0.8), 5 mL of that pre-culture was pelleted and stored at −80˚C for the T0 reference in the fitness analysis. The remaining cells were used to inoculate the different fitness assay conditions.

Inoculations

For each RB-TnSeq fitness assay, $7*10^6$ cells of the library pre-culture were inoculated by spreading evenly on a 100 mm petri dish containing 10% CCA, pH seven after having been washed in PBS1x-Tween0.05%. This represents on average 50 cells per insertion mutant. For each pairwise assay, $7*10^6$ cells of the partner were co-inoculated with the library. For the community assay, $7*10^6$ cells of *H. alvei* JB232 and *G. candidum* as well as $7*10^5$ cells of *P. camemberti* were co-inoculated with the library. For each condition, assays were performed in triplicate.

Harvest

Harvests were performed at T = 24 hr, 48 hr and 72 hr. Sampling was done by flooding a plate with 1.5 mL of PBS1X-Tween0.05% and gently scraping the cells off. The liquid was then transferred into a 1.5 mL microfuge tube and cells were pelleted by centrifugation. After removing the supernatant, the cells were washed in 1 mL of RNA-protect solution (Qiagen, Hilden, Germany), pelleted and stored at −80˚C before further experiments.

gDNA and mRNA extraction

gDNA and mRNA were simultaneously extracted by a phenol-chloroform extraction (pH 8) from samples of the competitive assays. For each extraction: 125 µL of 425–600 µm acid-washed beads and 125 µL of 150–212 µm acid-washed beads were poured in a screw-caped 2 mL tube. 500 µL of 2X buffer B (200 mM NaCl, 20 mM EDTA) and 210 µL of SDS 20% were added to the tube as well as the pellet and 500 µL of Phenol:Chloroform (pH 8). Cells were lysed by vortexing the tubes for 2 min at maximum speed. Aqueous and organic phases were separated by centrifugation at 4˚C, 8,000 RPM for 3 min and 450 µL of the aqueous phase (upper phase) was recovered in a 1.5 mL eppendorf tube. 45 µL of sodium acetate 3M and 450 µL of ice cold isopropanol were added before incubating the tubes at −80˚C for 10 min. The tubes were then centrifuged for 5 min at 4˚C at 13,000 RPM. The pellet was then washed in 750 µL of 70% ice cold ethanol and re-suspended in 50 µL of DNAse/RNAse free water. Each sample was split into 2 times 25 µL and stored at −80˚C until further analysis.

Library preparation and sequencing

After gDNA extraction, the 98˚C BarSeq PCR as described in ***Wetmore et al., 2015*** was used to amplify only the barcoded region of the transposons. Briefly, PCR was performed in a final volume of 50 µL: 25 µL of Q5 polymerase master mix (New England Biolab), 10 µL of GC enhancer buffer (New England Biolab), 2.5 µL of the common reverse primer (BarSeq_P1 – ***Wetmore et al., 2015***) at 10 µM, 2.5 µL of a forward primer from the 96 forward primers (BarSeq_P2_ITXXX) at 10 µM and 50 ng to 2 µg of gDNA. For each triplicate, the PCR was performed with the same forward primer so all replicates of a condition could be pooled and have the same sequencing multiplexing index. For *E. coli* analysis, we performed 46 PCRs (T0 sample and 45 harvest samples) involving 16 different multiplexing indexes. For *P. psychrophila* JB418 analysis, we performed 46 PCR (T0 sample and 45 harvest samples) involving 16 other multiplexing indexes. We used the following PCR program: (i) 98˚C - 4 min, (ii) 30 cycles of: 98˚C – 30 s; 55˚C – 30 s; 72˚C – 30 s, (iii) 72˚C – 5 min. After the PCR, 10 µL of each of the 92 PCR products were pooled together to create the BarSeq library(920 µL) and 200 µL of the pooled library were purified using the MinElute purification kit (Qiagen). The final elution of the BarSeq library was performed in 30 µL in DNAse and RNAse free water.

The BarSeq library was then quantified using Qubit dsDNA HS assay kit (Invitrogen) and sequenced on HiSeq4000 (50 bp, single-end reads), by the IGM Genomics Center at the University of California San Diego. The sequencing depth for each condition varied between 1.5 and 7.5 million reads.

Data processing and fitness analysis

BarSeq data processing and gene fitness calculation were performed separately for the *E. coli* and the *P. psychrophila* JB418 experiments. For each library, BarSeq reads were processed using the Perl script BarSeqTest.pl from (***Wetmore et al., 2015***). This script combines two Perl scripts essential for the BarSeq data processing. After the raw reads have been de-multiplexed, the computational pipeline: (i) identifies individual barcodes and the associated number of reads, (ii) calculates the strain fitness for each insertion mutant and (iii) calculates the normalized fitness value for each gene along with a t-statistic value (t-score). The following parameters were applied during the fitness calculations: (i) only insertion mutants located within the central region of genes (10%–90%) were considered, (ii) barcodes with less than three reads in the T0 were ignored and (iii) genes with less than 30 counts across all barcodes in T0 were ignored. For each library, the pipeline uses a table where each barcode is mapped to a location in the genome. The Arkin lab (Physical Biosciences Division, Lawrence Berkeley National Laboratory, Berkeley, California, USA) kindly provided the TnSeq table for the *E. coli* library and we generated a TnSeq table for *P. psychrophila* strain JB418. The different scripts used for this analysis originate from (***Wetmore et al., 2015***) and are publicly available on https://bitbucket.org/berkeleylab/feba.

We calculated *E. coli* and *P. psychrophila* JB418 genes fitnesses at T = 24 hr (Day1), 48 hr (Day2) and 72 hr (Day3) in the following conditions: growth alone, growth with *H. alvei*, growth with *G. candidum*, growth with *P. camemberti* and growth with the community.

First, strain fitness for each insertion mutant that met the criteria described above is calculated as the log2 of the ratio of the insertion mutant's abundance at the time of the harvest (number of reads of the associated barcode) and its abundance in the T0 sample. Un-normalized gene fitness is then calculated as the weighted average of strain fitness of all the insertion mutants of a gene. Un-normalized fitness values are then normalized, first by subtracting the smoothed median of the un-normalized fitness values. This is performed to account for changes in gene copy number along the chromosome as genes close to the replication fork might have multiple copies in diving cells. Then, the final normalization step relies on the assumption that disruption of most of the genes leads to little to no fitness effect. This normalization is performed by subtracting the mode of the gene fitness. Thus, most of the genes are expected to have a fitness of 0. Genes whose disruption is deleterious will have a negative fitness and genes whose disruption is beneficial a positive fitness. A t-score is calculated along with each gene fitness to evaluate how reliably different from zero the gene fitness is. The t-score is a moderated t-statistic calculated as the ratio of the gene fitness and its standard deviation. More details can be found in ***Wetmore et al., 2015***.

In this study, all our experiments and genes fitness values met the quality requirements to be further analyzed (***Figure 1—figure supplement 7***).

Keio collection mutant competition assays for RB-TnSeq validation

We used mutants from the Keio collection to validate the genes identified by RB-TnSeq as having a significant fitness in *E. coli* growth alone on CCA (see list in ***Figure 1—figure supplement 5***). Each mutant was grown in a competition assay with the non-kanamycin resistant wild-type (Keio ME9062 –(***Baba et al., 2006***)). 1000 cells of a specific mutant were inoculated with 1000 cells of the wild type (WT) on the surface of the same cheese plug in a 96 well plate containing 10% CCA, pH7. The number of the mutant cells and the WT cells were calculated at T0 and day one after harvesting and homogenizing the cheese plug, plating serial dilutions and counting CFUs. Experimental fitness of each mutant was calculated as the log2 of the ratio of the mutant abundance (mutant CFUs divided by total CFUs (WT +mutant)) after 24 hr and its abundance at T0.

RNASeq and differential expression analysis

RNASeq library preparation

Libraries were prepared in duplicate for the following conditions: *E. coli* growth alone, with *H. alvei*, with *G. candidum*, with *P. camemberti* and with the community for T = 24 hr, 48 hr and 72 hr. RNA samples from the *E. coli* BarSeq experiment were used to produce the RNASeq library.

Each library was prepared as follows. First, RNA samples were treated with DNAse using the 'Rigorous DNAse treatment' for the Turbo DNA-free kit (AMBION, Life Technologies, Waltham, MA) and RNA concentration was measured by nucleic acid quantification in Epoch Microplate Spectrophotometer (BioTek, Winooski, VT). Then, transfer RNAs and 5S RNA were removed using the MEGAclear Kit Purification for Large Scale Transcription Reactions (AMBION, Life Technologies) following manufacturer instructions. Absence of tRNA and 5S RNA was verified by running 100 ng of RNA on a 1.5% agarose gel and RNA concentration was quantified by nucleic acid quantification in Epoch Microplate Spectrophotometer. Also, presence of trace amounts of genomic DNA was assessed by PCR using universal bacterial 16S PCR primers (Forward primer: AGAGTTTGATCCTGGCTCAG, Reverse Primer: GGTTACCTTGTTACGACTT). The PCR was performed in a final volume of 20 µL: 10 µL of Q5 polymerase master mix (New England Biolabs), 0.5 µL of forward primer 10 uM, 0.5 µL of reverse primer 10 uM and 5 µL of non-diluted RNA. PCR products were run on a 1.7% agarose gel and if genomic DNA was amplified, another DNAse treatment was performed as well as a new verification of absence of genomic DNA. Ribosomal RNA depletion was performed using the Ribo-Zero rRNA removal kit by Illumina (Illumina, San Diego, CA). According to manufacturer instructions; we used 1 µL of RiboGuard RNAse Inhibitor in each sample as suggested and followed instructions for 1–2.5 ug of RNA input and we used a 2:1 mix of bacterial Ribo-Zero Removal solution and yeast Ribo-Zero Removal solution. rRNA depleted samples were recovered in 10 µL after ethanol precipitation. Concentrations after ribodepletion were measured using Qubit RNA HS Assay Kits (Invitrogen). The RNASeq library was produced using the NEBNextUltraTM RNA Library Prep Kit for Illumina for purified mRNA or ribosome depleted RNA. We prepared a library with fragments size of 300 nucleotides and used the 10 uM NEBNext Multiplex Oligos for Illumina (Set 1, NEB #E7335) lot 0091412 and the NEBNext multiplex Oligos for Illumina (Set 2, NEB #E7500) lot 0071412. We performed PCR product purification with 0.8X Agencourt AMPure XP Beads instead of 0.9X. Library samples were quantified with Qubit DNA HS Assay Kits before the quality and fragment size were validated by TapeStation (HiSensD1000 ScreenTape). Library samples were pooled at a concentration of 15 nM each and were sequenced on HiSeq4000 (50 bp, single-end).

Differential expression analysis

RNASeq reads were mapped to the concatenated genome of *Escherichia coli* K12 BW25113 (***Grenier et al., 2014***) and *H. alvei* using Geneious version R9 9.1.3 (http://www.geneious.com, [***Kearse et al., 2012***]). Only the reads that uniquely mapped to a single location on the *E. coli* genome section were conserved. *E. coli* and *H. alvei* genome are divergent enough so 50 nucleotide reads potentially originating from *H. alvei* mRNA would not map to the *E. coli* genome and few reads from *E. coli* would map on the *H. alvei* genome.

E. coli expression analysis was performed using the following R packages: Rsamtool (R package version 1.30.0), GenomeInfoDb (R package version 1.14.0.), GenomicFeatures (***Lawrence et al., 2013***), GenomicAlignments, GenomicRanges (***Lawrence et al., 2013***) and DESeq2 (***Love et al., 2015***). We followed the workflow described by Love et al. and performed the differential expression

analysis using the package DESeq2. Differentially expressed genes between two conditions were selected with an adjusted p-value lower than 1% (Benjamini-Hochberg correction for multiple testing) and an absolute log2 of fold change equal to or greater than 1.

KEGG pathway enrichment analysis

Functional enrichment analysis was performed using the R package clusterProfiler (***Yu et al., 2012***). We used the latest version of the package org.EcK12.eg.db for *E. coli* annotations (R package version 3.5.0.). We used Benjamini-Hochberg for multiple comparison correction and only the KEGG pathways enriched with an adjusted p-value lower than 5% were considered.

Acknowledgments

The authors would like to thank: the Arkin lab and the Deutschbauer lab at UC-Berkeley for the *E. coli* Keio_ML9 library and their help for the RB-TnSeq analysis, Steven Villareal and Tyler Nelson for their help in the competitive assays, Kristen Jepsen at the IGM Genomics Center at the University of California San Diego for assistance with sequencing, Ben Wolfe and Sandeep Venkataram for their constructive comments on this work as well as all the Dutton lab members for their input. Nanopore sequencing of *P. psychrophila* JB418 was supported in part by NSF Grant No. PHY17-48958, NIH Grant No. R25GM067110, and the Gordon and Betty Moore Foundation Grant No. 2919.01

Additional information

Funding

Funder	Grant reference number	Author
CJS INRA/INRIA		Manon Morin
National Institutes of Health	5 T32 GM 7240-40	Emily C Pierce
David and Lucile Packard Foundation	#2016-65131	Rachel J Dutton
Pew Charitable Trusts	Pew Scholar in Biomedical Sciences	Rachel J Dutton
National Institutes of Health	P50 GM068763	Rachel J Dutton

The funders had no role in study design, data collection and interpretation, or the decision to submit the work for publication.

Author contributions

Manon Morin, Conceptualization, Data curation, Software, Formal analysis, Validation, Investigation, Visualization, Methodology, Writing—original draft, Writing—review and editing; Emily C Pierce, Data curation, Software, Formal analysis, Investigation, Visualization, Writing—review and editing; Rachel J Dutton, Conceptualization, Resources, Data curation, Supervision, Funding acquisition, Writing—original draft, Project administration, Writing—review and editing

Author ORCIDs

Manon Morin http://orcid.org/0000-0003-2158-0473
Emily C Pierce http://orcid.org/0000-0002-9960-0270
Rachel J Dutton http://orcid.org/0000-0002-2944-2182

Decision letter and Author response

Decision letter https://doi.org/10.7554/eLife.37072.031
Author response https://doi.org/10.7554/eLife.37072.032

Additional files

Supplementary files

• Supplementary file 1. Differential expression analysis of *E. coli* growth in community versus pairwise conditions. We used RNASeq to investigate changes in *E. coli* gene expression between growth in the community and in each pairwise conditions (with *H. alvei*, *G. candidum* or *P. camemberti*). Using DESeq2 (***Love et al., 2015***), we identified up and downregulated genes during growth in community versus growth in each pairwise condition individually. Only genes associated with an adjusted p-value lower than 1% (Benjamini-Hochberg correction for multiple testing) and an absolute log of fold change higher than one were considered differentially expressed.

DOI: https://doi.org/10.7554/eLife.37072.024

• Transparent reporting form

DOI: https://doi.org/10.7554/eLife.37072.025

Data availability

The Pseudomonas psychrophila JB418 genome is publicly available at https://img.jgi.doe.gov/ (IMG Genome ID 2751185442).

The following dataset was generated:

Author(s)	Year	Dataset title	Dataset URL	Database, license, and accessibility information
Rachel J Dutton, Emily C Pierce	2017	Pseudomonas psychrophila JB418	https://img.jgi.doe.gov/cgi-bin/m/main.cgi?section=TaxonDetail&page=taxonDetail&taxon_oid=2751185442	Publicly available at the IMG website (Genome ID 2751185442)

References

Albar AH, Almehdar HA, Uversky VN, Redwan EM. 2014. Structural heterogeneity and multifunctionality of lactoferrin. *Current Protein & Peptide Science* **15**:778–797. DOI: https://doi.org/10.2174/1389203715666140919124530, PMID: 25245670

Baba T, Ara T, Hasegawa M, Takai Y, Okumura Y, Baba M, Datsenko KA, Tomita M, Wanner BL, Mori H. 2006. Construction of Escherichia coli K-12 in-frame, single-gene knockout mutants: the keio collection. *Molecular Systems Biology* **2**:2006.0008. DOI: https://doi.org/10.1038/msb4100050, PMID: 16738554

Belenguer A, Duncan SH, Calder AG, Holtrop G, Louis P, Lobley GE, Flint HJ. 2006. Two routes of metabolic cross-feeding between Bifidobacterium adolescentis and butyrate-producing anaerobes from the human gut. *Applied and Environmental Microbiology* **72**:3593–3599. DOI: https://doi.org/10.1128/AEM.72.5.3593-3599.2006, PMID: 16672507

Billick I, Case TJ. 1994. Higher order interactions in ecological communities: what are they and how can they be detected? *Ecology* **75**:1529–1543. DOI: https://doi.org/10.2307/1939614

Boutrou R, Aziza M, Amrane A. 2006b. Enhanced proteolytic activities of Geotrichum candidum and Penicillium camembertii in mixed culture. *Enzyme and Microbial Technology* **39**:325–331. DOI: https://doi.org/10.1016/j.enzmictec.2005.11.003

Boutrou R, Guéguen M. 2005. Interests in Geotrichum candidum for cheese technology. *International Journal of Food Microbiology* **102**:1–20. DOI: https://doi.org/10.1016/j.ijfoodmicro.2004.12.028, PMID: 15924999

Boutrou R, Kerriou L, Gassi J-Y. 2006a. Contribution of Geotrichum candidum to the proteolysis of soft cheese. *International Dairy Journal* **16**:775–783. DOI: https://doi.org/10.1016/j.idairyj.2005.07.007

Cashel M, Rudd KE. 1996. The Stringent Response. In: Neidhart FC, Ingraham JL, Brooks L. K, Magasanik B, Schaechter M, Edwin U. H (Eds). *Escherichia coli and Salmonella; Cellular and Molecular Biology 2*. American Society for Microbiology. p. 1410–1438.

Chorianopoulos NG, Giaouris ED, Kourkoutas Y, Nychas GJ. 2010. Inhibition of the early stage of Salmonella enterica serovar Enteritidis biofilm development on stainless steel by cell-free supernatant of a Hafnia alvei culture. *Applied and Environmental Microbiology* **76**:2018–2022. DOI: https://doi.org/10.1128/AEM.02093-09, PMID: 20097823

Coia JE, Johnston Y, Steers NJ, Hanson MF. 2001. A survey of the prevalence of Escherichia coli O157 in raw meats, raw cow's milk and raw-milk cheeses in south-east Scotland. *International Journal of Food Microbiology* **66**:63–69. DOI: https://doi.org/10.1016/S0168-1605(00)00490-6, PMID: 11407549

Croucher NJ, Thomson NR. 2010. Studying bacterial transcriptomes using RNA-seq. *Current Opinion in Microbiology* **13**:619–624. DOI: https://doi.org/10.1016/j.mib.2010.09.009, PMID: 20888288

De Vuyst L, Leroy F. 2011. Cross-feeding between bifidobacteria and butyrate-producing colon bacteria explains bifdobacterial competitiveness, butyrate production, and gas production. *International Journal of Food Microbiology* **149**:73–80. DOI: https://doi.org/10.1016/j.ijfoodmicro.2011.03.003, PMID: 21450362

Dieuleveux V, Van Der Pyl D, Chataud J, Gueguen M. 1998. Purification and characterization of anti-Listeria compounds produced by Geotrichum candidum. *Applied and Environmental Microbiology* **64**:800–803. PMID: 9464426

Dorel C, Lejeune P, Rodrigue A. 2006. The Cpx system of Escherichia coli, a strategic signaling pathway for confronting adverse conditions and for settling biofilm communities? *Research in Microbiology* **157**:306–314. DOI: https://doi.org/10.1016/j.resmic.2005.12.003, PMID: 16487683

Falkowski PG, Fenchel T, Delong EF. 2008. The microbial engines that drive Earth's biogeochemical cycles. *Science* **320**:1034–1039. DOI: https://doi.org/10.1126/science.1153213, PMID: 18497287

Faust K, Raes J. 2012. Microbial interactions: from networks to models. *Nature Reviews Microbiology* **10**:538–550. DOI: https://doi.org/10.1038/nrmicro2832, PMID: 22796884

Flint HJ, Scott KP, Louis P, Duncan SH. 2012. The role of the gut microbiota in nutrition and health. *Nature Reviews Gastroenterology & Hepatology* **9**:577–589. DOI: https://doi.org/10.1038/nrgastro.2012.156, PMID: 22945443

Frank JF, Marth EH, Olson NF. 1977. Survival of Enteropathogenic and Non-Pathogenic Escherichia coli During the Manufacture of Camembert Cheese. *Journal of Food Protection* **40**:835–842. DOI: https://doi.org/10.4315/0362-028X-40.12.835

Freilich S, Zarecki R, Eilam O, Segal ES, Henry CS, Kupiec M, Gophna U, Sharan R, Ruppin E. 2011. Competitive and cooperative metabolic interactions in bacterial communities. *Nature Communications* **2**:589. DOI: https://doi.org/10.1038/ncomms1597, PMID: 22158444

Friedman J, Higgins LM, Gore J. 2017. Community structure follows simple assembly rules in microbial microcosms. *Nature Ecology & Evolution* **1**:109. DOI: https://doi.org/10.1038/s41559-017-0109, PMID: 28812687

Galia W, Leriche F, Cruveiller S, Garnier C, Navratil V, Dubost A, Blanquet-Diot S, Thevenot-Sergentet D. 2017. Strand-specific transcriptomes of Enterohemorrhagic Escherichia coli in response to interactions with ground beef microbiota: interactions between microorganisms in raw meat. *BMC Genomics* **18**:574. DOI: https://doi.org/10.1186/s12864-017-3957-2, PMID: 28774270

Gambino M, Cappitelli F. 2016. Mini-review: Biofilm responses to oxidative stress. *Biofouling* **32**:167–178. DOI: https://doi.org/10.1080/08927014.2015.1134515, PMID: 26901587

Ghrist AC, Heil G, Stauffer GV. 2001. GcvR interacts with GcvA to inhibit activation of the Escherichia coli glycine cleavage operon. *Microbiology* **147**:2215–2221. DOI: https://doi.org/10.1099/00221287-147-8-2215, PMID: 11495998

Ghrist AC, Stauffer GV. 1995. Characterization of the Escherichia coli gcvR gene encoding a negative regulator of gcv expression. *Journal of Bacteriology* **177**:4980–4984. DOI: https://doi.org/10.1128/jb.177.17.4980-4984.1995, PMID: 7665475

Goldford JE, Lu N, Bajić D, Estrela S, Tikhonov M, Sanchez-Gorostiaga A, Segrè D, Mehta P, Sanchez A. 2018. Emergent simplicity in microbial community assembly. *Science* **361**:469–474. DOI: https://doi.org/10.1126/science.aat1168, PMID: 30072533

Goodman AL, McNulty NP, Zhao Y, Leip D, Mitra RD, Lozupone CA, Knight R, Gordon JI. 2009. Identifying genetic determinants needed to establish a human gut symbiont in its habitat. *Cell Host & Microbe* **6**:279–289. DOI: https://doi.org/10.1016/j.chom.2009.08.003, PMID: 19748469

Grenier F, Matteau D, Baby V, Rodrigue S. 2014. Complete genome sequence of Escherichia coli BW25113. *Genome Announcements* **2**. DOI: https://doi.org/10.1128/genomeA.01038-14, PMID: 25323716

Guinee TP. 2004. Salting and the role of salt in cheese. *International Journal of Dairy Technology* **57**:99–109. DOI: https://doi.org/10.1111/j.1471-0307.2004.00145.x

Gunsalus RP. 1992. Control of electron flow in Escherichia coli: coordinated transcription of respiratory pathway genes. *Journal of Bacteriology* **174**:7069–7074. DOI: https://doi.org/10.1128/jb.174.22.7069-7074.1992, PMID: 1331024

Hallatschek O, Hersen P, Ramanathan S, Nelson DR. 2007. Genetic drift at expanding frontiers promotes gene segregation. *PNAS* **104**:19926–19930. DOI: https://doi.org/10.1073/pnas.0710150104, PMID: 18056799

Hider RC, Kong X. 2010. Chemistry and biology of siderophores. *Natural Product Reports* **27**:637–657. DOI: https://doi.org/10.1039/b906679a, PMID: 20376388

Kanehisa M, Sato Y, Morishima K. 2016. BlastKOALA and GhostKOALA: KEGG Tools for Functional Characterization of Genome and Metagenome Sequences. *Journal of Molecular Biology* **428**:726–731. DOI: https://doi.org/10.1016/j.jmb.2015.11.006, PMID: 26585406

Kastman EK, Kamelamela N, Norville JW, Cosetta CM, Dutton RJ, Wolfe BE. 2016. Biotic Interactions Shape the Ecological Distributions of Staphylococcus Species. *mBio* **7**. DOI: https://doi.org/10.1128/mBio.01157-16, PMID: 27795388

Kearse M, Moir R, Wilson A, Stones-Havas S, Cheung M, Sturrock S, Buxton S, Cooper A, Markowitz S, Duran C, Thierer T, Ashton B, Meintjes P, Drummond A. 2012. Geneious Basic: an integrated and extendable desktop software platform for the organization and analysis of sequence data. *Bioinformatics* **28**:1647–1649. DOI: https://doi.org/10.1093/bioinformatics/bts199, PMID: 22543367

Koren S, Walenz BP, Berlin K, Miller JR, Bergman NH, Phillippy AM. 2017. Canu: scalable and accurate long-read assembly via adaptive *k*-mer weighting and repeat separation. *Genome Research* **27**:722–736. DOI: https://doi.org/10.1101/gr.215087.116, PMID: 28298431

Landini P. 2009. Cross-talk mechanisms in biofilm formation and responses to environmental and physiological stress in Escherichia coli. *Research in Microbiology* **160**:259–266. DOI: https://doi.org/10.1016/j.resmic.2009.03.001, PMID: 19345733

Lawrence M, Huber W, Pagès H, Aboyoun P, Carlson M, Gentleman R, Morgan MT, Carey VJ. 2013. Software for computing and annotating genomic ranges. *PLoS Computational Biology* **9**:e1003118. DOI: https://doi.org/10.1371/journal.pcbi.1003118, PMID: 23950696

Love MI, Anders S, Kim V, Huber W. 2015. RNA-Seq workflow: gene-level exploratory analysis and differential expression. *F1000Research* **4**:1070. DOI: https://doi.org/10.12688/f1000research.7035.1, PMID: 26674615

Markowitz VM, Chen IM, Palaniappan K, Chu K, Szeto E, Grechkin Y, Ratner A, Jacob B, Huang J, Williams P, Huntemann M, Anderson I, Mavromatis K, Ivanova NN, Kyrpides NC. 2012. IMG: the Integrated Microbial Genomes database and comparative analysis system. *Nucleic Acids Research* **40**:D115–D122. DOI: https://doi.org/10.1093/nar/gkr1044, PMID: 22194640

McAdam PR, Richardson EJ, Fitzgerald JR. 2014. High-throughput sequencing for the study of bacterial pathogen biology. *Current Opinion in Microbiology* **19**:106–113. DOI: https://doi.org/10.1016/j.mib.2014.06.002, PMID: 25033019

Momeni B, Xie L, Shou W. 2017. Lotka-Volterra pairwise modeling fails to capture diverse pairwise microbial interactions. *eLife* **6**:e25051. DOI: https://doi.org/10.7554/eLife.25051, PMID: 28350295

Monnet C, Back A, Irlinger F. 2012. Growth of aerobic ripening bacteria at the cheese surface is limited by the availability of iron. *Applied and Environmental Microbiology* **78**:3185–3192. DOI: https://doi.org/10.1128/AEM.00085-12, PMID: 22367081

Montet MP, Jamet E, Ganet S, Dizin M, Miszczycha S, Dunière L, Thevenot D, Vernozy-Rozand C. 2009. Growth and survival of Acid-Resistant and Non-Acid-Resistant Shiga-Toxin-Producing Escherichia coli strains during the manufacture and ripening of camembert cheese. *International Journal of Microbiology* **2009**:1–10. DOI: https://doi.org/10.1155/2009/653481, PMID: 20016668

Olson MA, Siebach TW, Griffitts JS, Wilson E, Erickson DL. 2018. Genome-Wide identification of fitness factors in Mastitis-Associated *Escherichia coli*. *Applied and Environmental Microbiology* **84**. DOI: https://doi.org/10.1128/AEM.02190-17, PMID: 29101196

Pacheco AR, Moel M, Segre D. 2018. Costless metabolic secretions as drivers of interspecies interactions in microbial ecosystems. *bioRxiv*. DOI: https://doi.org/10.1101/300046

Price MN, Wetmore KM, Waters RJ, Callaghan M, Ray J, Liu H, Kuehl JV, Melnyk RA, Lamson JS, Suh Y, Carlson HK, Esquivel Z, Sadeeshkumar H, Chakraborty R, Zane GM, Rubin BE, Wall JD, Visel A, Bristow J, Blow MJ, et al. 2018. Mutant phenotypes for thousands of bacterial genes of unknown function. *Nature* **557**:503–509. DOI: https://doi.org/10.1038/s41586-018-0124-0, PMID: 29769716

Raymond KN, Dertz EA, Kim SS. 2003. Enterobactin: an archetype for microbial iron transport. *PNAS* **100**:3584–3588. DOI: https://doi.org/10.1073/pnas.0630018100, PMID: 12655062

Sanchez-Gorostiaga A, Bajić D, Osborne ML, Poyatos JF, Sanchez A. 2018. Deep annotation of protein function across diverse. *bioRxiv*. DOI: https://doi.org/10.1101/333534

Sezonov G, Joseleau-Petit D, D'Ari R. 2007. Escherichia coli physiology in Luria-Bertani broth. *Journal of Bacteriology* **189**:8746–8749. DOI: https://doi.org/10.1128/JB.01368-07, PMID: 17905994

Stubbendieck RM, Straight PD. 2016. Multifaceted Interfaces of Bacterial Competition. *Journal of Bacteriology* **198**:2145–2155. DOI: https://doi.org/10.1128/JB.00275-16, PMID: 27246570

Traxler MF, Seyedsayamdost MR, Clardy J, Kolter R. 2012. Interspecies modulation of bacterial development through iron competition and siderophore piracy. *Molecular Microbiology* **86**:628–644. DOI: https://doi.org/10.1111/mmi.12008, PMID: 22931126

Trmčić A, Chauhan K, Kent DJ, Ralyea RD, Martin NH, Boor KJ, Wiedmann M. 2016. Coliform detection in cheese is associated with specific cheese characteristics, but no association was found with pathogen detection. *Journal of Dairy Science* **99**:6105–6120. DOI: https://doi.org/10.3168/jds.2016-11112, PMID: 27289158

van Opijnen T, Camilli A. 2013. Transposon insertion sequencing: a new tool for systems-level analysis of microorganisms. *Nature Reviews Microbiology* **11**:435–442. DOI: https://doi.org/10.1038/nrmicro3033, PMID: 23712350

Wackwitz B, Bongaerts J, Goodman SD, Unden G. 1999. Growth phase-dependent regulation of nuoA-N expression in Escherichia coli K-12 by the Fis protein: upstream binding sites and bioenergetic significance. *Molecular and General Genetics MGG* **262**:876–883. DOI: https://doi.org/10.1007/s004380051153, PMID: 10628873

Walker BJ, Abeel T, Shea T, Priest M, Abouelliel A, Sakthikumar S, Cuomo CA, Zeng Q, Wortman J, Young SK, Earl AM. 2014. Pilon: an integrated tool for comprehensive microbial variant detection and genome assembly improvement. *PLoS One* **9**:e112963. DOI: https://doi.org/10.1371/journal.pone.0112963, PMID: 25409509

Wetmore KM, Price MN, Waters RJ, Lamson JS, He J, Hoover CA, Blow MJ, Bristow J, Butland G, Arkin AP, Deutschbauer A. 2015. Rapid quantification of mutant fitness in diverse Bacteria by sequencing randomly bar-coded transposons. *mBio* **6**:e00306-15. DOI: https://doi.org/10.1128/mBio.00306-15, PMID: 25968644

Wolfe BE, Button JE, Santarelli M, Dutton RJ. 2014. Cheese rind communities provide tractable systems for in situ and in vitro studies of microbial diversity. *Cell* **158**:422–433. DOI: https://doi.org/10.1016/j.cell.2014.05.041, PMID: 25036636

Yu G, Wang LG, Han Y, He QY. 2012. clusterProfiler: an R package for comparing biological themes among gene clusters. *OMICS: A Journal of Integrative Biology* **16**:284–287. DOI: https://doi.org/10.1089/omi.2011.0118, PMID: 22455463

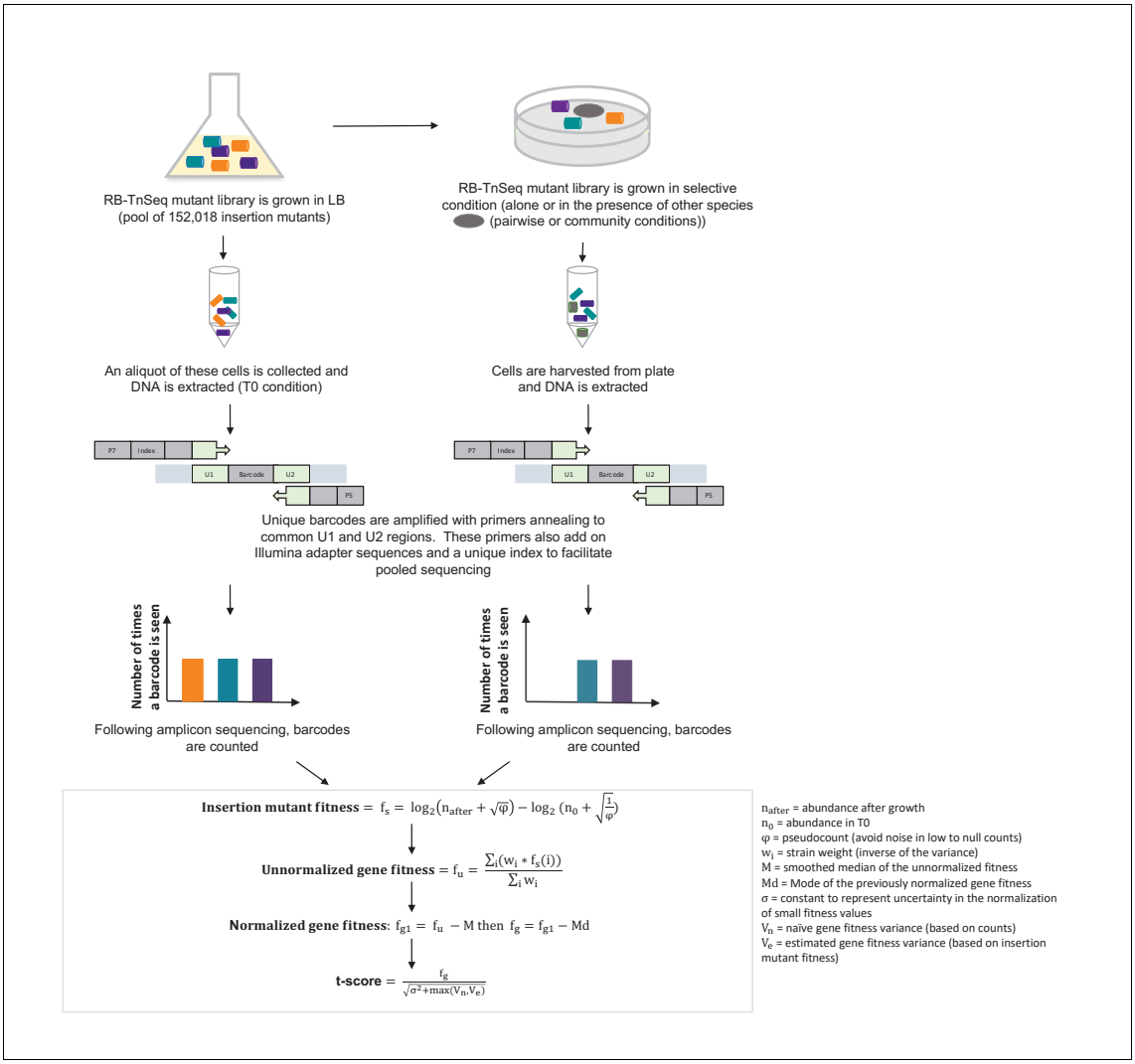

Figure 1—figure supplement 1. Pipeline of RB-TnSeq experiment using the *E. coli* Keio M9 library: from experimental set-up to normalized gene fitness and t-score calculation. Calculation of gene fitness from the Illumina sequencing files was performed using the Perl script BarSeqTest.pl from (***Wetmore et al., 2015***). The detailed description of the pipeline can be found in (***Wetmore et al., 2015***).

DOI: https://doi.org/10.7554/eLife.37072.004

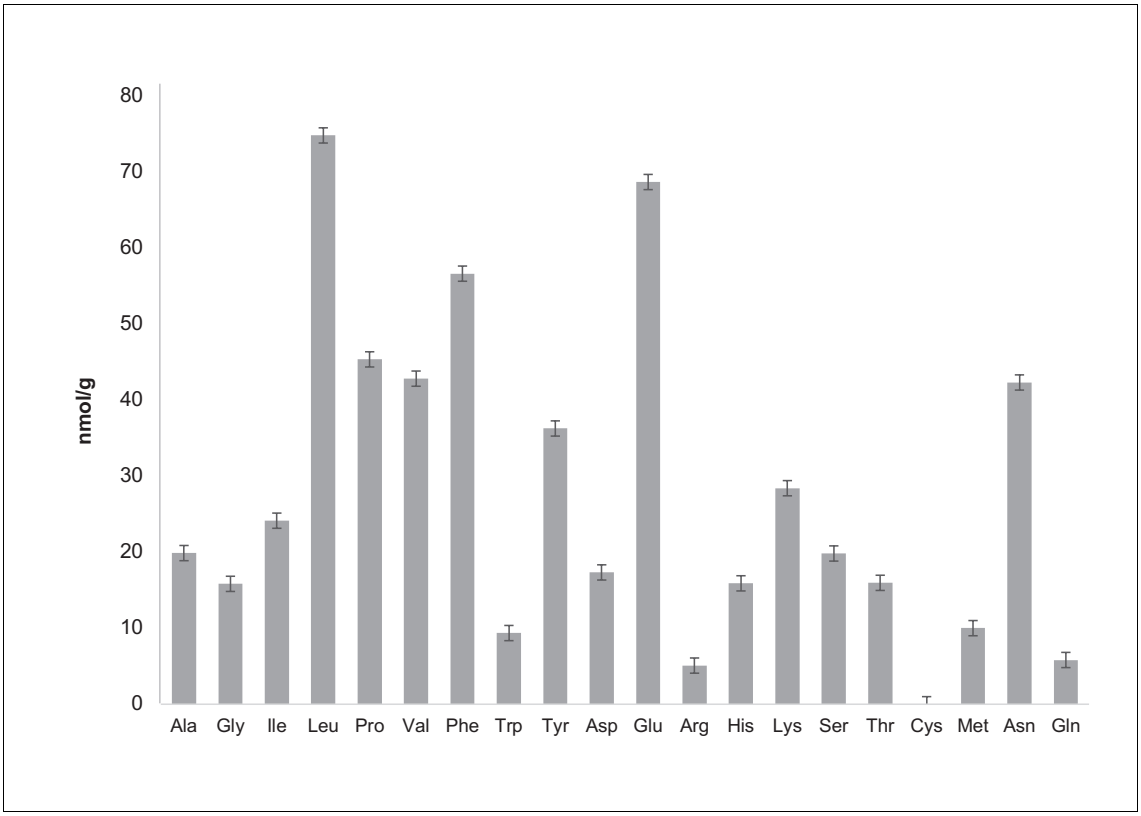

Figure 1—figure supplement 2. Quantification of free amino acids in CCA. Free amino acid characterization and quantification have been carried out by the Proteomics and Mass Spectrometry Facility of the Donald Danforth Plant Science Center and each analysis has been performed in triplicate. Samples were prepared as recommended by the Proteomics and Mass Spectrometry Facility of the Donald Danforth Plant Science Center instructions. For free amino acid analysis, 150 mg CCA was frozen in liquid nitrogen and ground in the presence of 600 µL of water:chloroform:methanol (3:5:12 v/v). Tubes were then centrifuged at full speed for two minutes and supernatant was recovered in a new 2 mL eppendorf tube. A second extraction with 600 uL of water:chloroform:methanol was performed followed by a two minute centrifugation at maximum speed. Supernatant was then recovered and combined with the previous supernatant in a 2 mL eppendorf tube. Then 300 uL of chloroform and 450 uL of water were added before centrifugation at full speed for two minutes. The upper phase was recovered and transferred to a new tube. Samples were dried in a speedvac overnight and stored at −20°C. The total concentration of free amino acids in CCA is 75.3 nmol/mL. Analysis of total amino acids was also performed by the Proteomics and Mass Spectrometry Facility of the Donald Danforth Plant Science Center. It highlights that free aminos are a very small fraction of total amino acid whose concentration is 16.5 ± 2.97 µmol/mL (six times less than the LB concentration measured by ***Sezonov et al. (2007)***). Ala: alanine, Gly: glycine, Ile: isoleucine, Leu: leucine, Pro: proline, Val: valine, Phe: phenylalanine, Trp: tryptophan, Tyr: tyrosine, Asp: aspartate, Glu: glutamate, Arg: arginine, His: histidine, Lys: lysine, Ser: serine, Thr: threonine, Cys: cysteine, Met: methionine, Asn: asparagine, Gln: glutamine.

DOI: https://doi.org/10.7554/eLife.37072.005

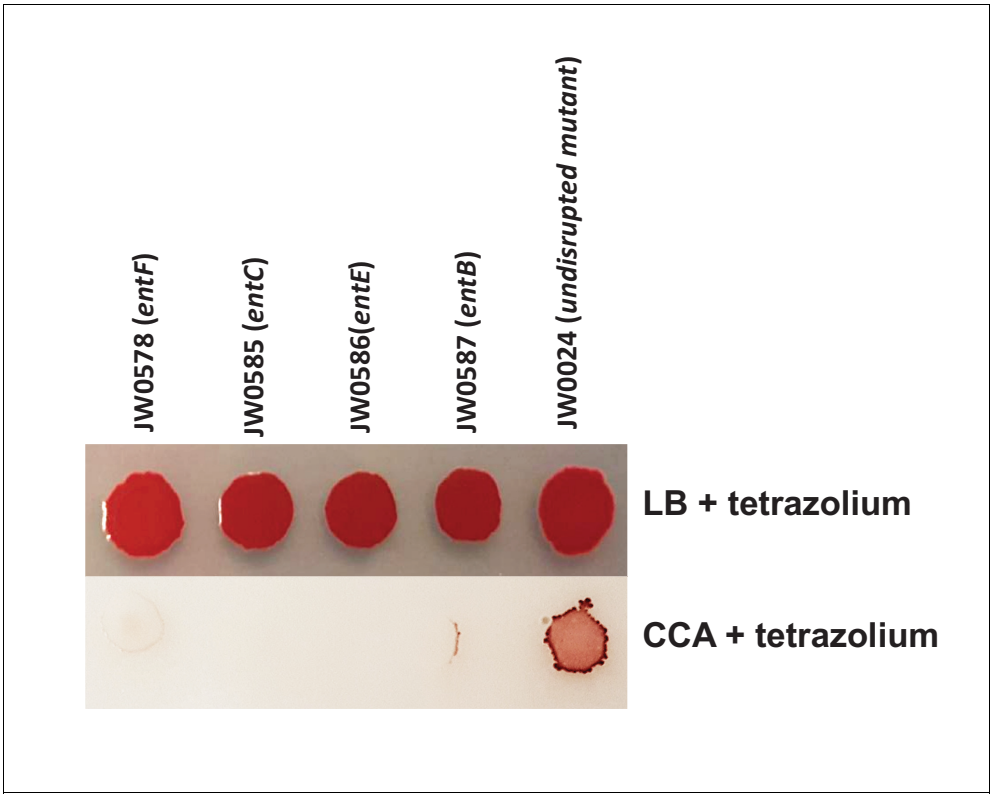

Figure 1—figure supplement 3. Comparison of individual growth of enterobactin biosynthesis mutants on LB and CCA. 5% tetrazolium solution (100 uL/L of medium) was added to the media to color colonies and make them visible on CCA. We selected 4 mutants of enterobactin biosynthesis from the Keio collection. 5 µL of each mutant culture was spotted on either LB-tetrazolium or CCA-tetrazolium and grown at room temperature for 3 days. The wild-type strain JW0024 was used as a control.

DOI: https://doi.org/10.7554/eLife.37072.006

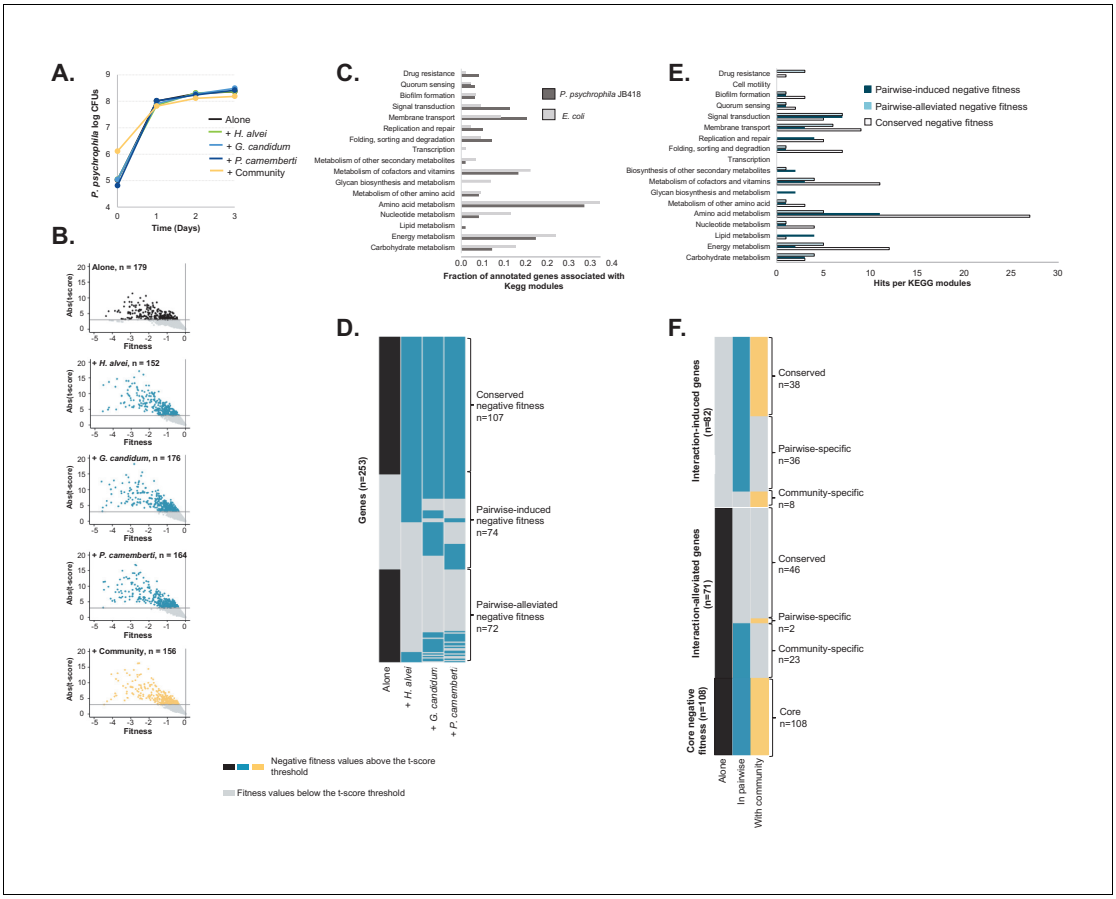

Figure 1—figure supplement 4. RB-TnSeq experiments using the P. psychrophila JB418 library. (**A**) We grew *P. psychrophila* JB418 alone, in pairwise conditions with *H. alvei*, *G. candidum* or *P. camemberti* and with the full community on CCA. (**B**) Using the transposon library of *P. psychrophila* JB418 generated in the laboratory, we identified genes with negative fitness at 1, 2 and 3 days of growth. In each volcanoplot, data from the three timepoints have been grouped. We identified 179 genes important for *P. psychrophila* JB418, 152 genes important for growth with *H. alvei*, 176 genes with *G. candidum*, 164 with *P. camemberti* and 156 genes important for growth with the community (Source data 5). (**C**) We annotated *P. psychrophila* JB418 using KEGG KOALA Blast (***Kanehisa et al., 2016***). 98 of the 179 genes important for growth alone were attributed a KEGG annotation. To compare the relative importance of functions for growth alone observed for *P. psychrophila* JB418 and for *E. coli* we represented, per KEGG module, the ratio between the number of hits for the module and the number of genes with KEGG annotation. (**D**) For *P. psychrophila* JB418, we then compared the genes with negative fitness for growth alone and the genes with negative fitness for growth in pairwise. We identified three categories: (**i**) the core negative fitness: genes with negative fitness for growth alone and all the pairwise conditions, (ii): Pairwise-induced negative fitness: genes with negative fitness in at least one pairwise condition but no negative fitness alone and, (iii): pairwise-alleviated: genes with negative fitness in growth alone and no negative fitness in at least one pairwise condition. (**E**) We further investigated the KEGG functions associated with the core negative fitness, pairwise-induced negative fitness and pairwise alleviated negative fitness. (**F**) We then compared the community-induced negative fitness and community-alleviated negative fitness for *P. psychrophila* JB418 with the pairwise-induced and pairwise-alleviated negative fitness.

DOI: https://doi.org/10.7554/eLife.37072.007

Keio strain	Gene name	RB-TNSeq fitness	Experimental Fitness value	SEM of Experimental Fitness value	z-score
JW3140	argG	-0.43	-1.38	0.06	23.90
JW0391	brnQ	-2.42	-0.45	0.37	1.21
JW3789	corA	-2.27	-4.37	0.30	14.58
JW2407	cysK	-1.38	-1.72	0.91	1.90
JW2974	exbB	-1.42	-1.48	0.05	27.25
JW2973	exbD	-1.46	-3.25	0.08	43.16
JW5086	fepA	-0.95	-1.97	0.46	4.28
JW0584	fepB	-1.11	-1.60	0.13	12.42
JW0580	fepC	-0.80	-3.11	0.74	4.21
JW0582	fepD	-1.02	-3.13	0.64	4.85
JW0581	fepG	-0.76	-2.07	1.02	2.03
JW0576	fes	-1.91	-1.98	0.08	24.75
JW0742	galE	-1.53	-3.69	0.41	8.89
JW2464	gcvR	-1.89	-3.56	0.42	8.54
JW3377	nfuA	-2.70	-4.09	0.29	14.07
JW0018	nhaA	-4.09	-1.82	0.40	4.56
JW3627	recG	-2.10	-0.63	0.28	2.23
JW2755	relA	-0.86	-2.49	0.19	13.39
JW3624	rpoZ	-2.23	-1.17	0.26	4.43
JW2880	serA	-1.54	-0.24	0.30	0.79
JW4351	serB	-2.41	-1.04	0.18	5.81
JW0890	serC	-1.43	-1.01	0.15	6.85
JW5576	trkH	-0.89	-0.57	0.10	5.49
JW5856	trxA	-2.21	-0.75	0.54	1.39
JW3434	zntA	-1.50	-0.64	0.19	3.37

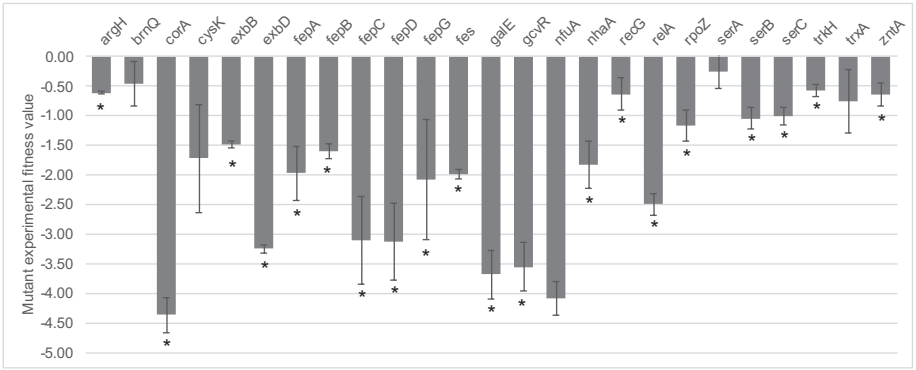

Figure 1—figure supplement 5. Competitive assays of 25 mutants of the Keio collection (***Baba et al., 2006***). Competition assays between single knockouts and the wild-type strain have been carried out for 25 strains associated with genes identified as important for *E. coli* growth using RB-TnSeq (Significant fitness lower than -1 after 1 day of growth). * highlights fitness values different from 0 with a confidence higher than 95%. The competitive assays were performed in at least triplicates. SEM stands for: standard deviation of the mean: $SEM = \frac{\sigma}{\sqrt{n}}$, where $\sigma$is the standard deviation and $n$the number of replicates. Then, $z - score = \frac{0-\mu}{SEM}$where $\mu$is the experimental fitness value (average of the replicates).

DOI: https://doi.org/10.7554/eLife.37072.009

Genome size	6.07 Mbp
Number of protein-coding genes (PCG)	5788
Number of mapped barcodes	272329
Number of mutants with central insertions in PCG	143491
Median of barcode per gene	18
Number of PCG with central insertion	4811

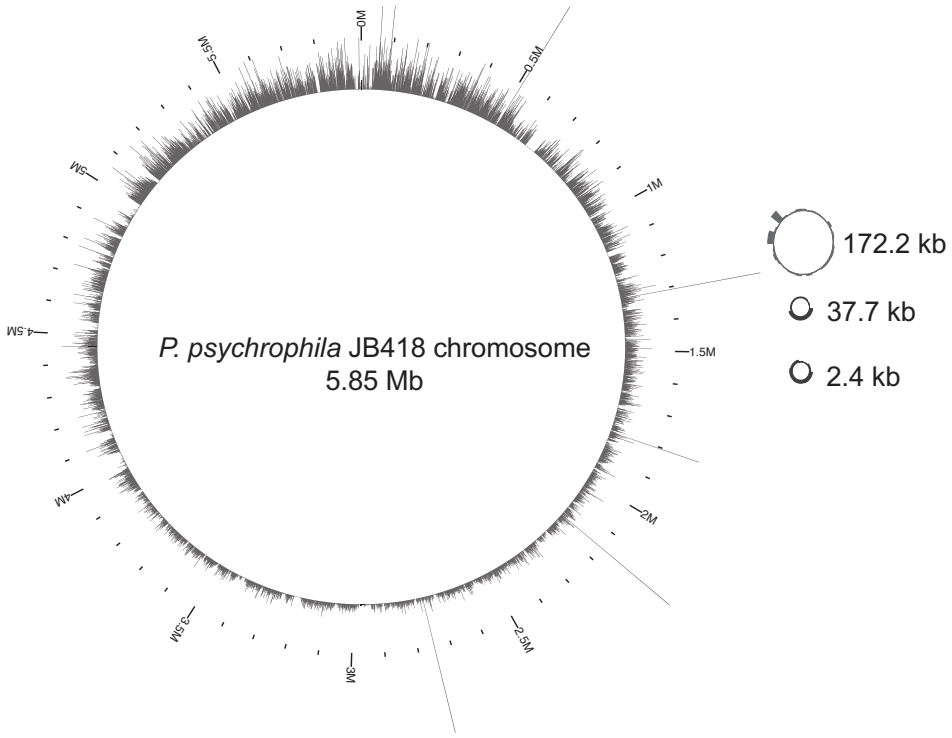

Figure 1—figure supplement 6. Map of the JB418_ECP1 transposon library generated in *P. psychrophila* JB418. We built a barcoded-transposon library in the cheese isolate *P. psychrophila* JB418. 272,329 insertions were mapped to the genome and 143,491 barcodes were located in the central region of a gene. The median of number of insertion mutants per gene is 18, similar to *E. coli*'s library. 4811 genes have at least one insertion in the

Figure 1—figure supplement 6 continued on next page

Figure 1—figure supplement 6 continued

central part of the gene, thus the library covers 83% of *P. psychrophila* JB418 genome. On the chromosome and the plasmids, each bar represents the number of insertions per kb.

DOI: https://doi.org/10.7554/eLife.37072.010

E. coli RB-TnSeq experiments

Sample	gMed	cor12	mad12	adjcor	gccor	quality-test
Alone-Day1	255	0.1723879	0.26568155	0.09779835	0.03594243	TRUE
with *H. alvei* -Day1	784.5	0.16093804	0.22950086	0.01344365	0.10109925	TRUE
with *P. camemberti* -Day1	694	0.15246077	0.24130197	-0.0288577	0.0781625	TRUE
with *G. candidum* -Day 1	615	0.21262254	0.22411822	0.05631649	0.08865255	TRUE
with Community -Day1	705.5	0.16833782	0.22670031	7.35E-05	0.10804874	TRUE
Alone-Day2	210	0.16670639	0.2659591	0.03893953	0.01551325	TRUE
with *H. alvei* -Day2	643	0.20284412	0.22711697	0.06134974	0.08684969	TRUE
with *P. camemberti* -Day2	850.5	0.19586525	0.21875375	-0.0188038	0.06885679	TRUE
with *G. candidum* -Day 2	486.5	0.1828237	0.23211583	-0.0169854	0.08628507	TRUE
with Community -Day2	795	0.18553046	0.22467727	-0.0046128	0.09393122	TRUE
Alone-Day3	277	0.16459242	0.26477063	0.04099767	0.03896542	TRUE
with *H. alvei* -Day3	839.5	0.24571319	0.22925674	0.05041216	0.0668381	TRUE
with *P. camemberti* -Day3	907	0.18509847	0.22954482	-0.0146138	0.06294131	TRUE
with *G. candidum* -Day 3	1013	0.18533261	0.22785847	-0.044744	0.08140464	TRUE
with Community -Day3	814.5	0.1677215	0.23602283	-0.0172009	0.07646943	TRUE

P. psychrophila JB 418 RB-TnSeq experiments

Sample	gMed	cor12	mad12	adjcor	gccor	quality-test
Alone-Day1	99	0.17009447	0.36313709	0.08167588	-0.0248871	TRUE
with *H. alvei* -Day1	315.5	0.25863873	0.26542377	0.13810483	0.00523254	TRUE
with *P. camemberti* -Day1	375	0.23178696	0.28072116	0.09827563	0.01019754	TRUE
with *G. candidum* -Day 1	337	0.28177362	0.265721	0.16133524	0.00608864	TRUE
with Community -Day1	316	0.24654972	0.2770101	0.13833535	0.0128327	TRUE
Alone-Day2	113	0.1955332	0.40382365	0.03113561	-0.0225443	TRUE
with *H. alvei* -Day2	385.5	0.23498414	0.27329519	0.06481841	0.00739981	TRUE
with *P. camemberti* -Day2	312	0.22238257	0.26684366	0.02676088	-0.002133	TRUE
with *G. candidum* -Day 2	301	0.21420476	0.27356635	0.0526742	0.00032401	TRUE
with Community -Day2	285	0.17817419	0.28575851	0.02095246	0.01214387	TRUE
Alone-Day3	87	0.15654554	0.35633263	0.03285248	-0.0118369	TRUE
with *H. alvei* -Day3	403	0.20618922	0.27800945	0.0131201	0.00328971	TRUE
with *P. camemberti* -Day3	310	0.20855776	0.27447156	0.02202981	-0.0002405	TRUE
with *G. candidum* -Day 3	403	0.19856088	0.27713564	0.03743198	0.00727052	TRUE
with Community -Day3	323	0.20256391	0.26672818	0.01716005	0.00867084	TRUE

Figure 1—figure supplement 7. Quality assessment of all RB-TnSeq experiments. For each RB-TnSeq experiment different parameters are calculated to assess the quality of each RB-TnSeq experiment. If all quality parameters are met, then the gene fitness values can be further analyzed. These parameters include: (i) median gene has at least 50 counts (gMed ≥50), (ii) the median of the absolute difference in fitness between the two halves of the gene is less or equal to 0.5 (mad12 ≤0.5), (iii) the Spearman correlation in fitness between the two halves of the gene is at least 0.1 (cor12 ≥0.1), (iv) the correlation between gene GC content and fitness is less or equal to 0.2 (gccor ≤0.2), (v) the Spearman correlation of adjacent genes on different

Figure 1—figure supplement 7 continued on next page

Figure 1—figure supplement 7 continued

insertion mutants is not greater than 0.25 (adjcor ≤0.25), and (vi): the sample is not a T0 sample. More details about these metrics can be found in the supplementary material of Wetmore et al. 2015. All of our RB-TnSeq experiments met the required criteria (quality-test = TRUE).

DOI: https://doi.org/10.7554/eLife.37072.011

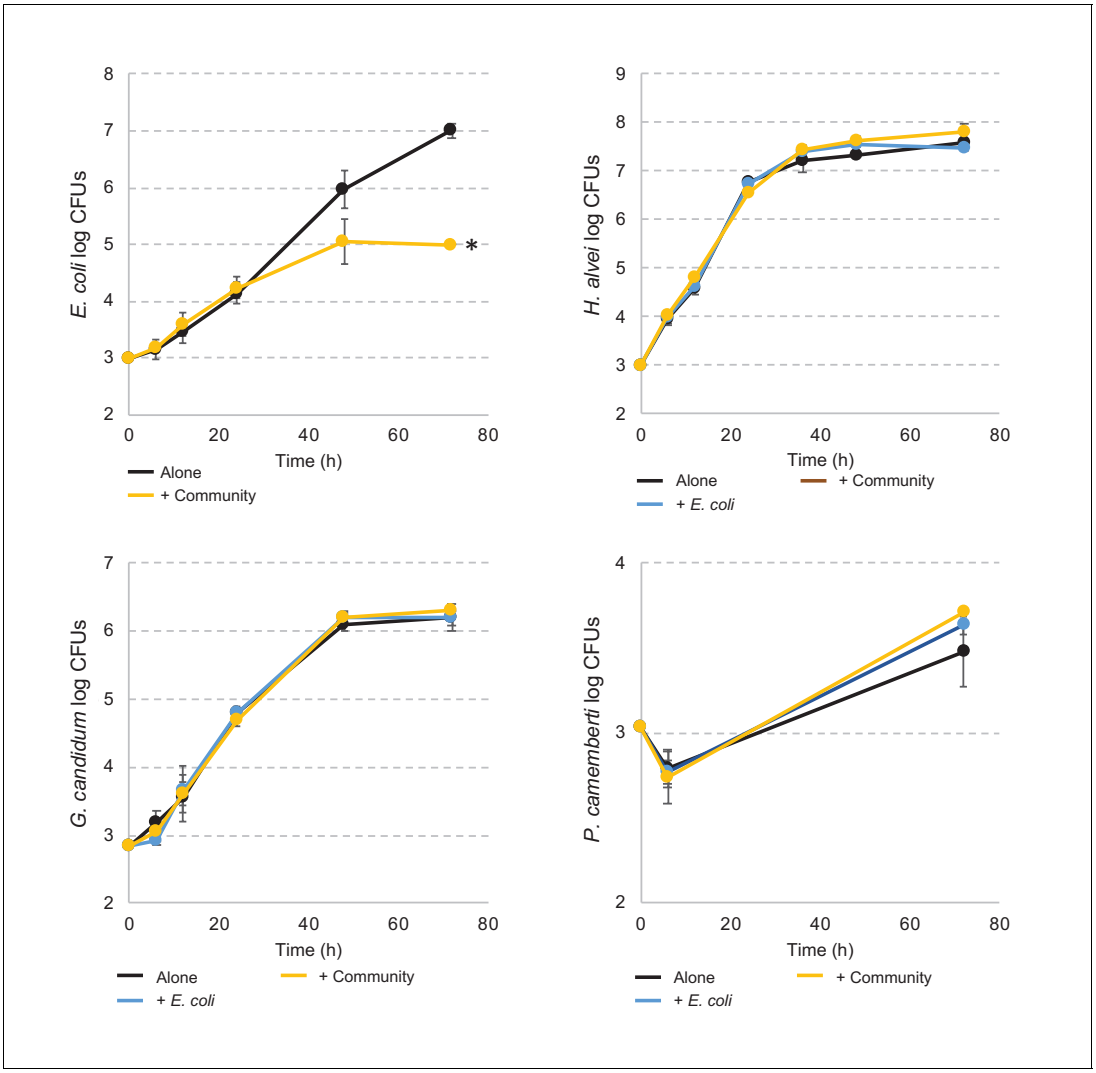

Figure 2—figure supplement 1. *E. coli* and community member growth curves alone, in pairwise conditions or during community growth. Each graph represents the growth over time of *E. coli*, *H. alvei*, *G. candidum*, or *P. camemberti* alone, in pairwise growth or with the community. Assays have been performed in triplicates. Dunnett's tests have been performed for each species at day three to compare the number of CFUs of that species in interactive conditions versus growth alone. * adjusted p-value≤5%.

DOI: https://doi.org/10.7554/eLife.37072.014

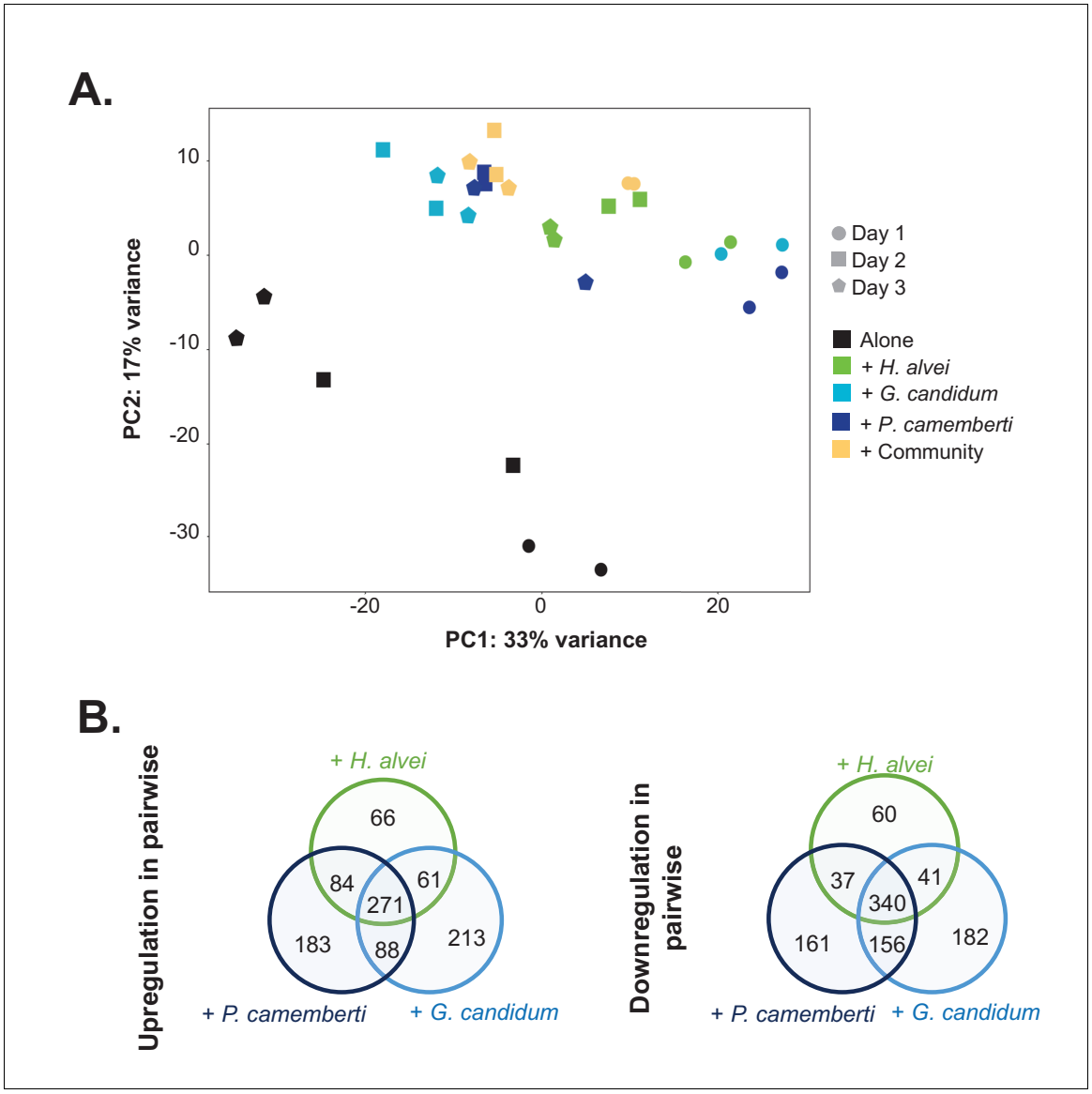

Figure 4—figure supplement 1. RNASeq analysis of *E. coli* gene expression during growth alone and in pairwise conditions. We used RNASeq to investigate *E. coli* gene expression at three timepoints (1, 2 and 3 days) during growth on CCA alone, in pairwise conditions (with *H. alvei*, *G. candidum* or *P. camemberti*) and with the community. (**A**) We carried out a principal component analysis on the rlog transformed expression data (***Love et al., 2015***). (**B**) For each pairwise condition, we identified up and downregulated genes compared to alone at each timepoint. Then, for each pairwise condition, we pooled together upregulated genes at any timepoint and did the same for downregulated genes. Comparing the up or downregulated genes in the different pairwise conditions, we observe overlapping as well as specific responses depending on the partner.

DOI: https://doi.org/10.7554/eLife.37072.020

2.3 Acknowledgments

Chapter 2 is made up of a reprint of the following published manuscript: Morin, Manon, Emily C. Pierce, and Rachel J. Dutton. Changes in the genetic requirements for microbial interactions with increasing community complexity. *elife* 7 (2018): e37072. The dissertation author was the secondary author of this paper.

CHAPTER 3: The Genetic Basis of Diverse Bacterial-Fungal Interactions

3.1 Chapter Summary

Chapter 2 described how we used pre-existing tools to identify genes impacting bacterial fitness in a 3-member model cheese community. Chapter 3 describes the work that followed this initial study. In the process of completing the *eLife* manuscript, we realized that the available RB-TnSeq analysis tools did not fully enable the desired analyses. Namely, we wanted to quantitatively compare gene fitness values between alone and interactive conditions in order to statistically group genes into categories of those having or not having a differential fitness in the presence of a growth partner. In the *eLife* paper, we were able to make hypotheses based on comparing lists of genes that were significant in each condition, but for genes significant in multiple conditions, we had no power to say whether the gene fitness values across these conditions were the same or different. One of the goals following this paper was thus to develop a set of computational tools to accomplish this.

The second goal of the succeeding work was to delve into the genetic basis of bacterial-fungal interactions across a diverse set of interaction partners. Previous work in cheese rind communities had shown that fungi impact bacterial growth (Wolfe et al. 2014), bacterial dispersal (Zhang et al. 2018), and bacterial community composition (Kastman et al. 2016), suggesting that cheese is a powerful model system for studying bacterial-fungal interactions. We therefore aimed to use RB-TnSeq to investigate fungal impacts on bacteria using a range of cheese-associated fungal species (both yeasts and filamentous fungi).

These two goals were accomplished in the *Nature Microbiology* paper presented in Section 3.2, on which I am first author. In this work, we characterized bacterial-fungal

interactions across 16 bacterial-fungal pairs. Fungal partners included 8 cheese-associated fungi, and bacterial partners included *E. coli* and a cheese-associated *Pseudomonas psychrophila.* We collaborated with other labs to enable the use of a combination of RB-TnSeq, RNA-Seq, metabolomics (Sanchez lab, University of Illinois at Chicago), bacterial cytological profiling (Pogliano lab, University of California San Diego), and fungal genetics (Keller lab, University of Wisconsin-Madison) to identify key themes in these interactions. These themes included fungal provision of access to iron, competition for biotin, and fungal production of antimicrobial molecules. This paper also describes a custom R computational pipeline designed for quantitative comparison of multiple RB-TnSeq conditions.

3.2 Characterization of Bacterial-Fungal Interactions using RB-TnSeq

nature microbiology

ARTICLES

https://doi.org/10.1038/s41564-020-00800-z

Check for updates

Bacterial–fungal interactions revealed by genome-wide analysis of bacterial mutant fitness

Emily C. Pierce[1], Manon Morin[1], Jessica C. Little[2], Roland B. Liu[1], Joanna Tannous[3], Nancy P. Keller[3,4,5], Kit Pogliano[1], Benjamin E. Wolfe[6], Laura M. Sanchez[2] and Rachel J. Dutton[1,7]✉

Microbial interactions are expected to be major determinants of microbiome structure and function. Although fungi are found in diverse microbiomes, their interactions with bacteria remain largely uncharacterized. In this work, we characterize interactions in 16 different bacterial–fungal pairs, examining the impacts of 8 different fungi isolated from cheese rind microbiomes on 2 bacteria (*Escherichia coli* and a cheese-isolated *Pseudomonas psychrophila*). Using random barcode transposon-site sequencing with an analysis pipeline that allows statistical comparisons between different conditions, we observed that fungal partners caused widespread changes in the fitness of bacterial mutants compared to growth alone. We found that all fungal species modulated the availability of iron and biotin to bacterial species, which suggests that these may be conserved drivers of bacterial–fungal interactions. Species-specific interactions were also uncovered, a subset of which suggested fungal antibiotic production. Changes in both conserved and species-specific interactions resulted from the deletion of a global regulator of fungal specialized metabolite production. This work highlights the potential for broad impacts of fungi on bacterial species within microbiomes.

Despite growing awareness that fungi have an immense capacity to affect ecosystems, fungi are frequently overlooked in microbiome studies[1,2]. Recently, fungi and other microeukaryotes have received increased attention in sequencing-based studies[3–6], and there is growing interest in exploring the roles that fungi and bacterial–fungal interactions play in environmental and host-associated microbiomes[7–10]. While specific interaction mechanisms have been elucidated for pairwise bacterial–fungal associations, including important pathogenic bacteria and fungi[11–14], analysing a greater diversity of bacterial–fungal interactions could lead to a better ability to predict when and how these interactions contribute to microbiome diversity and function. However, a broader characterization of bacterial–fungal interactions has been challenging given the complexity of many microbiomes.

Cheese rind biofilms have been developed as experimentally tractable systems to study microbiomes. These multi-kingdom biofilms form on the surface of cheese during the ageing process. Prior work using this system has demonstrated that fungi can affect bacterial growth[15]. For example, fungi were shown to cross-feed amino acids to bacteria when grown on a cheese-based medium[16]. Fungal hyphal networks can also alter the composition of a rind microbiome community by providing a means of dispersal for certain community members[17].

Here, we combined the high-throughput genetic screening method random barcode transposon-site sequencing (RB-TnSeq)[18] with RNA sequencing (RNA-seq), bacterial cytological profiling and metabolomics to investigate bacterial–fungal interactions. Building on existing tools, we created a customized computational RB-TnSeq[18] pipeline that enabled us to specifically examine the differences in bacterial growth alone versus in the presence of a fungal partner to highlight pathways that are important during interactions. We examined pairwise combinations of eight fungal species isolated from cheese rinds (two yeasts and six filamentous fungi) and two bacteria, *Pseudomonas psychrophila* strain (str.) JB418 and *Escherichia coli* K12.

We observed broad changes in bacterial mutant fitness in the presence of fungi compared to growth alone. A consistent impact across fungal species was the alleviation of the requirement by *E. coli* for its own siderophore, enterobactin. Further genetic analysis suggested that this alleviation is due to the uptake of siderophores produced by filamentous fungi. We observed similar alleviation when *E. coli* was grown with soil and skin fungi, which suggests that fungal siderophores may affect bacterial growth in other systems. In addition, we found evidence to indicate that fungi increase the need for biotin biosynthesis in both *E. coli* and *P. psychrophila*. Furthermore, multiple lines of evidence suggested that several filamentous fungal species produce antimicrobials. Deletion of *laeA*, a gene encoding a global regulator of fungal specialized metabolite production, led to a large decrease in the number of affected pathways in bacteria, which suggests that specialized metabolites play an important role in bacterial–fungal interactions.

Results

Characterization of bacterial genes with differential fitness in the presence of fungal partners. We selected a panel of eight fungi commonly found in cheese rind microbiomes, all of which belong to the phylum Ascomycota (Fig. 1). They include two yeasts, *Candida* sp. str. 135E and *Debaryomyces* sp. str. 135B, and six filamentous fungi, *Penicillium* sp. str. 12, *Penicillium* sp. str. SAM3, *Penicillium* sp. str. RS17, *Fusarium* sp. str. 554A, *Scopulariopsis* sp. str. JB370 and *Scopulariopsis* sp. str. 165-5. These genera are also found in the human gut mycobiome[19], in soil microbiomes[20], in other agricultural microbiomes[21] and in marine environments[22].

[1]Division of Biological Sciences, University of California, San Diego, La Jolla, CA, USA. [2]Department of Pharmaceutical Sciences, College of Pharmacy, University of Illinois at Chicago, Chicago, IL, USA. [3]Department of Medical Microbiology and Immunology, University of Wisconsin–Madison, Madison, WI, USA. [4]Department of Bacteriology, University of Wisconsin–Madison, Madison, WI, USA. [5]Food Research Institute, University of Wisconsin–Madison, Madison, WI, USA. [6]Department of Biology, Tufts University, Medford, MA, USA. [7]Center for Microbiome Innovation, Jacobs School of Engineering, University of California, San Diego, La Jolla, CA, USA. ✉e-mail: rjdutton@ucsd.edu

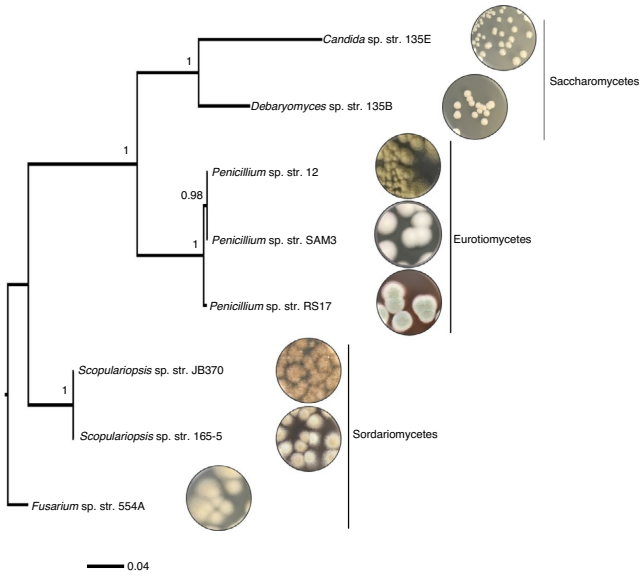

Fig. 1 | Fungal interaction partners span the phylogenetic and morphological diversity of the cheese ecosystem. A phylogenetic tree based on the large subunit ribosomal RNA of the cheese fungi used as interaction partners in this study. The tree was built using Bayesian phylogenetic inference with MrBayes[68] and the Jukes and Cantor substitution model[98]. Branch labels display posterior probability values.

The selected bacterial interaction partners were two species of Gammaproteobacteria, *P. psychrophila* str. JB418 and *E. coli* K12 BW25113. Proteobacteria are common inhabitants of cheese rind communities and are responsive to the presence of fungi in experimental community conditions[15] (Supplementary Figs. 1 and 2). *P. psychrophila* str. JB418 was originally isolated from a cheese rind. *E. coli* K12 was selected as a bacterial partner to take advantage of the genetic resources available for this organism. Furthermore, *E. coli* can be a causative agent of foodborne illness in cheese and other foods[23,24].

Using a pooled library of barcoded transposon-insertion mutants, RB-TnSeq[18] generates a fitness value for each gene that reflects the importance of a gene for survival in the experimental condition. A negative fitness value indicates that disruption of a given gene leads to decreased growth relative to a wild-type (WT) strain, whereas a positive value indicates enhanced growth, with values further from 0 indicating stronger effects of gene disruption. To identify bacterial mutants with a significantly different fitness value in the presence of a fungal partner compared to growth alone, pooled *P. psychrophila*[16] or *E. coli*[18] RB-TnSeq mutant libraries were grown for 7 days on solid cheese curd agar (CCA) plates[25] either alone or mixed with one of the eight fungal species. As sporulation is associated with production of many fungal specialized metabolites, we selected the 7-day time point to capture interactions related to these metabolites[26]. A custom computational pipeline allowed us to quantitatively compare fitness values between conditions (Extended Data Fig. 1 and Supplementary Method 1; https://github.com/DuttonLab/RB-TnSeq-Microbial-interactions). The difference between these fitness values is hereafter referred to as 'interaction fitness' (Fig. 2 and Extended Data Fig. 2). In some cases, the presence of a fungus increased the fitness of a mutant (positive interaction fitness), whereas in others, the fitness of a mutant decreased (negative interaction fitness) (Supplementary Tables 1 and 2).

In total, we found 731 *E. coli* and 1,606 *P. psychrophila* genes whose disruption led to a change in fitness in the presence of at least one of the fungal partners (Supplementary Tables 3 and 4). This represents an average of 216 ± 50 *E. coli* genes per fungal condition and 576 ± 122 *P. psychrophila* genes per fungal condition that have an interaction fitness. For *E. coli*, interaction fitness values ranged from −5.66 to 5.71, and for *P. psychrophila*, −6.18 to 5.74, which highlights the large positive and negative impacts of fungi on bacteria.

To assess the degree of conservation of these fitness effects, we identified homologous genes between *E. coli* and *P. psychrophila* (Supplementary Tables 5 and 6 and Extended Data Fig. 3). The set of 88 genes with interaction fitness for both *E. coli* and *P. psychrophila* in the same set of fungal conditions was enriched for genes in amino acid biosynthesis, including isoleucine/valine biosynthesis. The isoleucine/valine biosynthesis genes have a negative interaction fitness with both bacteria, which suggests that fungi may be competing for amino acids available from cheese (Supplementary Table 7). We have previously seen[16] that these genes are important for *E. coli* growth alone on cheese, which suggests that these amino acids may be limited in this medium.

To assess the specificity of fungal impacts on bacteria, we evaluated the intersections of gene sets across the entire set of fungal interaction conditions (Fig. 3a, Extended Data Fig. 4 and Supplementary Tables 8 and 9). Around 21% ($n = 152$) of the interaction-related genes for *E. coli* and 32% ($n = 508$) for *P. psychrophila* were common to at least four out of the eight fungal interaction conditions (Fig. 3b). In addition to conserved effects, we observed a large number of fungal species-specific effects. For *E. coli*, 45% of the genes with interaction fitness were specific to a single fungus ($n = 329$), whereas for *P. psychrophila*, it was 37% ($n = 599$). For both *E. coli* and *P. psychrophila*, growth with *Penicillium* sp. str. 12 and *Penicillium* sp. str. SAM3 resulted in a large number of the same genes with significant interaction fitness ($n = 83$ and $n = 318$, respectively; Fig. 3b). These species also clustered away from the other fungi in a principal component analysis (Extended Data Fig. 5).

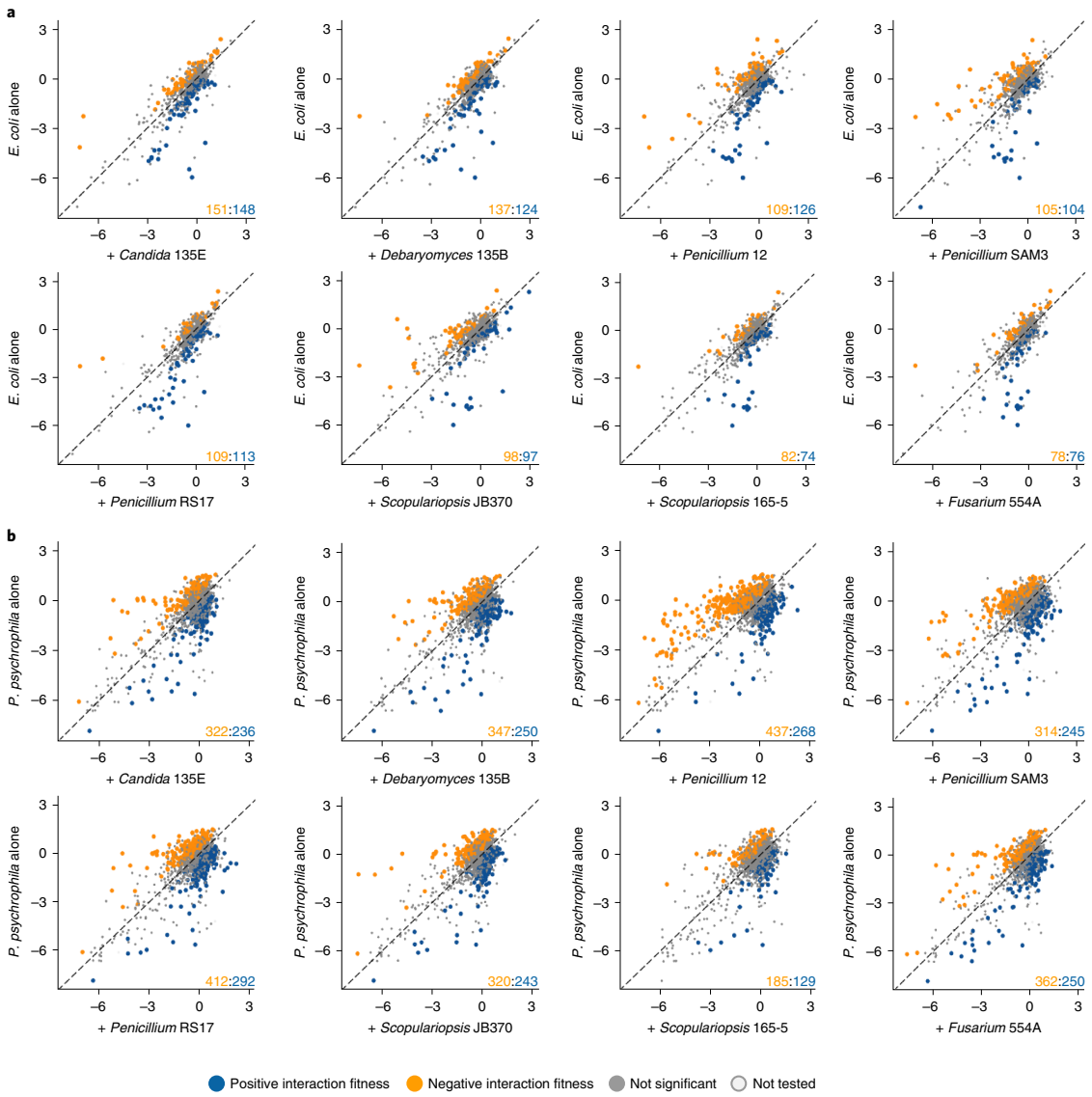

Fig. 2 | Comparison of bacterial gene fitness with fungi against growth alone and identification of bacterial genes with significant interaction fitness across fungal partners. a,**b**, Gene fitness values for *E. coli* (**a**) and *P. psychrophila* (**b**) were calculated for each gene during growth with a fungal partner (*x* axis) and during growth alone (*y* axis). Each point represents a gene, with coloured points indicating genes with a significant difference between gene fitness during growth alone versus with a fungal partner identified by a two-sided *t*-test and an adjusted *P* value lower than 5% using Benjamini–Hochberg correction for multiple comparison testing[75]. This difference is hereafter referred to as 'interaction fitness'. Exact *P* values are provided in Supplementary Tables 1 and 2. The coloured numbers in the lower right-hand corner indicate how many genes have either positive (blue) or negative (orange) interaction fitness. Positive interaction fitness indicates that a gene fitness value is significantly higher in the presence of the fungal partner compared to growth alone while negative interaction fitness indicates a lower fitness value in the presence of the fungal partner. Nonsignificant points are plotted smaller to aid in the visualization of significant genes. Genes not included in the *t*-test are labelled as not tested.

***Penicillium* sp. str. 12 and *Penicillium* sp. str. SAM3 induce bacterial envelope stress.** We used the following combination of methods to identify potential mechanisms underlying bacterial–fungal interactions: categorization of clusters of orthologous genes (COG), analysis of functional enrichment and analysis of the conservation of the effect across fungal species (Fig. 3c, Supplementary Tables 10 and 11 and Extended Data Fig. 6). *Penicillium* sp. str. 12 and *Penicillium* sp. str. SAM3 consistently shared effects on bacterial mutant fitness, as seen by their large number of network connections (Fig. 3a). The gene sets affected

by these fungi suggest that these two fungal species are creating bacterial envelope stress, potentially through the production of antibiotic molecules, as they include drug efflux pumps, envelope stress response systems, penicillin-binding proteins and lipopolysaccharide/peptidoglycan biosynthesis genes (Supplementary Table 12). For example, disruption of the multidrug efflux pump MdtK resulted in a decreased fitness specifically in the presence of these two fungi (gene fitness alone = 0.34, with *Penicillium* sp. str. 12 = −2.49, with *Penicillium* sp. str. SAM3 = −1.92).

We performed bacterial cytological profiling (BCP)[27], a microscopy-based method used to predict the mechanism of action for antibiotics, on WT or Δ*mdtK E. coli* grown alone or in a mixed biofilm with *Penicillium* sp. str. 12 or *Penicillium* sp. str. SAM3. Microscopy analysis showed a strong change in cell morphology for both WT and Δ*mdtK E. coli* when grown with *Penicillium* compared to growth alone (Fig. 4a). When cultured with these fungi, *E. coli* cells were significantly more round, which is consistent with a reduction in cell wall integrity (Fig. 4b). Δ*mdtK* cells were strongly affected and were spheroplasted, which is indicative of the complete loss of structural integrity. Control experiments with known antibiotic compounds showed that this effect is similar to that of antibiotics that target cell wall biosynthesis, such as mecillinam and amoxicillin (Fig. 4 and Extended Data Fig. 7).

Previous studies have shown that fungal specialized metabolite production in other ascomycete fungi is controlled by the global regulator LaeA[28,29]. To test the contribution of this gene to the potential antibiotic activity observed, we generated a Δ*laeA* mutant in *Penicillium* sp. str. 12. WT *E. coli* cells were significantly less round when grown with *Penicillium* sp. str. 12 Δ*laeA*, which suggests that loss of this global regulator has potentially decreased fungal antibiotic production (Fig. 4). Neither of these two fungal strains are known producers of penicillin, and an analysis of the *Penicillium* sp. str. 12 draft genome failed to detect penicillin biosynthesis gene clusters[30]. However, both fungi were causing consistent morphological and genetic effects that suggest that these fungi induce cell envelope stress similar to that seen with β-lactam antibiotics.

Fungi increase the bacterial need for biotin biosynthesis. *P. psychrophila* RB-TnSeq data showed that the disruption of genes associated with biotin biosynthesis (*bioB*, *bioD*, *bioF*, *bioA*, *bioH* and *bioC*) results in a negative interaction fitness with most fungi (average fitness alone = 0.08, average fitness across fungi = −2.97) (Fig. 3c). This gene set represents all genes needed to synthesize biotin from pimeloyl-CoA. Biotin is present in our CCA medium at 73 nmol mg^{-1} and represents an essential cofactor for enzymes involved in key cellular functions such as amino acid metabolism and lipid synthesis[31]. In *E. coli*, biotin biosynthesis genes exhibited a neutral fitness alone and did not show interaction fitness in our RB-TnSeq experiments. However, RNA-seq of WT *E. coli* grown either alone or in the presence of *Penicillium* sp. str. 12, a predicted biotin prototroph, showed that *bioA*, *bioB*, *bioC*, *bioD* and *bioF* were all significantly upregulated in the presence of *Penicillium* sp. str. 12, with an average fold change of 4.4 (Supplementary Table 13). This highlights an increased need for bacterial biotin synthesis in both *P. psychrophila* and *E. coli*, which suggests that there is competition for available biotin in the medium or that bacteria have higher biotin requirements in the presence of these fungi.

Fungi increase iron availability for bacterial partners. Because cheese is an iron-limited environment (with free iron levels of approximately 3 ppm[32]), microbial species require iron chelators such as siderophores to grow[16,32,33]. Our RB-TnSeq fitness data revealed that *E. coli* mutants that are defective in the transport of its siderophore, enterobactin, grow poorly in the alone condition (fitness < −4). However, the presence of any fungal partner significantly improved the growth of mutants in the *fep* operon (*fepC*, *fepG*, *fepA* and *fepB*), which encodes enterobactin transport functions (average positive interaction fitness of 3.11) (Fig. 3c, Fig. 5a and Supplementary Table 10). The positive effect of fungi on growth was further supported by competitive mutant fitness assays with isolated enterobactin uptake mutants (Fig. 5b).

Although siderophore production and uptake have not been previously characterized in *P. psychrophila* str. JB418, three putative iron-related genes have an effect similar to that seen with *E. coli fep* genes (having a fitness defect alone, but a positive interaction fitness with any fungus): Ga0212129_113525, Ga0212129_115698 and Ga0212129_114260. These genes are annotated as iron-complex outer membrane receptor protein, as putative iron-dependent peroxidase and as uncharacterized iron-regulated membrane protein, respectively. Immediately upstream of Ga0212129_114260, we found a ferric enterobactin receptor (FepA) and the PfeR–PfeS two-component regulatory system required for the ferric enterobactin receptor[34]. Although pyochelin and pyoverdine are two well-known *Pseudomonas* siderophores[35], antiSMASH did not predict these siderophores in *P. psychrophila*.

RNA-seq analysis of WT *E. coli* revealed 34 genes (out of a total of 348 significantly upregulated genes) involved in iron acquisition that were specifically upregulated in the presence of *Penicillium* sp. str. 12 (Supplementary Table 14). We observed upregulation of enterobactin biosynthesis and uptake (*ent*- and *fep*-associated genes), which suggests that even in the presence of fungi, *E. coli* still produces and utilizes its native siderophore (Fig. 5c). In addition to the enterobactin uptake system, *E. coli* possesses the Fhu system, which enables the uptake of hydroxamate-type siderophores, including those produced by fungi, such as ferrichrome and coprogen[36,37]. Notably, our RNA-seq data showed upregulation of *fhuA* (which encodes an outer membrane receptor for ferrichrome)

Fig. 3 | Cross-comparison and functional characterization of bacterial genes with interaction fitness in the presence of fungi. a, Network of *E. coli* (left) or *P. psychrophila* (right) genes with an interaction fitness based on RB-TnSeq. Each orange node represents a fungal partner and is labelled as follows: fungal partner (number of genes with interaction fitness; number of genes with interaction fitness unique to this condition). Each green node represents a bacterial gene. Green nodes are shaded by the number of fungal conditions in which this gene has an interaction fitness, as shown in the legend below, and are sized by the average strength of interaction fitness across partners. **b**, UpSet[99] plots showing the intersections of *E. coli* (left) or *P. psychrophila* (right) gene sets with interaction fitness across fungal partners. These UpSet plots are conceptually similar to Venn diagrams. The connected circles indicate which fungal conditions are included in the intersection, and the size of the intersection (the number of genes that have an interaction fitness in all the highlighted conditions) is displayed in the main bar chart. The horizontal bar chart displays the number of genes with significant interaction fitness per fungal condition. Intersections with fewer than five genes are not shown for *E. coli* and fewer than ten genes are not shown for *P. psychrophila*. For example, in the *E. coli* panel, 17 genes have an interaction fitness with all partners (all fungi circles are connected), while 16 other genes have an interaction fitness with *Penicillium* sp. str. 12 and with *Penicillium* sp. str. SAM3 (only *Penicillium* sp. str. 12 and *Penicillium* sp. str. SAM3 circles are connected). Intersections are green colour-coded based on the number of fungal partners sharing the interaction as in Fig. 3a. **c**, Comparison of *E. coli* (left) or *P. psychrophila* (right) gene fitness values alone compared to fitness values with a fungal partner, coloured by COG category and sized by the conservation of effect among fungal partners (one to eight fungal species). Genes that are discussed further in the main text related to *E. coli* enterobactin uptake and *P. psychrophila* biotin biosynthesis are labelled.

and *fhuE* (which encodes an outer membrane receptor for coprogen) in the presence of *Penicillium*, which suggests that this fungus may alleviate the growth defects seen in the *fep* mutants through the provision of hydroxamate-type siderophores taken up by the Fhu system.

All filamentous fungi in this study, but not yeast, produce siderophores detectable by the chrome azurol S (CAS) assay (Extended Data Fig. 8). In addition, liquid chromatography–mass spectrometry (LC–MS and LC–MS/MS) showed evidence of the hydroxamate fungal siderophores coprogen and ferrichrome in *Fusarium*

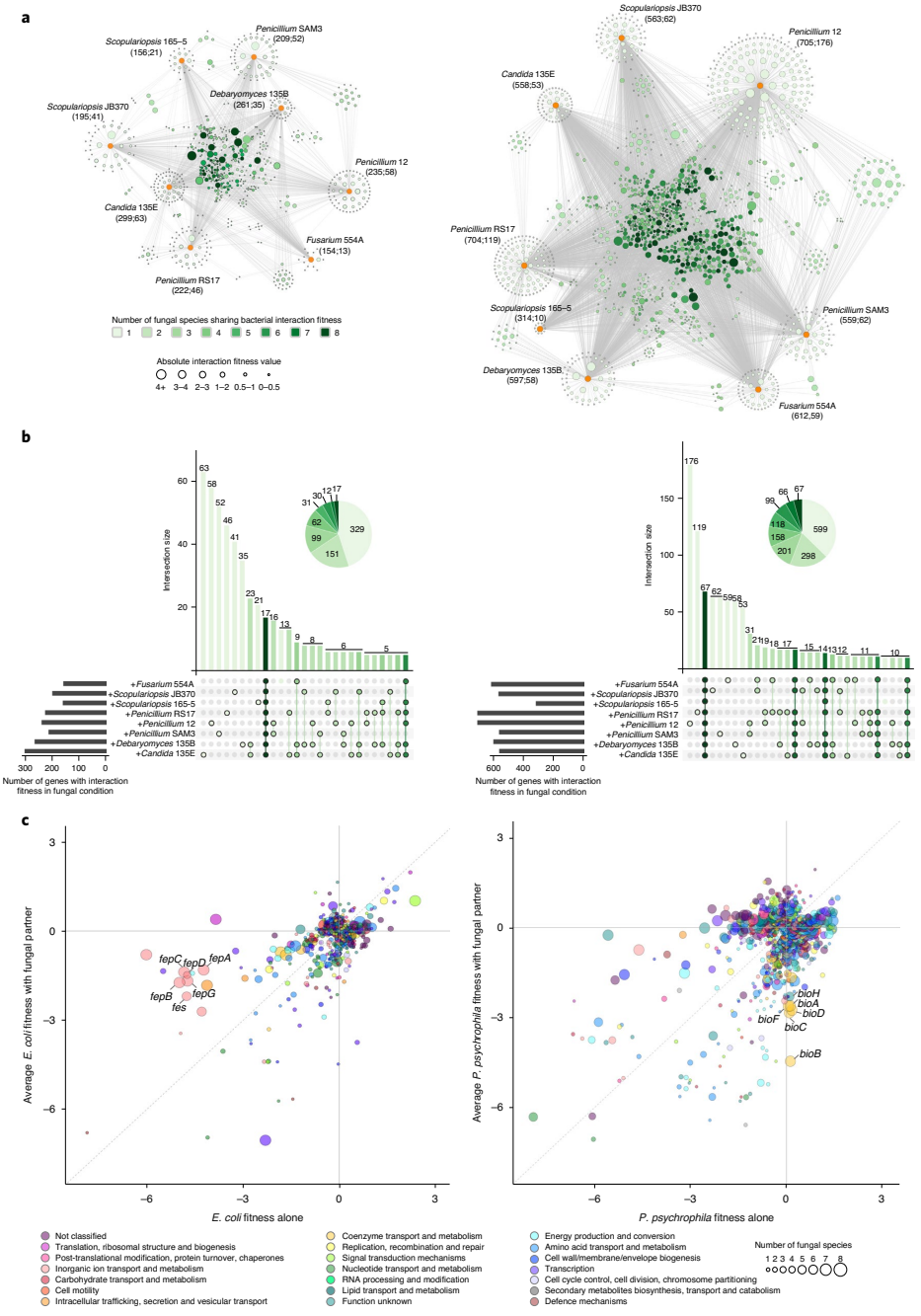

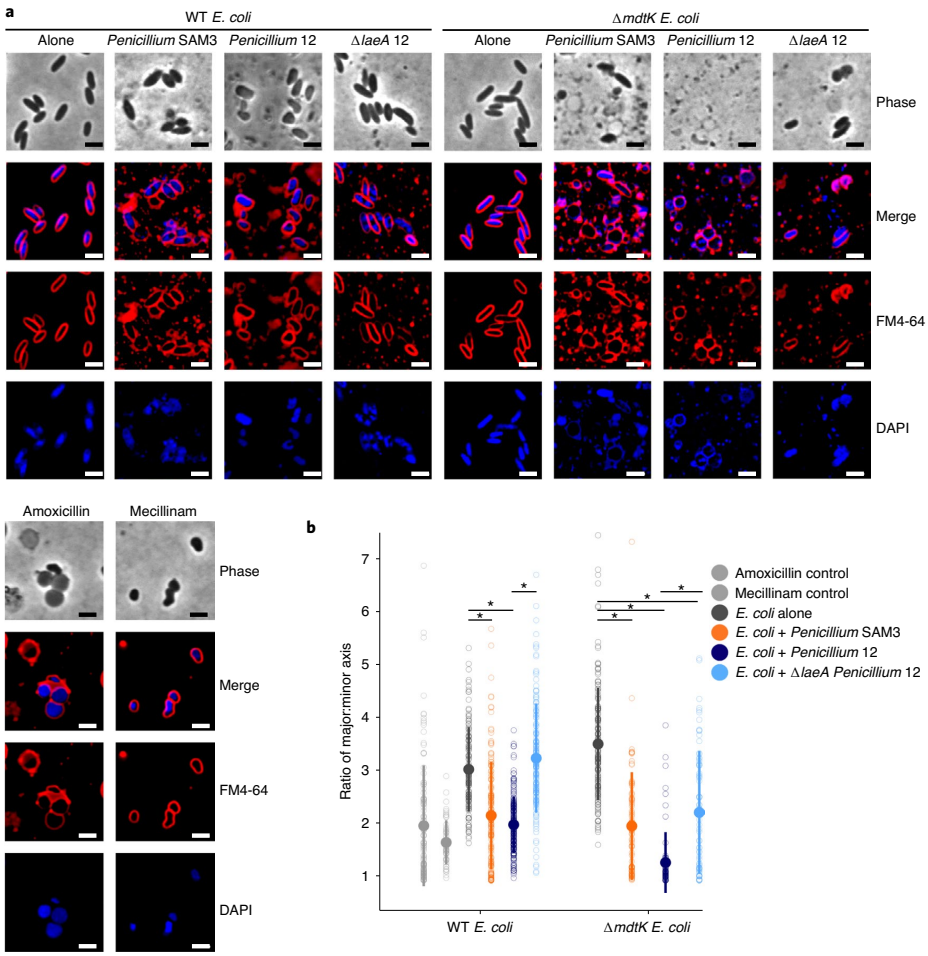

Fig. 4 | BCP of *E. coli* grown with *Penicillium* sp. str. SAM3, *Penicillium* sp. str. 12 or Δ*laeA Penicillium* sp. str. 12 on CCA plates. a, The phenotype of *E. coli* grown with these fungi is similar to that seen when *E. coli* is exposed to antibiotics targeting cell wall biosynthesis. This effect is more dramatic in *E. coli* lacking the *mdtK* multidrug efflux pump. Representative fields of deconvoluted images are displayed. DAPI dye stains DNA and FM4-64 dye stains bacterial membranes. Scale bars, 2 μm. **b**, Quantification of microscopy results. The major and minor axes of individual cells were measured (all cells in the image for multiple images), and the ratio of these measurements was used as an indicator of cell roundness. Each empty circle represents an individual cell (from left to right, $n = 110$, 53, 121, 136, 181, 144, 153, 79, 70 and 73 cells examined from one independent experiment per condition). The filled circle displays the mean, and the thick bar extending from the mean displays the standard deviation. WT *E. coli* has a ratio of about 3, and the cells become rounder as the ratio approaches 1. Asterisks indicate significantly different roundness in the presence of a fungus relative to growth alone or significantly different roundness in the presence of WT *Penicillium* sp. str. 12 relative to Δ*laeA Penicillium* sp. str. 12 (unpaired two-sample Wilcoxon test $P < 0.05$). Exact P values are as follows: *E. coli–Penicillium* SAM3 versus *E. coli* alone $= 3.05 \times 10^{-13}$; *E. coli–Penicillium* 12 versus *E. coli* alone $= 3.55 \times 10^{-28}$; *E. coli–Penicillium* 12 versus *E. coli–ΔlaeA Penicillium* 12 $= 5.21 \times 10^{-37}$; Δ*mdtK E. coli–Penicillium* SAM3 versus Δ*mdtK E. coli* alone $= 4.13 \times 10^{-25}$; Δ*mdtK E. coli–Penicillium* 12 versus Δ*mdtK E. coli* alone $= 1.14 \times 10^{-41}$; Δ*mdtK E. coli–ΔlaeA Penicillium* 12 versus Δ*mdtK E. coli* alone $= 2.68 \times 10^{-13}$; Δ*mdtK E. coli–Penicillium* 12 versus Δ*mdtK E. coli–ΔlaeA Penicillium* 12 $= 1.16 \times 10^{-7}$.

and *Penicillium* species (Fig. 5d). Although not detected in these extracts, *Scopulariopsis* sp. str. JB370 is predicted to make dimethylcoprogen based on an antiSMASH analysis of the draft genome[38].

To confirm that hydroxamate siderophores could rescue *fep* mutants via the Fhu pathway, we verified that purified coprogen and ferrichrome rescued the growth defect of Δ*fepA* or Δ*fepC* mutants grown on CCA (Fig. 5e). As expected, *fhuA* or *fhuE* mutants alone did not show a growth defect on CCA, probably because the enterobactin system is intact. Thus, to specifically examine whether these genes are required for the uptake of the purified siderophores, we constructed *fhuA* or *fhuE* mutants in an enterobactin-uptake-defective background (Δ*fepC* or Δ*fepA*). The combined loss of enterobactin uptake and *fhuA* eliminated the alleviation seen with ferrichrome, whereas loss of either *fhuA* or *fhuE* in the Δ*fepA* background seemed to eliminate the alleviation seen with coprogen (Fig. 5e). This suggests that *E. coli* requires *fhuA* for ferrichrome uptake, and both *fhuA* and *fhuE* for coprogen uptake.

We next examined whether the presence of fungal species changed the growth of strains defective in siderophore uptake (Fig. 5f and Extended Data Fig. 9). Growth of the Δ*fepA* and Δ*fepC* mutants was restored closest to the filamentous fungi, but not when grown near yeasts. For filamentous fungi, this effect was dependent on either *fhuA* or *fhuE*. Thus, *E. coli* is likely to use and benefit from fungal hydroxamate siderophores produced by filamentous fungi that are taken up by the Fhu system independently of the enterobactin uptake system.

Because iron limitation is a common challenge across many environments, we wanted to examine whether fungal species from other ecosystems could also be producing siderophores that are accessible to neighbouring bacterial species. We performed similar assays with *Aspergillus fumigatus*, a soil-dwelling filamentous ascomycete, and *Malassezia pachydermatis*, a basidiomycete yeast that is a commensal resident on animal skin. Our results suggested that *A. fumigatus* produces a siderophore capable of being imported through FhuA (Fig. 5f). We saw a similar effect using *M. pachydermatis*, which suggests that bacteria are able to utilize siderophores from a yeast species using the Fhu system (Fig. 5f). We performed an antiSMASH[38] analysis on a previously published genome of this *M. pachydermatis* strain and were able to identify a nonribosomal peptide synthetase (NRPS) biosynthetic gene cluster containing a ferrichrome peptide synthetase[38,39]. In summary, our results suggest that cheese-associated filamentous fungi, and select fungi from other environments, can reduce bacterial dependence on their own siderophores.

Loss of a fungal secondary metabolite regulator alters the profile of interaction fitness. The cases above show that bacterial gene fitness is affected by the production of fungal specialized metabolites, including siderophores and potentially antibiotics. To determine the extent to which the global regulator LaeA is responsible for fungal-induced changes in bacterial fitness, we performed RB-TnSeq experiments with the *Penicillium* sp. str. 12 Δ*laeA* mutant. Despite comparable fungal growth between WT and Δ*laeA*, we saw only 65 *E. coli* genes with interaction fitness when grown with Δ*laeA* compared with 204 with WT, which suggests that many of the fitness effects we saw may be due to fungal specialized metabolite production (Fig. 6a and Extended Data Fig. 10).

Given that siderophore production in other fungi is controlled by LaeA, we would expect that *E. coli* enterobactin uptake mutants would not have positive interaction fitness with the Δ*laeA* mutant. Indeed, we no longer saw a positive interaction fitness for *fes*, *fepA*, *fepB*, *fepC*, *fepD* and *fepG* genes when *E. coli* was grown with Δ*laeA* *Penicillium* sp. str. 12 (Supplementary Table 15). Additionally, we saw a negative interaction fitness for the hydroxamate siderophore transport genes *fhuB* and *fhuC* with WT *Penicillium* sp. str. 12 but not with Δ*laeA*. Liquid CAS assays demonstrated that Δ*laeA* *Penicillium* sp. str. 12 produced fewer siderophores than WT on cheese medium (Fig. 6b). Overall, these results demonstrate that loss of the LaeA regulator decreases siderophore production in *Penicillium* sp. str. 12 and abolishes the positive interaction effect seen for *fep* genes grown with WT fungus.

We next examined whether there were changes in the fitness of genes related to responses to antibiotics. A number of genes involved in cell envelope maintenance showed a negative interaction fitness with WT but not Δ*laeA* *Penicillium* sp. str. 12 (Supplementary Table 12). These genes included *dacA*, which encodes penicillin-binding protein 5. Loss of this gene can increase the susceptibility of *E. coli* to β-lactam antibiotics[40]. Mutants in the gene encoding the MdtK efflux protein had improved fitness with Δ*laeA* relative to WT *Penicillium* sp. str. 12. As seen in our BCP analysis, maintenance of cell envelope integrity is important for *E. coli* growing with WT *Penicillium* sp. str. 12, but less so in the absence of LaeA.

RNA-seq results showed that 14% of the *Penicillium* sp. str. 12 genome was differentially expressed between WT and Δ*laeA* (Fig. 6c and Supplementary Table 16). This is consistent with previous findings in *A. fumigatus* that LaeA influenced the expression of around 10% of the fungal genome[41]. Gene Ontology (GO) term enrichment analysis identified a number of specialized metabolite biosynthesis pathways overrepresented in the genes that were more expressed in the WT strain (Supplementary Table 17). Of the biosynthetic gene clusters predicted by the antiSMASH[38] analysis, 11 were downregulated in Δ*laeA*, including 1 terpene cluster, 2 type I polyketide synthase clusters and 8 NRPS clusters. Consistent with our findings of decreased siderophore production in Δ*laeA*, one NRPS cluster contained four genes with homology to *sidD*, *sidF*, *sidH* and *sitT*; these genes are associated with siderophore biosynthesis and transport in *Aspergillus*[42].

LC–MS comparison of WT and Δ*laeA* *Penicillium* sp. str. 12 showed differential production of many metabolites, 94 of which showed a greater than tenfold change between the two (Supplementary Table 18). Of these, 93 were less abundant in the Δ*laeA* mutant, which is consistent with the loss of secondary metabolite production in the Δ*laeA* mutant (Fig. 6d). Cyclopenol, a biosynthetic intermediate for viridicatol[43], was the only molecule reported to have antibiotic activity identified in the LC–MS data; it was produced by the WT *Penicillium* sp. str. 12 in more than tenfold higher quantity than Δ*laeA*. However, further work is needed to determine whether this molecule is related to the antibacterial activity seen in BCP. In summary, these data highlight an important diminution of specialized metabolite production in the Δ*laeA* strain.

Fig. 5 | Utilization of fungal siderophores by *E. coli*. a, RB-TnSeq fitness values for *fep* operon genes in alone or with fungi conditions showing an increase in fitness in the presence of fungal species. Fitness values are not shown for nonsignificant differences from alone condition. Error bars show the standard deviation of fitness values from the mean. **b**, Colony-forming units of WT *E. coli* and Δ*fep* mutants after 7 days of 1:1 competitive growth on CCA, pH 7. Competitions between the two *E. coli* strains were performed with either no fungus present (alone) or with *Penicillium* sp. str. 12 or *Scopulariopsis* sp. str. JB370 (*Scop.* JB370). $n = 4$ biologically independent experiments, and error bars show the standard deviation from the mean (black circle). Asterisks indicate significantly different growth in the presence of a fungus relative to growth without the fungus (alone) based on a two-sided two-sample *t*-test $P < 0.05$. Exact *P* values associated with asterisks are as follows (from left to right): 0.001, 0.007, 0.034, 0.022, 0.0001 and 0.0006. **c**, *E. coli* iron-related genes upregulated in the presence of *Penicillium* sp. str. 12. Significance cut-off was made at abs($\log_2$[fold change]) >1.5 and adjusted $P < 0.05$. Differential expression analysis was performed using the default function DESeq[87], which performs a Wald test with Benjamini–Hochberg[75] correction for multiple comparison testing. Exact *P* values are available in Supplementary Table 14. The schematic on the right displays key proteins involved in siderophore uptake in *E. coli*. These proteins are coloured based on the upregulation of their corresponding genes. Fes and FhuF aid in removal of iron from siderophores inside the cell. **d**, Fungal siderophores identified by MS. The inset in the left box shows the node that represents the desferrichrome fragmentation pattern depicted, while the network on the right represents coprogen-related molecules. Coprogen B and ferrichrome were found by matching fragmentation patterns to library spectra. Both identifications were confirmed using retention time and fragmentation matching to a purchased standard. **e**, Visual assays of Δ*fep* mutant growth with purified siderophores coprogen and ferrichrome. **f**, Visual assays of *E. coli* mutant growth at varying distances from pre-cultured cheese fungi, *A. fumigatus* (soil, human pathogen) and *M. pachydermatis* (skin commensal). For **e** and **f**, growth was performed on CCA. Tetrazolium chloride, a red indicator of cellular respiration, was added to the medium to visualize colony growth on the opaque CCA.

Discussion

Fungi have the potential to strongly affect bacterial neighbours in diverse systems, from soil to polymicrobial infections[44–48]. We combined the high-throughput genetic screen RB-TnSeq with BCP, RNA-seq and metabolomics to identify a diversity of bacterial genes involved in, and the associated fungal contributors to, bacterial–fungal interactions in our system. This study provides new insight into the wide range of fungal impacts on bacteria that can occur

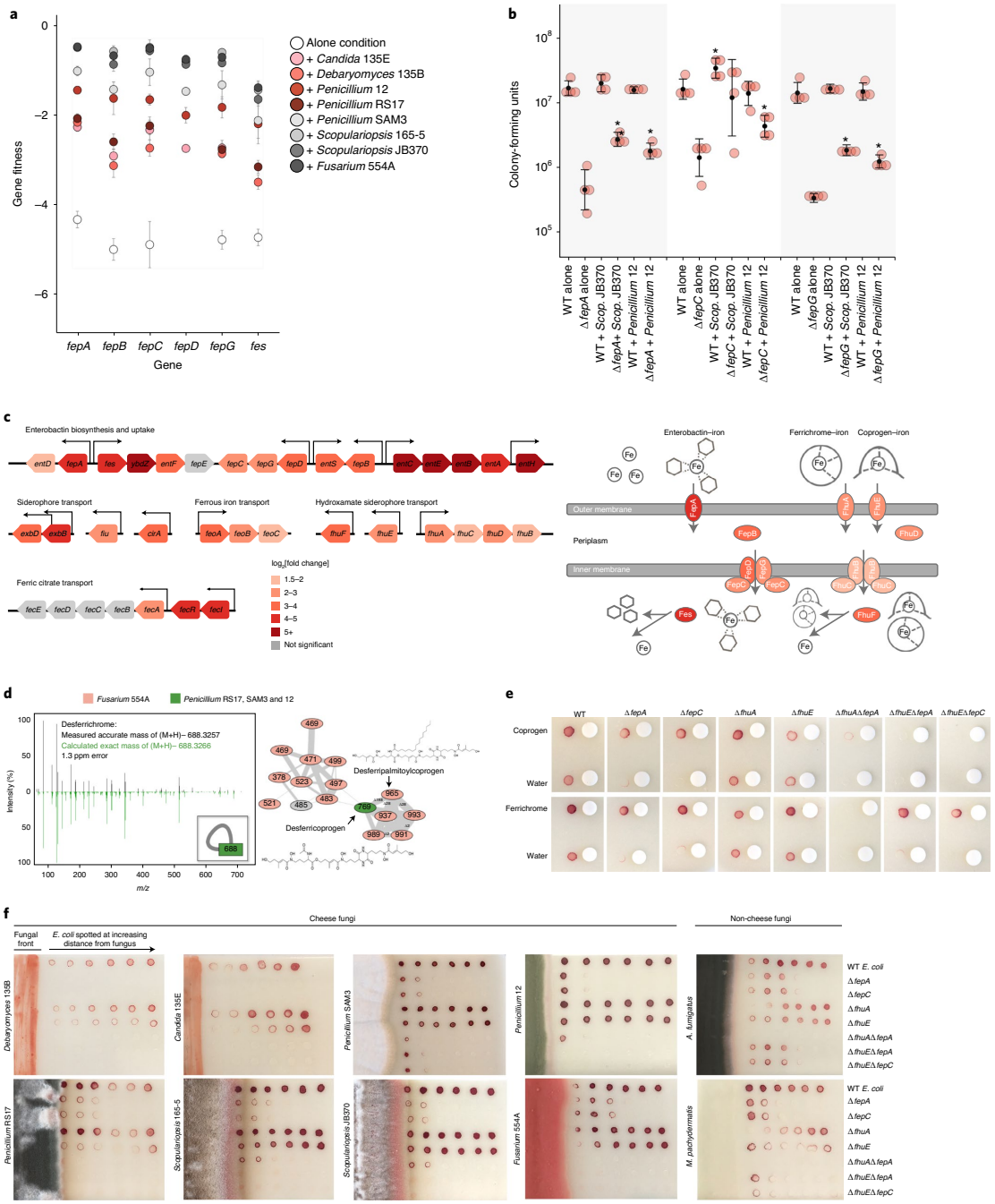

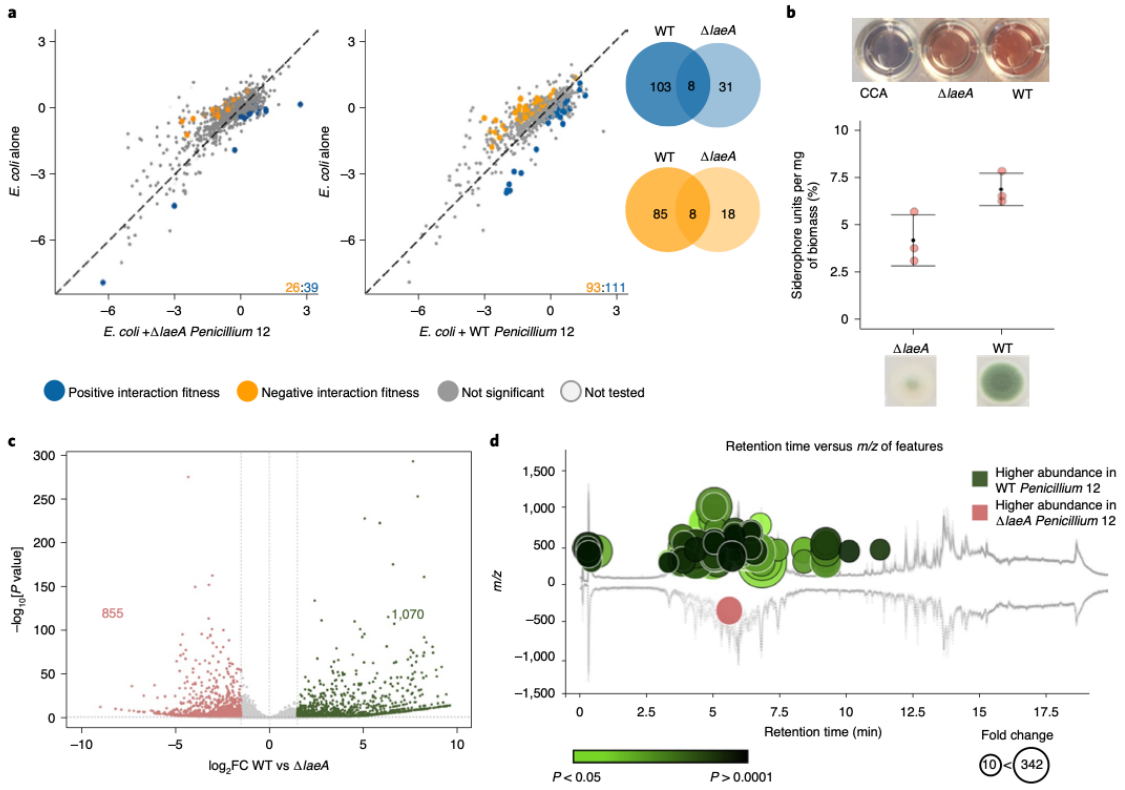

Fig. 6 | Fungal metabolite production affects bacterial–fungal interactions. a, *E. coli* genes with significant interaction fitness with Δ*laeA* or WT *Penicillium* sp. str. 12. Each point represents a gene, with coloured points indicating genes with interaction fitness. The *x* and *y* values (plus fungal partner on the *x* axis; alone on *y* axis) indicate gene fitness values in each condition, and the numbers in the lower right-hand corner indicate how many genes have either positive (blue) or negative (orange) interaction fitness. The Venn diagrams display the overlap of these gene sets. **b**, Liquid CAS assay of supernatants from blank control CCA medium, Δ*laeA* or WT *Penicillium* sp. str. 12 normalized to fungal biomass. $n = 3$ biologically independent experiments, and error bars show the standard deviation from the mean. The asterisk indicates significantly different siderophore production (two-sided two-sample *t*-test, $P = 0.04$). **c**, Differential expression of WT *Penicillium* sp. str. 12 relative to Δ*laeA* after 3 days of growth on CCA. Labelled on the volcano plot are the number of genes with a $\log_2$ fold change (FC) of >1.5 (green) or <−1.5 (red) and adjusted $P < 0.05$. Differential expression analysis was performed using the default function DESeq[87], which performs a Wald test with Benjamini–Hochberg[75] correction for multiple comparison testing. **d**, The metabolomics data analysis platform XCMS[100] was used to compare features detected by LC–MS analyses of Δ*laeA* and WT *Penicillium* sp. str. 12 extracts (two-sided Welch's *t*-test for unequal variances). Features of higher abundance in WT relative to Δ*laeA* are depicted as green nodes on the top of the mirror plot, and features of lower abundance in WT relative to Δ*laeA* are depicted as red nodes on the bottom. The node radius is proportional to the fold change of the detected features, and the colour intensity is dependent on the *P* value. The graph displays only those features with a *P* value less than or equal to 0.05, a fold change higher than or equal to 10, a *m/z* between 200 and 2,000 Da, and an intensity higher than 500. Exact *P* values are provided in Supplementary Table 18.

even in a relatively simple system with pairwise combinations of bacteria and fungi. Our study focused on fungi from Ascomycota because this phylum is abundant in cheese rinds, and therefore represents a small sampling of the full genomic and functional diversity across fungi. It remains to be seen how these interactions might change with a more diverse set of partners, in conditions with varying ratios of bacteria and fungi, in varied environmental conditions or with increasing community complexity[16].

Our study highlighted several important areas that contribute to bacterial–fungal interactions. First, multiple lines of evidence suggest that cheese-isolated *Penicillium* species exhibit antibiotic-like activity, although the mechanism underlying this activity is currently unknown. Although *Penicillium* species produce a wide range of specialized metabolites, detection of known antibiotics such as penicillin in food products is limited[30]. Second, we found an increased need for biotin biosynthesis in the presence of fungi, which suggests that there is fungal competition for available biotin. Previous studies have pointed to roles of B vitamins in bacterial–fungal and even plant–bacterial interactions[49,50]. Third, the strongest and most widespread bacterial–fungal interaction that we observed suggests that fungal species can dramatically modulate access to iron through the provision of fungal siderophores such as ferrichrome and coprogen. It has long been known that bacteria grown in isolation are able to take up purified fungal siderophores, but the ecological relevance of this putative interaction has not been demonstrated[36,51]. Our results demonstrate that this exchange takes

place between bacteria and filamentous fungi growing in a biofilm and that this exchange can have impacts on the competitive fitness of bacteria. Our data suggest that cheese-associated yeast species may alleviate bacterial iron limitation through a different mechanism, as we did not detect siderophore production by these species.

Owing to the importance of iron in bacterial physiology and the prevalence of fungi in microbial ecosystems, we expect that iron-based bacterial–fungal interactions are important in other microbiomes. For example, growth of non-siderophore-producing mutants of soil-dwelling *Streptomyces coelicolor* was restored by the presence of siderophores from airborne contaminant *Penicillium*[52]. Moreover, many filamentous fungi outside the genera studied here can produce siderophores[53]. In addition to filamentous fungi, we showed that the basidiomycete skin yeast *M. pachydermatis* alleviated bacterial iron limitation. Human skin microbiome yeasts *Malassezia restricta* and *Malassezia globosa* have previously been found to possess genes for siderophore biosynthesis[54,55]. Fungal growth may also be affected by inter-kingdom siderophore exchange, as some fungal species have evolved mechanisms of utilizing bacterial siderophores while others are inhibited by bacterial siderophores[56–58].

FhuE and FhuA receptors are widespread in Proteobacteria, further suggesting that inter-kingdom siderophore exchange could play an important role in diverse systems. Hydroxamate siderophore uptake systems have also been identified in Gram-positive bacterial pathogens[59,60]. Additionally, hydroxamate siderophore uptake systems affect bacterial fitness, as shown in a murine infection model[61]. *Bacteroides fragilis*, a human gut symbiont, is able to use ferrichrome to grow in iron-limiting conditions, and *fhu* genes are expressed by *E. coli* in colonic mucus[62,63]. Fermented foods are known to contain fungal siderophores, which could be a source of fungal siderophores in the gut in addition to potential siderophore production by gut-resident species[64,65].

We anticipated that by looking for fungal impacts on *E. coli*, we could leverage the genetic information available for this species. However, even in this well-characterized organism, 38% of genes identified as having interaction fitness are annotated as hypothetical, uncharacterized or putative. For *P. psychrophila*, 27% of genes with interaction fitness are hypothetical proteins. Similarly, the chemical identity and ecological relevance of most of the specialized metabolites we identified in our *Penicillium* species are unknown. This highlights that many genes and molecules involved in interspecies interactions are yet to be characterized, and that studying microbes in the context of their interactions with other species, and not just in monoculture, provides an avenue for uncovering new areas of biology.

Methods

Source information for strains and libraries. Source information for strains and libraries used in this study is provided in Supplementary Table 19.

Sequencing of the fungal ribosomal RNA gene. Genomic DNA (gDNA) was extracted using phenol–chloroform (pH 8) from cultures of the eight cheese fungal species used in this study. For each extraction, 125 µl of 425–600-µm acid-washed beads and 125 µl of 150–212-µm acid-washed beads were poured into a screw-capped 2-ml tube. A total of 500 µl of 2× buffer B (200 mM NaCl, 20 mM EDTA) and 210 µl of SDS 20% were added to the tube containing fungal material and 500 µl of phenol–chloroform (pH 8). Cells were lysed by vortexing the tubes for 2 min at maximum speed. Aqueous and organic phases were separated by centrifugation at 4 °C, 8,000 r.p.m. for 3 min, and 450 µl of the aqueous phase (upper phase) was recovered in a 1.5-ml Eppendorf tube. Sodium acetate (3 M, 45 µl) and ice-cold isopropanol (450 µl) were added before incubating the tubes at −80 °C for 10 min. The tubes were then centrifuged for 5 min at 4 °C at 13,000 r.p.m. The pellet was then washed in 750 µl of 70% ice-cold ethanol and resuspended in 50 µl of DNase/RNase-free water. Following DNA extraction, LROR (ACCCGCTGAACTTAAGC) and LR6 (CGCCAGTTCTGCTTACC)[66] primers were used to amplify the large subunit of the ribosomal RNA, and for *Penicillium* species, Bt2a (GGTAACCAAATCGGTGCTGCTTTC) and Bt2b (ACCCTCAGTGTAGTGACCCTTGGC)[67] primers were used to amplify the β-tubulin gene. PCR was performed in a final volume of 50 µl (25 µl of Q5 polymerase master mix (New England Biolabs), 2.5 µl of the forward primer at 10 µM, 2.5 µl of the reverse primer at 10 µM, 100 ng of gDNA, and water) using the following PCR programmes: (1) for LSU: 98 °C for 30 s, then 35 cycles of 98 °C for 10 s, 52 °C for 30 s, followed by 72 °C for 1.5 min, and finally 72 °C for 5 min; (2) for β-tubulin: 98 °C for 30 s, then 35 cycles of 98 °C for 10 s; 57 °C for 30 s, followed by 72 °C for 1 min, and finally, 72 °C for 5 min. PCR products were purified using a QIAquick PCR purification kit (Qiagen) and sequenced using the forward and reverse primers by Eton Bioscience. Consensus sequences from forward and reverse sequencing reactions of the LROR/LR6 PCR product were aligned using Geneious v.R9 9.1.8 (http://www.geneious.com). The MrBayes[68] plugin for Geneious was used to build the phylogenetic tree with the following parameters: Substitution model- JC69; Rate variation- gamma; Outgroup- *Fusarium* sp. str. 554A; Gamma categories-4; Chain Length- 1100000; Subsampling freq- 200; Heated chains-4; Burn-in length- 100000; Heated chain temp- 0.2; Random seed-1160; Unconstrained branch lengths- 1, 0.1, 1, 1. FigTree v.1.4.4 was used for visualization (https://github.com/rambaut/figtree/releases).

Bacterial–fungal growth assays. To approximate a 1:1 ratio of bacteria and fungi based on cell size, we inoculated 60,000 bacterial cells alone or with 6,000 fungal spores per well on 10% CCA medium[25] adjusted to pH 7 in a 96-well plate. Each bacterial or bacterial–fungal assay was done in triplicate. After 7 days of growth at room temperature, the entire well was collected and homogenized in 1×PBS–Tween 0.05% before dilution and plating on LB medium with 20 µg ml^{-1} cycloheximide (for bacterial counts) or plate count agar supplemented with 0.1% milk and 1% salt (PCAMS) with 50 µg ml^{-1} chloramphenicol (for fungal spore counts). Counts were done at inoculation and after collection. Final growth counts were then compared between the co-culture condition relative to growth alone to identify interaction effects. Significant growth effects were determined based on Dunnett's test[69], $P < 0.05$. Plots were made using the R package ggplot (v.2 3.2.1)[70].

Microbial culturing for LC–MS/MS extraction. All fungal cultures were grown on PCAMS. Plates were kept at room temperature and spores were collected at 7 days of growth (or after sporulation was observed) for subsequent experiments. Spores collected from fungi were normalized to an optical density at 600 nm (OD_{600}) of 0.1 in PBS for a working stock.

Extraction of cultures. Three biological replicates of each condition were plated (distinct samples) and extracted from solid agar. For extraction from solid agar plates, 5 µl of fungal working stock was spotted onto 10% CCA medium adjusted to pH 7. Following 7 days of growth, agar was removed from the Petri dish and placed into 50-ml Falcon tubes. Acetonitrile (10 ml) was added to each tube and all were sonicated for 30 min. All Falcon tubes were centrifuged, and liquid was removed from the solid agar pieces and transferred to 15-ml Falcon tubes. The 15-ml Falcon tubes containing liquid were then centrifuged and liquid was again removed from any residual solid debris and transferred to glass scintillation vials. These liquid extractions were then dried in vacuo. Dried extracts were weighed and diluted with methanol to obtain 1 mg ml^{-1} solutions, which were stored at −20 °C until analysis via LC–MS/MS.

LC–MS/MS data collection. High-resolution LC–MS and LC–MS/MS data were collected on a Bruker impact II qTOF in positive mode with the detection window set from 50 to 1,500 Da on a 2.1 × 150-mm C18 Cortecs UPLC column with a flow rate of 0.5 ml min^{-1} for a gradient of 10–100% acetonitrile with 0.1% formic acid over 16 min. For each sample, 10 µl of a 1 mg ml^{-1} solution was injected. The electrospray ionization conditions were set with the capillary voltage at 4.5 kV. For MS^2, dynamic exclusion was used, and the top nine precursor ions from each MS^1 scan were subjected to collision energies scaled according to the mass and charge state for a total of nine data-dependent MS^2 events per MS^1. MS^2 data for pooled biological replicates have been deposited under MassIVE accession number MSV000085070. MS^1 and MS^2 data for *ΔlaeA* and WT *Penicillium* sp. str. 12 have been deposited under MassIVE accession number MSV000085054 and were collected under identical conditions on a Bruker compact qTOF.

Molecular networking. For all extractions, all precursor *m/z* values that were found in solvent and agar controls (based on both retention time and mass tolerance) were removed before input into Global Natural Products Social molecular networking (GNPS) using the BLANKA algorithm[71]. A molecular network (https://gnps.ucsd.edu/ProteoSAFe/status.jsp?task=464b331ef9d54de9957d23b4f9b9db14) was created using the online workflow in GNPS. The data were filtered by removing all MS/MS peaks within ±17 Da of the precursor *m/z*. MS/MS spectra were window filtered by choosing only the top six peaks in the ±50-Da window throughout the spectrum. The data were then clustered with MS-Cluster with a parent mass tolerance of 0.02 Da and a MS/MS fragment ion tolerance of 0.02 Da to create consensus spectra. Furthermore, consensus spectra that contained fewer than two spectra were discarded. A network was then created whereby edges were filtered to have a cosine score above 0.7 and more than six matched peaks. Further edges between two nodes were kept in the network only if each of the nodes appeared in each other's respective top ten most similar nodes. The spectra

in the network were then searched against the spectral libraries of the GNPS. The library spectra were filtered in the same manner as the input data. All matches kept between network spectra and library spectra were required to have a score above 0.7 and at least six matched peaks. Solvent and agar control files were also loaded into the networks to perform removal based on fragmentation patterns. All nodes with precursor masses less than 200 Da were also removed. The extensive background and low *m/z* Da value removal was done to more accurately reflect the metabolomic profiles of fungal genera in an attempt to represent only true metabolites. The Dereplicator algorithm[72,73] was used to annotate MS/MS spectra. The molecular networks were visualized using Cytoscape software[74].

RB-TnSeq assays. All RB-TnSeq assays were performed on 10% CCA medium adjusted to pH 7. Before inoculation, one aliquot of each library was thawed and inoculated into 25 ml of liquid LB with kanamycin (50 μg ml^{-1}). This is the same medium used for creating the initial library and is expected to be nonselective. Once the culture reached mid-log phase (OD = 0.6–0.8), 5 ml of that pre-culture was pelleted and stored at −80 °C for the T0 reference in the fitness analysis. The remaining cells were used to inoculate the fitness assay conditions. For each RB-TnSeq fitness assay, we aimed to inoculate 7,000,000 cells of the bacterial library (on average 50 cells per insertion mutant). For fitness assays including a fungal partner, 700,000 fungal cells were inoculated based on spore counts. We inoculated ten times more bacterial cells than fungal spores to approximate a 1:1 volume ratio of bacteria:fungi, as fungal cells are approximately ten times larger than bacterial cells. Pre-cultured cells were washed in 1×PBS–Tween 0.05%, mixed with appropriate volumes of quantified fungal spore stocks, and then inoculated by spreading evenly on a 100-mm Petri dish containing 10% CCA medium, pH 7. For each condition, assays were performed in triplicate (three distinct samples). After 7 days, each plate was flooded with 1.5 ml of 1×PBS–Tween 0.05% and cells were scraped off, taking care not to disturb the CCA. The liquid was then transferred into a 1.5-ml microcentrifuge tube and cells were pelleted by centrifugation. After removing the supernatant, the cells were washed in 1 ml of RNAprotect solution (Qiagen), pelleted and stored at −80 °C until gDNA extraction. gDNA was extracted with phenol–chloroform (pH 8) using the same protocol used for fungal gDNA extraction described above. Samples were stored at −80 °C until further analysis.

After gDNA extraction, extracts containing *Penicillium* sp. str. 12 DNA were purified using a OneStep PCR Inhibitor Removal kit (Zymo Research). Then, the 98 °C BarSeq PCR protocol as previously described in Wetmore et al.[18] was used to amplify only the barcoded region of the transposons. PCR was performed in a final volume of 50 μl with the following content: 25 μl of Q5 polymerase master mix (New England Biolabs), 10 μl of GC enhancer buffer (New England Biolabs), 2.5 μl of the common reverse primer (BarSeq_P1 – Wetmore et al.[18]) at 10 μM, 2.5 μl of a forward primer from the 96 forward primers (BarSeq_P2_ITXXX) at 10 μM and either 200 ng of gDNA for growth-alone conditions or 2 μg of gDNA for fungal interaction conditions. For *E. coli* analysis, we performed 84 PCR assays (T0 sample and 28 collected samples in triplicate) involving 28 different multiplexing indices. For *P. psychrophila* str. JB418 analysis, we performed 84 PCR assays (T0 sample and 28 collected samples in triplicate) involving 28 different multiplexing indices. We used the following PCR programme: (1) 98 °C for 4 min; (2) 30 cycles of 98 °C for 30 s, 55 °C for 30 s and 72 °C for 30 s; and (3) 72 °C for 5 min. After the PCR, for both *E. coli* and *P. psychrophila*, 10 μl of each of the PCR products was pooled together to create the BarSeq sequencing library, and 200 μl of the pooled library was purified using a MinElute purification kit (Qiagen). The final elution of the BarSeq library was performed in 30 μl of DNase- and RNase-free water. The BarSeq libraries were then quantified using a Qubit dsDNA HS assay kit (Invitrogen) and sequenced on a HiSeq4000 (75 bp, single-end reads) by the IGM Genomics Center at the University of California, San Diego. The sequencing depth for each condition varied between 6.1 and 11.7 million reads for *E. coli* and 5.8 and 13.3 million reads for *P. psychrophila*.

RB-TnSeq data processing. Custom R scripts were used to determine the average fitness scores for each gene across three RB-TnSeq assay replicates. These scripts are available at https://github.com/DuttonLab/RB-TnSeq-Microbial-interactions. The Readme document provides an in-depth explanation of all the data processing steps performed in these scripts. Insertion mutants that did not have a sufficient T0 count (3) in each condition or that were not centrally inserted (10–90% of gene) were removed from the analysis. Counts as determined using the scripts described by Wetmore et al.[18] were then normalized using a set of five reference genes (*glgP*, *acnA*, *modE*, *leuA* and *idnK* in *E. coli* (average of 52 strains each) and the respective closest protein BLAST matches Ga0212129_11488, Ga0212129_114557, Ga0212129_111416, Ga0212129_112128 and Ga0212129_112491 (average of 74 strains each) in *P. psychrophila*) to be able to compare across conditions and to account for differences in sequencing depth. These genes have an absolute fitness effect of <0.6 in all conditions for all replicates in any condition based on a former fitness determination developed by Wetmore et al.[18]. Strain fitness (f_s) was then calculated per insertion mutant as the $\log_2$ of the ratio of the normalized counts in the condition and the normalized counts in the T0 sample (equation (1)).

$$f_s = \log_2\left(\frac{Cc}{Ct0}\right) \quad (1)$$

with *Cc* representing normalized counts in condition *C* and *Ct*0 representing normalized counts in T0.

Gene fitness and variance were next calculated by averaging insertion mutants within a gene. These values were then normalized based on the position of the gene along the chromosome using a smoothed median on a window of 251 genes as described in Wetmore et al.[18]. These steps were all done on individual replicates. For all conditions, replicates were highly correlated, with an averaged Pearson correlation coefficient of 0.85 for *E. coli* and 0.84 for *P. psychrophila*. Next, the average gene fitness (f_g) (equation (2)) and associated standard deviation (σ_g) (equation (3)) were calculated using the inverse of variance weighted average of the fitness values across the three different replicates.

$$f_g = \frac{\sum_{i=1}^{n} w_i \times f_{gi}}{\sum_{i=1}^{n} w_i} \quad (2)$$

$$\sigma_g = \sqrt{\left(\frac{n}{n-1}\right) \times \left(\frac{\sum_{i=1}^{n} w_i \times \left(f_g - \underline{f_{wg}}\right)^2}{\sum_{i=1}^{n} w_i}\right)} \quad (3)$$

With w_i representing the inverse of the gene fitness variance for each replicate, n the number of replicates and $\underline{f_{wg}}$ the weighted gene fitness average across the n replicates.

Final fitness values were then compared between fungal interaction conditions and bacteria alone conditions using two-sided *t*-tests (when the equality of variance was verified by Fisher test) and correction for multiple comparison (Benjamini–Hochberg method[75]). Comparisons associated with an adjusted *P* value lower than 5% were considered a significant interaction fitness (alphaF parameter=0.002 and alphaT parameter=0.05 in Script3_2conditions_FitnessComparison.Rmd code). The overall pipeline is described in Extended Data Fig. 1, and Supplementary Method 1 provides an example for a complete run. Networks of fitness values were visualized in Cytoscape (v.3.5.1)[74], and principal component analysis plots were made using the R packages ggplot2 (v.3.2.1)[70] and ggfortify (v.0.4.7)[76]. COG category mapping of *E. coli* and *P. psychrophila* protein sequences was done using eggNOG-mapper (v.2)[77].

Functional enrichment analysis of bacterial gene sets. ClusterProfiler[78] was used for GO functional enrichment analysis of bacterial gene sets with a false discovery rate *P* value adjustment cut-off of 0.1. For *E. coli*, the *E. coli* K12 database (org.EcK12.eg.db)[79] was used. For *P. psychrophila*, a custom annotation database was created using eggNOG-mapper v.2 (ref. [77]) GO assignments using AnnotationForge[80] in R.

Bacterial cytological profiling. Approximately 7,000,000 WT *E. coli* K12 strain BW25113 or Keio collection *mdtK* mutant cells[81] were inoculated alone or co-inoculated with 700,000 *Penicillium* sp. str. 12, *Penicillium* sp. str. 12 Δ*laeA* or *Penicillium* sp. str. SAM3 spores on 10% CCA pH 7. After 7 days of growth, 1 ml of T-Base buffer was added to the surface of the biofilms, and biofilms were scraped into the buffer. For co-culture conditions, the sample was filtered through a 0.5-μm filter to specifically remove fungal material. A total of 2 μl of concentrated dye mix (1 μl of 1 mg ml^{-1} FM4-64, 1 μl of 2 mg ml^{-1} 4,6-diamidino-2-phenylindole (DAPI) in 48 μl of T-Base) was added to 20 μl of filtrate. The dye filtrate mix was spotted onto agarose–LB pads (1% agarose, 20% LB liquid medium, 80% ddH_2O) and imaged by fluorescence and phase contrast microscopy using an Applied Precision Deltavision Spectris imaging system with an Olympus UPLFLN100XO2PH objective. Control compound references on CCA medium were obtained by spotting and drying 30 μl of 5-, 10-, 25- and 100-times minimum inhibitory concentration dilutions of antibiotics onto quadrants on CCA medium pH 7 plates and then spread-plating 200 μl of log-phase (OD of 0.1) *E. coli* cultures. After 2 days of growth, cells near the edge of the zone of inhibition on appropriate dilution spots were resuspended in 10 μl of prediluted dye mix (1 μl 1 mg ml^{-1} FM4-64, 1 μl 2 mg ml^{-1} DAPI in 998 μl of T-Base) and spotted onto agarose–LB pads and imaged as described above. Resulting images were deconvoluted using Deltavision SoftWorx software (Applied Precision), analysed using Fiji[82] and assembled in Adobe Photoshop (Adobe). Brightness was altered linearly in Fiji to aid visualization. For quantification of cell roundness, we defined the cell major axis as the longest possible line along the cell, and the cell minor axis was measured as the longest possible line orthogonal to the cell major axis. Cell measurements were obtained via the measure tool in Fiji[82], and single-cell major and minor axes measurements were collated. The pixel to micron ratio was set as 15.6 as per the microscope specifications. The major/minor axis ratio was calculated for all cells in the field. The number of fields was chosen to ensure measurement of at least 50 cells for each experimental condition. Individual ratio values for each cell were plotted via the R package ggplot2 (v.3.2.1)[70], and differences in major/minor ratios in the presence of a fungus relative to growth alone or with WT *Penicillium* sp. str. 12 relative to Δ*laeA Penicillium* sp. str. 12 were determined based on an unpaired two-sample Wilcoxon test $P < 0.05$.

CCA medium biotin quantification. Biotin quantification of CCA medium was performed on three replicate samples by Creative Proteomics as follows: 100 mg of each sample was homogenized in water (10 µl mg^{-1}) for 1 min three times with the aid of 5-mm metal balls on a MM400 mill mixer. Methanol (10 µl mg^{-1}) was then added. Water-soluble vitamins were extracted by vortex mixing for 2 min and sonication in a water batch for 5 min. After centrifugation, the clear supernatants were cleaned up by solid-phase extraction on a Strata-X (60 mg ml^{-1}) cartridge. The eluted fractions containing water-soluble vitamins were collected, pooled and then dried under a gentle nitrogen gas flow in a nitrogen evaporator. The residues were dissolved in 200 µl of 10% methanol. Aliquots (20 µl) were injected to run on a UPLC–MRM/MS with the use of a C18 UPLC column and with (+) ion detection and (−) ion detection. Calibration curves were prepared by injection of serially diluted mixed standard solutions of water-soluble vitamins. Concentrations of detected vitamins were calculated by interpolating the linear calibration curves.

Δ*fep* mutant competitive growth assays. Approximately 60,000 bacterial cells (a 1:1 ratio of WT cells and Δ*fepA*, Δ*fepC* or Δ*fepG* Keio collection[81] mutant cells) were inoculated either alone (no fungus) or co-inoculated with approximately 6,000 *Penicillium* sp. str. 12 or *Scopulariopsis* sp. str. JB370 spores on 10% CCA pH 7 in a 96-well plate in four replicates each (four distinct samples). After 7 days of growth, the entire well was collected and homogenized in 1×PBS–Tween 0.05% before dilution and plating on LB with 20 µg ml^{-1} cycloheximide (total bacterial counts) or with 20 µg ml^{-1} cycloheximide and 50 µg ml^{-1} kanamycin (bacterial mutant counts). Final growth counts were then compared in fungal co-culture conditions relative to bacterial growth alone to identify interaction effects. Significant growth effects were determined by significantly different growth in the presence of a fungus relative to growth alone based on a two-sided two-sample *t*-test $P < 0.05$. Plots made using the R package ggplot2 (v.3.2.1)[70].

Siderophore detection with CAS assays. The following methods were adapted from those described by Schwyn and Neilands[83] and Payne[84]. All glassware, caps and stir bars were cleaned with 6 M HCl and rinsed with deionized water. Plastic spatulas and doubly deionized water were used for solution preparation. A 2 mM CAS stock solution was prepared and stored in the dark at room temperature, and a 1 mM $FeCl_3$ stock solution was prepared. Piperazine buffer was prepared by dissolving 4.3095 g of anhydrous piperazine in 30 ml of water and adding 5 M HCl until the pH reached 5.635. To prepare the CAS reagent, 1.1202 ml of 0.05 M hexadecyltrimethylammonium bromide (HDTMA) was added to 50 ml of water. Then, 1.5 ml of 1 mM $FeCl_3$ stock solution was mixed with 7.5 ml of 2 mM CAS solution and added to the HDTMA solution. Last, the piperazine buffer was added to the solution and stirred. The resulting CAS assay solution was stored in the dark at room temperature. A 0.2 M shuttle solution was prepared with 5-sulfosalicylic acid dihydrate in water. The shuttle solution was stored in the dark at room temperature.

For detection of siderophore presence, fungal species were inoculated in triplicate into liquid 2% CCA pH 7, and cultures were grown at room temperature for 12 days. For filamentous fungi, cultures were left standing without shaking. After 12 days, supernatants were filtered through a 0.22-µm filter. Before use, the CAS assay solution was vortexed until all precipitates were resuspended. CAS assay incubations were performed in the dark at room temperature. For each fungal supernatant or CCA filtrate, 100 µl of CAS assay solution was added to 100 µl of supernatant. The resulting solution was mixed by pipetting and incubated for 15 min. After incubation, 2 µl of shuttle solution was added to the solution and mixed by pipetting. The solution was incubated for an additional 30 min. Sample absorbance of 630-nm light was measured in a 96-well plate using an Epoch 2 plate reader (BioTek).

For CAS assay comparisons of relative siderophore production in WT and Δ*laeA Penicillium* sp. str. 12, 200,000 spores of WT or Δ*laeA* were inoculated in triplicate in 3 ml of liquid 2% CCA pH 7. After 7 days of growth at room temperature without shaking, the biomass of the fungal mat was removed from the top of the culture and the entire supernatant was filtered through a 0.22-µm filter. Total filtrate was measured. Fungal mats were dried in a 60 °C drying oven for 2 days before being weighed. Filtrates were concentrated 3× in a SpeedVac Vacuum Concentrator and 100 µl of three replicates each of WT, Δ*laeA* and 2% liquid CCA were added to 100 µl of CAS solution, and CAS assays were performed as described above. Following CAS measurements, the percentage siderophore units were normalized to the entire volume of 1× filtrate and expressed as per mg of dried fungal biomass.

RNA-seq and differential expression analysis of *E. coli* with *Penicillium* sp. str. 12. Approximately 7,000,000 *E. coli* cells were inoculated in triplicate (three distinct samples) either alone or with approximately 700,000 *Penicillium* sp. str. 12 spores on 10% CCA pH 7 in standard petri dishes. After 3 days, the biofilms were collected for RNA extraction and washed with 1 ml of RNAprotect. RNA was extracted by a phenol–chloroform extraction (pH 8) using the same extraction protocol as for gDNA. Extractions were then purified using a OneStep PCR Inhibitor Removal kit (Zymo Research).

Sequencing libraries were prepared as follows: RNA samples were treated with DNase using the 'Rigorous DNase treatment' for the Turbo DNA-free kit (Ambion, Life Technologies), and the RNA concentration was measured by nucleic acid quantification in an Epoch microplate spectrophotometer (BioTek). Transfer RNAs and 5S RNA were then removed using a MEGAclear kit Purification for Large Scale Transcription Reactions (Ambion, Life Technologies) following the manufacturer's instructions. Absence of tRNA and 5S RNA was verified by running 100 ng of RNA on a 1.5% agarose gel, and the RNA concentration was quantified by nucleic acid quantification in an Epoch microplate spectrophotometer. Also, the presence of gDNA was assessed by PCR using universal bacterial 16S PCR primers (forward primer: AGAGTTTGATCCTGGCTCAG; reverse primer: GGTTACCTTGTTACGACTT). The PCR was performed in a final volume of 20 µl (10 µl of Q5 polymerase master mix (New England Biolabs), 0.5 µl of forward primer 10 µM, 0.5 µl of reverse primer 10 µM and 5 µl of non-diluted RNA). PCR products were run on a 1.7% agarose gel and if gDNA was amplified, another DNase treatment was performed as well as a new verification of absence of gDNA.

Ribosomal RNA depletion was performed using a RiboMinus Transcriptome Isolation kit (yeast and bacteria) for the *E. coli* alone samples and using both a RiboMinus Transcriptome Isolation kit (yeast and bacteria) and a RiboMinus Eukaryote kit v.2 for the mixed *E. coli–Penicillium* sp. str. 12 samples (ThermoFisher Scientific). For the *E. coli* alone samples, each sample was divided into two for treatment and then repooled for RNA recovery with ethanol precipitation. For the *E. coli–Penicillium* sp. str. 12 samples, an equal volume of the eukaryotic probe and RiboMinus Bacterial Probe Mix were used to deplete both bacterial and fungal ribosomal RNA, and RNA was recovered by ethanol precipitation. Concentrations after ribosomal RNA depletion were measured using Qubit RNA HS Assay kits (Invitrogen). The RNA-seq library was produced using a NEBNext Ultra RNA Library Prep kit for Illumina for purified mRNA or ribosome-depleted RNA. We prepared a library with a fragment size of 300 nucleotides and used the 10 µM NEBNext Multiplex Oligos for Illumina (Set 1, NEB E7335, lot 0091412) and the NEBNext multiplex Oligos for Illumina (Set 2, NEB E7500, lot 0071412). We performed PCR product purification with 0.8× Agencourt AMPure XP Beads. Library samples were quantified using Qubit DNA HS Assay kits before the quality and fragment size were validated by TapeStation (HiSensD1000 ScreenTape). Library samples were pooled at a concentration of 15 nM each and were sequenced on a HiSeq4000 (50 bp, single-end). TapeStation assays and sequencing were performed by the IGM Genomics Center at the University of California, San Diego.

Following sequencing, reads were mapped to the concatenated genome of *E. coli* K12 BW25113 (ref. [85]) and *Penicillium* sp. str. 12 using Geneious v.R9 9.1.8 (http://www.geneious.com). Only the reads that uniquely mapped to a single location on the *E. coli* genome section were kept. *E. coli* expression analysis was performed using the following R packages: Rsamtools (R package v.2.0.3), GenomeInfoDb (R package v.1.20.0), GenomicFeatures[86] (R package v.1.36.4), GenomicAlignments[86] (R package v.1.20.1), GenomicRanges[86] (R package v.1.36.1) and DESeq2 (ref. [87]) (R package v.1.20.1). We followed the workflow described by Love et al. 2014 (ref. [87]) and performed the differential expression analysis using the package DESeq2. Differentially expressed genes between conditions were selected using an adjusted *P* value lower than 5% (Benjamini–Hochberg correction for multiple testing[75]) and an absolute $\log_2$ fold change equal to or greater than 1.5.

Construction of *E. coli* mutants and visual interaction assays. *Visual assays for purified hydroxamate siderophore stimulation.* Antibiotic assay discs (Whatman) were placed on CCA medium pH 7 with 0.005% tetrazolium chloride (an indicator of cellular respiration) and 20 µl of water, or 10 µM coprogen or ferrichrome (EMC Microcollections) solutions (in water) were slowly pipetted onto the disc and allowed to absorb. Aliquots (2.5 µl) of 37 °C overnight LB cultures of *E. coli* K12 BW25113 WT, Δ*fepA*, Δ*fepC*, Δ*fhuE*, Δ*fhuA*, Δ*fepA*Δ*fhuE*, Δ*fepC*Δ*fhuE* or Δ*fepA*Δ*fhuA* mutants[81] were spotted next to the discs. Double mutants were constructed as described below. Plates were left at room temperature until development of red colour resulting from tetrazolium chloride, an indicator of respiration.

Visual assays for fungal stimulation of bacterial mutants. Fungal spores were inoculated on CCA pH 7 with 0.005% tetrazolium chloride. After fungal pre-culturing at room temperature (cheese fungal isolates) or 30 °C (*A. fumigatus* and *M. pachydermatis*), 2.5 µl of *E. coli* overnight cultures grown in LB medium at 37 °C were spotted at increasing distances from the fungal front. Plates were left at room temperature until red colour developed. The *A. fumigatus* isolate AF293 was received from N. Keller, University of Wisconsin–Madison. *M. pachydermatis* was originally isolated from the ear of a dog in Sweden (ATCC14522 from ATCC).

Creation of Δ*fepA*Δ*fhuE* and Δ*fepC*Δ*fhuE*. Chemically competent cells for Δ*fepA* or Δ*fepC* mutants were created. An overnight culture of Δ*fepA* or Δ*fepC* mutants was diluted 1:100 and grown at 37 °C until OD of 0.4–0.6. The culture was placed on ice for 20 min and then centrifuged at 4 °C for 10 min at 6,000 r.p.m. to collect the cells. The supernatant was removed, and cells were resuspended in half the previous volume of pre-cooled 0.1 M $CaCl_2$. After incubating on ice for 30 min, centrifugation was repeated, and supernatant was removed before resuspension in one-quarter of the original volume of pre-cooled 0.1 M $CaCl_2$/15% glycerol. Cells were aliquoted and stored at −80 °C until transformation. These cells were transformed with the pKD46 plasmid[88], recovered at 30 °C, and plated

on LB plates with 100 μg ml^{-1} ampicillin and grown at 30 °C. Overnight cultures were started from individual colonies for the creation of electrocompetent cells. Overnight cultures of Δ*fepC*-pkD46 or Δ*fepA*-pkD46 were diluted 1:100 in fresh LB with 100 μg ml^{-1} ampicillin and grown at 30 °C until an OD of 0.1. A total of 20 μl of fresh 1 M L-arabinose was added, and growth was continued at 30 °C until OD 0.4–0.6. Cells were then chilled on ice for 15 min and then centrifuged for 10 min at 4,000 r.c.f. at 4 °C. Cells were resuspended in 1 ml of ice water and centrifuged for 10 min at 4,000 r.c.f. at 4 °C. Cells were resuspended in 0.5 ml of ice water and centrifuged for 10 min at 4,000 r.c.f. at 4 °C. Cells were resuspended in 50 μl of ice water and kept on ice until transformation. The chloramphenicol resistance cassette was amplified from the pKD3 plasmid[88] using the following custom primers: FhuEcatF (CAGATGGCTGCCTTTTTTACAGGTGTTATTCA-GAATTGATACGTGCCGGTAATGGCGCGCCTTACGCCCC) and FhuEcatR (CCTCCTCCGGCATGAGCCTGACGACAACATAAACCAAGAGATTTCAAA-TGCTGGGCCAACTTTTGGCGAA). The following PCR conditions were used: (1) 98 °C for 30 s; (2) 30 cycles of 98 °C for 10 s, 70 °C for 20 s and 72 °C for 3 s; and (3) 72 °C for 5 min. Amplification was performed on 4 ng of pKD3 plasmid using Q5 High-Fidelity 2× Master Mix (New England Biolabs). The PCR product was digested for 1 h with the restriction enzymes DpnI and ClaI at 37 °C and then the PCR product was run on a 1% agarose gel. The PCR product was extracted using a QIAquick Gel Extraction kit (Qiagen) and then dialysed for 4 h with TE buffer. A total of 1.5 μl of dialysed PCR product was used to transform the electrocompetent Δ*fepC*-pkD46 or Δ*fepA*-pkD46 cells. After 2 h of recovery in SOC medium with 1 mM arabinose at 37 °C, the transformants was plated on LB with 50 mg ml^{-1} kanamycin and chloramphenicol. Transformants were confirmed to be Δ*fhuE* with Eton Bioscience sequencing of the chloramphenicol cassette.

Creation of Δ*fepA*Δ*fhuA*. Creation was done as for Δ*fepA*Δ*fhuE*, except that the chloramphenicol resistance cassette was amplified from pKD3 (ref. [88]) using FhuAcatF (ATCATTCTCGTTTACGTTATCATTCACTTT ACATCAGAGATATACCAATGAATGGCGCGCCTTACGCCCCAATGG CGCGCCTTACGCCCC) and FhuAcatR (GCACGGAAATCCGTGCCC-CAAAAGAGAAATTAGAAACGGAAGGTTGCGGTCTGGGCCAAC-TTTTGGCGAACTGGGCCAACTTTTGGCGAA) custom primers.

***Penicillium* sp. str. 12 genome sequencing, assembly and annotation.** gDNA was extracted from *Penicillium* sp. str. 12 using the gDNA extraction protocol described above. High molecular weight DNA (average 16 kilobases) was sequenced on an Oxford Nanopore MinION with a R.9.5 flow cell using 1D[2] sequencing adaptors from kit SQK-LSK308 (Oxford Nanopore Technologies). Raw data were base called using guppy 3.3.0 (Oxford Nanopore Technologies) (guppy_basecaller -config dna_r9.5_450bps.cfg -fast5_out) for 1D base calls and these were used to also obtain higher accuracy 1D[2] base calls (guppy_basecaller_1d2 -i 1Dbasecall/ workspace/ -config dba_r9.5_450bps_1d2_raw.cfg -index_file 1Dbasecall/ sequencing_summary.txt). These reads were assembled by canu 1.8 (ref. [89]) and polished by racon 1.4.3 (ref. [90]) four times and by pilon 1.23 (ref. [91]) once. The final assembly is 38 Mbp and consists of 52 contigs.

Penicillium sp. str. 12 genome annotations were obtained by combining genomic and transcriptomic information from RNA-seq. To obtain the gene expression profile of *Penicillium* sp. str. 12, approximately 700,000 WT *Penicillium* sp. str. 12 spores were inoculated in triplicate on 10% CCA pH 7 in standard petri dishes. After 3 days, the biofilms were collected for RNA extraction and washed with 1 ml of RNAprotect. RNA was extracted and RNA-seq libraries were prepared as described above with the following modification: ribosomal RNA depletion was performed using a RiboMinus Eukaryote kit v1, and RNA was recovered by ethanol precipitation. After sequencing, the RNA-seq reads from these *Penicillium* sp. str. 12 alone cultures were concatenated with RNA-seq reads from the previously described *E. coli*–*Penicillium* sp. str. 12 co-culture conditions that uniquely mapped to a single location on the *Penicillium* sp. str. 12 genome. The full set of transcriptomic reads was then used as input into the FunGAP annotation pipeline and 77 million of these reads were mapped[92]. This pipeline predicted 13,261 protein-coding genes in the *Penicillium* sp. str. 12 genome. Interproscan[93] was used within the FunGAP pipeline for function prediction of genes. This Whole Genome Shotgun project has been deposited at DDBJ/ENA/GenBank under the accession JAASRZ000000000. The version described in this paper is version JAASRZ010000000.

Creation and confirmation of *Penicillium* sp. str. 12 *laeA* deletion mutant. The deletion cassette design strategy involved knocking out *laeA* in *Penicillium* sp. str. 12, whereby the isolate was first screened for hygromycin and phleomycin resistance. *Penicillium* sp. str. 12 showed a confirmed sensitivity to both antibiotics. A three-round PCR deletion strategy was used to replace the *laeA* open reading frame (ORF) with the *hph* gene, whose expression confers selection on hygromycin[94]. A schematic representation of the *laeA* gene replacement with the *hph* gene is depicted in Supplementary Fig. 3. The deletion cassette (5′flank- hph- 3′flank) was constructed using three sequential PCR reactions. In the first PCR round, about 1 kilobase of the genome sequence flanking either the 5′ or 3′ end of the *laeA* ORF was amplified using the primer sets P12_KOlaeA_5′F (CTCCGTTGGGCCCTCAC) and 5′R (GCAATTTAACTGTGATAAACTACCGCATTAAAGCTGTTGATATCGGC AATCAATCAATG) or P12_KOlaeA_3′F (GGTGGGCCTTGACATGTGCAGCC GGTGGAGCGGCGCCTGGTGAATCCTACCCACATGG) and 3′R (CGTTGG GAGGAAAAGCTTCTGCG), respectively. The *hph* gene was amplified from plasmid pUCH2-8 using primers hph_F (AGCTTTAATGCGGTAGTTTATCA CAG) and hph_R (CTCCACCGGCTGCACATGTC). A second PCR reaction was performed to assemble the three individual fragments from the first round of PCR by homologous recombination. The deletion cassettes were finally amplified using the nested primer set P12_KOlaeA_NestedF (CAGACGGTCCGCATCCCG) and P12_KOlaeA_NestedR (GGTCCAGGTGCAGTAGTACTG).

To generate the deletion strains, a protoplast-mediated transformation protocol was employed. Briefly, 109 fresh spores were cultured in 500 ml of liquid minimal medium for 12 h at 25 °C and 280 r.p.m. Newly born hyphae were collected by centrifugation at 8,000 r.p.m. for 15 min and hydrolysed in a mixture of 30 mg Lysing Enzyme from Trichoderma (Sigma-Aldrich) and 20 mg Yatalase (Fisher Scientific) in 10 ml of osmotic medium (1.2 M $MgSO_4$, 10 mM NaPB, pH 5.8). The quality of the protoplasts was monitored under the microscope after 4 h of shaking at 28 °C and 80 r.p.m. The protoplast mixture was later overlaid with 10 ml of trapping buffer (0.6 M sorbitol, 100 mM Tris-HCl pH 7.0) and centrifuged for 15 min at 4 °C and 5,000 r.p.m. Protoplasts were collected from the interface, overlaid with an equal volume of STC (1.2 M sorbitol, 10 mM Tris-HCL pH 7.5,10 mM $CaCl_2$) and decanted by centrifugation at 6,000 r.p.m. for 8 min. The protoplast pellet was resuspended in 500 μl STC and used for transformation. After 5 days of incubation at 25 °C, colonies grown on stabilized minimal medium plates supplemented with hygromycin were subjected to a second round of selection on hygromycin plates. In total, 25 hygromycin-resistant transformants were isolated after a rapid screening procedure on stabilized minimal medium supplemented with hygromycin. Single-spored transformants were later tested for proper homologous recombination at the ORF locus by PCR and Southern blot analysis.

The correct replacement of *laeA* with the *hph* gene was first verified by PCR analysis of gDNA from the transformant strains using the primer set P12_laeA_F (CACAATGGCTGAACACTCTCGG) and P12_laeA_R (GGGATATGGAGCATCGAAGTTGC) that amplify the *laeA* ORF. About 12% (3 out of 25) of the monoconidial lines generated from primary transformants of *Penicillium* sp. str. 12 were PCR-positive for the absence of the *laeA* ORF. The positive deletion strains were further checked for a single insertion of the deletion cassette by Southern blot analysis and revealed single-site integration of the deletion cassette in one transformant (Supplementary Fig. 3). Probes corresponding to the 5′ and 3′ flanks of the *laeA* gene in each strain were labelled using [α32P] dCTP (PerkinElmer) following the manufacturer's instructions.

RNA-seq analysis of WT and Δ*laeA Penicillium* sp. str. 12. To characterize the effect of the *laeA* deletion on the *Penicillium* sp. str. 12 gene expression profile, we performed RNA-seq analysis for Δ*laeA Penicillium* sp. str. 12. As for WT *Penicillium* sp. str. 12, 700,000 Δ*laeA Penicillium* sp. str. 12 spores were inoculated in triplicate (three distinct samples) on 10% CCA pH 7 in standard petri dishes, and biofilms were collected after 3 days. Collection, RNA extraction and library preparation were performed identically to that for WT *Penicillium* sp. str. 12. Then, *Penicillium* sp. str. 12 and Δ*laeA* differential expression analysis was performed as described for *E. coli*–*Penicillium* sp. str. 12 above. To look for enrichment of functions in the set of differentially expressed genes, we input the protein sequences of the genes into the gene-list enrichment function of KOBAS 3.0 (ref. [95]). Sequences were searched against the GO database[96,97] using *A. fumigatus* as a reference for GO assignment before conducting a hypergeometric test with Benjamini–Hochberg correction. Functions with a corrected $P < 0.05$ were considered enriched.

WT and Δ*laeA Penicillium* sp. str. 12 growth assays. For radial growth assays, 2,000 WT or Δ*laeA Penicillium* sp. str. 12 fungal spores were inoculated as spots in triplicate on 10% CCA pH 7 either alone or with 20,000 *E. coli* cells. The radius of fungal growth was measured after 7 days. For spore counting assays, we aimed to inoculate 6,000 WT or Δ*laeA Penicillium* sp. str. 12 fungal spores per well on 10% CCA pH 7 in a 96-well plate either alone or co-inoculated with 60,000 *E. coli* cells. Each assay was done in triplicate. After 7 days of growth, the entire well was collected and homogenized in 1× PBS–Tween 0.05% before dilution and plating on PCAMS with 50 μg ml^{-1} chloramphenicol (for fungal spore counts).

Availability of biological materials. All unique materials, including the described fungal strains isolated from cheese, the *P. psychrophila* JB418 strain and the RB-TnSeq library, the *Penicillium* sp. str. 12 *laeA* deletion mutant and the *E. coli* siderophore-uptake double mutants, are readily available from the authors upon request. The *E. coli* RB-TnSeq library and Keio strains can be requested from the groups that created these resources (PMID references are provided in Supplementary Table 19).

Reporting Summary. Further information on research design is available in the Nature Research Reporting Summary linked to this article.

Data availability

Sequence data that support the findings of this study (RB-TnSeq and RNA-seq) have been deposited in the NCBI SRA database with SRA accession codes SRR11514793–SRR11514872 and BioProject code PRJNA624168. MS data are available in the MassIVE database under accession numbers MSV000085070 and MSV000085054. The GNPS molecular network is available at https://gnps.ucsd.edu/ProteoSAFe/status.jsp?task=464b331ef9d54de9957d23b4f9b9db14. The *E. coli* annotation database used for GO functional enrichment is available at http://bioconductor.org/packages/release/data/annotation/html/org.EcK12.eg.db.html. The Whole Genome Shotgun project for *Penicillium* sp. str. 12, including reads, genome assembly and annotation has been deposited at DDBJ/ENA/GenBank under the accession JAASRZ000000000 in BioProject PRJNA612335 (BioSample SAMN14369290 and SRA SRR11536435). In addition to these sources, the data used to create Figs. 2, 3, 5 and 6 are available in the Supplementary Tables provided with the paper. Uncropped Southern blots associated with Supplementary Fig. 3 are provided with the manuscript as Supplementary Data. Source data are provided with this paper.

Code availability

The R scripts developed for processing RB-TnSeq data described in this manuscript are available at https://github.com/DuttonLab/RB-TnSeq-Microbial-interactions along with usage instructions. The perl scripts needed for initial processing of RB-TnSeq data published in Wetmore et al.[18] are available at https://bitbucket.org/berkeleylab/feba/src/master/.

Received: 30 March 2020; Accepted: 16 September 2020;
Published online: 02 November 2020

References

1. Laforest-Lapointe, I. & Arrieta, M.-C. Microbial eukaryotes: a missing link in gut microbiome studies. *mSystems* **3**, e00201-17 (2018).
2. Huseyin, C. E., O'Toole, P. W., Cotter, P. D. & Scanlan, P. D. Forgotten fungi—the gut mycobiome in human health and disease. *FEMS Microbiol. Rev.* **41**, 479–511 (2017).
3. Bergelson, J., Mittelstrass, J. & Horton, M. W. Characterizing both bacteria and fungi improves understanding of the *Arabidopsis* root microbiome. *Sci. Rep.* **9**, 24 (2019).
4. Huffnagle, G. B. & Noverr, M. C. The emerging world of the fungal microbiome. *Trends Microbiol.* **21**, 334–341 (2013).
5. Bradford, L. L. & Ravel, J. The vaginal mycobiome: a contemporary perspective on fungi in women's health and diseases. *Virulence* **8**, 342–351 (2017).
6. de Phillips, F., Laiola, M., Blaiotta, G. & Ercolini, D. Different amplicon targets for sequencing-based studies of fungal diversity. *Appl. Environ. Microbiol.* **83**, e00905-17 (2017).
7. Jiang, T. T. et al. Commensal fungi recapitulate the protective benefits of intestinal bacteria. *Cell Host Microbe* **22**, 809–816 (2017).
8. Wagg, C., Schlaeppi, K., Banerjee, S., Kuramae, E. E. & van der Heijden, M. G. A. Fungal–bacterial diversity and microbiome complexity predict ecosystem functioning. *Nat. Commun.* **10**, 4841 (2019).
9. Durán, P. et al. Microbial interkingdom interactions in roots promote *Arabidopsis* survival. *Cell* **175**, 973–983 (2018).
10. Tourneroche, A. et al. Bacterial–fungal interactions in the kelp endomicrobiota drive autoinducer-2 quorum sensing. *Front. Microbiol.* **10**, 1693 (2019).
11. Lindsay, A. K. & Hogan, D. A. *Candida albicans*: molecular interactions with *Pseudomonas aeruginosa* and *Staphylococcus aureus*. *Fungal Biol. Rev.* **28**, 85–96 (2014).
12. Xu, X.-L. et al. Bacterial peptidoglycan triggers *Candida albicans* hyphal growth by directly activating the adenylyl cyclase Cyr1p. *Cell Host Microbe* **4**, 28–39 (2008).
13. Spraker, J. E. et al. Conserved responses in a war of small molecules between a plant-pathogenic bacterium and fungi. *mBio* **9**, e00820-18 (2018).
14. Khalid, S. et al. NRPS-derived isoquinolines and lipopetides mediate antagonism between plant pathogenic fungi and bacteria. *ACS Chem. Biol.* **13**, 171–179 (2018).
15. Wolfe, B. E., Button, J. E., Santarelli, M. & Dutton, R. J. Cheese rind communities provide tractable systems for in situ and in vitro studies of microbial diversity. *Cell* **158**, 422–433 (2014).
16. Morin, M., Pierce, E. C. & Dutton, R. J. Changes in the genetic requirements for microbial interactions with increasing community complexity. *eLife* **7**, e37072 (2018).
17. Zhang, Y., Kastman, E. K., Guasto, J. S. & Wolfe, B. E. Fungal networks shape dynamics of bacterial dispersal and community assembly in cheese rind microbiomes. *Nat. Commun.* **9**, 336 (2018).
18. Wetmore, K. M. et al. Rapid quantification of mutant fitness in diverse bacteria by sequencing randomly bar-coded transposons. *mBio* **6**, e00306-15 (2015).
19. Hallen-Adams, H. E. & Suhr, M. J. Fungi in the healthy human gastrointestinal tract. *Virulence* **8**, 352–358 (2017).
20. Frąc, M., Hannula, S. E., Bełka, M. & Jędryczka, M. Fungal biodiversity and their role in soil health. *Front. Microbiol.* **9**, 707 (2018).
21. Dukare, A. S. et al. Exploitation of microbial antagonists for the control of postharvest diseases of fruits: a review. *Crit. Rev. Food Sci. Nutr.* **59**, 1498–1513 (2019).
22. Richards, T. A., Jones, M. D. M., Leonard, G. & Bass, D. Marine fungi: their ecology and molecular diversity. *Ann. Rev. Mar. Sci.* **4**, 495–522 (2012).
23. Choi, K.-H., Lee, H., Lee, S., Kim, S. & Yoon, Y. Cheese microbial risk assessments—a review. *Asian-Australas. J. Anim. Sci.* **29**, 307–314 (2016).
24. Perrin, F. et al. Quantitative risk assessment of haemolytic and uremic syndrome linked to O157:H7 and non-O157:H7 shiga-toxin producing *Escherichia coli* strains in raw milk soft cheeses: quantitative risk assessment of HUS linked to pathogenic STEC in cheese. *Risk Anal.* **35**, 109–128 (2015).
25. Cosetta, C. M. & Wolfe, B. E. Deconstructing and reconstructing cheese rind microbiomes for experiments in microbial ecology and evolution. *Curr. Protoc. Microbiol.* **56**, e95 (2020).
26. Calvo, A. M., Wilson, R. A., Bok, J. W. & Keller, N. P. Relationship between secondary metabolism and fungal development. *Microbiol. Mol. Biol. Rev.* **66**, 447–459 (2002).
27. Nonejuie, P., Burkart, M., Pogliano, K. & Pogliano, J. Bacterial cytological profiling rapidly identifies the cellular pathways targeted by antibacterial molecules. *Proc. Natl Acad. Sci. USA* **110**, 16169–16174 (2013).
28. Bok, J. W. & Keller, N. P. LaeA, a regulator of secondary metabolism in *Aspergillus* spp. *Eukaryot. Cell* **3**, 527–535 (2004).
29. Kosalková, K. et al. The global regulator LaeA controls penicillin biosynthesis, pigmentation and sporulation, but not roquefortine C synthesis in *Penicillium chrysogenum*. *Biochimie* **91**, 214–225 (2009).
30. Laich, F., Fierro, F. & Martín, J. F. Production of penicillin by fungi growing on food products: identification of a complete penicillin gene cluster in *Penicillium griseofulvum* and a truncated cluster in *Penicillium verrucosum*. *Appl. Environ. Microbiol.* **68**, 1211–1219 (2002).
31. Streit, W. R. & Entcheva, P. Biotin in microbes, the genes involved in its biosynthesis, its biochemical role and perspectives for biotechnological production. *Appl. Microbiol. Biotechnol.* **61**, 21–31 (2003).
32. Kastman, E. K. et al. Biotic interactions shape the ecological distributions of *Staphylococcus* species. *mBio* **7**, e01157-16 (2016).
33. Bonham, K. S., Wolfe, B. E. & Dutton, R. J. Extensive horizontal gene transfer in cheese-associated bacteria. *eLife* **6**, e22144 (2017).
34. Dean, C. R. & Poole, K. Expression of the ferric enterobactin receptor (PfeA) of *Pseudomonas aeruginosa*: involvement of a two-component regulatory system. *Mol. Microbiol.* **8**, 1095–1103 (1993).
35. Schalk, I. J., Rigouin, C. & Godet, J. An overview of siderophore biosynthesis among fluorescent Pseudomonads and new insights into their complex cellular organization. *Environ. Microbiol.* **22**, 1447–1466 (2020).
36. Fecker, L. & Braun, V. Cloning and expression of the *fhu* genes involved in iron(III)-hydroxamate uptake by *Escherichia coli*. *J. Bacteriol.* **156**, 1301–1314 (1983).
37. Sauer, M., Hantke, K. & Braun, V. Ferric-coprogen receptor FhuE of *Escherichia coli*: processing and sequence common to all TonB-dependent outer membrane receptor proteins. *J. Bacteriol.* **169**, 2044–2049 (1987).
38. Blin, K. et al. antiSMASH 5.0: updates to the secondary metabolite genome mining pipeline. *Nucleic Acids Res.* **47**, W81–W87 (2019).
39. Triana, S. et al. Draft genome sequence of the animal and human pathogen malassezia pachydermatis strain CBS 1879. *Genome Announc.* **3**, e01197-15 (2015).
40. Sarkar, S. K., Chowdhury, C. & Ghosh, A. S. Deletion of penicillin-binding protein 5 (PBP5) sensitises *Escherichia coli* cells to β-lactam agents. *Int. J. Antimicrob. Agents* **35**, 244–249 (2010).
41. Perrin, R. M. et al. Transcriptional regulation of chemical diversity in *Aspergillus fumigatus* by LaeA. *PLoS Pathog.* **3**, e50 (2007).
42. Haas, H. Fungal siderophore metabolism with a focus on *Aspergillus fumigatus*. *Nat. Prod. Rep.* **31**, 1266–1276 (2014).
43. Luckner, M. [On the synthesis of quinoline alkaloids in plants. 2. Fermentativ conversion of the penicillin alkaloids cyclopenin and cyclopenol to viridicatin and viridicatol]. *Eur. J. Biochem.* **2**, 74–78 (1967).
44. Peters, B. M., Jabra-Rizk, M. A., O'May, G. A., Costerton, J. W. & Shirtliff, M. E. Polymicrobial interactions: impact on pathogenesis and human disease. *Clin. Microbiol. Rev.* **25**, 193–213 (2012).
45. Scherlach, K., Graupner, K. & Hertweck, C. Molecular bacteria–fungi interactions: effects on environment, food, and medicine. *Annu. Rev. Microbiol.* **67**, 375–397 (2013).
46. de Boer, W., Folman, L. B., Summerbell, R. C. & Boddy, L. Living in a fungal world: impact of fungi on soil bacterial niche development. *FEMS Microbiol. Rev.* **29**, 795–811 (2005).
47. Johansson, J. F., Paul, L. R. & Finlay, R. D. Microbial interactions in the mycorrhizosphere and their significance for sustainable agriculture. *FEMS Microbiol. Ecol.* **48**, 1–13 (2004).

48. Tarkka, M. T., Sarniguet, A. & Frey-Klett, P. Inter-kingdom encounters: recent advances in molecular bacterium–fungus interactions. *Curr. Genet.* **55**, 233–243 (2009).
49. Taga, M. E. & Walker, G. C. *Sinorhizobium meliloti* requires a cobalamin-dependent ribonucleotide reductase for symbiosis with its plant host. *Mol. Plant. Microbe Interact.* **23**, 1643–1654 (2010).
50. Deveau, A. et al. Role of fungal trehalose and bacterial thiamine in the improved survival and growth of the ectomycorrhizal fungus *Laccaria bicolor* S238N and the helper bacterium *Pseudomonas fluorescens* BBc6R8. *Environ. Microbiol. Rep.* **2**, 560–568 (2010).
51. Hantke, K. Identification of an iron uptake system specific for coprogen and rhodotorulic acid in *Escherichia coli* K12. *Mol. Gen. Genet.* **191**, 301–306 (1983).
52. Arias, A. A. et al. Growth of desferrioxamine-deficient *Streptomyces* mutants through xenosiderophore piracy of airborne fungal contaminations. *FEMS Microbiol. Rev.* **91**, fiv080 (2015).
53. Haas, H., Eisendle, M. & Turgeon, B. G. Siderophores in fungal physiology and virulence. *Annu. Rev. Phytopathol.* **46**, 149–187 (2008).
54. Park, M., Cho, Y.-J., Lee, Y. W. & Jung, W. H. Understanding the mechanism of action of the anti-dandruff agent zinc pyrithione against *Malassezia restricta*. *Sci. Rep.* **8**, 12086 (2018).
55. Gründlinger, M. et al. Fungal siderophore biosynthesis is partially localized in peroxisomes. *Mol. Microbiol.* **88**, 862–875 (2013).
56. Heymann, P., Ernst, J. F. & Winkelmann, G. A gene of the major facilitator superfamily encodes a transporter for enterobactin (Enb1p) in *Saccharomyces cerevisiae*. *Biometals* **13**, 65–72 (2000).
57. Sass, G. et al. Studies of *Pseudomonas aeruginosa* mutants indicate pyoverdine as the central factor in inhibition of *Aspergillus fumigatus* biofilm. *J. Bacteriol.* **200**, e00345-17 (2017).
58. Briard, B. et al. *Pseudomonas aeruginosa* manipulates redox and iron homeostasis of its microbiota partner *Aspergillus fumigatus* via phenazines. *Sci. Rep.* **5**, 8220 (2015).
59. Clancy, A. et al. Evidence for siderophore-dependent iron acquisition in group B streptococcus. *Mol. Microbiol.* **59**, 707–721 (2006).
60. Jin, B. et al. Iron acquisition systems for ferric hydroxamates, haemin and haemoglobin in *Listeria monocytogenes*. *Mol. Microbiol.* **59**, 1185–1198 (2006).
61. Mishra, R. P. N. et al. *Staphylococcus aureus* FhuD2 is involved in the early phase of staphylococcal dissemination and generates protective immunity in mice. *J. Infect. Dis.* **206**, 1041–1049 (2012).
62. Rocha, E. R. & Krykunivsky, A. S. Anaerobic utilization of Fe(III)-xenosiderophores among *Bacteroides* species and the distinct assimilation of Fe(III)-ferrichrome by *Bacteroides fragilis* within the genus. *MicrobiologyOpen* **6**, e00479 (2017).
63. Li, H. et al. The outer mucus layer hosts a distinct intestinal microbial niche. *Nat. Commun.* **6**, 8292 (2015).
64. Ong, S. A. & Neilands, J. B. Siderophores in microbially processed cheese. *J. Agric. Food Chem.* **27**, 990–995 (1979).
65. David, L. A. et al. Diet rapidly and reproducibly alters the human gut microbiome. *Nature* **505**, 559–563 (2014).
66. Rehner, S. A. & Samuels, G. J. Molecular systematics of the Hypocreales: a teleomorph gene phylogeny and the status of their anamorphs. *Can. J. Bot.* **73**, 816–823 (1995).
67. Glass, N. L. & Donaldson, G. C. Development of primer sets designed for use with the PCR to amplify conserved genes from filamentous ascomycetes. *Appl. Environ. Microbiol.* **61**, 1323–1330 (1995).
68. Ronquist, F. & Huelsenbeck, J. P. MrBayes 3: Bayesian phylogenetic inference under mixed models. *Bioinformatics* **19**, 1572–1574 (2003).
69. Dunnett, C. W. A multiple comparison procedure for comparing several treatments with a Control. *J. Am. Stat. Assoc.* **50**, 1096–1121 (1955).
70. Wickham, H. *ggplot2: Elegant Graphics for Data Analysis* (Springer Science+Business Media, 2009).
71. Cleary, J. L., Luu, G. T., Pierce, E. C., Dutton, R. J. & Sanchez, L. M. BLANKA: an algorithm for blank subtraction in mass spectrometry of complex biological samples. *J. Am. Soc. Mass. Spectrom.* **30**, 1426–1434 (2019).
72. Mohimani, H. et al. Dereplication of microbial metabolites through database search of mass spectra. *Nat. Commun.* **9**, 4035 (2018).
73. Mohimani, H. et al. Dereplication of peptidic natural products through database search of mass spectra. *Nat. Chem. Biol.* **13**, 30–37 (2017).
74. Shannon, P. et al. Cytoscape: a software environment for integrated models of biomolecular interaction networks. *Genome Res.* **13**, 2498–2504 (2003).
75. Benjamini, Y. & Hochberg, Y. Controlling the false discovery rate: a practical and powerful approach to multiple testing. *J. R. Stat. Soc. Ser. B Stat. Methodol.* **57**, 289–300 (1995).
76. Tang, Y., Horikoshi, M. & Li, W. ggfortify: unified interface to visualize statistical result of popular R packages. *R Journal* **8**, 474–485 (2016).
77. Huerta-Cepas, J. et al. eggNOG 5.0: a hierarchical, functionally and phylogenetically annotated orthology resource based on 5090 organisms and 2502 viruses. *Nucleic Acids Res.* **47**, D309–D314 (2019).
78. Yu, G., Wang, L.-G., Han, Y. & He, Q.-Y. clusterProfiler: an R package for comparing biological themes among gene clusters. *OMICS* **16**, 284–287 (2012).
79. Carlson, M. org.EcK12.eg.db: Genome wide annotation for *E. coli* strain K12. R package version 3.8.2. (Bioconductor, 2019).
80. Carlson, M. & Pagès, H. AnnotationForge: tools for building SQLite-based annotation data packages. R package version 1.26.0 (Bioconductor, 2019).
81. Baba, T. et al. Construction of *Escherichia coli* K-12 in-frame, single-gene knockout mutants: the Keio collection. *Mol. Syst. Biol.* **2**, 2006.0008 (2006).
82. Schindelin, J. et al. Fiji: an open-source platform for biological-image analysis. *Nat. Methods* **9**, 676–682 (2012).
83. Schwyn, B. & Neilands, J. B. Universal chemical assay for the detection and determination of siderophores. *Anal. Biochem.* **160**, 47–56 (1987).
84. Payne, S. M. Detection, isolation, and characterization of siderophores. *Methods Enzymol.* **235**, 329–344 (1994).
85. Grenier, F., Matteau, D., Baby, V. & Rodrigue, S. Complete genome sequence of *Escherichia coli* BW25113. *Genome Announc.* **2**, e01038-14 (2014).
86. Lawrence, M. et al. Software for computing and annotating genomic ranges. *PLoS Comput. Biol.* **9**, e1003118 (2013).
87. Love, M. I., Huber, W. & Anders, S. Moderated estimation of fold change and dispersion for RNA-seq data with DESeq2. *Genome Biol.* **15**, 550 (2014).
88. Datsenko, K. A. & Wanner, B. L. One-step inactivation of chromosomal genes in *Escherichia coli* K-12 using PCR products. *Proc. Natl Acad. Sci. USA* **97**, 6640–6645 (2000).
89. Koren, S. et al. Canu: scalable and accurate long-read assembly via adaptive *k*-mer weighting and repeat separation. *Genome Res.* **27**, 722–736 (2017).
90. Vaser, R., Sović, I., Nagarajan, N. & Šikić, M. Fast and accurate de novo genome assembly from long uncorrected reads. *Genome Res.* **27**, 737–746 (2017).
91. Walker, B. J. et al. Pilon: an integrated tool for comprehensive microbial variant detection and genome assembly improvement. *PLoS ONE* **9**, e112963 (2014).
92. Min, B., Grigoriev, I. V. & Choi, I.-G. FunGAP: fungal genome annotation pipeline using evidence-based gene model evaluation. *Bioinformatics* **33**, 2936–2937 (2017).
93. Jones, P. et al. InterProScan 5: genome-scale protein function classification. *Bioinformatics* **30**, 1236–1240 (2014).
94. Lim, F. Y., Sanchez, J. F., Wang, C. C. C. & Keller, N. P. Toward awakening cryptic secondary metabolite gene clusters in filamentous fungi. *Methods Enzymol.* **517**, 303–324 (2012).
95. Xie, C. et al. KOBAS 2.0: a web server for annotation and identification of enriched pathways and diseases. *Nucleic Acids Res.* **39**, W316–W322 (2011).
96. The Gene Ontology Consortium. The Gene Ontology Resource: 20 years and still GOing strong. *Nucleic Acids Res.* **47**, D330–D338 (2019).
97. Ashburner, M. et al. Gene Ontology: tool for the unification of biology. *Nat. Genet.* **25**, 25–29 (2000).
98. Jukes, T. H. & Cantor, C. R. in *Mammalian Protein Metabolism* Vol. 3 (ed. Munro, H. N.) 21–132 (Academic Press, 1969).
99. Conway, J. R., Lex, A. & Gehlenborg, N. UpSetR: an R package for the visualization of intersecting sets and their properties. *Bioinformatics* **33**, 2938–2940 (2017).
100. Patti, G. J. et al. A view from above: cloud plots to visualize global metabolomic data. *Anal. Chem.* **85**, 798–804 (2013).

Acknowledgements

The authors would like to thank the following people and groups: the Arkin Lab and the Deutschbauer Lab at UC Berkeley for the *E. coli* Keio_ML9 RB-TnSeq library; K. Jepsen at the IGM Genomics Center at the University of California, San Diego for assistance with sequencing; S. Kryazhimskiy (UCSD) for his input on RB-TnSeq data processing; C. Dinh (UCSD) for assistance with fungal genome assembly; W. Bushnell (UCSD) for assistance with fitness validation experiments; S. Beyhan (JCVI) for advice on fungal genome annotation; L. Marotz (UCSD) for assistance with non-cheese yeasts; and members of the Dutton Lab, especially B. Anderson and C. Saak, for constructive comments on the manuscript. This work was supported by the National Institutes of Health grant nos. T32-AT007533 (to J.C.L.) and F31-AT010418 (to J.C.L.), the National Institutes of Health grant no. R01-AI117712 (to R.B.L), National Science Foundation grant no. MCB-1817955 (to L.M.S.), National Science Foundation grant no. MCB-1817887 (to R.J.D. and L.M.S.), National Science Foundation grant no. MCB-1715553 (to B.E.W.), the UCSD Center for Microbiome Innovation (to E.C.P.), the UCSD Ruth Stern Award (to E.C.P.), NIH Institutional Training grant no. 5 T32 GM 7240-40 (to E.C.P.) and the National Institutes of Health grant no. R01GM112739-01 (to N.P.K.).

Author contributions

R.J.D., L.M.S. and B.E.W. conceptualized the study. E.C.P., M.M., J.T., R.B.L. and J.C.L. performed the experiments. The R data processing pipeline was written by M.M. Data analyses were performed by E.C.P., J.C.L. and M.M. The article was written by E.C.P., M.M., L.M.S., J.C.L. and R.J.D. and revised with input from all authors. The figures were made by E.C.P. with input from L.M.S., J.C.L., R.J.D. and M.M., except for Fig. 4a and Extended Data Fig. 7 (R.B.L.), Fig. 6d (J.C.L.), Extended Data Figs. 1 and 2 (M.M.) and Supplementary Fig. 3 (J.T.). The study was supervised by R.J.D. and L.M.S.

Competing interests

The authors declare no competing interests.

Additional information

Extended data is available for this paper at https://doi.org/10.1038/s41564-020-00800-z.

Supplementary information is available for this paper at https://doi.org/10.1038/s41564-020-00800-z.

Correspondence and requests for materials should be addressed to R.J.D.

Peer review information Peer reviewer reports are available.

Reprints and permissions information is available at www.nature.com/reprints.

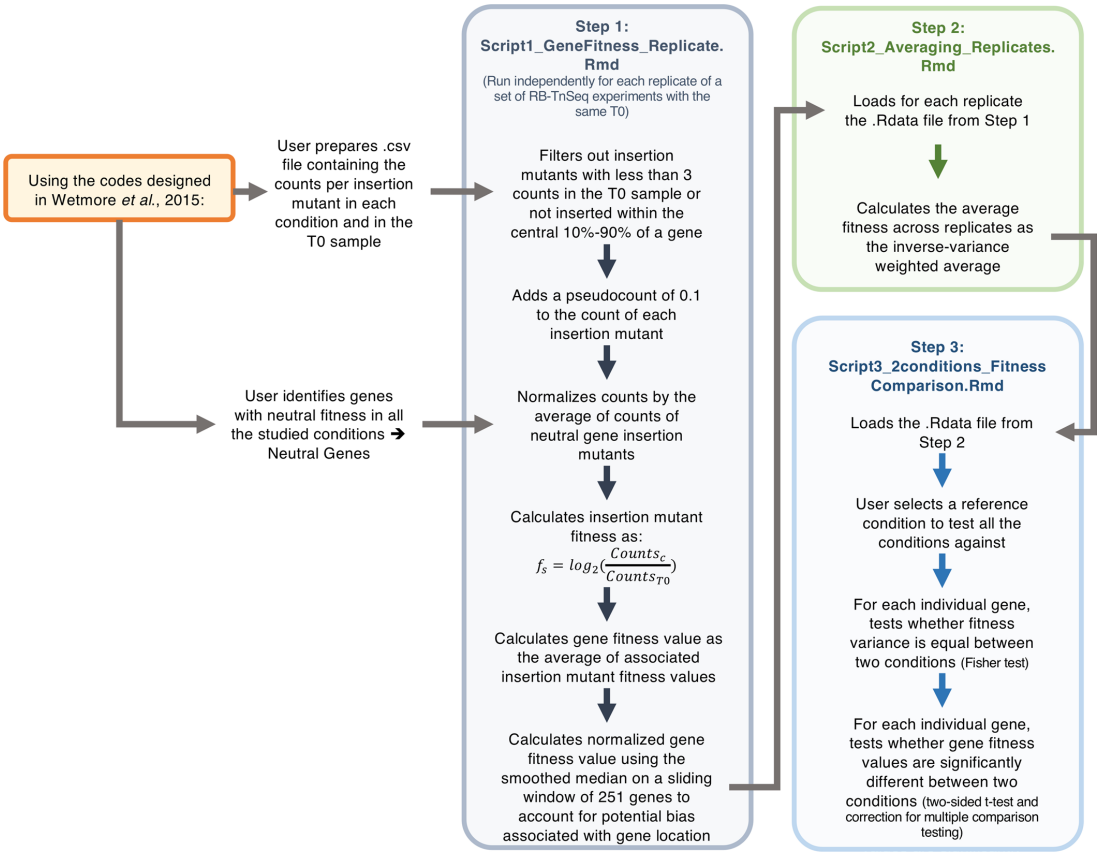

Extended Data Fig. 1 | RB-TnSeq R data processing pipeline for gene fitness comparison across multiple conditions. The pipeline is divided into three main scripts. Script 1 calculates the normalized gene fitness for each replicate of an RB-TnSeq experiment. This script has to be run for each replicate independently. Then, the .Rdata files from Script 1 are loaded in Script 2. Script 2 calculates for each RB-TnSeq condition the average gene fitness across replicates (inverse-variance weighted average). Finally, Script 3 compares gene fitness values of each RB-TnSeq condition against a chosen reference condition.

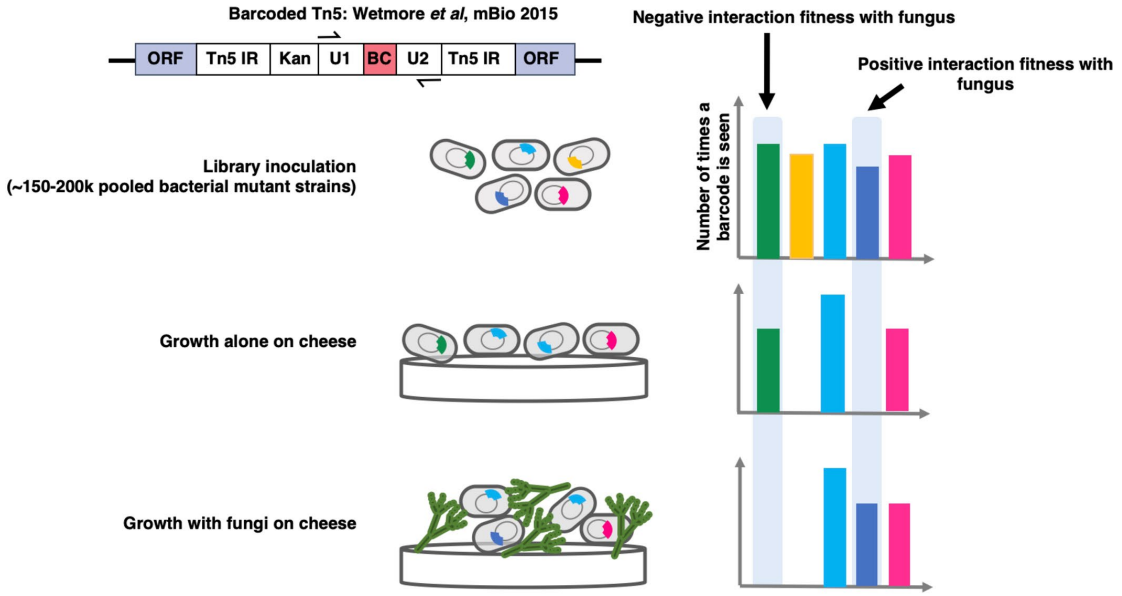

Extended Data Fig. 2 | RB-TnSeq assay for fungal impacts on bacterial gene fitness. Characterized pooled bacterial mutant libraries were grown in a biofilm either alone or with a fungal partner. After seven days of growth, mutant abundances were compared to the starting library abundances for each condition. Changes in barcode abundances were used to calculate gene fitness values. Genes with fitness values that differed significantly between co-culture and alone conditions (significant interaction fitness) were identified as potentially relevant to fungal interaction.

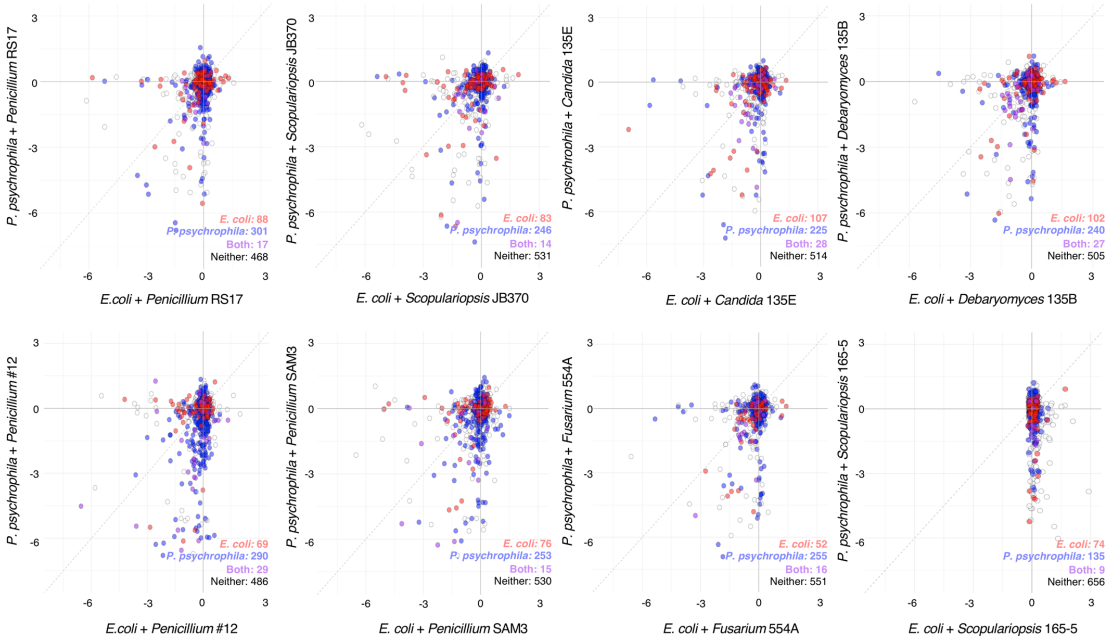

Extended Data Fig. 3 | Comparison of *E. coli* and *P. psychrophila* interaction fitness values for the 874 genes found in both bacteria. BLAST comparison (e-value cutoff of 1e-2) of protein sequences from *P. psychrophila* to those from *E. coli* and comparison of eggNOG gene assignments were used to find the best cross-species gene match for all genes with significant interaction fitness for at least one of the two bacterial species. A match was found for 874 genes. For each fungal condition, the fitness value of these genes with *E. coli* is on the x-axis and with *P. psychrophila* on the y-axis. In each condition, the genes are colored according to whether they have significant interaction fitness in the condition for *E. coli* (red), *P. psychrophila* (blue), both (purple), or neither (white).

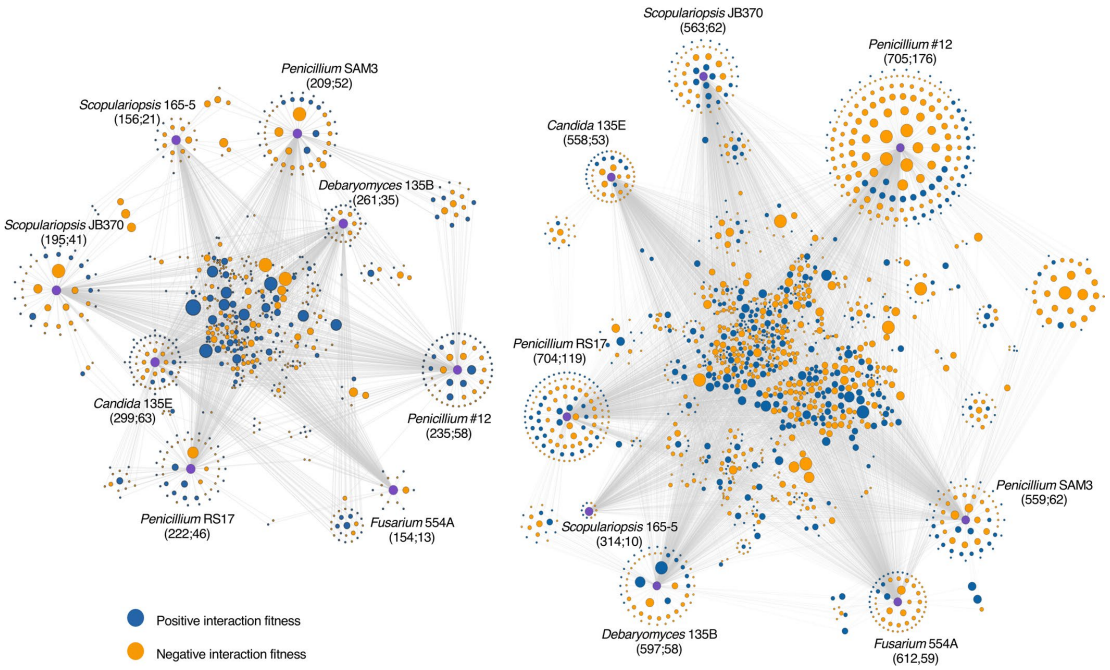

Extended Data Fig. 4 | Network of *E. coli* (left) or *P. psychrophila* (right) genes with positive and negative RB-TnSeq interaction fitness. Each purple node represents a fungal partner and is labeled as follows: fungal partner (number of genes with interaction fitness; number of genes with interaction fitness unique to this condition). Each blue or orange node represents a bacterial gene. Nodes are colored by whether the average interaction fitness is positive (blue) or negative (orange) as shown in the legend below and are sized by average strength of interaction fitness across partners.

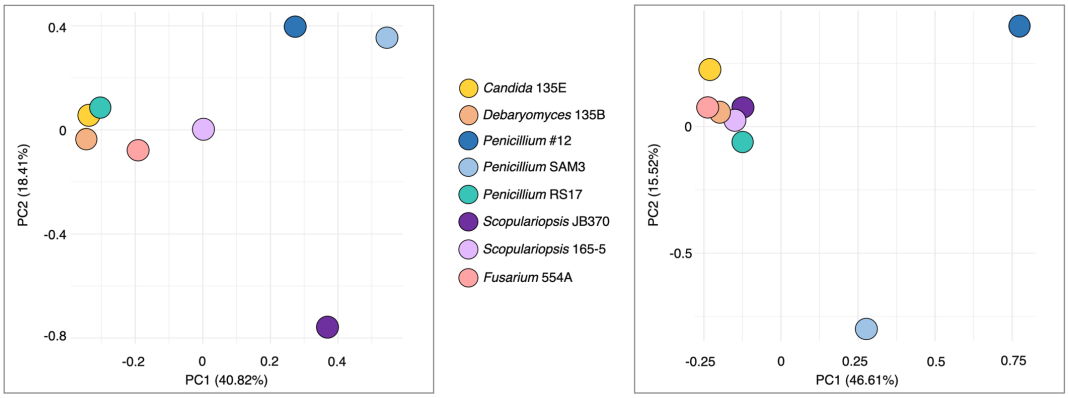

Extended Data Fig. 5 | Principal Component Analysis of RB-TnSeq data. Analysis was done on the fitness values in each fungal condition for all *E. coli* (left) or *P. psychrophila* (right) genes with an interaction fitness in at least one fungal condition. Each colored circle represents a fungal condition.

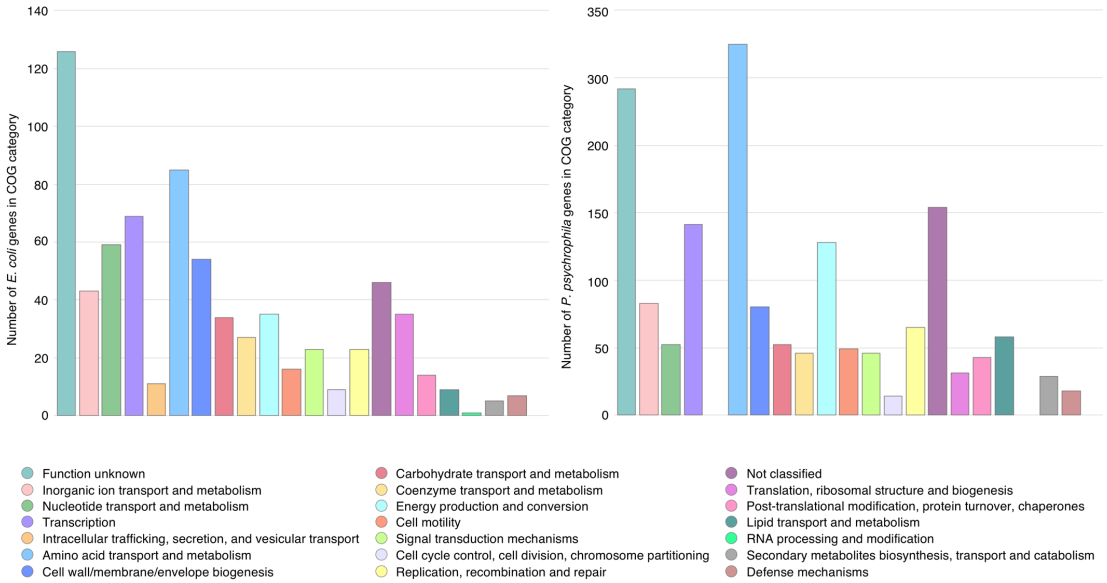

Extended Data Fig. 6 | Clusters of Orthologous Genes (COG) categories of genes with interaction fitness. Charts display the number of genes with interaction fitness that fall into each COG category for *E. coli* (left) or *P. psychrophila* (right).

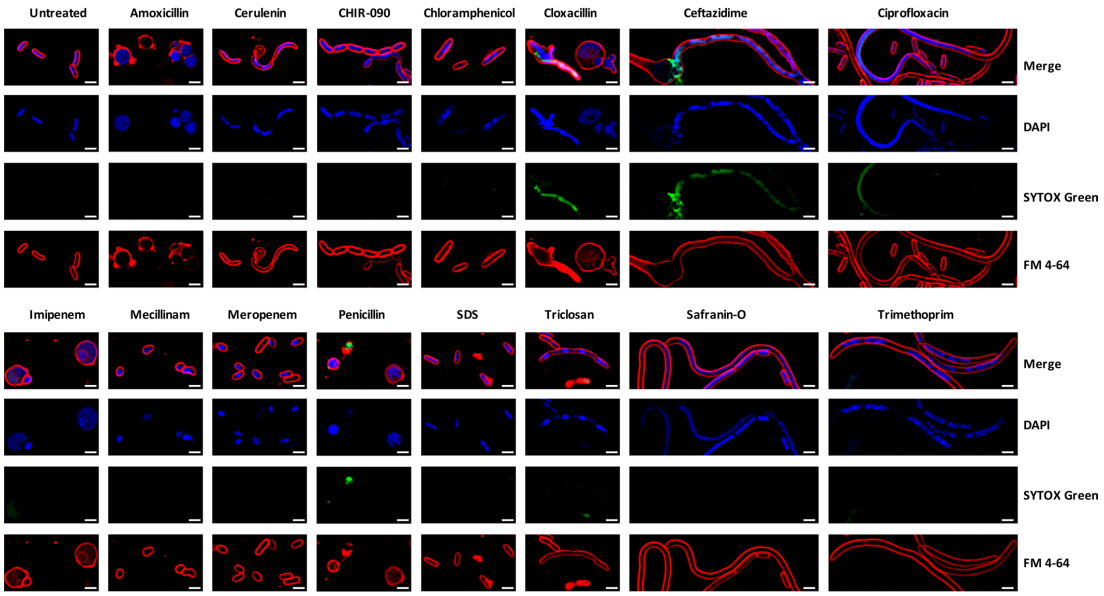

Extended Data Fig. 7 | Bacterial Cytological Profiling of Δ*tolC E.coli* treated with known antibiotic compounds on cheese curd agar. DAPI dye stains DNA and FM4-64 dye stains bacterial membranes. SYTOX green stains nucleic acids but cannot penetrate live cells. Scale bars represent 2 μm. Testing of each antibiotic at four concentrations was performed once, and cells from the edges of zones of clearing were imaged for at least 5 fields from each condition to ensure consistency in phenotype.

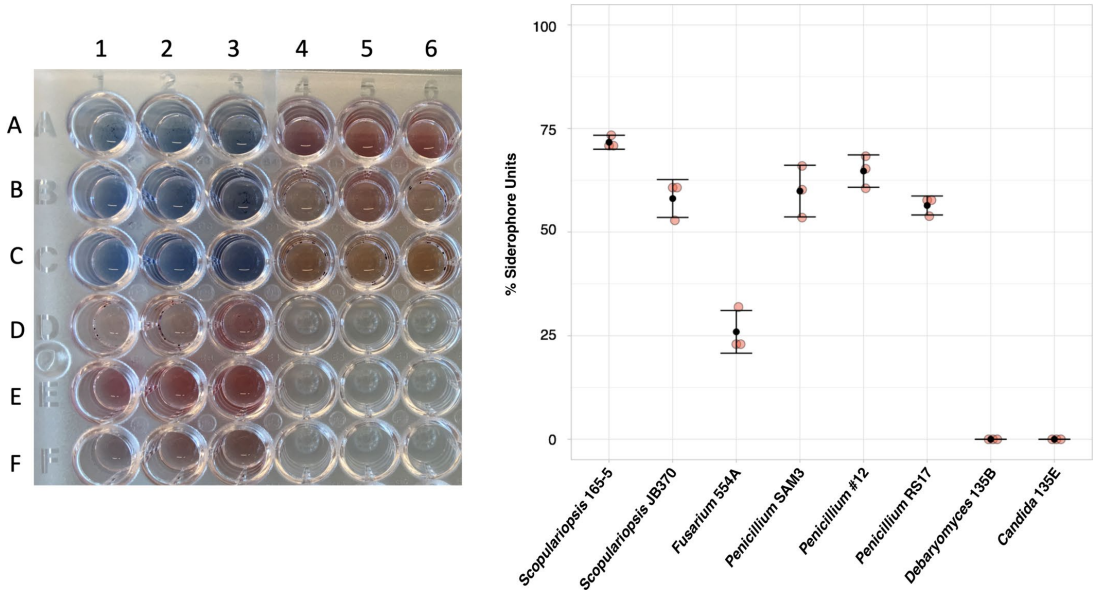

Extended Data Fig. 8 | Siderophore production by filamentous fungi. Liquid CAS assay was performed on filtered and concentrated fungal supernatants from three replicates grown in 2% liquid cheese pH 7 for 12 days. Row A) 1-3: Liquid cheese control 4-6: *Penicillium* SAM3. Row B) 1-3: *Debaryomyces* 135B 4-6: *Penicillium* #12. Row C) 1-3: *Candida* 135E. 4-6: *Penicillium* RS17. Row D) 1-3: *Scopulariopsis* 165-5 Row E) 1-3: *Scopulariopsis* JB370. Row F) 1-3: *Fusarium* 554A. % Siderophore units calculated as $[(A_r - A_s)/(A_r)]*100$, where A_r is the absorbance of the cheese curd agar supernatant blank and A_s is the absorbance of the sample. N=3 biologically independent samples, error bars show standard deviation and black point is the mean.

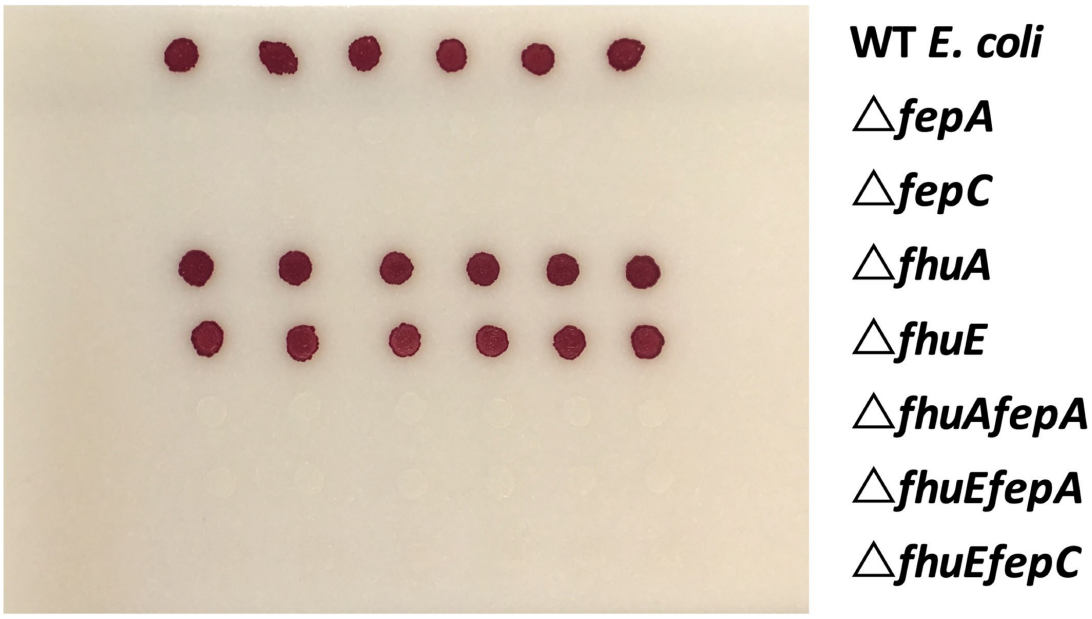

Extended Data Fig. 9 | Fitness defect of Δ*fep* mutants on iron-limiting CCA. Visual assays of *E. coli* mutant growth spotted alone on CCA pH 7 supplemented with tetrazolium chloride, an indicator of respiration.

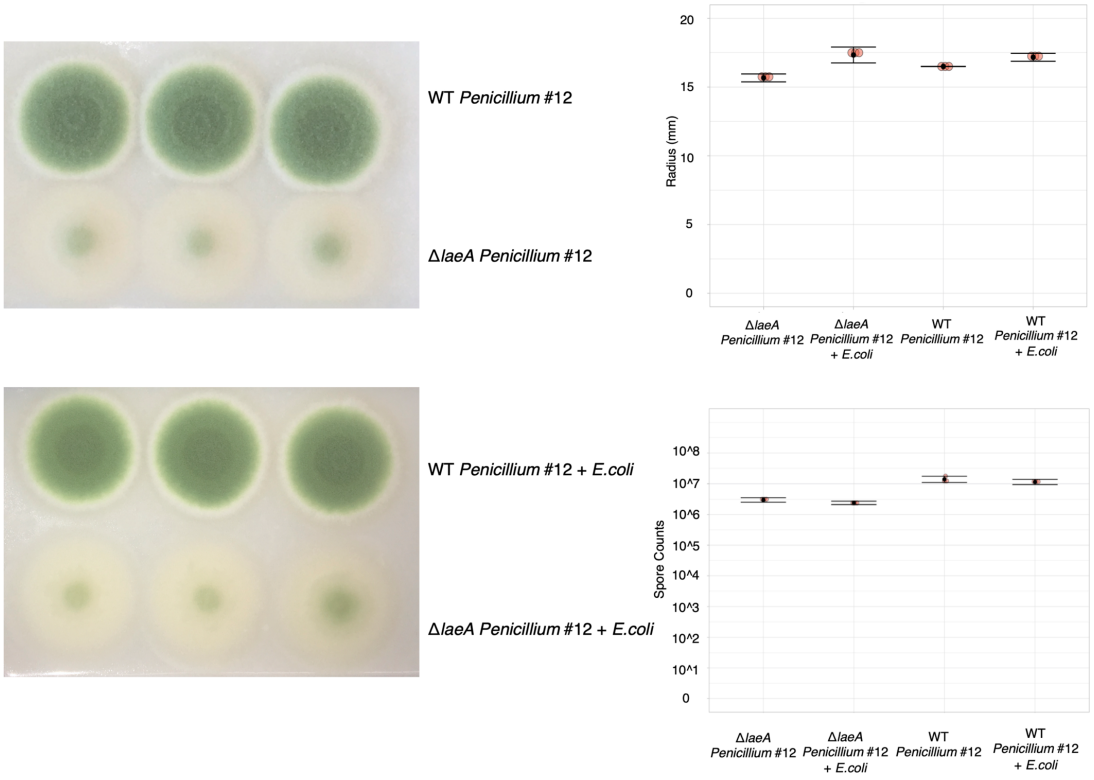

Extended Data Fig. 10 | Comparison of *Penicillium* sp. str. 12 WT and *laeA* deletion mutant growth on CCA. Radial growth assay, including quantification, of *Penicillium* sp. str. 12 WT and *laeA* deletion mutant grown alone or with *E. coli* on CCA pH 7 (N=3 biologically independent experiments, error bars show standard deviation and black point is the mean). Spore counts from *Penicillium* sp. str. 12 WT and *laeA* deletion mutant grown alone or with *E. coli* for 7 days on CCA are also shown (N=3 biologically independent samples, error bars show standard deviation and black point is the mean).

Supplementary Method 1:

Illustration of the analytical pipeline of RB-TnSeq analysis and identification of interaction fitness

This document provides examples of the different steps of the computational analysis of RB-TnSeq data and identification of interaction fitness. They rely on 3 principal custom R scripts.

Script 1 (Script1_GeneFitness_Replicate.Rmd): Calculates gene fitness for of one replicate of a set of RB-TnSeq experiments of the same library and relying on the same T0 sample. Therefore, this script has to be run independently for each replicate of RB-TnSeq experiment using the same T0. In this exemple, we use 5 RB-TnSeq experiments (Condition 1 to 5) sharing the same T0 and performed in triplicate. While this script has to be run for each replicate independently, here, we only display the run for the first replicate to illustrate the script.

Script 2 (Script2_Averaging_Replicates.Rmd): Averages gene fitness values across replicates.

To run this script, you need the output of Script 1 for each replicate of the experiment. Then the script combines all the replicates of the 5 example conditions.

Note: Even if we only display the Script 1 run for the first replicate, we also run Script 1 for the second and third replicate of this example as required to run Script 2.

Script 3 (Script3_2conditions_Fitness_Comparison.Rmd): Performs the gene fitness comparisons between a given reference condition and the other conditions and identifies interaction fitness.

Here, we used the run that compared the final gene fitness of Conditions 2 to 5 to gene fitness of reference condition, Condition 1

STEP 1:Gene fitness values and associated variance for 1 replicate of a set of RB-TnSeq experiments (Same T0)

Script: Script1_GeneFitness_Replicate.Rmd

That script processes the raw counts data from the allpoolcounts.tab file generated by the perl script BarSeqTest.pl (Wetmore **et al.**, 2015). This script processes 1 biological replicate This script produces a final file containing normalized gene fitness and associated fitness variance. Plots are generated during data processing to visually follow data transformation.

Example description

This run illustrates the first step of RB-TnSeq analysis to identify interaction fitness. This is the run for the first replicate of an example comprised of 5 RB-TnSeq experiments using the *E. coli* RB-TnSeq library.

Run

Packages and functions

```
rm(list=ls())

# Step 1: Packages

library(ggplot2)
library(dplyr)
```

```
##
## Attaching package: 'dplyr'
```

```
## The following objects are masked from 'package:stats':
##
##     filter, lag
```

```
## The following objects are masked from 'package:base':
##
##     intersect, setdiff, setequal, union
```

```
library(tidyr)
library(gridExtra)
```

```
##
## Attaching package: 'gridExtra'
```

```
## The following object is masked from 'package:dplyr':
##
##     combine
```

```
# Step 2: Sourcing functions required in that script
source("Data_prep_viz10KB.R")
source("Ref_counts_CorrandNorm.R")
source("Gene_fitness.R")
source("Loc_smoothmed_norm.R")
```

Input data and parameters set up

```
# Step 3: Parameters set up and data import

 #Different parameters have to be defined by the user:
  # org_locId: depending on your genome annotations, the locus_Id may be numerics or characters
  # cdnb: number of analyzed conditions (including T0)
  # scaffold: Set up the chromosome scaffold (for plot purposes only)
  # Indicate the locusId of the gene you will use as a reference to normalize counts

org_locId="Num"   # "Num" if numeric , "Char" if characters
cdnb=6
scaffoldX=7023
ref=c(17490,15396,14886,14220,18293) # here you write the locusId of your reference gene CAREFUL, depending
on the locusId Type, it might be a numeric  or character

 # You need to import the table containing the number of counts per barcodes in each condition (allpoolcount
s.tab transformed as a csv file - make sure to keep all columns)
 # The first 7 columns of your table should be: barcodes, rbarcode, scaffold, strand, pos, locusId and f, th
en each column should be a condition ==> THIS IS IMPORTANT THAT THE FIRST 7 COLUMNS ARE NOT COUNTS
 # ALSO COLUMN 8 MUST BE NAMED T0
 # THE CONDITIONS MUST HAVE THE SAME NAME IN EACH REPLICATE
 # You also need to import the genes.GC (as a .txt file) file used to run the perl script TestBarSeq.pl (Wet
more et al., 2015).

Data_original=read.csv("Ex_Run_R1.csv")  # import your allpoolcounts file

genes.tab <- readr::read_delim("genes.GC.txt",
                               "\t", escape_double = FALSE, trim_ws = TRUE)  # import your gene.GC file
```

```
## Parsed with column specification:
## cols(
##   locusId = col_double(),
##   sysName = col_character(),
##   type = col_double(),
##   scaffoldId = col_double(),
##   begin = col_double(),
##   end = col_double(),
##   strand = col_character(),
##   name = col_character(),
##   desc = col_character(),
##   GC = col_double(),
##   nTA = col_double()
## )
```

Original data visualization

```
# Step 4: Data pre-visualization

 # Before processing the data we represent, for each condition (T0 included) the number of counts per 10kB a
nd the distribution of number of counts per insertion mutant

Data=Data_original

    # Number of counts per 10kB

Data_prep=Data_prep_viz10KB(Data,cdnb,scaffoldX)    # format the data for vizualisation as counts per 10kB

dat_format <- data.frame(Data_prep[ncol(Data_prep)], stack(Data_prep[1:cdnb]))
colnames(dat_format)=c("Rank","Counts","Cdt")

plot1=ggplot(dat_format, aes(x=Rank,y=Counts,col=Cdt)) + geom_point(shape=19) +
  theme(axis.text.x = element_text(size=5),axis.text.y = element_text(size=5)) +
  ggtitle("Counts per 10kb interval") +
  facet_grid(Cdt ~ .) + labs(x = "Chromosome position (10kB)", y="Counts per 10kb interval")

#Note:if a couple of outliers points prevent from accuretely observing the number of counts per 10kB, you ca
n change y=Counts to y=log10(Counts)

# Distribution of number of counts per insertion mutant

Data_distr=gather(Data,"Cond","Counts",T0:ncol(Data))

plot1a=ggplot(Data_distr, aes(x=Counts,col=Cond)) + geom_density() +
  theme(axis.text.x = element_text(size=5),axis.text.y = element_text(size=5)) +
  ggtitle("Distribution of counts per insertion mutant") +
  facet_grid(Cond ~ .) + labs(x = "Counts per insertion mutant")



grid.arrange(plot1, plot1a, nrow=2)
```

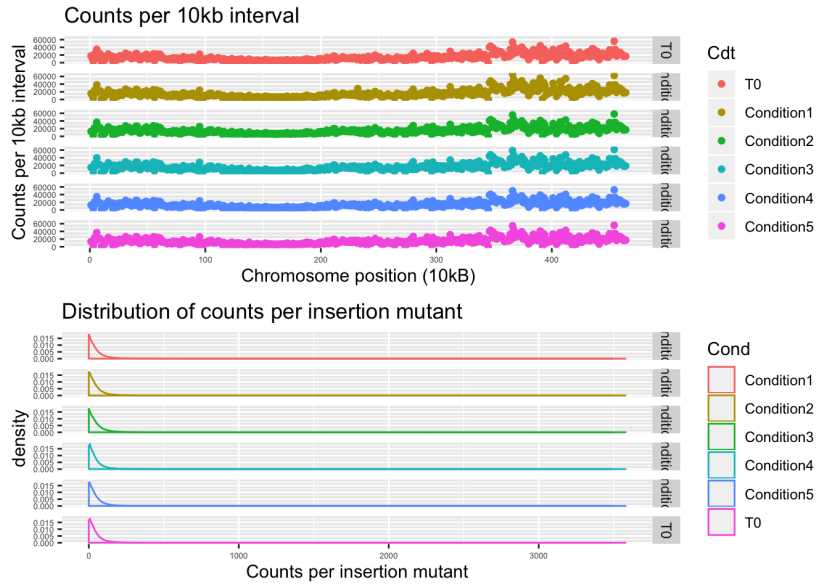

Selection of insertion mutants, followed by counts correction and normalization

Selection: raw counts have to be processed prior to fitness calculation. Insertion mutants in intergenic regions and that are located outside of the ORF (f<0.1 and f>0.9) are filtered out. Also, any mutants with a low abundance in the T0 condition are filtered out.

Count correction: a pseudocount of .1 is added to all counts to avoid counts of 0

Normalization: corrected counts are normalized by the average number of reads per insertion mutant calculated using a set of reference genes associated with neutral fitness in all tested conditions

```
# Step 5: Count correction before fitness calculation

 # A pseudocount of .1 is added to each count to avoid counts of 0
 # Insertions mutants that are outside of the ORF (f<0.1 and f>0.9) are filtered out
 # Insertion mutants that do not pass the T0 count threshold (before correction relative to reference ; Coun
ts<3.1) are filtered out
 # Counts are normalized using at least one reference gene (no fitness effect in all tested conditions) - Th
e reference are used to calculate the average number of read per insertion mutant which is in turn used for
normalization
 # Data are visualized again after correction (Number of corrected counts per 10kb and Distribution of corre
cted counts)

  # The function Data_counts_CorrandNorm perform all the aformentioned modifications
Data_ref_corrected=Ref_counts_CorrandNorm(Data, ref, cdnb)

  # Number of corrected counts per 10kB
Dat_viz=Data_prep_viz10KB(Data_ref_corrected,cdnb,scaffoldX)
dat_format <- data.frame(Dat_viz[ncol(Dat_viz)], stack(Dat_viz[1:cdnb]))
colnames(dat_format)=c("Rank","Counts","Cdt")

plot2=ggplot(dat_format, aes(x=Rank,y=Counts,col=Cdt)) + geom_point(shape=19) +
  theme(axis.text.x = element_text(size=5),axis.text.y = element_text(size=5)) + ggtitle("Corrected counts p
er 10kb interval") +
  facet_grid(Cdt ~ .) + labs(x = "Chromosome position (10kB)", y="Counts per 10kb interval")

#Note:if a couple of outliers points prevent from accurately observing the number of counts per 10kB, you ca
n change y=Counts to y=log10(Counts)

  # Distribution of number of counts per insertion mutant

Data_distr=gather(Data_ref_corrected,"Cond","Counts",T0:ncol(Data_ref_corrected))

plot2a=ggplot(Data_distr, aes(x=Counts,col=Cond)) + geom_density() +
  theme(axis.text.x = element_text(size=5),axis.text.y = element_text(size=5)) +
  ggtitle("Distribution of corrected counts per insertion mutant") +
  facet_grid(Cond ~ .) + labs(x = "Counts per insertion mutant after correction and normalization")



grid.arrange(plot2, plot2a, nrow=2)
```

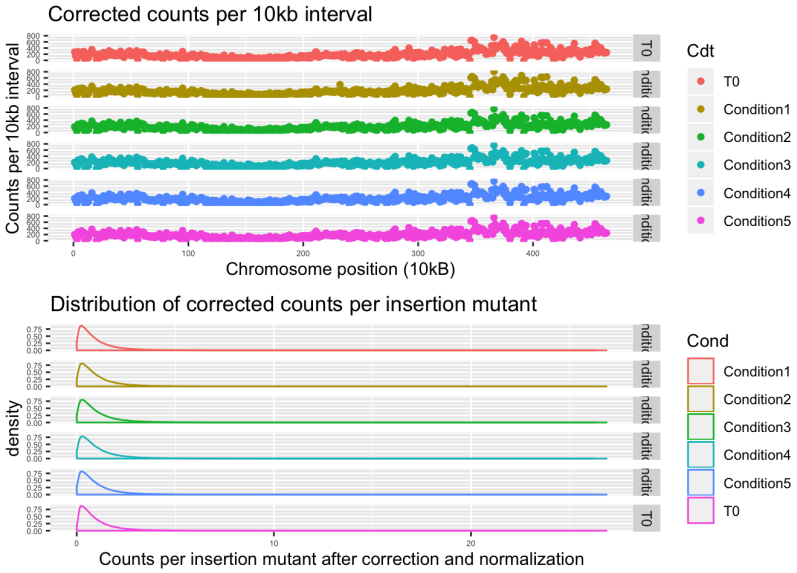

Calculation of gene fitness values

A gene fitness value is calculated as the average of the fitness values of associated insertion mutants. The fitness of insertion mutants is the log2 of the ratio of the insertion mutant's normalized counts in a given condition and at T0.

```
# Step 6: Calculation of gene fitness
 # Calculation of the strain fitness (fitness for each insertion with central insertion as the log2 of the r
atio of the corrected counts in the condition and the corrected counts in the T0)
 # Calculation of gene fitness values along with associated variance (average of all the insertion mutants f
itness in that gene)
 # Vizualization of the gene fitness values (along the chromose (plot3) or as a distribution (plot4))

Data_for_fit=Data_ref_corrected
cdnbF=(cdnb-1)    # number of conditions for which we will get a fitness values (=everything but T0)

# The following function returns a list containing 3 tables: "Strain fitness": strain fitness values, "Gene_
fitness": unnormalized gene fitness values and "Gene_fitness_variance": variance assocaited with gene fitnes
s values

Raw_values=Gene_fitness(Data_for_fit,cdnbF,genes.tab,org_locId)

Table_GeneFitness_Raw=Raw_values[[2]]  # We extract the table with the unnormalized fitness values for data
vizualisation

 #We format the data to vizualise them
dat_format <- data.frame(Table_GeneFitness_Raw[1], Table_GeneFitness_Raw[(ncol(Table_GeneFitness_Raw)-1):nco
l(Table_GeneFitness_Raw)], stack(Table_GeneFitness_Raw[2:(2+cdnbF-1)]))
colnames(dat_format)=c("locusId","sysName","begin","RawFitness","Cdt")

plot3=ggplot(dat_format, aes(x=begin,y=RawFitness,col=Cdt)) + geom_point(shape=19) +
  theme(axis.text.x = element_text(size=5),axis.text.y = element_text(size=5)) + ggtitle("Unnormalized gene
fitness") +
  facet_grid(Cdt ~ .) + labs(x = "Chromosome position", y="Fitness value")

plot4=ggplot(dat_format, aes(x=RawFitness,col=Cdt)) + geom_density(aes(fill=Cdt)) +
  theme(axis.text.x = element_text(size=5),axis.text.y = element_text(size=5))+ ggtitle("Distribution of gen
e unnormalized fitness values") +
  facet_grid(Cdt ~ .) + labs(x = "Fitness value", y="Density")


grid.arrange(plot3, plot4, ncol=1)
```

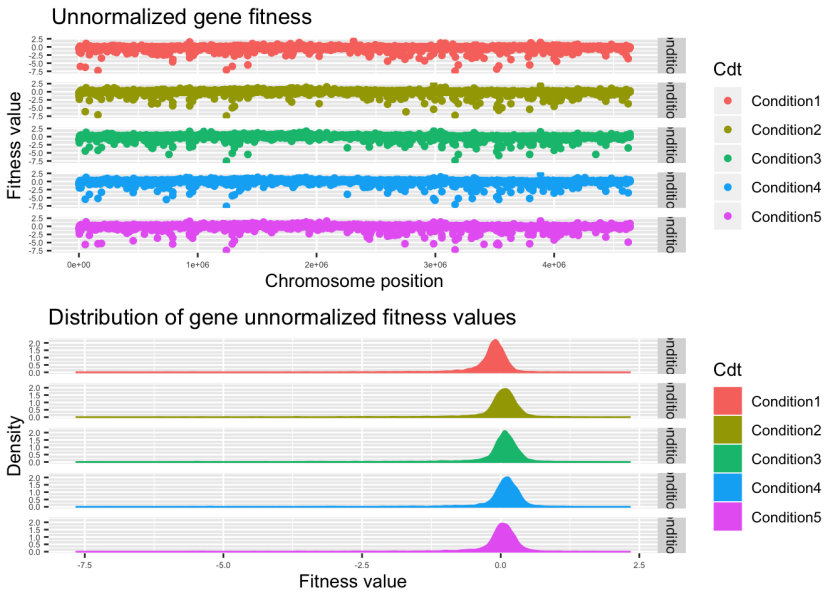

Chromosome position normalization of gene fitness values

As described in Wetmore *et al.*, 2015, gene fitness values are normalized based on the gene location on the chromosome using the smoothed median.

```
# Step 7: Gene fitness normalization
 # Normalize gene fitness based on the position of the gene on the chromosome (smooth median normalization ; Wetmore et al., 2015)
 # Data visualization like Step 6

Data_to_norm=Table_GeneFitness_Raw
Data_norm_loc=Loc_smoothmed_norm(Data_to_norm,genes.tab,cdnbF,org_locId)  # we obtain the gene fitness values normalized by the smoothed median ==> normalization for gene location


 # Data visualization
dat_format <- data.frame(Data_norm_loc[1:4], stack(Data_norm_loc[5:ncol(Data_norm_loc)]))
colnames(dat_format)=c("locusId","sysName","begin","scaffold","NormFitness","Cdt")
dat_format$begin=as.numeric(dat_format$begin)
dat_format$NormFitness=as.numeric(dat_format$NormFitness)

plot5=ggplot(dat_format, aes(x=begin, y=NormFitness, col=Cdt)) + geom_point(shape=19)+
  theme(axis.text.x = element_text(size=5),axis.text.y = element_text(size=5)) + ggtitle("Normalized gene fitness values (smoothed median)") +
  facet_grid(Cdt ~ .) + labs(x = "Chromosome position (10kB)", y="Fitness value")

plot6=ggplot(dat_format, aes(x=NormFitness, col=Cdt)) + geom_density(aes(fill=Cdt)) +
  theme(axis.text.x = element_text(size=5),axis.text.y = element_text(size=5)) + ggtitle("Distribution normalized gene fitness values (smoothed median)") + facet_grid(Cdt ~ .) + labs(y = "Density", x="Fitness value")

grid.arrange(plot5, plot6, ncol=1)
```

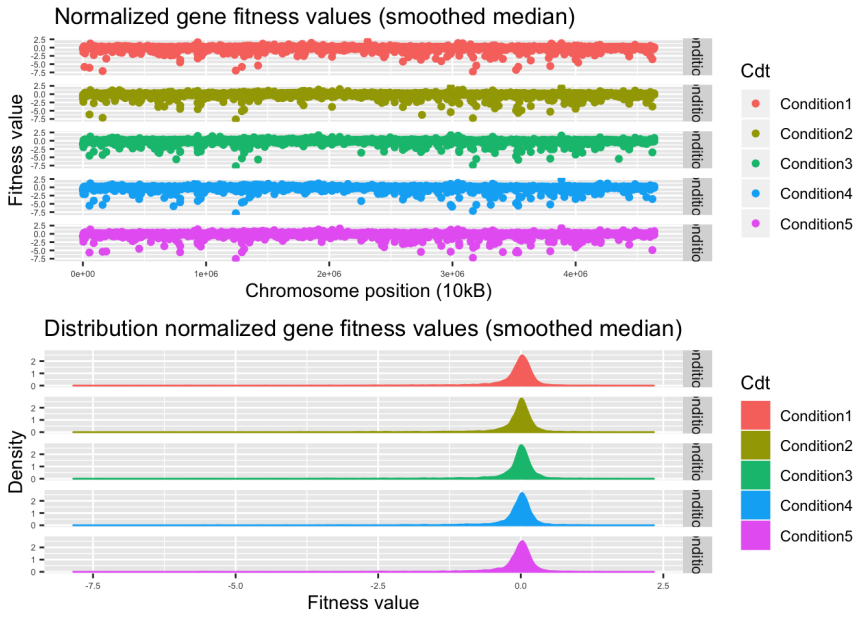

Saving data

```
# Step 8: Data formating and save

  # Data formating

Data_Fitness_Replicate=dat_format

Table_GeneFitness_VAR=Raw_values[[3]]
Data_Fitness_VAR=data.frame(Table_GeneFitness_VAR[1],
                            stack(Table_GeneFitness_VAR[2:ncol(Table_GeneFitness_VAR)]))
colnames(Data_Fitness_VAR)=c("locusId","Fitness_Variance","Cdt")


if (org_locId=="Num"){
  Data_Fitness_Replicate$locusId=as.numeric(Data_Fitness_Replicate$locusId)
}

All_data_Replicate=left_join(Data_Fitness_Replicate,Data_Fitness_VAR,by=c("locusId","Cdt"))
All_data_Replicate=All_data_Replicate[c(1,2,3,4,6,5,7)]


save(All_data_Replicate, Data_norm_loc,
     Raw_values, Data_ref_corrected, Data_original, genes.tab,
     file="Ex_Run_R1.RData")
```

STEP 2 :Gene fitness calculation: averaging across replicates

Script: Script2_Averaging_Replicates.Rmd

That second part of the analysis averages gene fitness across replicates. If all studied conditions have the same T0 sample, it requires for each replicate the .RData files generated in the first part of the analysis “Script1_GeneFitness_Replicate.Rmd”. If studied conditions have a different T0 sample, it requires the output of the script Multiple_T0s.R Before averaging replicates, we perform a quick analysis of correlation between replicates of the same condition. It produces a final file containing final normalized gene fitness and associated fitness variance across replicates. Plots are generated during data processing to visually follow data transformation.

Example description

This run illustrates the second step of RB-TnSeq analysis to identify interaction fitness. This is the run for averaging fitness values for all the replicates of the 5 conditions RB-TnSeq example.

Run

Packages and functions

```
rm(list=ls())

library(dplyr)
library(ggplot2)
library(ggrepel)
library(DescTools)
library(gridExtra)

source("Correlation_Rep.R")
source("Weighted_average.R")
```

Data upload and parameters set up

```
# Step1: Parameters set up and Data import
 # Import .Rdata files generated for each replicate in Script1_GeneFitness_Replicate.Rmd
 # Isolate and rename All_data_Replicate just after loading to avoid overwritting.
 # Note: if conditions have different T0s and have been processed independently in "Gene_Fitness_Replicate.R
", Step 1 is replaced by running the script: "Multiple_T0s.R"


  # Parameter set up
org_locId="Num"   # "Num" if numeric , "Char" if characters
multiT=FALSE  # Switch to TRUE if you used different T0s for a set of conditions and have to run Multiple_T0
to generate the table containing all replicates.

if (multiT==FALSE){
  load("Ex_Run_R1.Rdata") #load the .Rdata file from Gene_Fitness_Replicate.R for replicate 1
  Replicate1=All_data_Replicate

  load("Ex_Run_R2.Rdata") #load the .Rdata file from Gene_Fitness_Replicate.R for replicate 2
  Replicate2=All_data_Replicate

  load("Ex_Run_R3.Rdata") #load the .Rdata file from Gene_Fitness_Replicate.R for replicate 3
  Replicate3=All_data_Replicate

  # We bind all replicates together and add a column "Rep" to identify were it is coming from

  Replicate1$Rep="R1"
  Replicate2$Rep="R2"
  Replicate3$Rep="R3"

  AllReplicate=rbind(Replicate1,Replicate2,Replicate3)
  head(AllReplicate, n=5)
}
```

```
##   locusId sysName begin scaffold        Cdt NormFitness Fitness_Variance Rep
## 1   14146   b0001   190     7023 Condition1 -0.10763776      0.004234506  R1
## 2   14147   b0002   337     7023 Condition1 -0.39564492      0.158219137  R1
## 3   14148   b0003  2801     7023 Condition1 -0.60484100      0.198116180  R1
## 4   14149   b0004  3734     7023 Condition1 -1.37486386      0.416450536  R1
## 5   14150   b0005  5234     7023 Condition1  0.06967739      0.054488610  R1
```

```
if (multiT==TRUE){
  load(".Rdata")    #Generated in Multiple_T0s.R
  genes.tab <- readr::read_delim("genes.GC.txt",
                                 "\t", escape_double = FALSE, trim_ws = TRUE)  # import your gene.GC file
}
```

Side de by side Replicate visualization

```
# Step 2: Replicates visualization

  # Plots for fitness values or variance distribution in each condition and replicate
plot1_fit=ggplot(AllReplicate, aes(x=NormFitness,col=Cdt))+geom_density(aes(fill=Cdt)) + theme_light()+
  ggtitle("Distribution of gene fitness values") + facet_grid(Rep ~ Cdt) + labs(x = "Gene fitness value", y=
"Density")

plot1_var=ggplot(AllReplicate, aes(x=Fitness_Variance,col=Cdt))+geom_density(aes(fill=Cdt)) + theme_light()+
  ggtitle("Distribution of variance") + facet_grid(Rep ~ Cdt) + labs(x = "Variance associated with fitness v
alues", y="Density")

grid.arrange(plot1_fit, plot1_var, ncol=1)
```

```
## Warning: Removed 2145 rows containing non-finite values (stat_density).
```

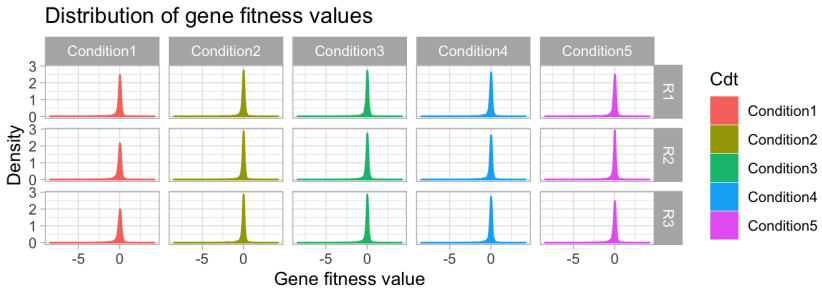

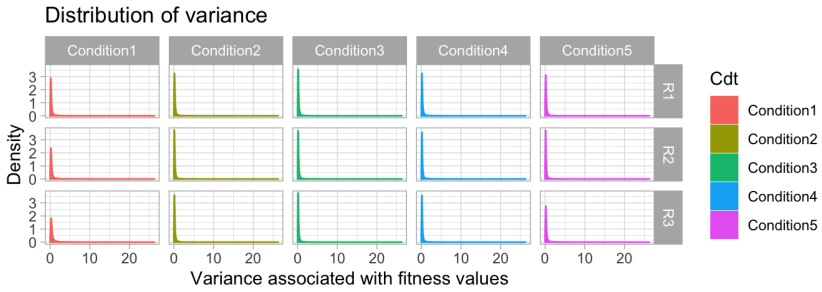

Replicates correlation analysis

Note for this example: while the script generates plots for each correlation analysis (Pearson, Spearman and Lin), here we only display the plot for the Pearson correlation

```
# Step 3: Replicate correlation calculation and visualization (for gene fitness values)
  # Determines the correlation between each replicate, stores them in a matrix
  # Visualizes correlation in two different ways: (i)  usual correlation plots and (ii) distribution of corr
elation across all conditions and replicates

  # Calculation of correlation for all pairs of replicate (and each condition) + plots
Correlation_table_fit=Correlation_Rep(AllReplicate) # Calculates different correlation coefficient + save pl
ots
```

```
## Warning: `data_frame()` is deprecated, use `tibble()`.
## This warning is displayed once per session.
```

```
Correlation_table_fit
```

```
## # A tibble: 15 x 5
##    Cond       Comp      P_Rsquared S_Rsquared L_Rsquared
##    <chr>      <chr>          <dbl>      <dbl>      <dbl>
##  1 Condition1 R2 vs R1       0.798      0.591      0.797
##  2 Condition1 R3 vs R1       0.768      0.572      0.763
##  3 Condition1 R3 vs R2       0.764      0.553      0.762
##  4 Condition2 R2 vs R1       0.866      0.696      0.865
##  5 Condition2 R3 vs R1       0.883      0.689      0.881
##  6 Condition2 R3 vs R2       0.873      0.711      0.873
##  7 Condition3 R2 vs R1       0.879      0.704      0.878
##  8 Condition3 R3 vs R1       0.882      0.703      0.881
##  9 Condition3 R3 vs R2       0.894      0.725      0.894
## 10 Condition4 R2 vs R1       0.836      0.669      0.835
## 11 Condition4 R3 vs R1       0.865      0.667      0.865
## 12 Condition4 R3 vs R2       0.846      0.687      0.845
## 13 Condition5 R2 vs R1       0.883      0.704      0.883
## 14 Condition5 R3 vs R1       0.837      0.652      0.836
## 15 Condition5 R3 vs R2       0.868      0.676      0.864
```

```
plot_allPcor_fit=ggplot(Correlation_table_fit, aes(x=Cond,y=P_Rsquared)) + geom_point(size=2, aes(col=Comp))
+
  theme_light() + labs(y = "Pearson Correlation coefficient", x="Condition") + ylim(0,1) +  ggtitle("Replica
te correlation: Pearson coefficient")

plot_allScor_fit=ggplot(Correlation_table_fit, aes(x=Cond,y=P_Rsquared)) + geom_point(size=2, aes(col=Comp))
+
  theme_light() + labs(y = "Spearman Correlation coefficient", x="Condition") + ylim(0,1) + ggtitle("Replica
te correlation: Spearman coefficient")

plot_allLcor_fit=ggplot(Correlation_table_fit, aes(x=Cond,y=P_Rsquared)) + geom_point(size=2, aes(col=Comp))
+
  theme_light() + labs(y = "Lin's Correlation coefficient", x="Condition") + ylim(0,1) + ggtitle("Replicate
correlation: Lin coefficient")

grid.arrange(plot_allPcor_fit, nrow=1)
```

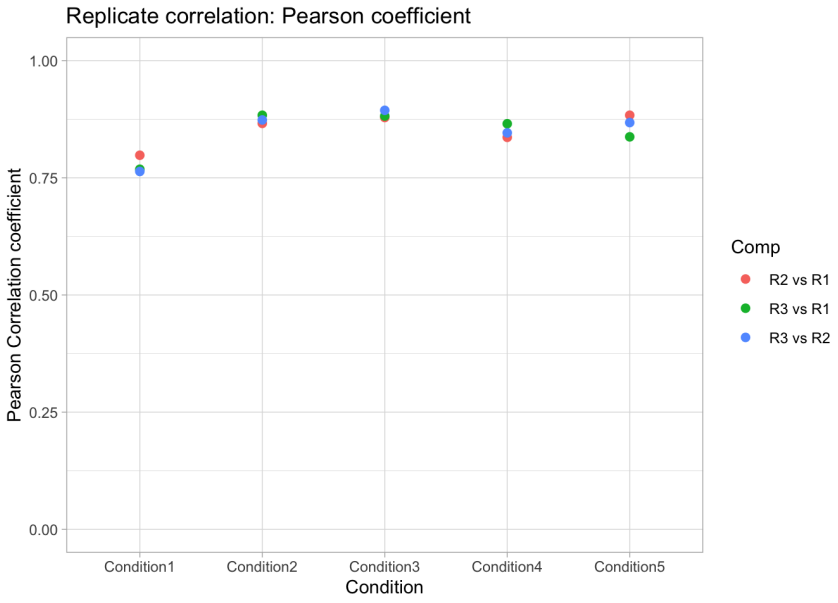

Averaging replicates

Gene fitness values are averaged across replicates using the inverse-variance weighted average. Associated squared standard error (var) and associated standard deviations are also calculated.

Note for this example: while the script generates plots for the average gene fitness, a plot for gene fitness variance and a plot for gene fitness standard deviation, here we only display the plot for the average fitness

```
# Step 4: Weighted average of gene fitness across replicate
 # Averages gene fitness values across replicates for each condition
 # Visualizes fitness values distrbutions, squared standard error (var) ditributions and standard deviation
distributions

Average_fitness=Weighted_average(AllReplicate, org_locId)

plot2_fit=ggplot(Average_fitness, aes(x=WeightedFit,col=Cdt))+geom_density(aes(fill=Cdt)) + theme_light()+
  ggtitle("Distribution of average fitness values across replicates") + facet_grid(Cdt ~ .) + labs(x = "Gene
fitness values", y="Density")

plot2_var=ggplot(Average_fitness, aes(x=WeightedVar,col=Cdt))+geom_density(aes(fill=Cdt)) + theme_light()+
  ggtitle("Distribution of squared standard error") + facet_grid(Cdt ~ .) + labs(x = "Squared standard error
associated with fitness values", y="Density")

plot2_sd=ggplot(Average_fitness, aes(x=Weightedsdev,col=Cdt))+geom_density(aes(fill=Cdt)) + theme_light()+
  ggtitle("Distribution of standard deviation") + facet_grid(Cdt ~ .) + labs(x = "Standard deviation associa
ted with fitness values", y="Density")

grid.arrange(plot2_fit, ncol=1)
```

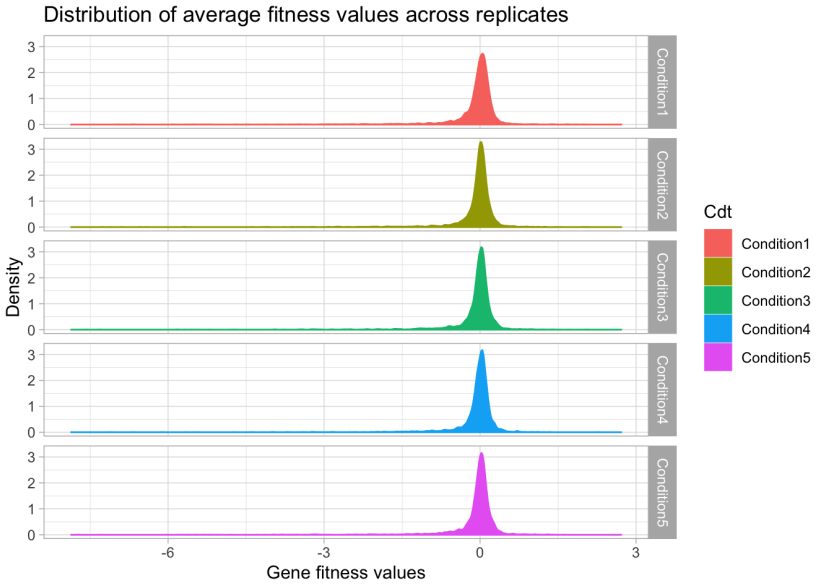

Saving data

```
# Step5: Saving data
if(org_locId=="Num"){
  Final_gene_Fitness=left_join(genes.tab,Average_fitness, by=c("locusId")) %>% select(-c(type,strand,GC,nTA)
)
  Final_gene_Fitness=na.omit(Final_gene_Fitness)
}

if(org_locId=="Char"){
  Average_fitness$locusId=as.character(Average_fitness$locusId)  # the locusId in the Mean table are factors
, we need to turn then into charcater for the left_join
  Final_gene_Fitness=left_join(genes.tab,Average_fitness, by=c("locusId")) %>% select(-c(type,strand,GC,nTA)
)
  Final_gene_Fitness$name="No_name"   #replace the NA by something else, otherwise the next NAomit removes e
verything
  Final_gene_Fitness=na.omit(Final_gene_Fitness)
}

write.csv(Final_gene_Fitness,"All_Fitness_Values_Exemple.csv")

save(Final_gene_Fitness, Average_fitness, genes.tab,
     Correlation_table_fit,AllReplicate, file="All_Fitness_Values_Exemple.RData")
```

STEP 3: Comparison of fitness values and identification of interaction fitness

Script: Script3_2condidtions_FitnessComparison.Rmd

Compares gene fitness values of all conditions against a chosen reference condition. Appends a “Category” to each compared gene to indicate if fitness values are significantly different or not based on chosen statistical criteria.

Example description

This run illustrates the third step of RB-TnSeq analysis to identify interaction fitness. This is the run that compares gene fitness values for E. coli growth in Conditions 2 to 5 versus Condition 1.

Packages and functions

```
rm(list=ls())

# Package and functions upload

library(ggplot2)
library(dplyr)
library(tidyr)
library(gridExtra)

source("Category_definition.R")
source("Comparison_test.R")
```

Data upload and parameters set up

```
# Step 1: Data import and parameters settings
  # Import the .Rdata file generated in Averaging_replicates.R
  # Set up org_locId
  # Set up your condition of reference (has to be one of your conditions)
  # Set up your alpha value for the T-test
  # Set up whether you want to performed correction for multiple comparison testing and screen on adjusted-p
value

load("All_Fitness_Values_Exemple.RData")   # here you upload the .RData ouput of Averaging_replicates.R
Data_Fitness=Final_gene_Fitness

org_locId="Num"  # Again, you set up your organisms whether "Ecoli" if the locusId are in numeric form or "P
seudo" if the locusId are in character form
Condition1="Condition1"  #here you write the name of one of the 2 conditions you want to compare. Make sure
it is the same name than previously used
alphaF=0.002    #here you choose any alpha you want for the Fisher test (Test for equal variance) You can ch
oose 0.05 or 0.002.
alphaT=0.05   #here you choose any alpha you want. Just be aware that it is where you can control the amount
of false discovery you allow
multi=1    # here you decide if you want to correct for multiple comparison (method=fdr) multi = 0 ==> no co
rrection; multi=1 correction
```

2 conditions comparison against a chosen reference condition (Condition 1)

In the following plots: “Sig” means that gene fitness values are significantly different for that gene between the compared conditions, “Not_Sig” means that fitness values are not significantly different, and “Not_tested” means that the comparison has not been performed for that gene due to unequal variances

```
# Step 2: Run the comparison for all conditions against the reference one
  # Each conditions that is not the reference is going to be tested against the refence one after the other
using a for loop embedding the comparison function


Table_all=data.frame() # creates a table to eventually store the data
List_plots=list(0,0,0,0,0,0,0) # creates a list to store comparison of plots for each comparison in the "for
loop" .
                               # needs to have as many spots in the list than you have comparison

Conditions=as.vector(unique(Data_Fitness$Cdt))
Conditions=Conditions[Conditions!=Condition1]# generates a vector with all the conditions to compare against
the reference one

for (i in 1:length(Conditions)){
  Cdt=Conditions[i]
  Condition2=paste(Cdt)
  Test1=Comparison_test(Data_Fitness,Condition1, Condition2, alphaT, alphaF, org_locId, multi)
  #You obtain a list
  #list[[1]]= the table containing all the genes tested + fitness + variance values in both conditions + Fca
lc (Fisher value calculates for the test of variance + Tcalc (Tscore value for the student test))
  # and the category column indicates if the difference of fitness is significant (Sig), if it is not (Not_S
ig) or if the student was not performed because of unequal variances (Not_tested)
  #list[[2]]=the scatter plot representing the data

  Table_all=rbind(Table_all, Test1[[1]])
  List_plots[[i]]= Test1[[2]]
}

#Visualize all the scatter plots
grid.arrange(List_plots[[1]],List_plots[[2]],List_plots[[3]],List_plots[[4]], nrow=2,ncol=2)
```

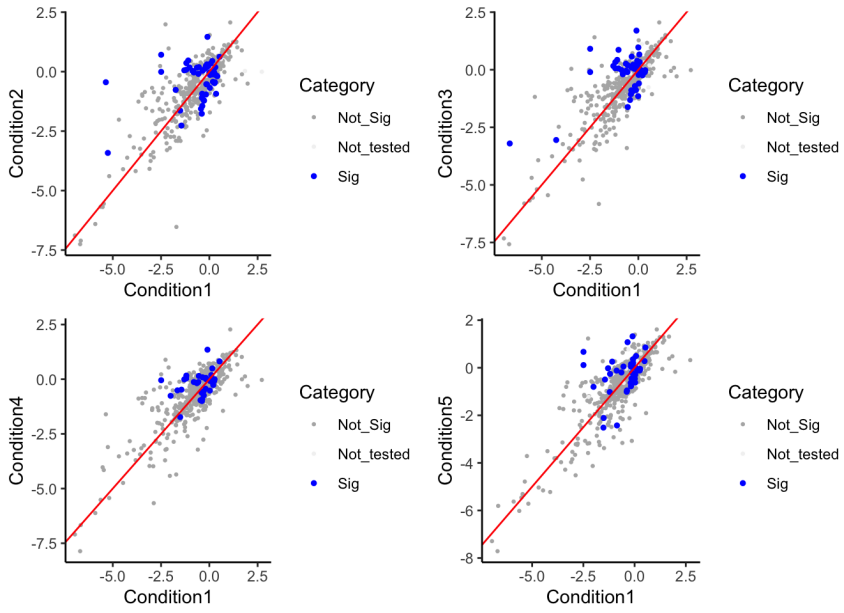


```
write.csv(Table_all, "Comparison_Ecoli_versusAlone.csv")
save(Table_all, List_plots, file="Comparison_Ecoli_versusAlone.RData")
```

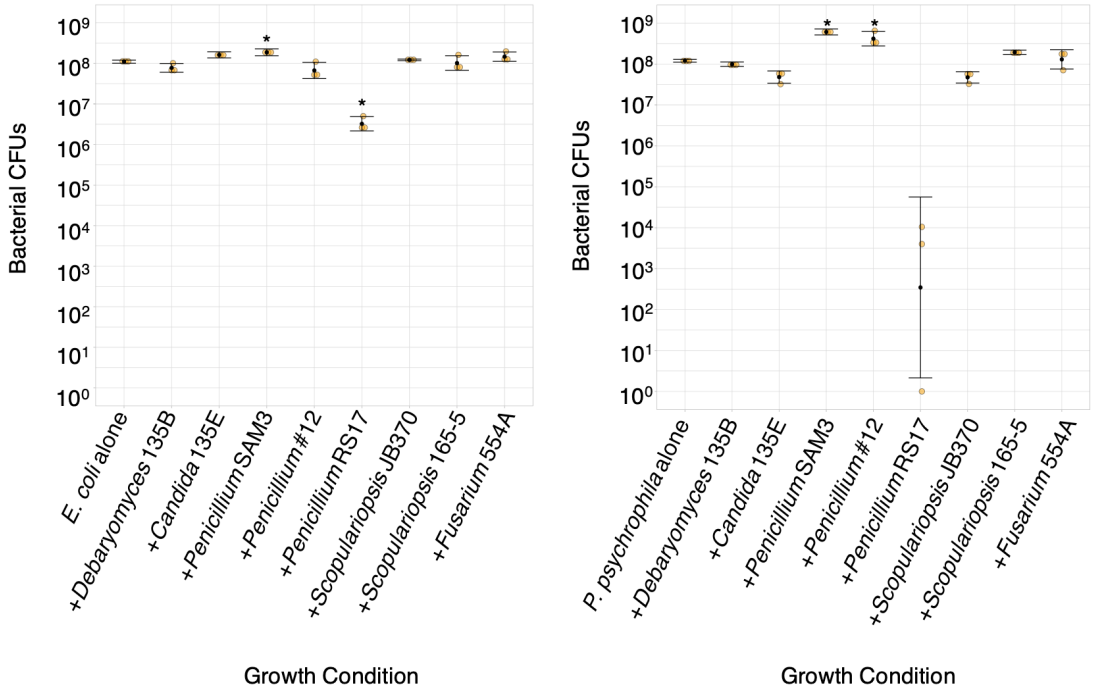

Supplementary Figure 1: **Impacts of fungal species on bacterial growth after 7 days of co-culture on cheese curd agar, pH 7**. CFU: colony forming units. N=3 biologically independent samples, error bars show standard deviation and black point is the mean. Asterisks represent a significant difference in bacterial growth in the presence of the fungal partner relative to alone (two-sided Dunnett's test, p-value <0.05). Exact p-values associated with asterisks (from left to right): 0.008, 0.002, 0.002, 0.02.

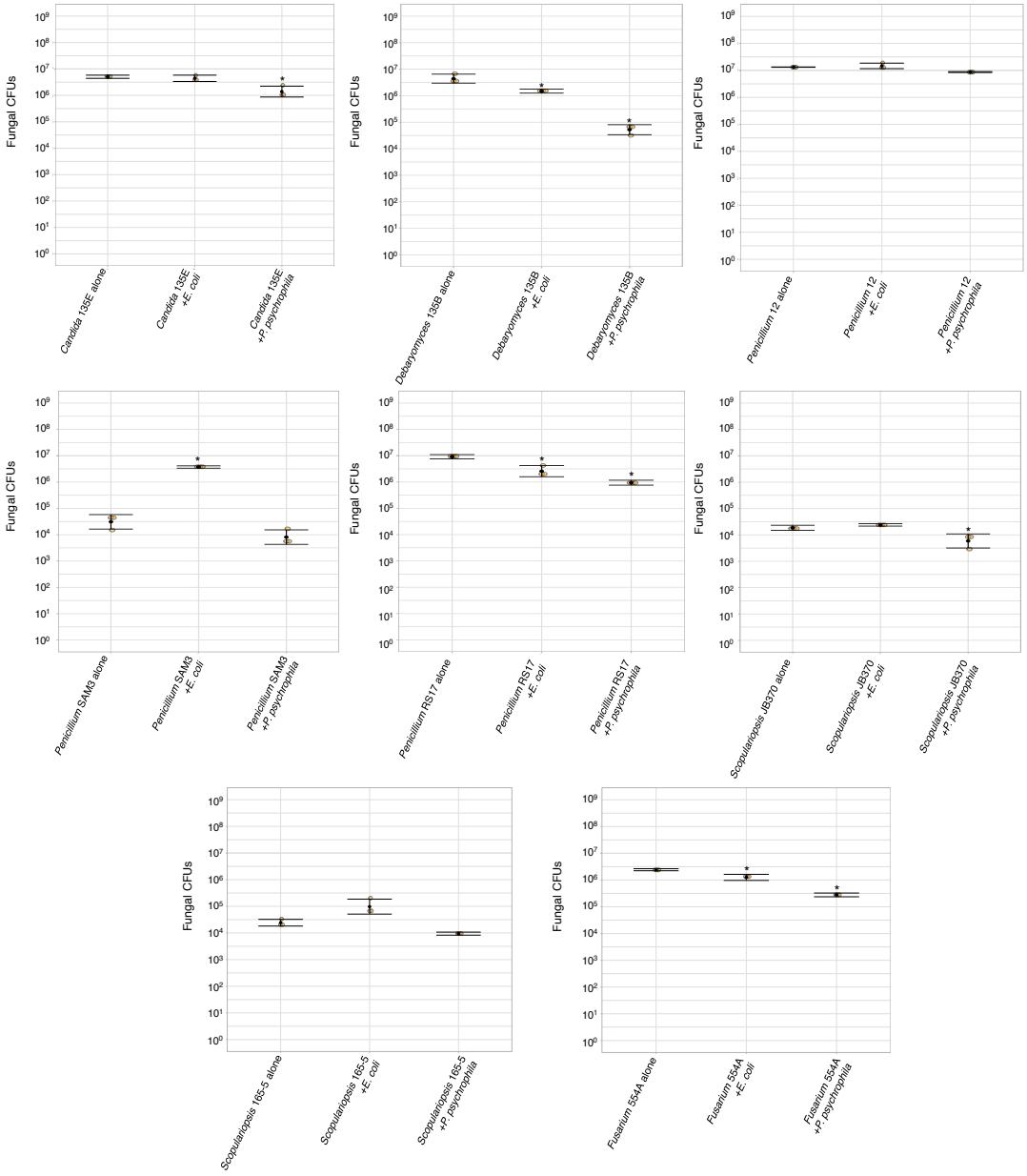

Supplementary Figure 2: **Impacts of bacterial species on fungal growth after 7 days of co-culture on cheese curd agar, pH 7**. For filamentous fungi, spore counts were used as a proxy for fungal CFUs. N=3 biologically independent samples, error bars show standard deviation and black point is the mean. Asterisks represent a significant difference in fungal growth in the presence of the bacterial partner relative to alone (two-sided Dunnett's test, p-value <0.05). Exact p-values associated with asterisks (from left to right, top to bottom): 0.004, 0.022, 0.004, 7.6e-05, 0.002, 0.00043, 0.013, 0.002, 6.2e-05.

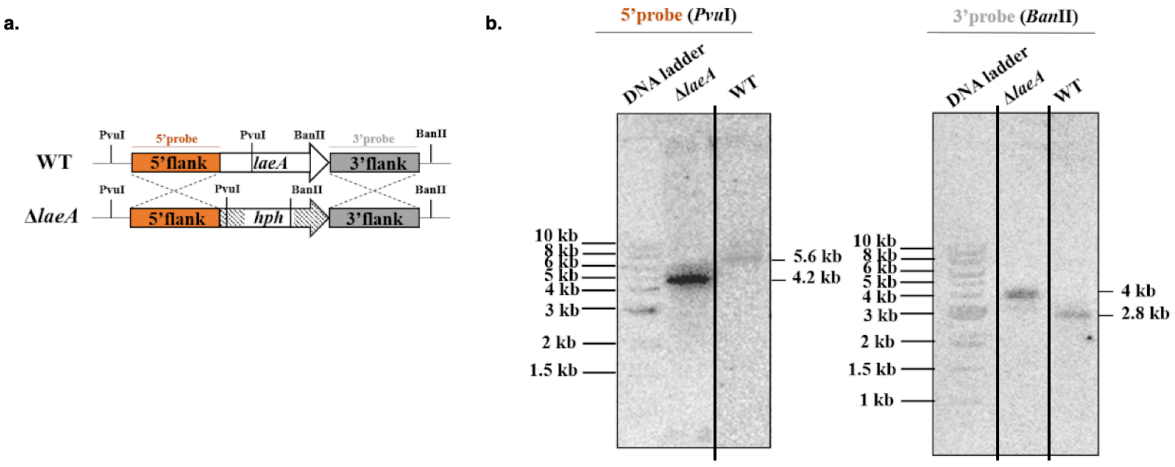

Supplementary Figure 3. Deletion of *laeA* gene in *Penicillium* sp. str. #12. **a,** Schematic representation of the genetic construct for *laeA* deletion in *Penicillium* sp. str. #12. The *hph* gene confers resistance to hygromycin. The positions of the restriction enzyme cutting sites are shown on the map. **b,** Southern blot analyses of genomic DNA from the WT and the Δ*laeA* strains. Ten micrograms of total DNA from each strain was digested with the appropriate enzymes and subjected to Southern blot analysis using respectively the 5' flank fragment (orange) and the 3'fragment (grey) as probes. The 1 kilobase DNA ladder from New England Biolabs was used to determine the size of the expected bands. The blot images were cropped to place the confirmed mutant adjacent to the WT strain. Black lines were added to the blot images to indicate where the cropping occurred. The blot images were also cropped on the top (around the wells) and bottom without interfering with the DNA ladder bands. The transformants that were confirmed to not have the correct insertion were not included in the figure. For the 3' blot image, an aligned overlay of the gel image and the blot was made allowing a clear visualization of the DNA ladder. Southern blots to confirm the Δ*laeA* strain were only performed once.

3.3 Acknowledgments

Chapter 3.2 is made up of a reprint of the following published manuscript: Pierce, EC, Morin, M, Little, JC, Liu, RB, Tannous, J, Keller, NP, Pogliano, K, Wolfe, BE, Sanchez, LM, and Dutton, RJ. Bacterial–fungal interactions revealed by genome-wide analysis of bacterial mutant fitness. *Nat Microbiol* (2020). https://doi.org/10.1038/s41564-020-00800- z. The dissertation author was the primary author of this paper.

CHAPTER 4: Further Work on Intermicrobial Interactions

4.1 Chapter Summary

Our initial work on bacterial-fungal interactions revealed a number of genes of unknown function that were involved in microbial interactions. In this chapter, three projects inspired by the work in Chapters 2 and 3 are discussed. In section 4.2 The Potential Role of *yjjZ* in Iron Uptake, we investigate an *E. coli* gene of unknown function. Preliminary work suggests that this gene may play a role in the uptake of hydroxamate-type siderophores. Section 4.3 Fungal Major Royal Jelly Protein summarizes initial work on a fungal protein implicated in bacterial-fungal interactions that potentially has antibiotic activity. Then, in section 4.4 Bacterial-bacterial Interactions, we apply the RB-TnSeq methods used to study bacterial-fungal interactions to investigate genes that are important for bacteria to grow with other bacterial species. Using pairwise combinations of bacterial RB-TnSeq libraries, we are able to get information on both perspectives of the interspecies interaction.

4.2 The Potential Role of *yjjZ* in Iron Uptake

Introduction

Despite advances in microbial genome sequencing, the function of many microbial genes remains a mystery. Even in the well-studied model organism *Escherichia coli,* 34.6% of genes lack experimental evidence of function (Ghatak et al. 2019). Our work in a three-member model Brie rind community indicated many unannotated genes in microbial interactions (Morin, Pierce, and Dutton 2018). Our investigation of genes relevant to bacterial-fungal interactions also highlighted 276 *E. coli* genes whose functions are annotated as hypothetical or unknown (Pierce et al. 2020). It is possible that the function of these genes may not have been previously

elucidated due to the common practice of studying bacteria in isolation rather than in interactive contexts.

As we had previously seen that access to iron is key to microbial growth on cheese, we wanted to further investigate unknown genes that might be related to iron uptake. One of these unknown genes was Fur-regulated DUF1435 domain-containing inner membrane protein *yjjZ.* Although this gene did not have significant RB-TnSeq interaction fitness, RNA-Seq showed that this gene was upregulated by *E. coli* in the presence of a filamentous fungus, suggesting that it may be important for bacterial-fungal interactions. It has been suggested that *yjjZ* encodes a small RNA (Chen et al. 2002). The only functional information available for this gene is that decreased expression of *yjjZ* led to increased tolerance to n-butanol, although it is unclear what role *yjjZ* might play in this tolerance (Otoupal and Chatterjee 2018). Based on its Fur regulation and our previous findings that iron plays a major role in bacterial-fungal interactions, we hypothesized that *yjjZ* might be involved in iron uptake (Figure 4.2-1a) (Pierce et al. 2020). Here, we begin to investigate the function of *yjjZ.*

Results

***YjjZ* co-localizes with *fhuF* and GGDEF genes in genomes throughout the Enterobacteriaceae family.** BLAST analysis of YjjZ (78 amino acids) showed that orthologs of this gene are present across the Enterobacteriaceae (Figure 4.2-1b) (Dehal et al. 2010). In *E. coli, yjjZ* is located next to *fhuF,* a membrane-associated protein that aids in the removal of iron from ferrichrome and coprogen, two siderophores produced by some fungi, including cheese filamentous fungi. We previously observed that fungal production of ferrichrome and coprogen impacted the fitness of *E. coli* mutants in siderophore biosynthesis, and that *fhuF* was

upregulated in co-culture conditions (in addition to *yjjZ*) (Pierce et al. 2020). *YjjZ* orthologs in *Salmonella, Citrobacter, Enterobacter, Klebsiella,* and *Cronobacter* are also located very close to *fhuF* orthologs (Figure 4.2-1b). In many species, *yjjZ* is located next to a diguanylate cyclase domain (GGDEF)-containing protein. Diguanylate cyclases regulate levels of cyclic di-GMP, a second messenger that regulates bacterial cell surface adhesiveness (D'Argenio and Miller 2004). Analysis of the *yjjZ* protein sequence shows three predicted transmembrane domains (Figure 4.2-1c).

Deletion of *yjjZ* impairs the ability of *E. coli* to use coprogen and ferrichrome. To survive in iron-limiting environments, *E. coli* normally excretes the siderophore enterobactin to harvest iron. Enterobactin uptake relies on the Fep system in *E. coli.* Loss of this system results in no *E. coli* growth on iron-limiting cheese curd agar (CCA) (Figure 3.2-5). Growth of ▵*fep* mutants can be rescued by ferrichrome and coprogen, whereas ▵*fep* ▵*fhu* double mutants cannot be rescued by these siderophores (Pierce et al. 2020). Consistent with the proposed role of *yjjZ* in hydroxamate siderophore uptake, deletion mutants of *yjjZ* in an enterobactin uptake-deficient (▵*fep*) background have diminished or no growth on CCA and cannot be rescued by these fungal siderophores (Figure 4.2-1d).

Discussion

Many genes in bacteria, even in well-studied organisms, do not have a known function. Based off of our previous work investigating bacterial-fungal interactions, we identified *yjjZ* as a candidate unknown gene for further study. Previous data and the genomic location of this gene indicated that *yjjZ* may be related to siderophore uptake. Growth assays with a *yjjZ* mutant in an

enterobactin-deficient background supports this hypothesis. YjjZ, in combination with a GGDEF protein, may play sensing/signaling role in hydroxamate siderophore uptake. However, further work is needed to determine the role of *yjjZ*.

Methods

RNA-Seq of *E. coli* with *Penicillium* sp. str. 12. This experiment and related methods are described in Pierce *et al.* 2020 (Pierce et al. 2020). The volcano plot was created in R using packages ggplot2 3.2.1 (Wickham 2009) and ggrepel 0.8.1 (Slowikowski 2018).

Analysis of *yjjZ* orthologs. MicrobesOnline (Dehal et al. 2010) was used to construct a Gene Tree for *yjjZ* using the full protein sequence and a clustering at 50% identity. The resulting tree image was edited in Inkscape 0.92.2.

Analysis of *yjjZ* protein domains. The InterPro 82.0 webserver (https://www.ebi.ac.uk/interpro/) was used to analyze protein domains.

Construction of *ΔfepΔyjjZ* double mutants. Overnight cultures of ΔfepC-pkD46 or ΔfepA-pkD46 *E. coli* (Pierce et al. 2020) were diluted 1:100 in fresh LB-100 µg/mL ampicillin and grown at 30 °C until an OD of 0.1. 20 µL of fresh 1 M L-arabinose were added, and growth was continued at 30 °C until OD 0.4-0.6. Cells were then chilled on ice for 15 minutes and then centrifuged for ten minutes at 4000 rcf 4 °C. Cells were resuspended in 1 mL of ice water and centrifuged for ten minutes at 4000 rcf at 4 °C. Cells were resuspended in 0.5 mL of ice water and centrifuged for ten minutes at 4000 rcf 4 °C. Cells were resuspended in 50 µL of ice water and kept on ice until transformation. The chloramphenicol resistance cassette was amplified from

the pKD3 plasmid using the following custom primers: Yjjz_catF (ATTATCATATGATATTGGTTATCATTATCAATGAAAGAGATGAAATCGTGTAGGCTGGAGCTGCTTC) and Yjjz_catR (CGCACCAATTATCTTTACTTCCTTTCTTGTTTCTTCCTTGATTTTATGGGAATTAGCCATGGTCC) and the following PCR conditions (i) 98 °C - 30 sec, (ii) 30 cycles of: 98 °C – 10 s; 70 °C – 20 s; 72 °C – 30 s, (iii) 72 °C – 5 min. Amplification was performed on 4 ng of pKD3 plasmid using Q5 High-Fidelity 2X Master Mix (New England Biolabs). The PCR product was digested for 1 hour with the restriction enzymes DpnI and ClaI at 37 °C and then the PCR product was run on a 1% agarose gel. The PCR product was extracted using the QIAquick Gel Extraction Kit (Qiagen) and then dialyzed overnight with TE buffer. 1.5 µL of dialyzed PCR product was used to transform the electrocompetent Δ*fepC*-pkD46 or Δ*fepA*-pkD46 cells. After 2 hours of recovery in SOC medium with 1 mM arabinose at 37 °C, the transformation was plated on LB with 50 mg/mL kanamycin and chloramphenicol. Transformants were confirmed to be Δ*yjjZ* with Eton Bioscience Inc. sequencing of the chloramphenicol cassette.

Tetrazolium growth assays with Δ*fep*Δ*yjjZ* double mutants. Antibiotic assay discs (Whatman) were placed on CCA medium pH 7 with 0.005% tetrazolium chloride (an indicator of cellular respiration) and 10 µL of water, or 10 mM coprogen, enterobactin, or ferrichrome (EMC Microcollections) solutions (in water) were slowly pipetted onto the disc and allowed to absorb. Aliquots (2.5 µL) of 37 °C overnight LB cultures of *E. coli* K12 BW25113 WT, Δ*fepA*, Δ*fepC*, Δ*fhuE*, Δ*fhuA* (Baba et al. 2006), Δ*fepA*Δ*fhuE*, Δ*fepA*Δ*fhuA*, Δ*fepA*Δ*yjjZ,* and Δ*fepC*Δ*yjjZ* mutants were spotted next to the discs. Plates were left at room temperature until development of red color resulting from tetrazolium chloride.

Figure

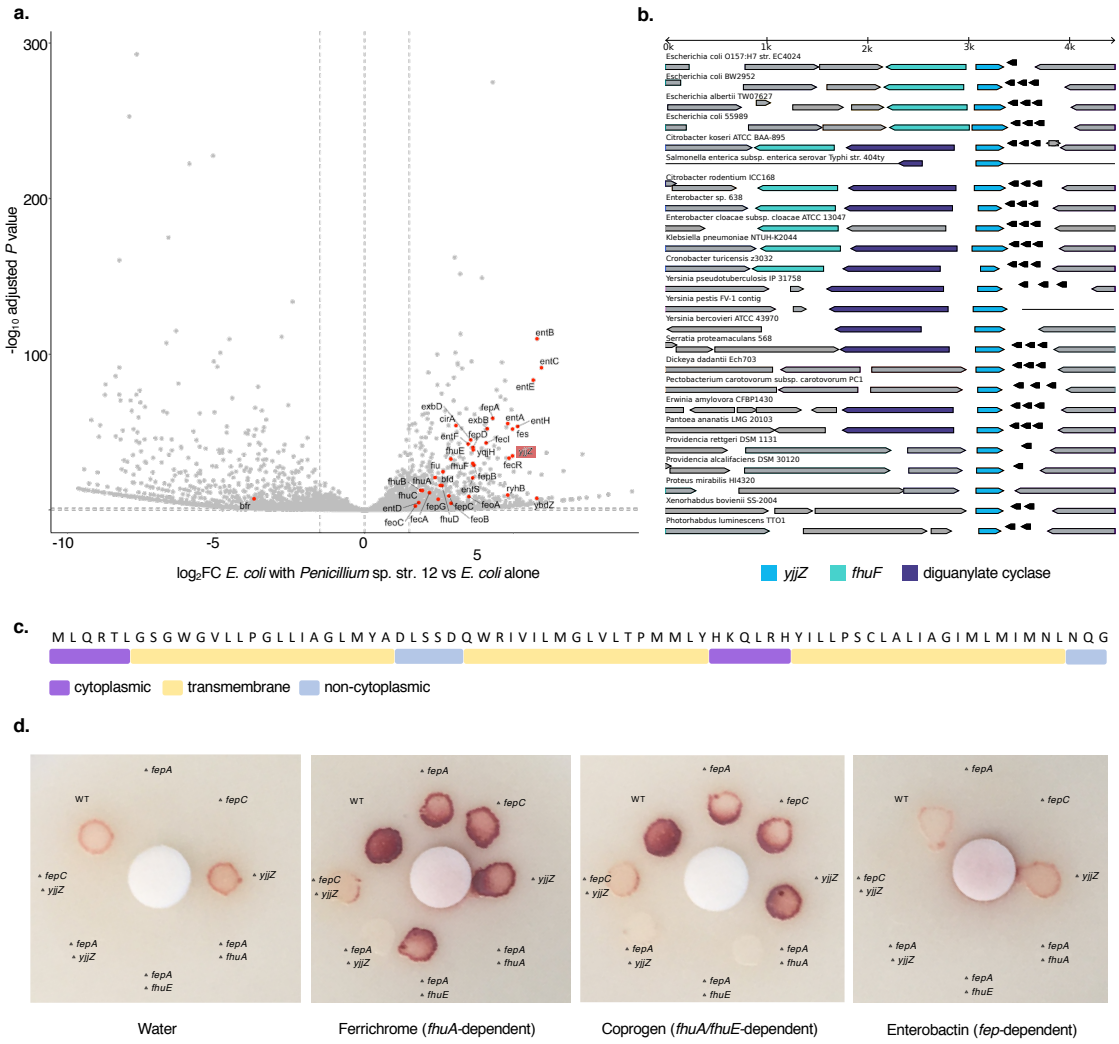

Figure 4.2-1. *YjjZ* may play a role in siderophore uptake in *E. coli*. a, Differential expression of *E. coli* grown with *Penicillium* sp. str. 12 relative to *E. coli* grown alone after 3 days of growth on CCA. Genes related to iron use with a log2 fold change (FC) of >1.5 or <−1.5 and adjusted P<0.05 are highlighted in red and *yjjZ* is boxed in red. **b,** Orthologs of *yjjZ* in other bacteria shown in their genomic context. *YjjZ, fhuF,* and GGDEF-domain containing genes are highlighted. **c,** Protein domain predictions of YjjZ. **d,** Visual assays of growth of iron uptake and *yjjZ* mutants with purified siderophores coprogen, ferrichrome, and enterobactin on CCA containing tetrazolium chloride, a red indicator of cellular respiration.

4.3 Fungal Major Royal Jelly Protein

Introduction

Royal jelly, a mix of proteins, sugars, lipids, vitamins, and salts, is a nurse honeybee secretion fed to bee larvae. Royal jelly is about 15% protein, the majority of which is made up of a family of nine major royal jelly proteins (MRJPs) (Buttstedt, Moritz, and Erler 2014). MRJPs are part of a *yellow*-like gene family found in insect species, bacteria, and fungi, but not in other eukaryotes. Analysis of *yellow*-like genes across genomes has led to the hypothesis that the presence of these genes in eukaryotes is the result of horizontal transfer from bacteria (Ferguson et al. 2011).

Although *yellow* genes are found across insects, the role of these genes is unknown in most species. In *Drosophila melanogaster,* the yellow gene impacts male mating success through changes in melanization of sex combs (Massey et al. 2019). Royal jelly has a variety of roles in honeybees (*Apis mellifera*), including impacts on caste differentiation. Only larvae that are fed royal jelly throughout development become queens, while worker bees are given royal jelly for a short time (Buttstedt et al. 2016). MRJP protein not only has interesting roles in bee development, but also has been researched for potential pharmacological activities (Nakaya et al. 2007; Kashima et al. 2014) , including antibiotic activity (Brudzynski, Sjaarda, and Lannigan 2015; Vezeteu et al. 2017).

Interestingly, MRJP has been shown to be upregulated in bees following bacterial challenge (Scharlaken et al., 2008). Additionally, the peptide jellein processed from the C-terminus of the bee MRJP1 has antibiotic activity similar to that seen with beta-lactam antibiotics (Brudzynski and Sjaarda, 2015). There has also been a report that full-length MRJP1 from bees inhibits the growth of bacteria relevant to larval diseases (Vezeteu et al. 2017). Previously, we had noticed that a fungal MRJP was among the highly upregulated genes in our *E. coli*/

Penicillium sp. str. 12 co-culture RNA-Seq experiment (Figure 4.3-1a). This fungal species had also been shown to have beta-lactam-like antibiotic activity against *E. coli* (Pierce et al. 2020). Here, we begin to investigate the potential role of *Penicillium* MRJP as an antibiotic.

Results

Bacterial cytological profiling (BCP) with MRJP peptides. Alignment of honeybee and *Penicillium* sp. str. 12 MRJP protein sequences showed some homology in the antibiotic peptide region at the C-terminus of the protein (Figure 4.3-1b). We ordered synthetic peptides of bee jellein and the aligned region from *Penicillium* sp. str. #12 to see if this peptide may be related to the activity seen with *Penicillium* sp. str. 12. *Bacillus subtilis* was used as a target bacterium due to a previous report that jellein activity was more evident in this bacterium than *E. coli* (Brudzynski and Sjaarda 2015). Preliminary BCP experiments with the bee and fungal peptide suggest that they may have antibiotic activity related to cell wall damage (Figure 4.2-1c).

Mass spectrometry to identify fungal MRJP peptides. To identify if the fungal peptide we synthesized was actually found in co-cultures of *E. coli* and *Penicillium* sp. str.12, we submitted supernatants of co-cultures on CCA for mass spectrometry analysis. This analysis was designed to look for peptides less than or equal to ten amino acids. However, we were not able to detect this peptide in *Penicillium* sp. str. 12 samples, perhaps because of high protein background in CCA, or because the peptide is either not processed or is longer than 10 amino acids.

Penicillium MRJP expression. As we have previously seen that *Penicillium* sp. str. 12 produces a large array of specialized metabolites, making it potentially harder to narrow down an active molecule, we decided to look for MRJP in *Penicillium camemberti* SAM3, a close relative of *Penicillium* sp. str. 12 that has been domesticated as an industrial starter for cheese

production. This strain had similar results to *Penicillium* sp. str. 12 in BCP and RB-TnSeq assays (Pierce et al. 2020). Although a MRJP gene was present in a publicly available *P. camemberti* genome, no genome existed for *Penicillium camemberti* SAM3. To determine if this strain possesses a MRJP gene, we sequenced the genome of this strain using a combination of long and short-read sequencing. The final assembly was 66 contigs and 36.5 Mb, in the size range of other *Penicillium* genomes (Figure 4.2-1d). BLAST of known *Penicillium* MRJP genes to this genome identified a single MRJP gene in *Penicillium camemberti* SAM3.

High protein background of CCA had previously made it difficult to identify MRJP peptides with mass spectrometry. In order to use a less complex medium for mass spectrometry, we first needed to confirm expression of *Penicillium* MRJP on other media. We grew *Penicillium camemberti* SAM3 on CCA, M9, and LB alone or with *E. coli* and used RT-PCR to look for MRJP expression. MRJP appears to be expressed on all three media, with or without *E. coli* present (Figure 4.2-1e).

Next steps. As *P. camemberti* SAM3 MRJP is expressed on less complex media, we will redo mass spectrometry analysis on CCA, M9, and LB looking for both full-length protein and short peptides. We will also heterologously express *P. camemberti* SAM3 MRJP in *E. coli* using vectors available from Matt Daugherty's lab at UCSD and coordinate with Chinmay Kalluraya from his lab to look into the horizontal gene transfer history of this gene. Nancy Keller's lab at UW Madison is also in the process of creating a MRJP deletion mutant in *Penicillium* sp. str. 12.

Discussion

MRJP, part of an ancient family of *yellow* proteins found in insects, is also found in cheese rind fungi. This protein is interesting not only for its potential antibiotic activity, but also

because it appears to have undergone two separate horizontal transfer events. Here, we have completed preliminary experiments to characterize MRJP in two cheese-associated *Penicillium* species. Follow-up mass spectrometry experiments on less complex media and heterologous expression experiments will further help us to identify the role of MRJP in microbial interactions in cheese rind communities and to determine if MRJP is related to the beta-lactam-like antibiotic activity previously observed in these fungi.

Methods

RNA-Seq of *E. coli* with *Penicillium* sp. str. 12. This experiment and related methods are described in Pierce *et al.* 2020 (Pierce et al. 2020). The volcano plot was created in R using package ggplot2 3.2.1(Wickham 2009).

Alignment of MRJPs. Protein alignment of *A. mellifera* (NCBI NP_001011579.1), *Penicillium* sp. str. 12 (GenBank KAF4769554.1), and *P. camemberti* str. SAM3 (contig 9 2251321-2252411) was performed with Geneious v.R9 9.1.8 (http://www.geneious.com).

BCP with MRJP peptides. The following custom peptides were synthesized (5-9 mg, >95% purity) by Thermo Fisher Scientific: jellein-TPFKISIHL, *Penicillium* sp. str. 12 C-term-NPSPIDHA. BCP was performed with 120 μg/ml^{-1} of peptide in an LB liquid culture of *Bacillus subtilis* PY79. After 30 minutes, 1.5 μL dye mix (1 μL of 1 mg ml^{-1} FM4-64, 1 μL of 200 μg ml^{-1} 4,6-diamidino-2-phenylindole (DAPI), 2 μL of 20 mM Sytox Green, in 46 μL of T-Base) was added to 6 μL of culture and cells were imaged as described below.

For the fungal co-culture assay, approximately 7,000,000 *B. subtilis* PY79 cells were inoculated alone or co-inoculated with 700,000 *Penicillium* sp. str. 12 spores on 10% CCA pH 7. After 3 days of growth, 1 ml of T-Base buffer was added to the surface of the biofilms, and

biofilms were scraped into the buffer. For co-culture conditions, the sample was filtered through a 0.5-μm filter to specifically remove fungal material. A total of 2 μL of concentrated dye mix (1 μL of 1 mg ml^{-1} FM4-64, 1 μL of 200 μg ml^{-1} 4,6-diamidino-2-phenylindole (DAPI), 2 μL of 20 mM Sytox Green, in 46 μL of T-Base) was added to 20 μL of filtrate. The dye-filtrate mix was spotted onto agarose–LB pads (1% agarose, 20% LB liquid medium, 80% ddH2O) and imaged by fluorescence and phase contrast microscopy using an Applied Precision Deltavision Spectris imaging system with an Olympus UPLFLN100XO2PH objective. Resulting images were deconvoluted using Deltavision SoftWorx software (Applied Precision), analyzed using Fiji and assembled in Adobe Photoshop (Adobe). Brightness was altered linearly in Fiji to aid visualization.

Sequencing of *Penicillium* SAM3 genome. *P. camemberti* SAM3 was grown in LB medium for 7 days at room temperature without shaking. The fungal mat floating on the surface was removed and ground in liquid nitrogen. Genomic DNA was then extracted from *P. camemberti* SAM3 using phenol–chloroform (pH 8). 125 μL of 425–600-μm acid-washed beads and 125 μL of 150–212-μm acid-washed beads were poured into a screw-capped 2-ml tube. A total of 500 μL of 2X buffer B (200 mM NaCl, 20 mM EDTA) and 210 μL of SDS 20% were added to the tube containing fungal material and 500 μL of phenol−chloroform (pH 8). Cells were lysed by vortexing the tubes for 2 min at maximum speed. Aqueous and organic phases were separated by centrifugation at 4 °C, 8,000 r.p.m. for 3 min, and 450 μL of the aqueous phase (upper phase) was recovered in a 1.5-ml Eppendorf tube. Sodium acetate (3 M, 45 μL) and ice-cold isopropanol (450 μL) were added before incubating the tubes at −80 °C for 10 min. The tubes were then centrifuged for 5 min at 4 °C at 13,000 r.p.m. The pellet was then washed in 750 μL of 70% ice-cold ethanol and resuspended in 50 μL of DNase/RNase-free water. High

molecular weight DNA (average 17 Kb) was then sequenced on four Flongle flow cells (Oxford Nanopore Technologies) using library preparation kit SQK-LSK309. Genomic DNA was also sequenced on Illumina iSeq for error correction (5 million PE reads). Raw Nanopore data were basecalled using guppy 4.0.15 (Oxford Nanopore Technologies) (guppy_basecaller -c dna_r9.4.1_450bps_hac.cfg) for 1D base calls. These reads were assembled by flye 2.8.1 (Kolmogorov et al. 2019) and polished by racon 1.4.3 (Vaser et al. 2017) four times and by DIAMOND 0.9.23 (Arumugam et al. 2019).

***Penicillium* MRJP RT-PCR.** Approximately 700,000 *P. camemberti* SAM3 cells were inoculated in duplicate (two distinct samples) either alone or with approximately 7,000,000 *E. coli* cells on 10% CCA pH 7, M9, or LB in standard petri dishes. Approximately 700,000 *Penicillium* sp. str. 12 cells were inoculated in duplicate (two distinct samples) either alone or with approximately 7,000,000 *E. coli* cells on 10% CCA pH 7. After 3 days at room temperature, the biofilms were collected in 1XPBS–Tween 0.05% for RNA extraction and resuspended in 300 µL of RNAprotect before storage at -80 °C prior to extraction. RNA was extracted by a phenol–chloroform extraction (pH 4.5) using the same extraction protocol as for gDNA described above, but samples were kept on ice when possible. RNA samples were treated with DNase using the 'Rigorous DNase treatment' for the Turbo DNA-free kit (Ambion, Life Technologies). Transfer RNAs and 5S RNA were then removed using a MEGAclear kit Purification for Large Scale Transcription Reactions (Ambion, Life Technologies) following the manufacturer's instructions. The presence of gDNA was assessed by PCR using universal bacterial 16S primers for samples with *E. coli* (forward primer: AGAGTTTGATCCTGGCTCAG; reverse primer: GGTTACCTTGTTACGACTT) and Bt2a (GGTAACCAAATCGGTGCTGCTTTC) and Bt2b (ACCCTCAGTGTAGTGACCCTTGGC) primers for fungal samples. The PCR was performed

in a final volume of 25 µL (12.5 µL of Q5 polymerase master mix (New England Biolabs), 1 µL of forward primer 10 µM, 1µl of reverse primer 10 µM and 1 µL of non-diluted RNA) with an annealing temperature of 57 °C, extension time of 45 seconds, and 35 cycles. PCR products were run on a 1.7% agarose gel and if gDNA was amplified, another DNase treatment was performed as well as a new verification of absence of gDNA. For RT-PCR, OneTaq One-Step Reaction Mix (New England BioLabs) was used (12.5 µL 2X reaction mix, 1 µL enzyme mix, 1 µL forward primer, 1 µL reverse primer, 100 ng RNA, water to 25 µL final volume) with the following conditions: (1) 48 °C for 30 min; (2) 94 °C for 1 min; (3) 40 cycles of 94 °C for 15 s, 58 °C for 30 s, 68 °C for 1 min; (4) 68 °C for 5 min. For *Penicillium* sp. str. 12 samples, pen12mrjpR (CACTCGATAGCGGCATCAAGG) and pen12mrjpF (GCTCAAGGAGACGTGACCAAG) primers were used to amplify MRJP cDNA. For *P. camemberti* SAM3 samples, sammrjpF (GAGCACGATGACCGTCTGAC) and sammrjpR (CAAGGCGACGACCGATTTGTG) primers were used to amplify MRJP cDNA.

Figure

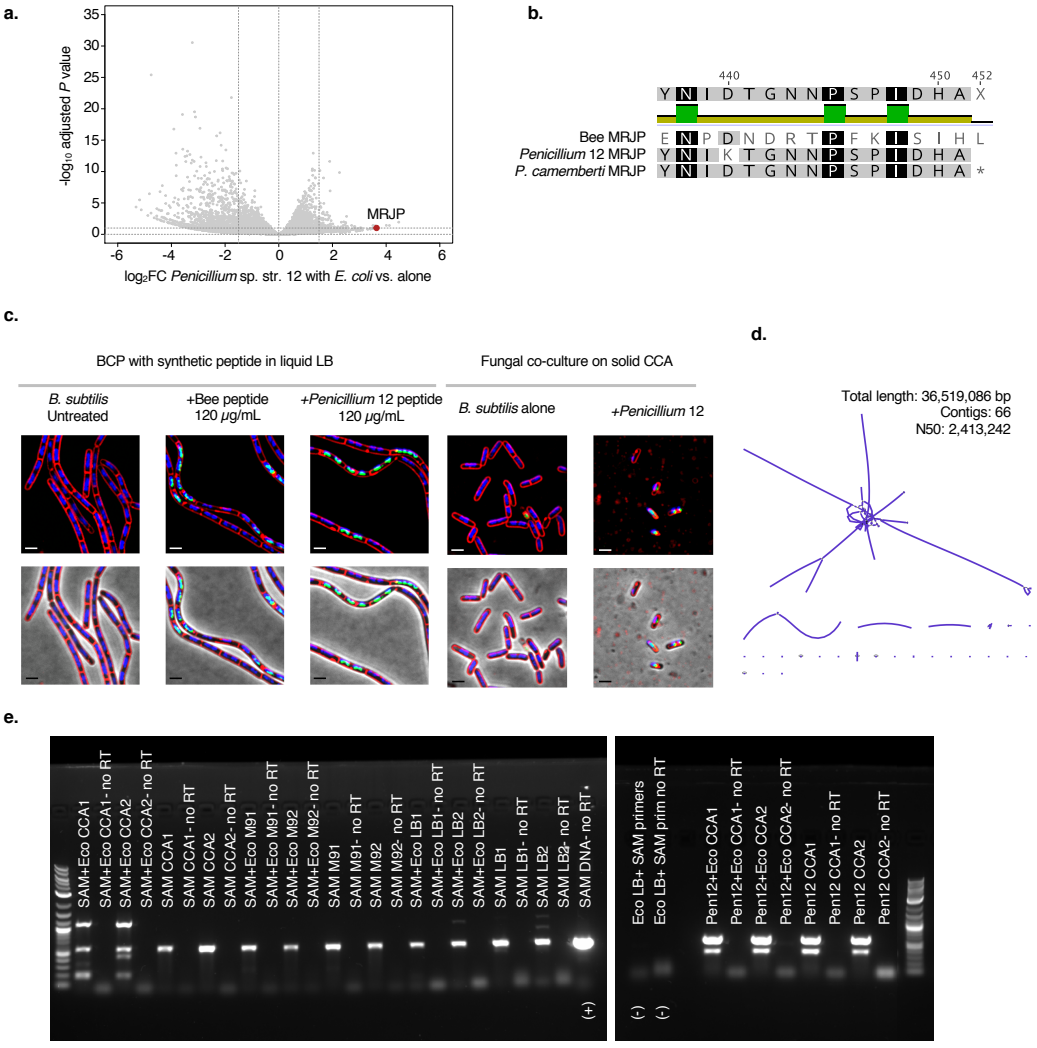

Figure 4.3-1. Characterization of *Penicillium major royal jelly protein*. a, MRJP is upregulated by *Penicillium* sp. str. 12 with a $\log_2$FC of ~ 4 when co-cultured with *E. coli*. **b,** Alignment of honeybee, *Penicillium* sp. str. 12, and *P. camemberti* SAM3 MRJP protein sequences. The last 16 amino acids at the C-terminus of the protein are shown. **c,** BCP assays of MRJP peptides with *B. subtilis* PY79 in liquid LB and of *B. subtilis* PY79 growing alone or mixed with *Penicillium* sp. str. 12 on cheese curd agar for three days. Teal color indicates damage to membrane integrity. **d,** Assembly graph of *P. camemberti* SAM3 genome assembly and assembly statistics. **e,** RT-PCR results looking at expression of MRJP of *P. camemberti* SAM3 (CCA pH 7, LB, or M9) and *Penicillium* sp. str. 12 (CCA pH 7) alone or co-cultured with *E. coli.* "No RT" indicates a control PCR reaction in which no reverse transcriptase was included. Results are shown for duplicate samples.

4.4 Bacterial-bacterial Interactions on Cheese

Introduction

Bacteria in cheese rind communities not only interact with fungi, but also with their bacterial neighbors. Bacteria have developed numerous strategies to cooperate and compete with each other, including motility, excretion of antibiotic compounds, disruption of competitors' signaling, and sequestration and cross-feeding of limited nutrients (Hibbing et al. 2010). They can also directly inject toxic molecules into other bacteria using type VI secretion systems (Russell, Peterson, and Mougous 2014).

To look at bacterial-bacterial interactions, RB-TnSeq experiments were done with bacterial libraries alone or with pairwise combinations of *E. coli, P. psychrophila* (cheese isolate), and *H. alvei* (cheese isolate) libraries on CCA. Because we can get RB-TnSeq information from both bacteria in the pairwise combination, we can see both perspectives of the interaction. These experiments provide preliminary information on genes important for bacterial fitness when growing with other bacteria.

Results

Genes with interaction fitness in bacterial-bacterial interactions. BarSeq (Wetmore et al. 2015) results from pairwise combinations of three bacterial libraries or from these libraries growing alone were analyzed using the pipeline previously developed for bacterial-fungal interactions to identify genes relevant to interactions (positive interaction fitness- gene has higher fitness with a partner than in growth alone; negative interaction fitness- gene has lower fitness with a partner than in growth alone) (Pierce et al. 2020). For *E. coli,* 70 genes have interaction fitness (IF) with *H. alvei* (max IF 1.4; min IF -1.3) and 84 genes have interaction fitness with *P.*

psychrophila (max IF 4.2; min IF -3.3). For *H. alvei,* 232 genes have interaction fitness with *P. psychrophila* (max IF 2.5; min IF -3.0) and 127 genes have interaction with *E. coli* (max IF 2.2; min IF -1.2). For *P. psychrophila,* 87 genes have interaction fitness with *H. alvei* (max IF 5.6; min IF -1.2) and 47 genes have interaction fitness with *E. coli* (max IF 4.4; min IF -2.1) (Figure 4.4-1a). For both cheese bacteria, there appear to be fewer impacts with *E. coli* than with the other cheese bacterium.

Bacterial-bacterial interactions are associated with amino acid metabolism, inorganic ion metabolism, and genes of unknown function. Genes with interaction fitness were classified into COG functional categories (Figure 4.4-1b). As we saw in the bacterial-fungal interaction data, all three bacteria have many genes of unknown function that have interaction fitness, again suggesting that unknown genes may have functions relevant to community contexts. For *H. alvei,* genes associated with nucleotide transport and metabolism seem to be mostly associated with positive interaction fitness with both partners, suggesting that *H. alvei* may benefit from nucleotide cross-feeding. Purine cross-feeding from *Rhodopseudomonas palustris* to *E. coli* has previously been observed in a synthetic bacterial mutualism (LaSarre et al. 2020). We see that *purF, purL,* and *purD* genes in *H. alvei* are among the genes with strongest positive interaction fitness with *P. psychrophila* (Figure 4.4-2).

For all three bacteria, amino acid metabolism is relatively highly represented (Figure 4.4-1b, Figure 4.4-2). However, for *H. alvei,* these genes are associated with positive interaction fitness, whereas for *E. coli,* most amino acid genes have negative interaction fitness (Figure 4.4-1b). For *E. coli, his* operon (histidine biosynthesis) genes have a negative interaction with *P. psychrophila* and *H. alvei. P. psychrophila his* genes have positive interaction fitness with *H. alvei,* whereas *H. alvei his* genes have negative interaction fitness with *P. psychrophila.* These

data suggest that histidine competition may play an important role in growth on CCA and that *P. psychrophila* may outcompete *H. alvei* for histidine.

As we saw in our previous work on bacterial-fungal interactions, access to iron is important for bacteria growing on iron-limiting CCA. *E. coli fep* genes related to uptake of its siderophore enterobactin have a positive fitness with both bacteria, suggesting that they may be pirating siderophores from the other species. For *P. psychrophila, fecA* and *fecR* have strong positive interaction fitness with both bacteria. These genes are part of an iron starvation response related to ferric citrate transport. In the presence of *H. alvei, P. psychrophila's fhuE* gene, which encodes a receptor for desferrioxamine uptake, has negative interaction fitness. AntiSMASH analysis predicts that *H. alvei* makes desferrioxamine, suggesting that the ability of *P. psychrophila* to use desferrioxamine produced by *H. alvei* provides a fitness advantage.

Next steps. To complement the RB-TnSeq data for these experiments, RNA-Seq experiments were done with the same conditions. These data will be integrated with the RB-TnSeq data to narrow down target genes for future mechanistic follow-up.

Discussion

In this section, we applied techniques previously developed for investigating bacterial-fungal interactions to investigate bacterial-bacterial interactions using RB-TnSeq. Initial results suggest that amino acid metabolism, access to iron, and genes of unknown function are among the main gene functions involved in bacterial-bacterial interactions. Follow-up experiments using RNA-Seq with these interaction partners will aid in the selection of gene candidates for mechanistic studies.

Methods

Bacterial-bacterial BarSeq. All RB-TnSeq assays were performed on 10% CCA medium adjusted to pH 7. Before inoculation, one aliquot of each library was thawed and inoculated into 25 ml of liquid LB with kanamycin (50 μg ml−1). This is the same medium used for creating the initial library and is expected to be nonselective. Once the culture reached mid-log phase (OD = 0.6–0.8), 5 ml of that pre-culture was pelleted and stored at −80 °C for the T0 reference in the fitness analysis. The remaining cells were used to inoculate the fitness assay conditions. For each BarSeq fitness assay, we aimed to inoculate 20,000,000 cells of each bacterial library. Libraries were inoculated alone or pairwise with one of the other bacterial libraries by spreading evenly on a 100-mm Petri dish. For each condition, assays were performed in triplicate (three distinct samples). After 3 days, each plate was flooded with 1.5 ml of 1×PBS–Tween 0.05% and cells were scraped off, taking care not to disturb the CCA. The liquid was then transferred into a 1.5-ml microcentrifuge tube and cells were pelleted by centrifugation before being stored at −80 °C until gDNA extraction. gDNA was extracted with phenol–chloroform (pH 8) as described in Pierce *et al*. 2020 (Pierce et al. 2020). Samples were stored at −80 °C until further analysis. The 98 °C BarSeq PCR protocol as previously described in Wetmore *et al*. (Wetmore et al. 2015) was used to amplify only the barcoded region of the transposons. PCR was performed in a final volume of 50 μL with the following content: 25 μL of Q5 polymerase master mix (New England Biolabs), 10 μL of GC enhancer buffer (New England Biolabs), 2.5 μL of the common reverse primer (BarSeq_P1 – Wetmore et al.18) at 10 μM, 2.5 μL of a forward primer from the 96 forward primers (BarSeq_P2_ITXXX) at 10 μM, and either 200 ng of gDNA for growth-alone conditions or 400 ng of gDNA for pairwise interaction conditions. We used the following PCR program: (1) 98 °C for 4 min; (2) 30 cycles of 98 °C for 30 s, 55 °C

for 30 s and 72 °C for 30 s; and (3) 72 °C for 5 min. After the PCR, 10 µL of each of the PCR products for conditions with a single species was pooled together to create the BarSeq sequencing library, and 200 µL of the pooled library was purified using a MinElute purification kit (Qiagen). The final elution of the BarSeq library was performed in 30 µL of DNase- and RNase-free water. The BarSeq libraries were then quantified using a Qubit dsDNA HS assay kit (Invitrogen) and sequenced on a HiSeq4000 (75 bp, single-end reads) by the IGM Genomics Center at the University of California, San Diego. The sequencing depth for each condition varied between 5.9 and 9.1 million reads for alone conditions and 17.5 and 28.2 for pairwise conditions. Wetmore *et al.* scripts (Wetmore et al. 2015) were used to count barcodes in each condition prior to processing with custom R scripts, as in Pierce *et al*. 2020 (Pierce et al. 2020). COG category mapping of protein sequences was done using eggNOG-mapper (v.2) (Huerta-Cepas et al. 2019) and visualized using R package ggplot2 (v.3.2.1)(Wickham 2009).

Figures

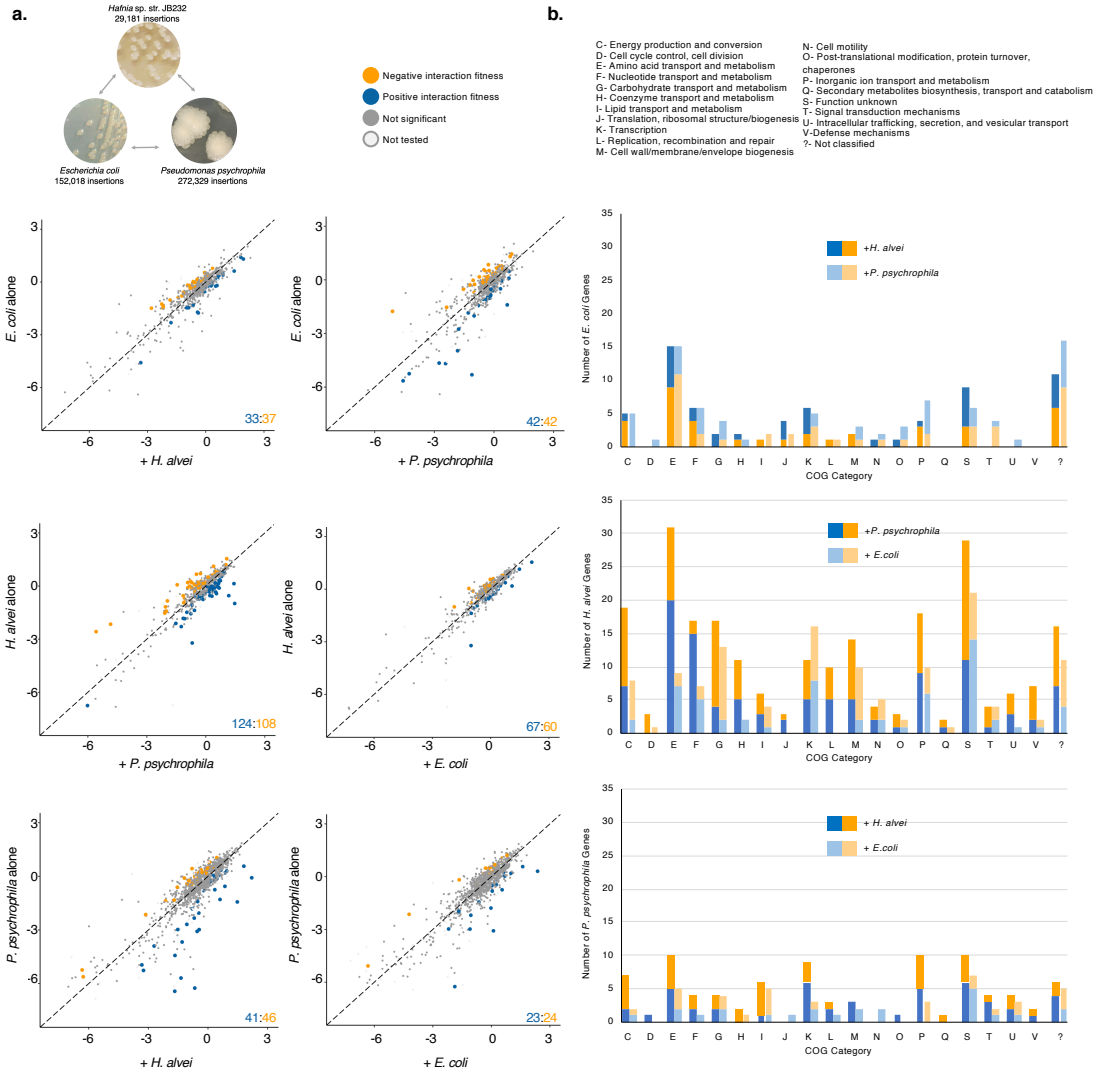

Figure 4.4-1. Comparison of bacterial gene fitness with a bacterial partner against growth alone and functional distribution of bacterial genes with significant interaction fitness. a, Gene fitness values were calculated for each gene during growth with a bacterial partner (x axis) and during growth alone (y axis). Each point represents a gene, with colored points indicating genes with a significant difference between gene fitness during growth alone versus with a partner identified by a two-sided t-test and an adjusted P value lower than 5% using Benjamini–Hochberg correction for multiple comparison testing. This difference is referred to as 'interaction fitness'. The colored numbers in the lower right-hand corner indicate how many genes have either positive (blue) or negative (orange) interaction fitness. Genes not included in the t-test are labeled as not tested. **b,** Number of genes with significant interaction fitness for each bacterium per COG functional category, colored by positive (blue) or negative (orange) interaction fitness.

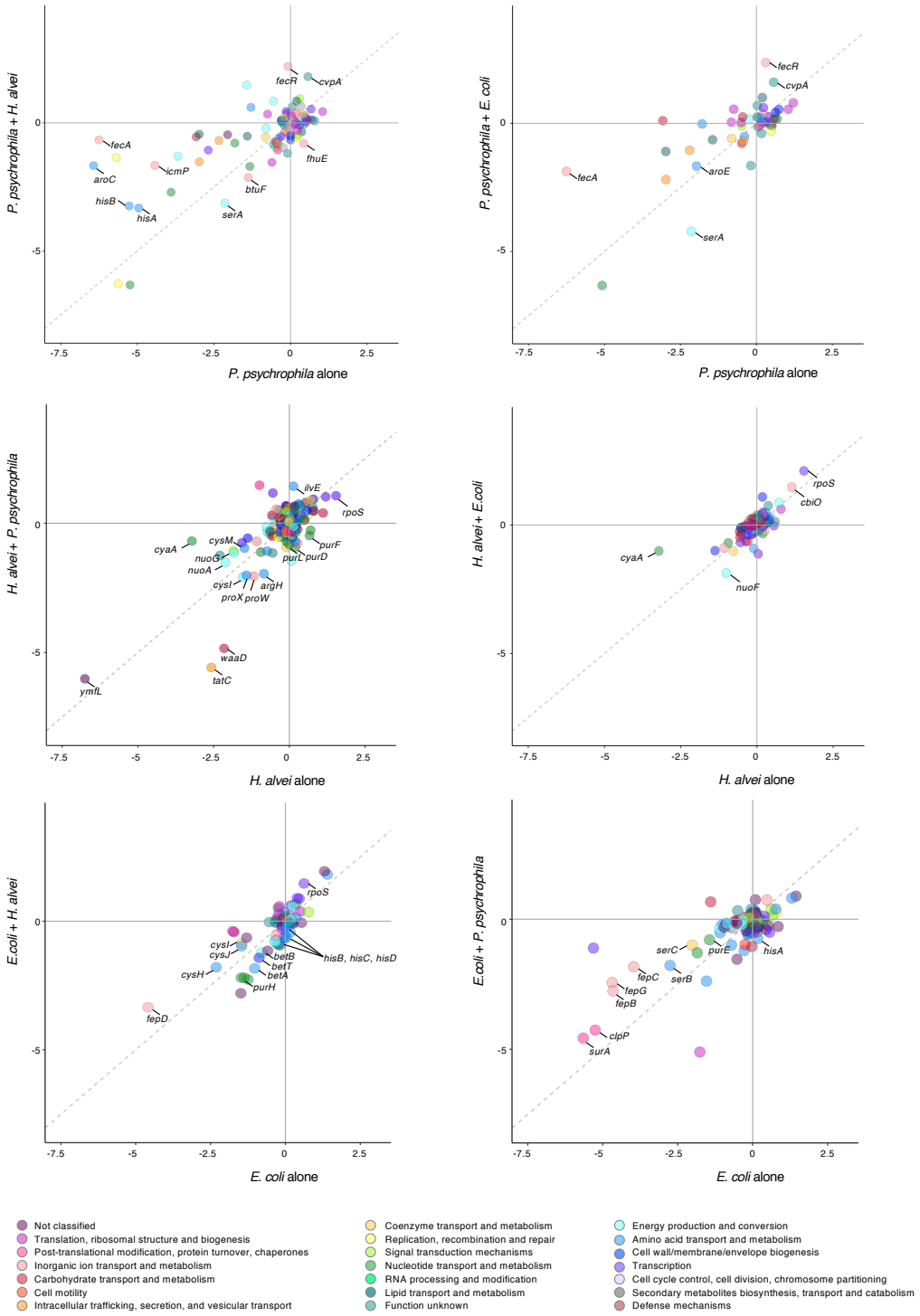

Figure 4.4-2. Functional comparison of bacterial gene fitness values alone compared to fitness values with a bacterial partner. Genes are colored by COG category and genes with strong interaction fitness or genes that may be of further interest are labeled.

4.5 Acknowledgments

Chapter 4 consists of unpublished material. The dissertation author is the primary author of this material. The following individuals are also authors on this work: Section 4.2- Rachel Dutton (UCSD); Section 4.3- Kit Pogliano (UCSD), Roland Liu (UCSD), Rachel Dutton (UCSD); Section 4.4- Manon Morin (UCSD), Rachel Dutton (UCSD).

CHAPTER 5: Conclusion

5.1 Future Directions

Pursuing genes of unknown function. One of the most interesting findings from the works discussed here was the implication of many unknown bacterial genes in interactions with other bacteria and with fungi. Many of these genes are from the model organism *E. coli* and have homologs in other bacterial species. Because much of microbiology research has been done with species growing in isolation, genes needed for growth with other species may not have been well explored, despite being key to bacterial life in natural environments. Because *E. coli* is extremely genetically tractable, it should be possible to explore the function of these genes in synthetic communities. Future work should take advantage of the rare ability that the cheese rind model provides to study gene function in community contexts.

One non-standard approach to further investigate the role of genes of unknown function would be to use interaction RB-TnSeq. In this technique, a second mutation in the gene of interest is added to all RB-TnSeq library members, enabling the determination of genetic interactions between this gene and the rest of the genome. This technique has previously been used in a cyanobacterium to find pathways related to a c-di-AMP cyclase but has so far to our knowledge not been applied to *E. coli* (Rubin et al. 2018). As there is already an existing *E. coli* RB-TnSeq library, and we already have the tools for making *E. coli* targeted knockouts, this approach should be technically feasible and could help us to determine processes related to genes with no known function. Although this process is not high-throughput as it requires individual mutant creation in the library background, genes could be prioritized based on RB-TnSeq data (*e.g.* fitness strength), whether we see the gene highlighted in other data sets (*e.g.* RNA-Seq),

and likelihood of interesting findings (*e.g.* homologs in pathogenic or otherwise important bacteria, encodes a protein that interacts with other proteins of interest).

Deeper characterization of fungi and fungal contributions to microbiomes. Due to limitations of genetic tools and knowledge for fungal species, especially filamentous fungi, most of the work described here on bacterial-fungal interactions was based on the bacterial perspective. However, we saw that many fungal impacts on bacteria were due to specialized metabolite production. While we did preliminary work to sequence the genomes of these fungi and catalog the metabolites produced by the fungi described here, the vast majority of these metabolites are unknown or of unknown ecological relevance. The huge array of undescribed cheese-associated fungal metabolites observed represents a rich source of potential future study, especially for the relatively unstudied *Scopulariopsis* molds.

We have also observed antibiotic activity not only in the two *Penicillium* species described above, but also in *Penicillium* sp. str. RS17 and in *Scopulariopsis* sp. str. JB370. Specialized metabolite analysis did not reveal any known antibiotics. Although attempts were made to isolate bioactive molecules, continued fractionation of extracts resulted in loss of activity, suggesting that the activity seen may be unstable or the result of multiple compounds acting in concert. Nevertheless, cheese fungal species, especially species that have not previously received much attention, could be an interesting source of novel antibiotics.

Fungi are undoubtedly very important players in the development and function of cheese rind and other microbiomes. To truly take advantage of the cheese rind model system, a system in which we can test hypotheses in community contexts, further work should be done on the development of genetic tools for cheese-associated fungal species. Further work on the annotation of fungal genomes, development of reliable dual RNA-Seq protocols, and

development of tools for in-house fungal mutant creation would all be advantageous for the further development of the cheese rind model.

Study of interactions in community contexts and cross-system comparisons of mechanisms of interaction. Much of the literature on intermicrobial interactions is descriptive rather than mechanistic and is solely based on net growth impacts or based on correlation patterns. When mechanistic studies are done, they are frequently done looking at an interaction between only two specific species, usually model or pathogenic organisms. One important future direction for studying intermicrobial interactions will be finding a way to bridge the gap between specific and theoretical studies. As studying each possible combination of species across all systems is not technically reasonable, higher level trends of how interactions impact microbiomes would ideally be found. Across many systems and for both interbacterial and interkingdom interactions, it is possible to see common intermicrobial interaction themes, such as cross-feeding, antagonism, and interactions related to pH. However, it is unclear how translatable findings are for similar organisms found in different systems. In this work, we focused on Ascomycete fungi and proteobacteria from cheese rind microbiomes. Future work should attempt to look at patterns of interaction mechanisms across different systems and with a more diverse range of organisms.

It will also be important to examine how these interactions change in multispecies communities and how relevant pairwise interactions are in more complex systems. We have previously seen evidence of higher order interactions in the Brie rind model system (Morin, Pierce, and Dutton 2018). However, this is a very simple three-member community. Future work should look at how the interactions found here change in the context of other species, whether

new interactions emerge, and whether these interactions have functional consequences in the cheese rind.

5.2 Concluding remarks

Using a combination of the high-throughput genetic screen RB-TnSeq, transcriptomics, metabolomics, and bacterial cytological profiling, we have investigated intermicrobial interactions between species associated with cheese rind microbiomes. To do this, we created and characterized barcoded transposon mutant libraries in two cheese-associated bacteria and developed an analytical pipeline for interpreting RB-TnSeq data relevant to microbial interactions. This pipeline can also be used for any two-condition comparison of fitness data. The development of these tools provides a foundation for mechanistic studies in the cheese rind model system. Using these tools, we have investigated both bacterial-bacterial and bacterial-fungal interactions. In addition to revealing several specific mechanisms of interaction, these works highlight a large number of uncharacterized genes and metabolites relevant to intermicrobial interactions, opening up new avenues of study that will enhance understanding of diverse microbial systems.

CHAPTER 6: References

Abdel-Haleem, Alyaa M., Vaishnavi Ravikumar, Boyang Ji, Katsuhiko Mineta, Xin Gao, Jens Nielsen, Takashi Gojobori, and Ivan Mijakovic. 2020. "Integrated Metabolic Modeling, Culturing, and Transcriptomics Explain Enhanced Virulence of Vibrio Cholerae during Coinfection with Enterotoxigenic Escherichia Coli." *MSystems* 5 (5). https://doi.org/10.1128/mSystems.00491-20.

Adamowicz, Elizabeth M., and William R. Harcombe. 2020. "Weakest-Link Dynamics Predict Apparent Antibiotic Interactions in a Model Cross-Feeding Community." *Antimicrobial Agents and Chemotherapy* 64 (11). https://doi.org/10.1128/AAC.00465-20.

Adamowicz, Elizabeth M., Michaela Muza, Jeremy M. Chacón, and William R. Harcombe. 2020. "Cross-Feeding Modulates the Rate and Mechanism of Antibiotic Resistance Evolution in a Model Microbial Community of Escherichia Coli and Salmonella Enterica." *PLoS Pathogens* 16 (7): e1008700.

Aranda-Díaz, Andrés, Benjamin Obadia, Ren Dodge, Tani Thomsen, Zachary F. Hallberg, Zehra Tüzün Güvener, William B. Ludington, and Kerwyn Casey Huang. 2020. "Bacterial Interspecies Interactions Modulate PH-Mediated Antibiotic Tolerance." *ELife* 9 (January). https://doi.org/10.7554/eLife.51493.

Armbruster, Chelsie E., Valerie Forsyth-DeOrnellas, Alexandra O. Johnson, Sara N. Smith, Lili Zhao, Weisheng Wu, and Harry L. T. Mobley. 2017. "Genome-Wide Transposon Mutagenesis of Proteus Mirabilis: Essential Genes, Fitness Factors for Catheter-Associated Urinary Tract Infection, and the Impact of Polymicrobial Infection on Fitness Requirements." *PLoS Pathogens* 13 (6): e1006434.

Arumugam, Krithika, Caner Bağcı, Irina Bessarab, Sina Beier, Benjamin Buchfink, Anna Górska, Guanglei Qiu, Daniel H. Huson, and Rohan B. H. Williams. 2019. "Annotated Bacterial Chromosomes from Frame-Shift-Corrected Long-Read Metagenomic Data." *Microbiome* 7 (1): 61.

Baba, Tomoya, Takeshi Ara, Miki Hasegawa, Yuki Takai, Yoshiko Okumura, Miki Baba, Kirill A. Datsenko, Masaru Tomita, Barry L. Wanner, and Hirotada Mori. 2006. "Construction of Escherichia Coli K-12 in-Frame, Single-Gene Knockout Mutants: The Keio Collection." *Molecular Systems Biology* 2 (February): 2006.0008.

Brudzynski, Katrina, and Calvin Sjaarda. 2015. "Honey Glycoproteins Containing Antimicrobial Peptides, Jelleins of the Major Royal Jelly Protein 1, Are Responsible for the Cell Wall Lytic and Bactericidal Activities of Honey." *PloS One* 10 (4): e0120238.

Brudzynski, Katrina, Calvin Sjaarda, and Robert Lannigan. 2015. "MRJP1-Containing Glycoproteins Isolated from Honey, a Novel Antibacterial Drug Candidate with Broad Spectrum Activity against Multi-Drug Resistant Clinical Isolates." *Frontiers in Microbiology* 6 (July): 711.

Butaitė, Elena, Michael Baumgartner, Stefan Wyder, and Rolf Kümmerli. 2017. "Siderophore Cheating and Cheating Resistance Shape Competition for Iron in Soil and Freshwater Pseudomonas Communities." *Nature Communications* 8 (1): 414.

Buttstedt, Anja, Christian H. Ihling, Markus Pietzsch, and Robin F. A. Moritz. 2016. "Royalactin Is Not a Royal Making of a Queen." *Nature* 537 (7621): E10-2.

Buttstedt, Anja, Robin F. A. Moritz, and Silvio Erler. 2014. "Origin and Function of the Major Royal Jelly Proteins of the Honeybee (Apis Mellifera) as Members of the Yellow Gene Family : Honeybee's Major Royals." *Biological Reviews* 89 (2): 255–69.

Chen, Shuo, Elena A. Lesnik, Thomas A. Hall, Rangarajan Sampath, Richard H. Griffey, Dave J. Ecker, and Lawrence B. Blyn. 2002. "A Bioinformatics Based Approach to Discover Small RNA Genes in the Escherichia Coli Genome." *Bio Systems* 65 (2–3): 157–77.

Claesen, Jan, Jennifer B. Spagnolo, Stephany Flores Ramos, Kenji L. Kurita, Allyson L. Byrd, Alexander A. Aksenov, Alexey V. Melnik, et al. 2020. "A Cutibacterium Acnes Antibiotic Modulates Human Skin Microbiota Composition in Hair Follicles." *Science Translational Medicine* 12 (570). https://doi.org/10.1126/scitranslmed.aay5445.

Cleary, Jessica L., Shilpa Kolachina, Benjamin E. Wolfe, and Laura M. Sanchez. 2018. "Coproporphyrin III Produced by the Bacterium Glutamicibacter Arilaitensis Binds Zinc and Is Upregulated by Fungi in Cheese Rinds." *MSystems* 3 (4). https://doi.org/10.1128/mSystems.00036-18.

Cooper, Matthew B., Elena Kazamia, Katherine E. Helliwell, Ulrich Johan Kudahl, Andrew Sayer, Glen L. Wheeler, and Alison G. Smith. 2019. "Cross-Exchange of B-Vitamins Underpins a Mutualistic Interaction between Ostreococcus Tauri and Dinoroseobacter Shibae." *The ISME Journal* 13 (2): 334–45.

Dal Co, Alma, Simon van Vliet, Daniel Johannes Kiviet, Susan Schlegel, and Martin Ackermann. 2020. "Short-Range Interactions Govern the Dynamics and Functions of Microbial Communities." *Nature Ecology & Evolution* 4 (3): 366–75.

D'Argenio, David A., and Samuel I. Miller. 2004. "Cyclic Di-GMP as a Bacterial Second Messenger." *Microbiology* 150 (8): 2497–2502.

Datta, Manoshi S., Elzbieta Sliwerska, Jeff Gore, Martin F. Polz, and Otto X. Cordero. 2016. "Microbial Interactions Lead to Rapid Micro-Scale Successions on Model Marine Particles." *Nature Communications* 7 (June): 11965.

Dehal, Paramvir S., Marcin P. Joachimiak, Morgan N. Price, John T. Bates, Jason K. Baumohl, Dylan Chivian, Greg D. Friedland, et al. 2010. "MicrobesOnline: An Integrated Portal for Comparative and Functional Genomics." *Nucleic Acids Research* 38 (Database issue): D396-400.

Enke, Tim N., Gabriel E. Leventhal, Matthew Metzger, José T. Saavedra, and Otto X. Cordero. 2018. "Microscale Ecology Regulates Particulate Organic Matter Turnover in Model

Marine Microbial Communities." *Nature Communications* 9 (1): 2743.

Evans, Kara C., Saida Benomar, Lennel A. Camuy-Vélez, Ellen B. Nasseri, Xiaofei Wang, Benjamin Neuenswander, and Josephine R. Chandler. 2018. "Quorum-Sensing Control of Antibiotic Resistance Stabilizes Cooperation in Chromobacterium Violaceum." *The ISME Journal* 12 (5): 1263–72.

Ferguson, Laura C., Jack Green, Alison Surridge, and Chris D. Jiggins. 2011. "Evolution of the Insect Yellow Gene Family." *Molecular Biology and Evolution* 28 (1): 257–72.

Flynn, Jeffrey M., Lydia C. Cameron, Talia D. Wiggen, Jordan M. Dunitz, William R. Harcombe, and Ryan C. Hunter. 2020. "Disruption of Cross-Feeding Inhibits Pathogen Growth in the Sputa of Patients with Cystic Fibrosis." *MSphere* 5 (2). https://doi.org/10.1128/mSphere.00343-20.

García-Bayona, Leonor, and Laurie E. Comstock. 2018. "Bacterial Antagonism in Host-Associated Microbial Communities." *Science* 361 (6408). https://doi.org/10.1126/science.aat2456.

Ghatak, Sankha, Zachary A. King, Anand Sastry, and Bernhard O. Palsson. 2019. "The Y-Ome Defines the 35% of Escherichia Coli Genes That Lack Experimental Evidence of Function." *Nucleic Acids Research* 47 (5): 2446–54.

Guillonneau, Richard, Claudine Baraquet, Alexis Bazire, and Maëlle Molmeret. 2018. "Multispecies Biofilm Development of Marine Bacteria Implies Complex Relationships Through Competition and Synergy and Modification of Matrix Components." *Frontiers in Microbiology* 9 (August): 1960.

Hall, James P. J., Ellie Harrison, and Michael A. Brockhurst. 2018. "Competitive Species Interactions Constrain Abiotic Adaptation in a Bacterial Soil Community." *Evolution Letters* 2 (6): 580–89.

Han, Yuying, Tietao Wang, Gukui Chen, Qinqin Pu, Qiong Liu, Yani Zhang, Linghui Xu, Min Wu, and Haihua Liang. 2019. "A Pseudomonas Aeruginosa Type VI Secretion System Regulated by CueR Facilitates Copper Acquisition." *PLoS Pathogens* 15 (12): e1008198.

Hansen, Bridget L., Rita de Cassia Pessotti, Monika S. Fischer, Alyssa Collins, Laila El-Hifnawi, Mira D. Liu, and Matthew F. Traxler. 2020. "Cooperation, Competition, and Specialized Metabolism in a Simplified Root Nodule Microbiome." *MBio* 11 (4). https://doi.org/10.1128/mBio.01917-20.

Hansen, Lea Benedicte Skov, Dawei Ren, Mette Burmølle, and Søren J. Sørensen. 2017. "Distinct Gene Expression Profile of Xanthomonas Retroflexus Engaged in Synergistic Multispecies Biofilm Formation." *The ISME Journal* 11 (1): 300–303.

Herschend, Jakob, Zacharias B. V. Damholt, Andrea M. Marquard, Birte Svensson, Søren J. Sørensen, Per Hägglund, and Mette Burmølle. 2017. "A Meta-Proteomics Approach to Study the Interspecies Interactions Affecting Microbial Biofilm Development in a Model

Community." *Scientific Reports* 7 (1): 16483.

Hibbing, Michael E., Clay Fuqua, Matthew R. Parsek, and S. Brook Peterson. 2010. "Bacterial Competition: Surviving and Thriving in the Microbial Jungle." *Nature Reviews. Microbiology* 8 (1): 15–25.

Hsu, Ryan H., Ryan L. Clark, Jin Wen Tan, John C. Ahn, Sonali Gupta, Philip A. Romero, and Ophelia S. Venturelli. 2019. "Microbial Interaction Network Inference in Microfluidic Droplets." *Cell Systems* 9 (3): 229-242.e4.

Huerta-Cepas, Jaime, Damian Szklarczyk, Davide Heller, Ana Hernández-Plaza, Sofia K. Forslund, Helen Cook, Daniel R. Mende, et al. 2019. "EggNOG 5.0: A Hierarchical, Functionally and Phylogenetically Annotated Orthology Resource Based on 5090 Organisms and 2502 Viruses." *Nucleic Acids Research* 47 (D1): D309–14.

Kashima, Yuri, Satoshi Kanematsu, Saori Asai, Mio Kusada, Suzuyo Watanabe, Takuji Kawashima, Tadashi Nakamura, Masaya Shimada, Tsuyoshi Goto, and Satoshi Nagaoka. 2014. "Identification of a Novel Hypocholesterolemic Protein, Major Royal Jelly Protein 1, Derived from Royal Jelly." *PloS One* 9 (8): e105073.

Kastman, Erik K., Noelani Kamelamela, Josh W. Norville, Casey M. Cosetta, Rachel J. Dutton, and Benjamin E. Wolfe. 2016. "Biotic Interactions Shape the Ecological Distributions of Staphylococcus Species." *MBio* 7 (5). https://doi.org/10.1128/mBio.01157-16.

Kehe, Jared, Anthony Kulesa, Anthony Ortiz, Cheri M. Ackerman, Sri Gowtham Thakku, Daniel Sellers, Seppe Kuehn, Jeff Gore, Jonathan Friedman, and Paul C. Blainey. 2019. "Massively Parallel Screening of Synthetic Microbial Communities." *Proceedings of the National Academy of Sciences of the United States of America* 116 (26): 12804–9.

Kim, Dongyeop, Arjun Sengupta, Tagbo H. R. Niepa, Byung-Hoo Lee, Aalim Weljie, Veronica S. Freitas-Blanco, Ramiro M. Murata, Kathleen J. Stebe, Daeyeon Lee, and Hyun Koo. 2017. "Candida Albicans Stimulates Streptococcus Mutans Microcolony Development via Cross-Kingdom Biofilm-Derived Metabolites." *Scientific Reports* 7 (January): 41332.

Kolmogorov, Mikhail, Jeffrey Yuan, Yu Lin, and Pavel A. Pevzner. 2019. "Assembly of Long, Error-Prone Reads Using Repeat Graphs." *Nature Biotechnology* 37 (5): 540–46.

Kramer, Jos, Özhan Özkaya, and Rolf Kümmerli. 2020. "Bacterial Siderophores in Community and Host Interactions." *Nature Reviews. Microbiology* 18 (3): 152–63.

LaSarre, Breah, Adam M. Deutschbauer, Crystal E. Love, and James B. McKinlay. 2020. "Covert Cross-Feeding Revealed by Genome-Wide Analysis of Fitness Determinants in a Synthetic Bacterial Mutualism." *Applied and Environmental Microbiology* 86 (13). https://doi.org/10.1128/AEM.00543-20.

Lewin, Gina R., Apollo Stacy, Kelly L. Michie, Richard J. Lamont, and Marvin Whiteley. 2019. "Large-Scale Identification of Pathogen Essential Genes during Coinfection with Sympatric and Allopatric Microbes." *Proceedings of the National Academy of Sciences of*

the United States of America 116 (39): 19685–94.

Liu, Wenzheng, Samuel Jacquiod, Asker Brejnrod, Jakob Russel, Mette Burmølle, and Søren J. Sørensen. 2019. "Deciphering Links between Bacterial Interactions and Spatial Organization in Multispecies Biofilms." *The ISME Journal* 13 (12): 3054–66.

Lloyd, Daniel G., and David E. Whitworth. 2017. "The Myxobacterium Myxococcus Xanthus Can Sense and Respond to the Quorum Signals Secreted by Potential Prey Organisms." *Frontiers in Microbiology* 8 (March): 439.

Lozano, Gabriel L., Juan I. Bravo, Manuel F. Garavito Diago, Hyun Bong Park, Amanda Hurley, S. Brook Peterson, Eric V. Stabb, Jason M. Crawford, Nichole A. Broderick, and Jo Handelsman. 2019. "Introducing THOR, a Model Microbiome for Genetic Dissection of Community Behavior." *MBio* 10 (2). https://doi.org/10.1128/mBio.02846-18.

Lozano, Gabriel L., Hyun Bong Park, Juan I. Bravo, Eric A. Armstrong, John M. Denu, Eric V. Stabb, Nichole A. Broderick, Jason M. Crawford, and Jo Handelsman. 2019. "Bacterial Analogs of Plant Tetrahydropyridine Alkaloids Mediate Microbial Interactions in a Rhizosphere Model System." *Applied and Environmental Microbiology* 85 (10). https://doi.org/10.1128/AEM.03058-18.

Massey, Jonathan H., Daayun Chung, Igor Siwanowicz, David L. Stern, and Patricia J. Wittkopp. 2019. "The Yellow Gene Influences Drosophila Male Mating Success through Sex Comb Melanization." *ELife* 8 (October). https://doi.org/10.7554/eLife.49388.

May, Alexander, Shrinath Narayanan, Joe Alcock, Arvind Varsani, Carlo Maley, and Athena Aktipis. 2019. "Kombucha: A Novel Model System for Cooperation and Conflict in a Complex Multi-Species Microbial Ecosystem." *PeerJ* 7 (September): e7565.

McCully, Lucy M., Adam S. Bitzer, Sarah C. Seaton, Leah M. Smith, and Mark W. Silby. 2019. "Interspecies Social Spreading: Interaction between Two Sessile Soil Bacteria Leads to Emergence of Surface Motility." *MSphere* 4 (1). https://doi.org/10.1128/mSphere.00696-18.

Morin, Manon, Emily C. Pierce, and Rachel J. Dutton. 2018. "Changes in the Genetic Requirements for Microbial Interactions with Increasing Community Complexity." *ELife* 7 (September). https://doi.org/10.7554/eLife.37072.

Nakaya, Mako, Hiroyuki Onda, Kyoko Sasaki, Akiko Yukiyoshi, Hirofumi Tachibana, and Koji Yamada. 2007. "Effect of Royal Jelly on Bisphenol A-Induced Proliferation of Human Breast Cancer Cells." *Bioscience, Biotechnology, and Biochemistry* 71 (1): 253–55.

Otoupal, Peter B., and Anushree Chatterjee. 2018. "CRISPR Gene Perturbations Provide Insights for Improving Bacterial Biofuel Tolerance." *Frontiers in Bioengineering and Biotechnology* 6 (September): 122.

Paharik, Alexandra E., Corey P. Parlet, Nadjali Chung, Daniel A. Todd, Emilio I. Rodriguez, Michael J. Van Dyke, Nadja B. Cech, and Alexander R. Horswill. 2017. "Coagulase-

Negative Staphylococcal Strain Prevents Staphylococcus Aureus Colonization and Skin Infection by Blocking Quorum Sensing." *Cell Host & Microbe* 22 (6): 746-756.e5.

Pierce, Emily C., Manon Morin, Jessica C. Little, Roland B. Liu, Joanna Tannous, Nancy P. Keller, Kit Pogliano, Benjamin E. Wolfe, Laura M. Sanchez, and Rachel J. Dutton. 2020. "Bacterial-Fungal Interactions Revealed by Genome-Wide Analysis of Bacterial Mutant Fitness." *Nature Microbiology*, November. https://doi.org/10.1038/s41564-020-00800-z.

Piewngam, Pipat, Yue Zheng, Thuan H. Nguyen, Seth W. Dickey, Hwang-Soo Joo, Amer E. Villaruz, Kyle A. Glose, et al. 2018. "Pathogen Elimination by Probiotic Bacillus via Signalling Interference." *Nature* 562 (7728): 532–37.

Ratzke, Christoph, Julien Barrere, and Jeff Gore. 2020. "Strength of Species Interactions Determines Biodiversity and Stability in Microbial Communities." *Nature Ecology & Evolution* 4 (3): 376–83.

Ratzke, Christoph, and Jeff Gore. 2018. "Modifying and Reacting to the Environmental PH Can Drive Bacterial Interactions." *PLoS Biology* 16 (3): e2004248.

Ross, Benjamin D., Adrian J. Verster, Matthew C. Radey, Danica T. Schmidtke, Christopher E. Pope, Lucas R. Hoffman, Adeline M. Hajjar, S. Brook Peterson, Elhanan Borenstein, and Joseph D. Mougous. 2019. "Human Gut Bacteria Contain Acquired Interbacterial Defence Systems." *Nature* 575 (7781): 224–28.

Ruaud, Albane, Sofia Esquivel-Elizondo, Jacobo de la Cuesta-Zuluaga, Jillian L. Waters, Largus T. Angenent, Nicholas D. Youngblut, and Ruth E. Ley. 2020. "Syntrophy via Interspecies H2 Transfer between Christensenella and Methanobrevibacter Underlies Their Global Cooccurrence in the Human Gut." *MBio* 11 (1). https://doi.org/10.1128/mBio.03235-19.

Russell, Alistair B., S. Brook Peterson, and Joseph D. Mougous. 2014. "Type VI Secretion System Effectors: Poisons with a Purpose." *Nature Reviews. Microbiology* 12 (2): 137–48.

Salinero-Lanzarote, Alvaro, Alba Pacheco-Moreno, Lucía Domingo-Serrano, David Durán, Ernesto Ormeño-Orrillo, Esperanza Martínez-Romero, Marta Albareda, José Manuel Palacios, and Luis Rey. 2019. "The Type VI Secretion System of Rhizobium Etli Mim1 Has a Positive Effect in Symbiosis." *FEMS Microbiology Ecology* 95 (5). https://doi.org/10.1093/femsec/fiz054.

Sharma, Kriti, Márton Palatinszky, Georgi Nikolov, David Berry, and Elizabeth A. Shank. 2020. "Transparent Soil Microcosms for Live-Cell Imaging and Non-Destructive Stable Isotope Probing of Soil Microorganisms." *ELife* 9 (November). https://doi.org/10.7554/eLife.56275.

Slowikowski, Kamil. 2018. "Ggrepel: Automatically Position Non-Overlapping Text Labels with 'Ggplot2'. R Package Version 0.8. 0." https://CRAN.R-project.org/package=ggrepel.

Soto-Martin, Eva C., Ines Warnke, Freda M. Farquharson, Marilena Christodoulou, Graham

Horgan, Muriel Derrien, Jean-Michel Faurie, Harry J. Flint, Sylvia H. Duncan, and Petra Louis. 2020. “Vitamin Biosynthesis by Human Gut Butyrate-Producing Bacteria and Cross-Feeding in Synthetic Microbial Communities.” *MBio* 11 (4). https://doi.org/10.1128/mBio.00886-20.

Speare, Lauren, Andrew G. Cecere, Kirsten R. Guckes, Stephanie Smith, Michael S. Wollenberg, Mark J. Mandel, Tim Miyashiro, and Alecia N. Septer. 2018. “Bacterial Symbionts Use a Type VI Secretion System to Eliminate Competitors in Their Natural Host.” *Proceedings of the National Academy of Sciences of the United States of America* 115 (36): E8528–37.

Spraker, Joseph E., Philipp Wiemann, Joshua A. Baccile, Nandhitha Venkatesh, Julia Schumacher, Frank C. Schroeder, Laura M. Sanchez, and Nancy P. Keller. 2018. “Conserved Responses in a War of Small Molecules between a Plant-Pathogenic Bacterium and Fungi.” *MBio* 9 (3). https://doi.org/10.1128/mBio.00820-18.

Stubbendieck, Reed M., Daniel S. May, Marc G. Chevrette, Mia I. Temkin, Evelyn Wendt-Pienkowski, Julian Cagnazzo, Caitlin M. Carlson, James E. Gern, and Cameron R. Currie. 2019. “Competition among Nasal Bacteria Suggests a Role for Siderophore-Mediated Interactions in Shaping the Human Nasal Microbiota.” *Applied and Environmental Microbiology* 85 (10). https://doi.org/10.1128/AEM.02406-18.

Thibault, Derek, Paul A. Jensen, Stephen Wood, Christine Qabar, Stacie Clark, Mara G. Shainheit, Ralph R. Isberg, and Tim van Opijnen. 2019. “Droplet Tn-Seq Combines Microfluidics with Tn-Seq for Identifying Complex Single-Cell Phenotypes.” *Nature Communications* 10 (1): 5729.

Thompson, Luke R., Jon G. Sanders, Daniel McDonald, Amnon Amir, Joshua Ladau, Kenneth J. Locey, Robert J. Prill, et al. 2017. “A Communal Catalogue Reveals Earth’s Multiscale Microbial Diversity.” *Nature* 551 (7681): 457–63.

Vaser, Robert, Ivan Sović, Niranjan Nagarajan, and Mile Šikić. 2017. “Fast and Accurate de Novo Genome Assembly from Long Uncorrected Reads.” *Genome Research* 27 (5): 737–46.

Vezeteu, Thomas V., Otilia Bobiş, Robin F. A. Moritz, and Anja Buttstedt. 2017. “Food to Some, Poison to Others - Honeybee Royal Jelly and Its Growth Inhibiting Effect on European Foulbrood Bacteria.” *MicrobiologyOpen* 6 (1). https://doi.org/10.1002/mbo3.397.

Wetmore, Kelly M., Morgan N. Price, Robert J. Waters, Jacob S. Lamson, Jennifer He, Cindi A. Hoover, Matthew J. Blow, et al. 2015. “Rapid Quantification of Mutant Fitness in Diverse Bacteria by Sequencing Randomly Bar-Coded Transposons.” *MBio* 6 (3). https://doi.org/10.1128/mBio.00306-15.

Wickham, Hadley. 2009. “Ggplot2: Elegant Graphics for Data Analysis.” Springer-Verlag New York. http://ggplot2.org.

Wolfe, Benjamin E., Julie E. Button, Marcela Santarelli, and Rachel J. Dutton. 2014. “Cheese Rind Communities Provide Tractable Systems for In Situ and In Vitro Studies of Microbial Diversity.” *Cell* 158 (2): 422–33.

Yannarell, Sarah M., Gabrielle M. Grandchamp, Shih-Yuan Chen, Karen E. Daniels, and Elizabeth A. Shank. 2019. “A Dual-Species Biofilm with Emergent Mechanical and Protective Properties.” *Journal of Bacteriology* 201 (18). https://doi.org/10.1128/JB.00670-18.

Zengler, Karsten, Kirsten Hofmockel, Nitin S. Baliga, Scott W. Behie, Hans C. Bernstein, James B. Brown, José R. Dinneny, et al. 2019. “EcoFABs: Advancing Microbiome Science through Standardized Fabricated Ecosystems.” *Nature Methods* 16 (7): 567–71.

Zhang, Yuanchen, Erik K. Kastman, Jeffrey S. Guasto, and Benjamin E. Wolfe. 2018. “Fungal Networks Shape Dynamics of Bacterial Dispersal and Community Assembly in Cheese Rind Microbiomes.” *Nature Communications* 9 (1): 336.